AN EXAMINATION OF ARCHING IN GRANULAR SOILS

by

CHARLES HUGHEY EVANS

B.S., Massachusetts Institute of Technology
(1979)

Submitted to the Department of
Civil Engineering
in Partial Fulfillment of the
Requirements of the Degree of

MASTER OF SCIENCE IN CIVIL ENGINEERING

at the

MASSACHUSETTS INSTITUTE OF TECHNOLOGY

February 1984

Signature of Author: _____
Department of Civil Engineering, October 1983

Certified by: _____
H.H. Einstein, Thesis Supervisor

Accepted by: _____
F. Morel, Chairman, Civil Engineering Department Committee

AN EXAMINATION OF ARCHING IN GRANULAR SOILS

by

CHARLES HUGHEY EVANS

Submitted to the Department of Civil Engineering on October 14, 1983 in partial fulfillment of the requirements for the Degree of Master of Science in Civil Engineering

ABSTRACT

Forces on underground structures are often different from the weight of ground above the structure. A major factor contributing to this behavior is the phenomenon of 'arching' whereby movements related to the structure's presence mobilize shear stresses within the ground. These shear stresses lead to load redistribution away from (active arching) or toward (passive arching) the structure, depending upon patterns of ground movement and relative flexibilities of the structure and ground.

This investigation reviews the literature on arching and then presents a theoretical approach to arching in granular soils which is based upon elementary plasticity theory. Laboratory experiments using sandboxes equipped with rectangular and circular trap doors were performed to observe soil deformations in the vicinity of a yielding structure as well as stresses on and adjacent to the structure. Results are presented and compared with those obtained by others as well as those predicted by the various theoretical approaches.

The experimental results indicate that active arching can reduce the loads on a buried structure by as much as 95 percent, while passive arching can increase the loads by several hundred percent. Factors determining the mobilized level of arching include: direction of relative movements of ground and structure, the magnitude of adjacent ground movement with respect to the structure's width, and the ratio between the depth of overburden and the structure's width. The mechanism of soil deformations above a translating trap door as well as the force on the door are reasonably well predicted by the proposed plasticity theory approach.

An additional series of tests simulated a tunnel heading advancing through a soil mass. Vertical stresses were monitored on and adjacent to the model tunnel. Considerable three-dimensional stress redistribution can be observed for at least one tunnel diameter ahead of and behind the face.

Thesis Supervisor: Herbert H. Einstein

Title: Professor of Civil Engineering

ACKNOWLEDGEMENTS

The author would like to extend his sincere gratitude to Professor Herbert Einstein for his insightful help and encouragement throughout the development of this thesis.

Thanks are owed to Dr. J. Germaine and Dr. R. T. Martin for advice and information which were helpful in development of an experimental device, and are due Ms. D. O'Neill for sharing her knowledge of laboratory equipment and procedures with the author.

Much of the equipment used in this thesis was built at the M.I.T. Student Hobby Shop. The use of these facilities and assistance of the staff are appreciated.

The author's parents have always provided support, encouragement, understanding, and love. Thanks, Mom and Dad.

Finally, I wish to thank my wife, Linda, for the immeasurable help in preparing this thesis, and for making the many sacrifices which allowed me to complete this work. I Love You.

TABLE OF CONTENTS

LIST OF FIGURES

LIST OF FIGURES (CONT'D)

LIST OF FIGURES (CONT'D)

LIST OF FIGURES (CONT'D)

LIST OF FIGURES (CONT'D)

LIST OF TABLES

CHAPTER 1: INTRODUCTION

1.1 General

The presence of any inclusion, such as a structure, within a ground mass will change the local distribution of stresses and alter the load one would expect to act upon the structure. In addition, the ground located adjacent to a structure can greatly increase its load-carrying ability compared to an identical unburied structure. Consequently, design of structures such as tunnels, caverns, culverts, and shafts cannot be performed using common above-ground design standards and with geostatic stresses as loads; such practices would lead to highly over or under-designed facilities. This research emphasizes the stress redistribution around buried structures while only briefly addressing the increased load-carrying capacity.

Three primary factors decide what level of stress redistribution occurs (McNulty, 1965): first, physical properties of the structure, especially its load-deformation behavior; second, properties of the surrounding ground, particularly its ability to transfer loads through mobilization of shear stresses in response to relative displacements; and third, the free field stresses which would exist if the structure were not present. Of these three, the least understood and one receiving the most attention herein, is the second. This process, whereby stresses are transferred away from or onto a buried structure through mobilization of shear stresses resulting from relative displacements, is termed 'arching'. A more detailed definition is presented in the following section. This research is largely directed at the arching behavior of granular soils and one will find this term herein used interchangably with granular mass and sand.

1.2 Definition of Arching

The most widely accepted definition of arching was

presented by Terzhaghi (1943). Briefly stated, if a portion of an otherwise rigid support of a soil mass yields (Figure 1.1), the adjoining soil moves with respect to the remainder of the soil mass. This movement is resisted by shearing stresses which reduce the pressure on the yielding portion of the support while increasing the pressure on the adjacent rigid portions. This phenomenon is 'arching', and it also occurs when one portion of a yielding support moves more than adjoining parts.

Depending upon relative movements of a structure and the adjacent ground, active and passive arching can be distinguished. Figure 1.2 shows active arching (sometimes called positive arching). A structure within a soil mass is more compressible than the surrounding soil. When pressure, due to overburden or a surcharge, is applied to the system, the structure deforms more than the soil. This can be seen at the planes of equal initial elevation (AA and BB) in Figures 1.2.A and 1.2.B. The resulting stress distribution across these planes is similar to that shown in Figure 1.2.C. The stresses on the structure are less than the geostatic stresses, while those on the adjacent soil are greater. If the structure is assumed to deform uniformly, the stress distribution on it would be as indicated, with lower stresses toward the edges (due to the mobilized shear stresses).

Figure 1.3 shows the situation for passive arching (also known as negative arching). Here the soil is more compressible than the structure, and therefore undergoes larger displacements, mobilizing shear stresses which increase the total pressure on the structure while decreasing the pressure in the adjacent soil. Assuming the structure deforms uniformly, the stresses are highest at the edges and lowest at the centerline.

If the soil and structure were to have identical load-deformation properties the stresses experienced throughout the soil and on the structure would be the geostatic stresses. No arching would be present. The occurrence of such a situation is unlikely, simply because of the difference in behavior between structural materials such as steel or concrete, and soils.

Commonly, underground structures do not deform uniformly,

which causes stress distributions to become more complicated than those shown in Figures 1.2 and 1.3. Such a structure is present in Figure 1.4. The horizontal and vertical faces are more flexible towards the centers of the spans. This gives rise to the deformation patterns depicted. Thus, arching will be greater at the spans' centers, leading to horizontal and vertical stress distributions similar to those shown. In this case the faces of the structure are experiencing both active and passive arching simultaneously.

Stress redistribution resulting from relative displacements is a behavior commonly experienced in both granular and cohesive soils. The permanence of this redistribution is not, however, the same for these two materials. With cohesive soils the phenomenom of creep causes stresses to relax over time and often return to magnitudes near those due to the weight of overburden (Peck, 1969). A similar relaxation process can occur in granular soils when subjected to external influences such as vibration; however, typical reductions observed within granular soils range from negligible values to only about 15 percent of the stress redistribution caused by arching (Spangler and Handy, 1973 and Proctor and White, 1977). From the standpoint of design, beneficial long-term load reduction due to arching can only be anticipated in granular soils.

1.3 Objectives of Research

The purpose of this study is to explore the phenomenon of arching under controlled conditions where it can be separated from other aspects of the soil-structure interaction problem. In this way, magnitudes of active and passive arching, values for displacements necessary to mobilize arching, and the extent of the zone of stress transfer can be investigated.

From a basic understanding of the fundamentals of arching, extensions can be made to illuminate its contribution to the complicated stress distributions around underground structures. Of particular importance in this sense is arching around a tunnel heading as it advances through a granular soil.

1.4 Scope of Research

The author conducted an extensive literature search to identify previous investigations on the topic of arching. After reviewing these, it was decided to construct a device wherein arching experiments would be performed. This device consists of a sand-filled container with non-flexible sides and base. Stiff trap doors located within the base are initially flush, but can be translated vertically into or away from the soil mass. While displacements are controlled directly, pressure transducers mounted flush within the trap doors and adjacent base indicate the distribution of vertical stresses before, during, and after trap door displacement.

Several potentially important parameters were identified and varied between tests to study their impact on results. Among these were: sand type, density, depth of cover, direction of trap door motion, shape of door, and magnitude of displacement.

A number of simple plane strain and three-dimensional experiments were conducted to evaluate the performance of the device, obtain information on the magnitudes of stress redistribution, and observe behavior within the soil as arching occurs. These were followed by a series of tests simulating arching around an advancing soft ground tunnel by lowering a line of rectangular trap doors in succession while observing the associated stress redistribution.

An analytical prediction for arching is derived which closely models the actual deformation behavior observed within the soil, and is based on plasticity theory. This prediction and those of several other researchers are compared with experimental results of this and other research.

The next chapter contains a summary of the most relevant previous experimental and theoretical research into arching. Chapter 3 presents this author's proposed analytical approach to arching, while Chapter 4 addresses the difficult question of ground movements around underground structures; specifically, the magnitude of movements necessary to mobilize arching and how the distributions of movements affect the size of the zone

of arching. The testing equipment used in the experimental portion of this research is described in Chapter Five, while results and comparisons appear in Chapter Six. A summary, conclusions, and some recommendations for further research can be found in Chapter Seven.

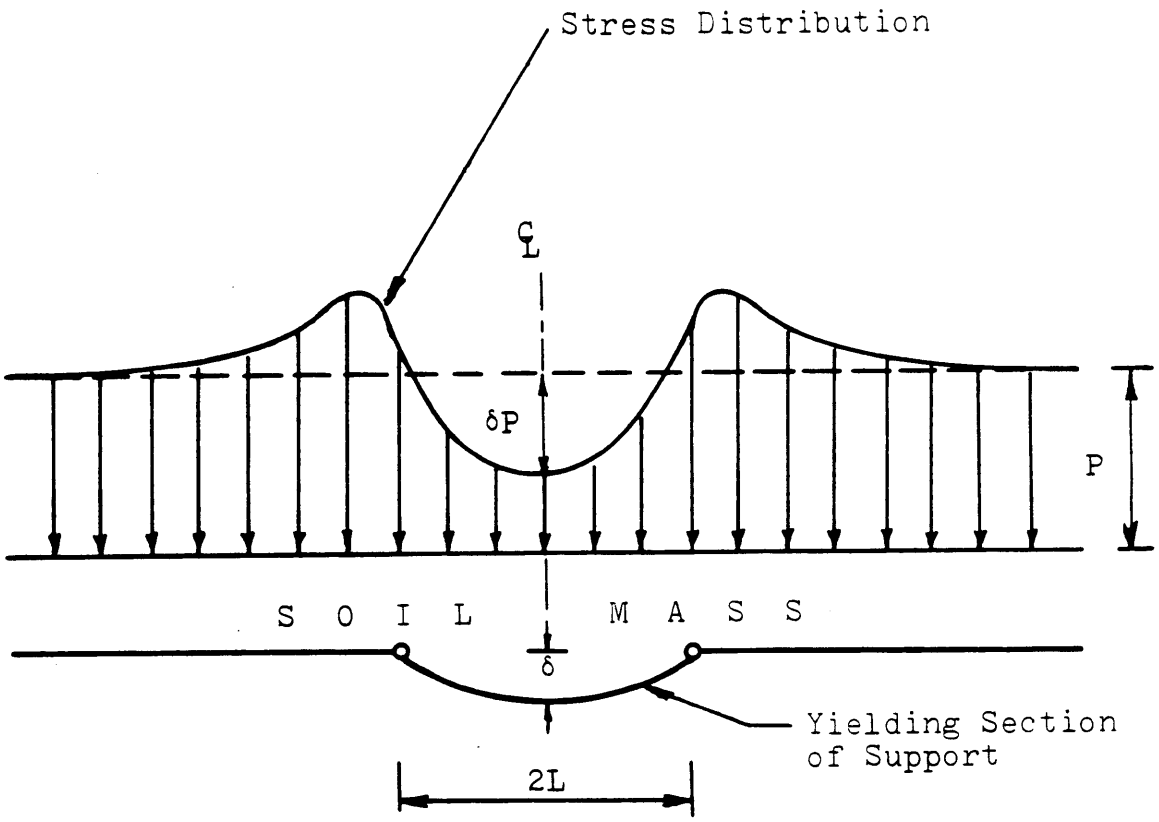

Figure 1.1 Arching within the Soil Above a Yielding Base

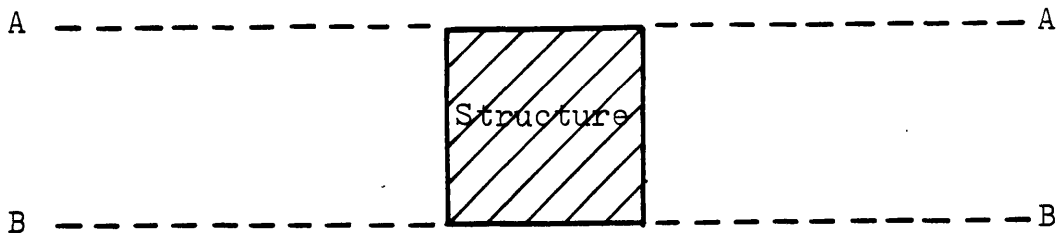

A. Structure within soil mass, no forces present

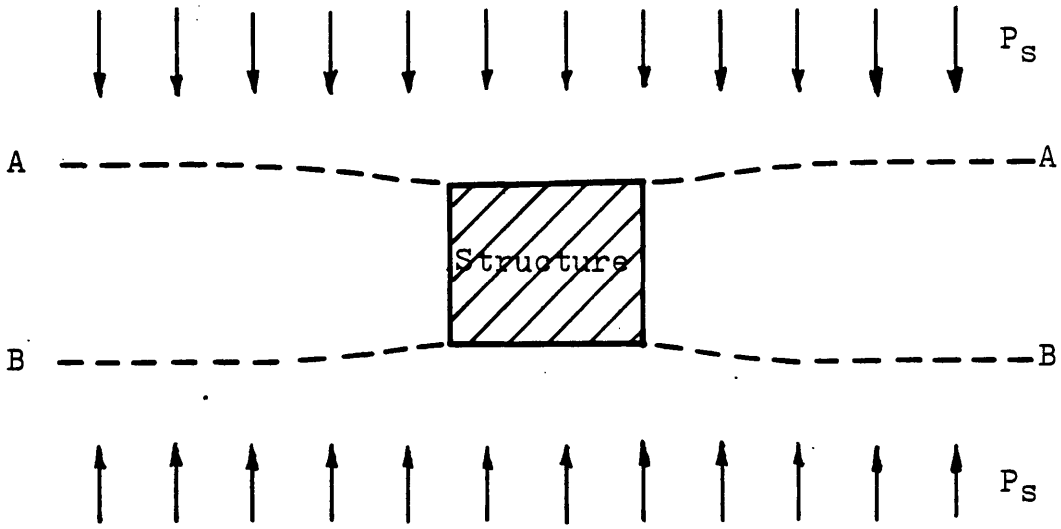

B. Displacements under pressure P_s when structure is more compressible than surrounding soil

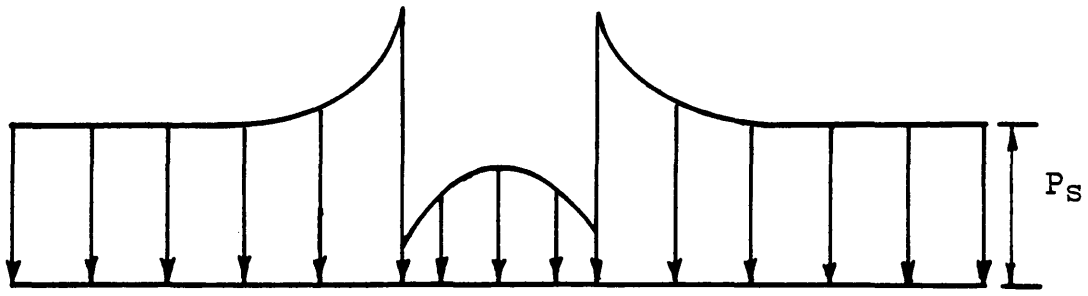

C. Stress distribution across plane AA or BB

Figure 1.2 Active Arching

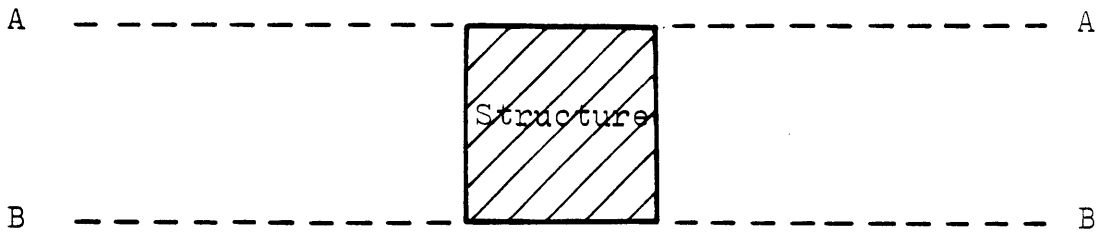

A. Structure within soil mass, no forces present

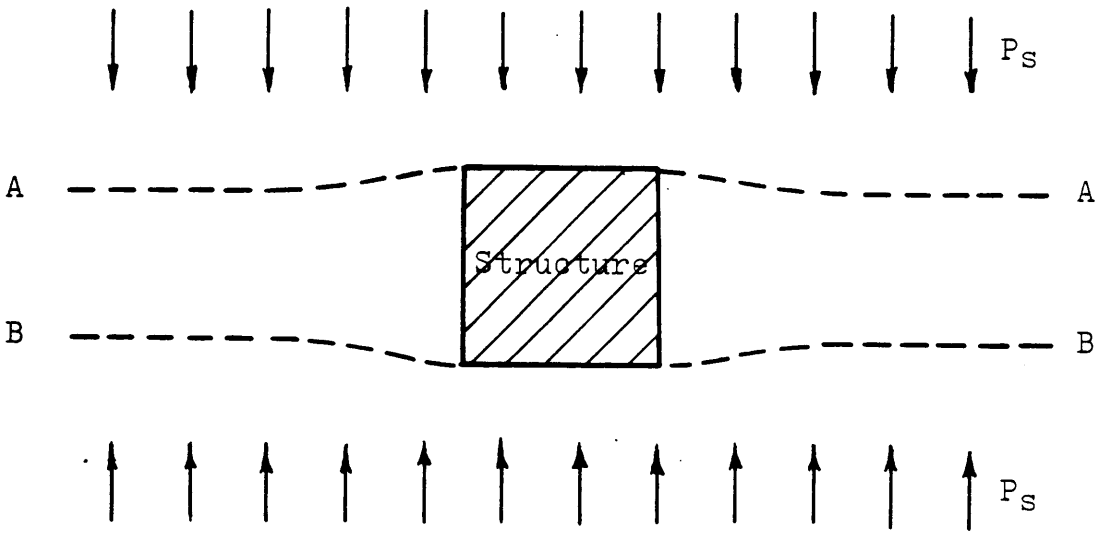

B. Displacement under pressure P_s when structure is less compressible than surrounding soil

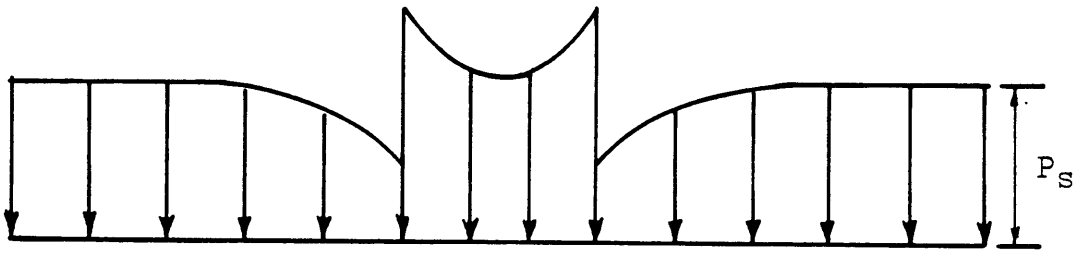

C. Stress distribution across plane AA or BB

Figure 1.3 Passive Arching

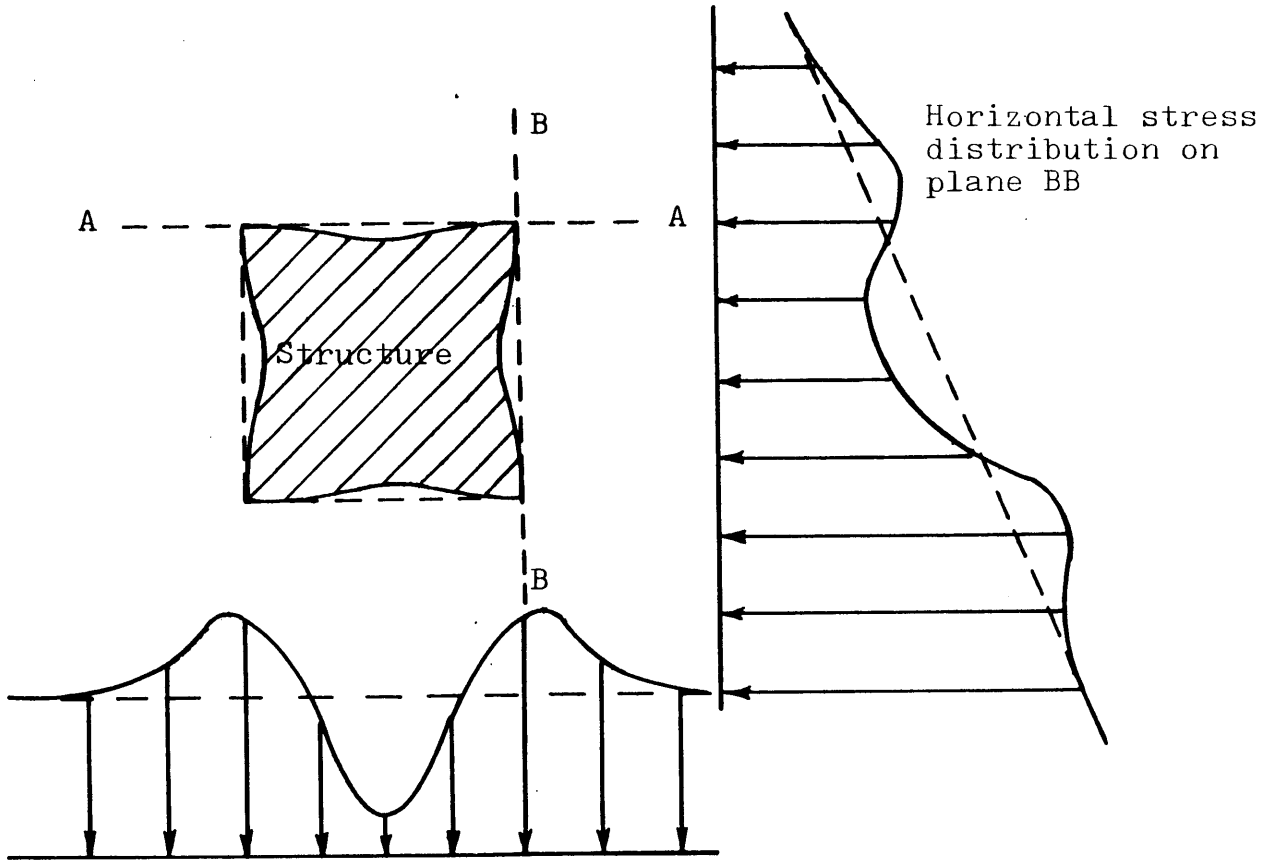

Figure 1.4 Typical deformation and stress distributions around a rectangular structure with flexible sides

CHAPTER 2: SUMMARY OF PREVIOUS RESEARCH

2.1 Historical Development

The phenomenon of arching has been recognized for over 150 years. Research has generally been sporadic, usually directed toward a particular area of importance at that point in time. This section summarizes this shifting emphasis of arching research. In subsequent sections the most significant theoretical and experimental investigations are presented, grouped by basic underlying approach.

As was shown in Chapter 1, arching is present in many geotechnical problems. However, arching was first recognized and investigated in a non-geotechnical context. During the early 1800's French military engineers were asked to design magazine silos (Feld, 1948). They found that the base of the silo only supported a fraction of the total weight of material above it, and the side walls carried far more load than anticipated. Experiments showed that if a small section of the base were detached and lowered, the resulting load the section experienced was independent of the height of material in the silo. They concluded an 'arch' had formed above this displaced section. In the latter 1800's this knowledge of the behavior within magazine silos was utilized in deriving an approach to the design of silos for grain and other particulate materials.

Around 1910 considerable land drainage projects were underway in the Midwest (Spangler and Handy, 1973). Engineers found that many of the drainage pipes they specified underwent structural failure subsequent to installation and backfilling. Anson Marston conducted extensive research at Iowa State University into the loads on underground conduits, finding that the loads may vary between a small fraction of the overburden and several times the overburden, depending upon the conduit's flexibility and the installation procedure. This variation was attributed to arching.

In the 1920's and 1930's the importance of arching around tunnels was recognized. Designers found that the

support loads were far less than the overburden and that considerable economy could be achieved if accurate predictions of load were possible. This gave rise to a great many empirical expressions for tunnel support loading, some of which are still in use today (Szechy, 1966). This interest in tunnel support loads also led to experimental and theoretical treatment of the problem, most notably by Terzaghi (1936, 1943 and in Proctor and White, 1946).

In the 1950's new interest in the loads on underground conduits was sparked by this county's decision to build an interstate highway system. More and larger culverts, with fill heights and culvert loadings greater than ever before, were required. Researchers reviewed and updated Marston's recommendations in light of experience obtained in the several decades since his investigations. Areas given particular concentration included the beneficial load redistribution around flexible culverts, and techniques for reducing the load on a culvert through specific backfilling procedures.

The direction of arching-related research shifted once again in the 1960's when the Defense Department sponsored considerable research into the area of soil-structure interaction. Techniques were needed for the design of hardened defense facilities and it was recognized that the arching phenomenon would allow facilities placed below ground to withstand nuclear attacks during war, which would destroy any surface facilities. Much of this research was presented at the "Symposium on Soil-Structure Interaction" held in 1964.

The last decade-and-a-half has seen the application of computer-based techniques (such as finite elements) to the arching problem. This creates the need for better models representing the behavior of actual soil masses, an area currently receiving much attention. In addition, more information from actual instrumented projects, such as culverts and tunnels, is becoming available, which aids in evaluating the appropriateness of the various approaches.

2.2 The Silo Theory

The commonly used formula for determining the force exerted on the base of a silo containing granular material was developed by H.A. Janssen in 1895 (Jakobson, 1958). By letting Figure 2.1 represent a silo of diameter B and height H which is full of material, one can determine F, the vertical force on the base.

Consider the forces acting on the horizontal differential element of height dh, diameter B, and at depth h (Figure 2.1). The lateral stress ($\sigma=4KV/\pi B^2$) is symmetric about the centerline, producing no net force on the element. Vertical forces on the element are the downward directed force on the top (V), the upward force on the bottom (V+dV), and the element's self weight ($W=\gamma\pi B^2 dh/4$). In addition, if the element is assumed to move downward with respect to the rigid walls of the silo, upward acting shear stresses ($\tau=4KV\tan\phi'/\pi B^2$, where $\tan\phi'$ is the coefficient of friction between the granular material and the silo's walls) develop. These shearing stresses contribute an upward acting vertical force on the element ($4KV\tan\phi' dh/\pi B^2$). The vertical equilibrium is therefore:

$$V + dV + \frac{4KV\tan\phi' dh}{\pi B^2} = V + \frac{\gamma\pi B^2 dh}{4} \qquad (2.1)$$

This is a linear differential equation, the solution for which is:

$$V = \frac{\gamma\pi B^3}{16K\tan\phi'}\left(1 - e^{-4K\tan\phi'(h/B)}\right) \qquad (2.2)$$

The value for force on the base (F) is obtained by substituting H for h in this expression.

There are two assumptions inherent in this derivation. First, the coefficient of lateral stress (K) has the same value at all depths, and second, the material settles with respect to the side walls sufficiently to develop shear stresses over the full depth of the silo.

2.3 Marston/Spangler Approach to Loads on Buried Conduits

Buried conduits may be grouped according to installation procedures. The two main categories are those installed in a ditch excavated through existing soil (ditch conduit), and those placed at existing ground level above which an embankment is subsequently constructed (projecting conduit).

Loads on a conduit equal the overburden if no relative motion occurs within the soil or between soil and conduit; however, this is seldom the case. Marston, assuming that sufficient movement occurs to mobilize shearing resistance on planes of sliding, used an analysis similar to that for the silo theory to determine potential loads on the conduit.

For the ditch conduit (Figure 2.2) the soil is divided into three zones: the prism (zone 1) where the ditch was excavated and backfilled, and the zones (2 and 3) on either side of this prism where natural ground remains. For analysis purposes the ditch is considered to have vertical sides, along which relative movement occurs, and a uniform width B_d. Suggested values of B_d for differently shaped ditches are found in Spangler and Handy (1973). Solution for the vertical force per unit length of ditch (V) on any vertical plane yields:

$$V = \gamma B_d^2 \frac{1 - e^{\mp 2K\tan\phi(h/B_d)}}{\pm 2K\tan\phi} \qquad (2.3)$$

The upper signs in this expression are for the center prism (zone 1 in Figure 2.2) moving downward compared with natural ground (active arching) and the lower signs apply when the center prism settles less than the natural ground (passive arching).

The expression for projecting conduits is identical, with the exception that sliding is assumed to develop along vertical surfaces (shown in Figure 2.2) extending upward from the sides of the conduit. This requires B_d in this formula to be replaced by B_c, the conduit's diameter.

The actual loads measured on conduits in laboratory experiments did not agree with theoretical values. It was

concluded that relative movement did not develop over the full depth, but rather only below an empirically determined plane called 'plane of equal settlement' (Spangler and Handy, 1973). This plane separates the lower part of the soil in the center prism, in which stress is being transferred by shear, from the upper part of the soil (in the center prism) which acts merely as a surcharge (see also section 2.4). To account for this an expression for load on the conduit (W_c) was introduced, $W_c = C\gamma B^2$ where B equals either B_d or B_c and C is a coefficient which can assume values within the two limits established by :

$$\left(\frac{1 - e^{\mp 2K\tan\phi(H/B)}}{\mp 2K\tan\phi}\right) \qquad (2.4)$$

Specific values for C can be obtained from laboratory experiments (described in Nielson, 1966), or from charts in Spangler and Hardy (1973) which give values for rigid and flexible conduits under various burial conditions.

2.4 Terzaghi's Investigations of Arching

Terzaghi conducted the most widely known experimental and theoretical investigations of arching. He also combined the knowledge obtained with information from many tunnelling projects to produce design values for tunnel support loads under various ground conditions (Proctor and White, 1946 and 1977). Many of Terzaghi's recommendations are still in wide use today.

Terzaghi (1936) reports the results of experiments conducted to improve understanding of the arching phenomenon in general and specifically the stress distribution around tunnels. A trap door, mounted flush with the base of a box containing sand (Figure 2.3.A) was translated downward while the total load on the door and its displacement were monitored. Horizontal and vertical stresses at various heights above the door were indirectly measured using the friction tape method.

Figures 2.3.B through 2.3.D show typical results reported by Terzaghi. As can be seen in Figure 2.3.B, the force on the

trap door decreases rapidly as displacement begins, with minimum values occurring at a displacement of only about 1% of the trap door width. These minimum values were less than 10% of the overburden and tended to be lower for dense sand than for loose sand. As displacement continued the 'structure' developed within the sand was believed to have disintegrated somewhat, causing the load to increase until a fairly constant value, still only a small fraction of the overburden, was obtained for trap door displacements greater than about 10% of the door's width. Dense and loose sand showed an ultimate trap door force of the same magnitude.

Figure 2.3.C shows measured vertical and horizontal stresses within the soil profile above the trap door, while Figure 2.3.D gives values for the coefficient of lateral stress (K) obtained from these results. For the case of 1% deflection K was approximately 1.0 directly above the trap door and increased to 1.6 at about one trap door width (B) above the door. At a distance of 2 to 2½ B above the door, K was essentially equal to K_o. Terzaghi describes K as an empirical constant and recommends that it be taken to equal 1.0 for analysis purposes.

In Terzaghi (1943) a theoretical approach to the arching problem in ideal soils is presented, which follows much the same reasoning as do the approaches in the previous two sections. This analysis is based on plane strain behavior within the soil. While actual sliding surfaces observed by Terzaghi in tests were believed to be shaped similar to those shown in Figure 2.4, surfaces rising vertically from the trap door edges were adopted in the analysis. In addition, it is assumed that vertical stress is constant across horizontal sections and that normal stress on the sliding planes equals $K\sigma_v$ where K is an empirical constant as discussed previously. Since his experimental results indicated that soil stresses at a distance more than 2B above the trap door were unaffected by the door's displacement, Terzaghi assumed that shearing resistance is only mobilized along the lower 2B of the sliding surface while the

remaining overburden acts as a surcharge. This is analogous to Spangler's 'plane of equal settlement' concept. Terzaghi also considers cohesion (c) to exist along the sliding surface, but he warns against treating it as a permanent condition. The equation obtained is:

$$F = \frac{B^2(\gamma - 2c/B)}{2K\tan\phi}\left(1 - e^{-2K\tan\phi(h/B)}\right) + Bqe^{-2K\tan\phi(h/B)} \qquad (2.5)$$

where F is force per unit length of trap door and q is any surcharge that might exist. When the soil layer is 2B or more in thickness and no external surcharge is present, this expression can be modified to:

$$F = \frac{B^2(\gamma - 2c/B)}{2K\tan\phi}\left(1 - e^{-4K\tan\phi}\right) + B(H - 2B)\,\gamma e^{-4K\tan\phi} \qquad (2.6)$$

These expressions can be applied to tunnels through sand by replacing the trap door width (B) by an equivalent width (B_e) (as shown in Figure 2.5) which can be expressed as:

$$B_e = B + 2D\tan(45^\circ - \phi/2) \qquad (2.7)$$

This expression was obtained by assuming the soil adjacent to the tunnel yields laterally toward the tunnel during construction. This creates an active earth pressure condition with boundaries for this zone of yielding inclined at about $45^\circ + \phi/2$. For a circular tunnel cross-section B_e is taken to equal the diameter of the tunnel.

Several researchers have duplicated the experiments conducted by Terzaghi. Among these are McNulty (1965), Ladanyi and Hoyaux (1969), Vardoulakis and Gudehus (1981), and Fricki and Fricker (1983). Vardoulakis and Gudehus modified Terzaghi's expressions to include a correlation factor which expresses σ_v along the sliding surfaces as a function of the free field stress. This function, however, is not readily known. Generally, no real advances have been made in recent years along the lines of Terzaghi's approach or in overcoming some of the limitations in his work.

There are several major limitations to the theories presented thus far in this chapter. First, they either do not address the distribution of stresses across the yielding surface, or else they assume it to be uniform, which does not agree with experimental results (see section 6.4). Second, they assume the trap door to displace rigidly whereas most buried structures possess some flexibility. The Marston/Spangler approach does take a conduit's flexibility somewhat into account through an empirical coefficient. Finally, the correct shape of the sliding surfaces is not always used, but rather an assumed shape is adopted which lends itself more easily to analytical treatment.

2.5 Ground Arch (Dome) Approaches

Several researchers have proposed a 'structural' analogy to explain the load redistribution around a yielding structure. They suggest that as the adjacent soil deforms, an arch or ring in the planar case, or a dome or sphere in the spatial case, forms within the soil (Figures 2.6 and 2.7). These 'ground-structures', once developed, redistribute loads away from the actual buried structure. Whitman, et.al. (1963) observed from tests on thin metal domes buried within sand that the level of pressure required to cause failure of the dome was several times that required for failure of an unburied dome. They postulated that a sand dome had developed above the structure, assuming some of the load which had previously acted upon the structure.

Luscher and Höeg (1965) attribute this increased load-carrying ability to the combination of three processes. First, the soil restrains deformation in a buried structure's second mode (for an explanation of a structure's modes of deformation see an elementary mechanics text such as Crandall and Dahl, 1959), causing stresses to redistribute to a more uniform configuration as the crown deflects vertically and the springlines horizontally. Second, deformation in the third and higher modes is restricted, creating increased load-carrying ability. Third,

deformation which does occur leads to development of these 'ground-arch/rings' and the redistribution of stresses away from the buried structure. A large number of data supporting the contention that buried structures exhibit a much higher load-carrying capacity are presented by Davis and Bacher (1968). They give magnitudes of actual loads experienced and ultimate capacities of culverts installed using several different backfills and backfilling techniques as well as load capacities of unburied culverts.

Luscher and Hoeg (1965) conducted experiments on buried flexible tubes, concluding that a sand ring (Figure 2.7.A) formed around the tube when deflection occurred. They suggest this soil-arch concept is more useful than the vertical sliding surface concept in the treatment of arching.

A differential soil arch, as shown in Figure 2.6.A was used by Nielson (1966) to determine arching over a buried conduit. The arch is assumed to be circular, with supports located on the surfaces of maximum shear stress (as determined by elasticity theory). The problem was solved using numerical procedures and a computer solution is presented. Nielson proposes the extension of this approach to non-circular (Figure 2.6.B) and three-dimensional (Figure 2.6.C) structures, but no attempt is made to formulate these solutions.

A structural analogy for arching was also proposed by Getzler, et.al. (1968) in experiments they conducted with structures having various roof shapes. The analytical model they proposed is shown in Figure 2.7.B, but no theoretical formulation is presented. An interesting conclusion from their experimental program is that buried structures with triangular or arch shape peaked roofs (i.e. higher at the center than at the edges), experience greater load reduction from arching than structures with flat roofs.

These 'structural' approaches have had little popularity in actual applications. Selig (1975) points out that they have never been fully developed, and in order to obtain any results one must make numerous assumptions as to the shape of

the arch (dome), location of and condition at supports, and interface behavior between elements.

2.6 Elastic Theory

A common approach to stress redistribution resulting from arching has been to apply elasticity theory solutions. While such approaches do predict stress redistribution as the ground-structure system deforms, they also contain the underlying assumption that behavior (including deformations and soil properties) is elastic. These solutions will be summarized here, however it should be noted that this author believes an approach (such as the one presented in Chapter 3), which models the ground surrounding a buried structure as behaving plastically, more closely resembles actual arching behavior (non-elastic) observed within soil.

Finn (1960) presents closed form solutions for the change in vertical stress resulting from translation or rotation of a trap door. He explicitly restricts his analysis to problems where displacements of the soil are very small and entirely elastic. A plane strain condition is assumed with the soil treated as a semi-infinite, elastic medium resting on a rigid horizontal boundary with a trap door located in it. The soil is considered to have no self weight.

A typical distribution of the change in vertical stress across the base for a downward translating door is shown in Figure 2.8. Infinite tensile stresses develop near the edges of the trap door, while infinite compressive stresses occur on the base next to the door.

Chelapati (1964) extended Finn's work to account for material self weight and a finite depth of cover. He superimposes stresses caused by the yielding trap door onto those due to material self weight plus any surcharges. The problem of infinite stresses at the trap door edges still exists. Since granular soil cannot sustain tension, the stress on the door is assumed to be zero wherever tensile stresses are indicated (see Figure 2.9). Compressive stresses on the base

adjacent to the door are then reduced, as shown, so as to produce no net change in total vertical force on the boundary (door plus base). A closed form solution is not obtained, rather results are presented graphically in terms of H, H/B, δ (trap door deflection), P_s (surcharge pressure), E (Young's Modulus), and μ (Poisson's Ratio).

Bjerrum, et.al. (1972) believed that Chelapati's elastic solution could be further extended to give approximate values for the change in vertical stress (δp) at the center of a flexible section located within a rigid horizontal boundary (Figure 2.10). They proposed the expression:

$$\delta p \simeq \alpha \frac{\delta}{L} E \qquad (2.8)$$

where α is a dimensionless coefficient whose value varies from about 0.3 to 1.0 depending upon the parameters: H, H/B, δ, P_s, E, and μ. They restricted the application of this expression to small values of δp, which makes the validity of this elastic approach questionable in light of the sizable stress reduction observed in the laboratory and field.

This type of approach was taken one step further by Burghignoli (1981) when investigating stress redistribution around underground structures with flexible roofs. He incorporated the elastic properties of the flexible section within the rigid boundary (similar to Figure 2.10) into the analysis. Results are once again presented in graphical form, and are only given for a few specific values of the previously mentioned parameters. Also, some iteration is necessary, because one must initially assume a value for centerline displacement. Some information on appropriate estimates is given.

Research has also been performed in the area of stress redistribution around an elastic cylindrical inclusion placed within a linear elastic medium. Approaches to this problem can be found in Burns and Richards (1964), Rohmaller (1968), Muir Wood (1975), and Highway Research Board (1971). Details of this work will not be presented here; however, due to the assumption of elastic behavior the results generally predict

thrusts and moments which are considerably larger than those actually measured in field and laboratory installations.

Peck (1975) questions the appropriateness of approaches to arching based on assumed elastic behavior and states, "The ground movements associated with construction, particularly in soft soils, are so large that the soil is likely to be stressed far beyond the limits of elasticity".

2.7 Empirical Methods

Over the years a group of methods for the loading developed on underground structures (particularly tunnels) which are primarily empirically based have evolved. Some have been obtained from very simple static analyses while others are entirely founded on the experience of the person proposing it. Szechy (1966), Markovic and Popovic (1970), Canizo (1973), and Bello (1978) present a number of these theories. One such method is shown in Figure 2.11 (Szechy, 1966). In general, they assume the existence of a zone of relaxation above the buried structure which often is given the shape of a triangle or parabola. The force acting on the structure is simply the weight of the material within the relaxation zone, plus in some cases a surcharge. Coefficients may be included to incorporate the condition and type of material present, but displacements of the soil or structure are not addressed.

These empirical methods are still often used by designers in conjunction with other approaches. They are very quick and simple, as well as giving fairly good results if one chooses a method which was derived from experiences with ground conditions and construction methods similar to those for the proposed structure. The method presented in Figure 2.11 is compared with experimental results in Chapter 6.

2.8 Finite Element and Finite Difference Approach

Perhaps the most comprehensive methods available for the analysis of stress redistribution around buried structures are the finite element and finite difference approaches. In their

most complete form they allow one to analyze problems with complications such as involved geometries, concentrated loads, non-homogeneity, and anisotropic behavior. Among the programs available are the ones in Selig (1975) and Rude (1982) (called CANDE) for culvert design, as well as a number of more general purpose programs, including ADINA, which are summarized in Einstein, et.al. (1980).

There are two main drawbacks to these formulations. First, the analysis can frequently become time-consuming and expensive, which limits their use. Second, the results are only as good as the chosen parameter values and constitutive relations modeled.

Getzler, et.al. (1970) performed a finite difference analysis of the plane strain trap door problem. Essentially, their formulation was the same elastic approach taken by Chelapati (1964) and presented in Section 2.6. The soil is linearly elastic and stresses associated with the trap door yielding and self weight of the material (plus any surcharge) are superimposed.

Ranken and Ghaboussi (1975) used an axisymmetric finite element program to simulate an advancing tunnel in isotropic, homogeneous, and continuous soil. They ran analyses for lined and unlined tunnels with three types of stress-strain behavior for the soil; linear elastic, elasto-plastic with strength independent of mean stress and angle of shear resistance, and elasto-plastic with the behavior being a function of these parameters.

Atkinson, et.al. (1977) used finite elements to predict the results of model tunnel tests they performed (Section 2.11); however, the predictions were disappointing and they chose not to publish them with the experimental results.

More recently, Rude (1982, 1983) used a linear elastic finite element program to predict the behavior of a culvert installed in a laboratory testing tank. He obtained good agreement between predicted and measured behavior.

2.9 Photoelasticity Methods

An experimental technique allowing study of stress distributions around structures of complex geometry is the photoelasticity method (Riley, 1964). Here, stresses are induced in an elastic material which is subsequently set, freezing the stresses in place. The material is then sliced and analyzed under polarizing filters. Application to arching at present is limited, since actual soil cannot be used as the medium for tests. Rather, an epoxy resin is commonly employed with properties considerably different from granular soil. If the method could be adapted to be more applicable to granular soils it could provide a powerful tool in examining arching and the associated stress redistribution around structures with very complicated geometries.

2.10 Other Theoretical Approaches to Arching

Truesdale and Vey (1964) investigated the load redistribution above a buried structure with a flexible roof having known elastic properties. They modeled the soil with a grid of rigid square elements which can transfer normal and shear forces across common boundaries, and are free to move as the structure yields (see Figure 2.12). An initial stress distribution is assumed to act upon the structure and its deflected shape is calculated. The soil elements then displace and the resulting stresses within the soil are determined. From these they find a new stress distribution on the structure and the process above is repeated until internally compatible stresses and displacements are obtained. A computer is required to solve for the stress redistribution and perform the iterations. The quality of results depends upon the relative size chosen for the individual soil elements with accuracy increasing as smaller elements are used.

The ideal approach to arching in granular soil would be to consider the equilibrium of individual particles. This, of course, is not generally practical; however, some research has been performed aimed at developing a simplified approach

of this type. The concept is termed 'systematic arching theory'. Soil is represented by single-sized two-dimensional particles in a regular packing (see Figure 2.13). Each particle is acted upon by six normal forces from adjacent particles. Imposing boundary conditions and static equilibrium, along with the assumptions that horizontal forces are zero and no force can be tensile, Trollope (1957, 1963) derived a solution for the arching beneath a triangular embankment on a flexible base. His results do not, however, agree very well with measured values. He also points out that only simple problem geometries can be modeled. Butterfield (1968) employed this concept in studies on the stresses developed within silos. His results were similar to those from the silo theory, but he gives little information as to how his model was set up.

2.11 Additional Experimental Investigations

This section summarizes several experimental programs which fall outside the topics of previous sections, but are important to the subject of arching.

A group at Cambridge University conducted a series of model tests to examine the behavior of shallow soft ground tunnels. The results are reported in Atkinson and Cairncross (1973), Atkinson, et.al. (1974, 1975, 1977), Atkinson and Orr (1976), and Atkinson and Potts (1977). Figure 2.14 shows the dimensions of the model. All boundaries are rigid except for the top where a pressure bag was installed to add surcharge loading. A grid of lead shot placed within the sand during deposition makes it possible to monitor displacements, as the test proceeds, using radiographic techniques (information on displacements will be presented in Chapter 4). The tunnel consists of a hollow flexible membrane which is initially pressurized to equal the overburden plus surcharge. Tests are conducted by slowly lowering the internal tunnel pressure until a sudden collapse occurs. The pressure just before collapse is analogous to the minimum active arching load. Conclusions

which can be drawn from the test results are: first, the tunnel pressure at collapse is nearly independent of overburden height, and second, with the same overburden, model tunnels in dense sand collapsed at lower tunnel pressures than those in loose sand (i.e. dense sand exhibits more arching).

Harris (1974) performed sandbox trap door experiments aimed at simulating the stress redistribution around a longwall coal mining operation. His apparatus is shown in Figure 2.15.A. It consists of a series of trap doors which can be lowered independently to model the advancing face. Diaphragm pressure cells are located as shown to facilitate stress measurement. By lowering the doors in succession, Harris could obtain the stress distribution from beyond the influence zone ahead of the face, till a constant distribution is obtained well back of the face. Typical results are shown in Figure 2.15.B. Areas of stress concentration (abutments) develop ahead of and to the side of the face. In addition, a less developed abutment (termed 'rear abutment area' in figure) appears within the extracted zone (above the lowered doors). Harris' results can also be interpreted as the stress distribution around an advancing tunnel face in soft ground. One can readily conclude that the stress field near the face is nothing like that predicted by most approaches, but is, rather a very complicated three-dimensional pattern. A constant stress distribution does not develop until one to two face widths behind the advancing face. Chapter 6 includes results from experiments similar to Harris'.

2.12 Concluding Remarks on Previous Research

As one has seen in this chapter, a wide spectrum of approaches to the load redistribution associated with arching exists. The purpose here has not been to provide indepth details on each approach, but rather to provide a short summary of what research was conducted, along with advantages and limitations of each approach. Each theoretical or experimental investigation has been grouped according to its basic underlying

principle.

In Chapter 3 another approach will be explored in more detail, that of plasticity theory. This author believes that plasticity theory can most correctly model and predict the actual arching behavior around a buried structure.

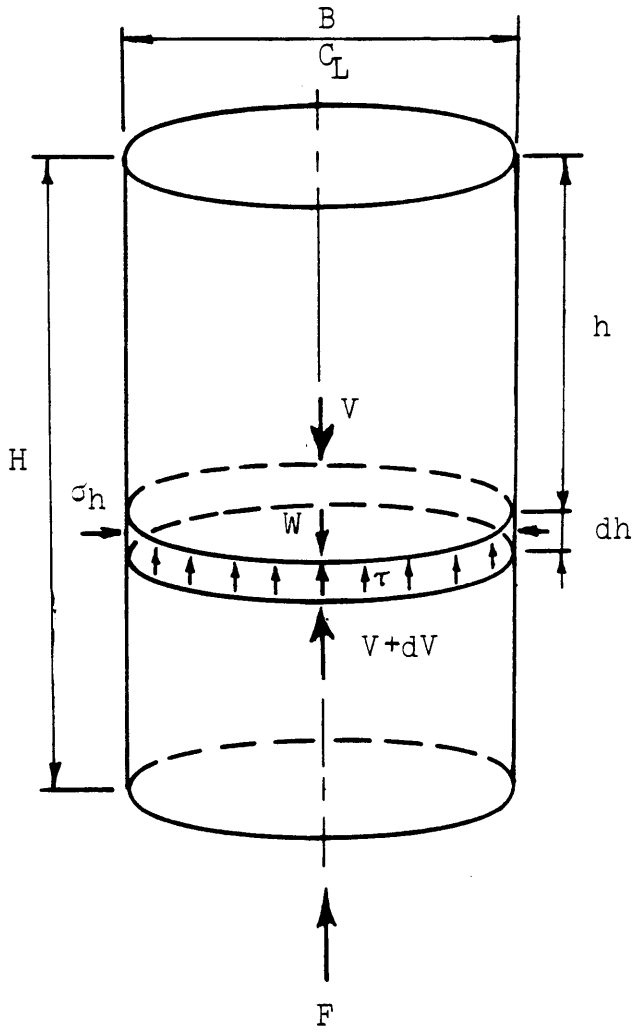

Figure 2.1 Free body diagram for silo theory

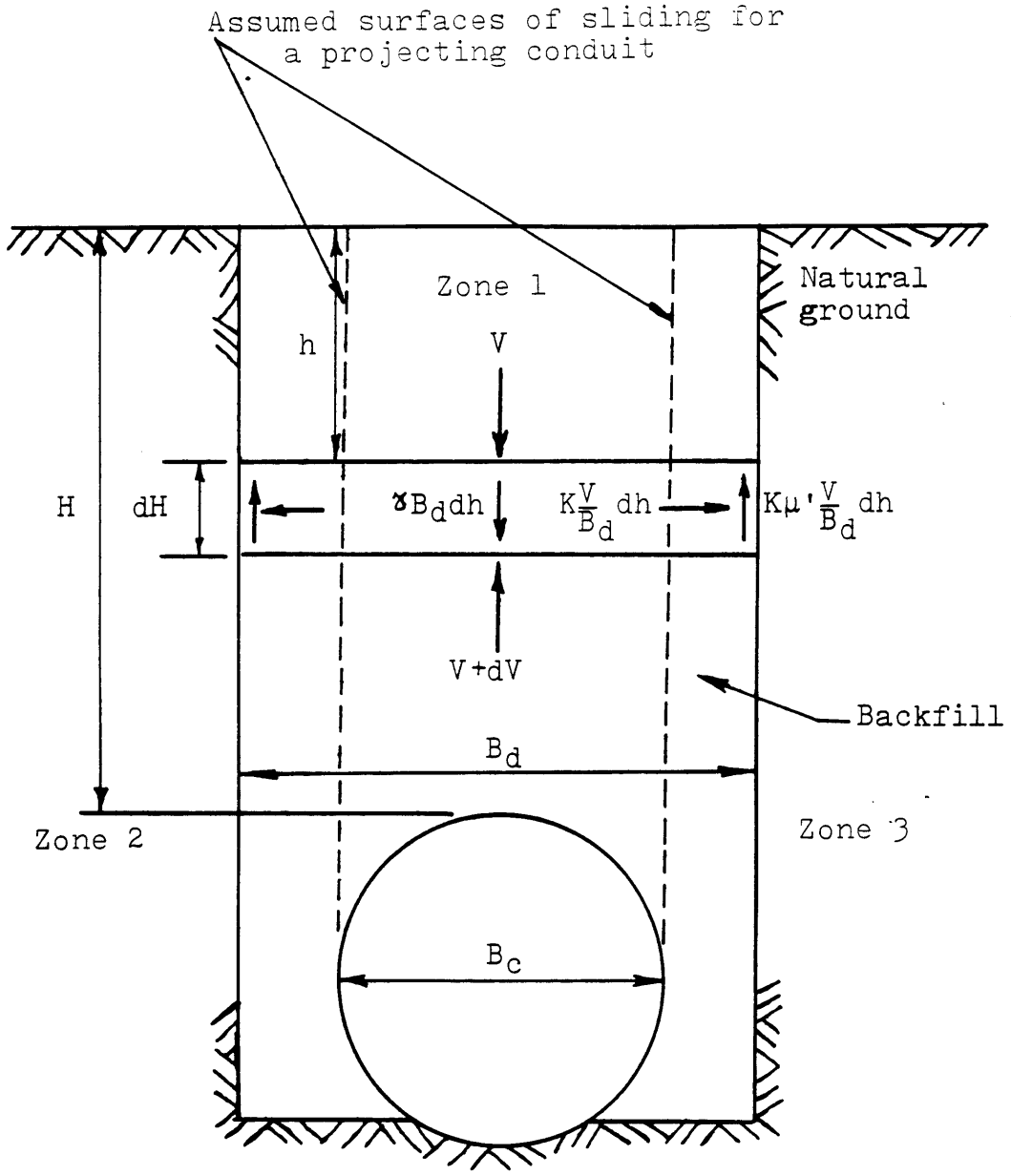

Figure 2.2 Free body diagram for a ditch conduit

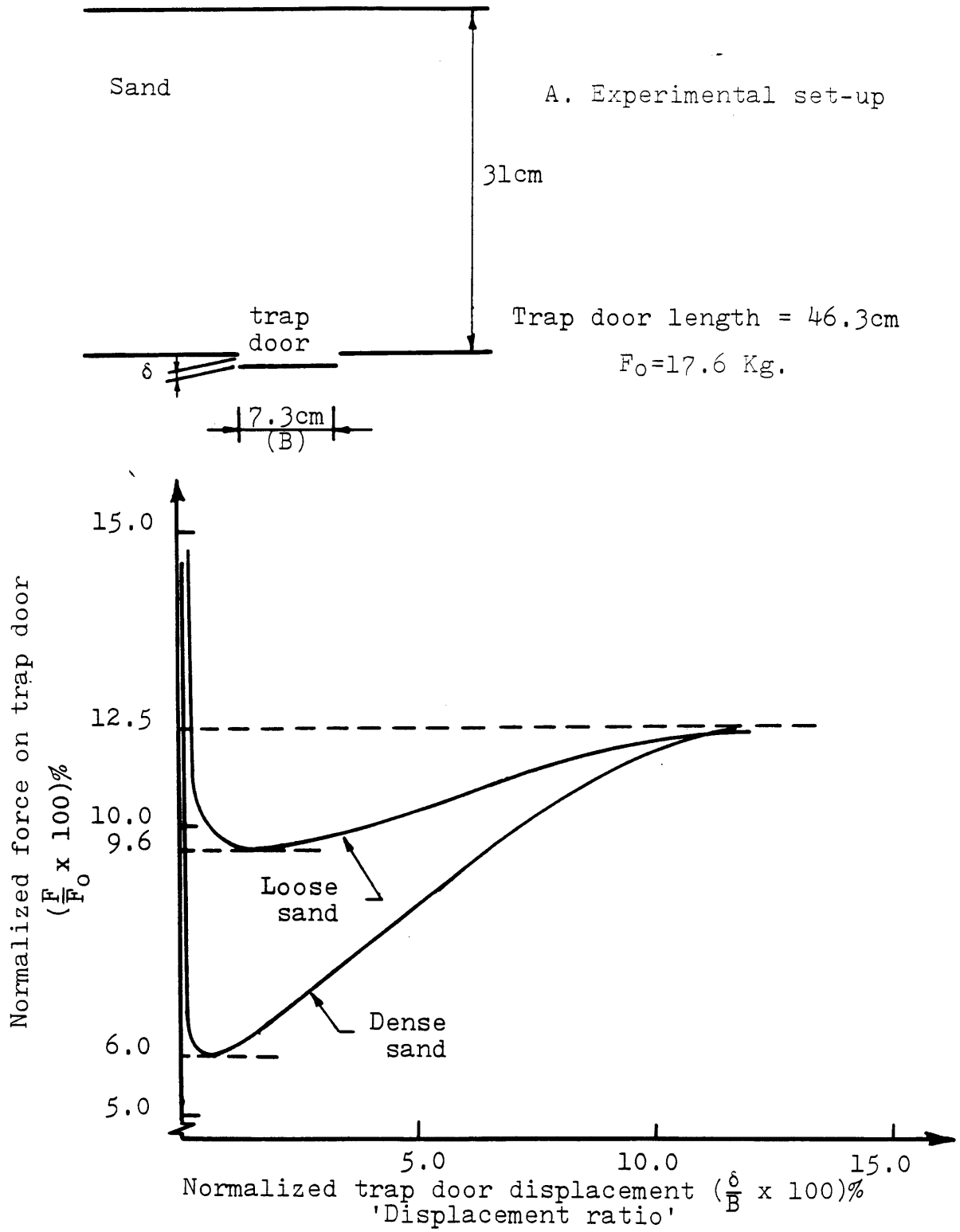

B. Vertical force on trap door vs. displacement

Figure 2.3 Terzaghi's trap door experiment

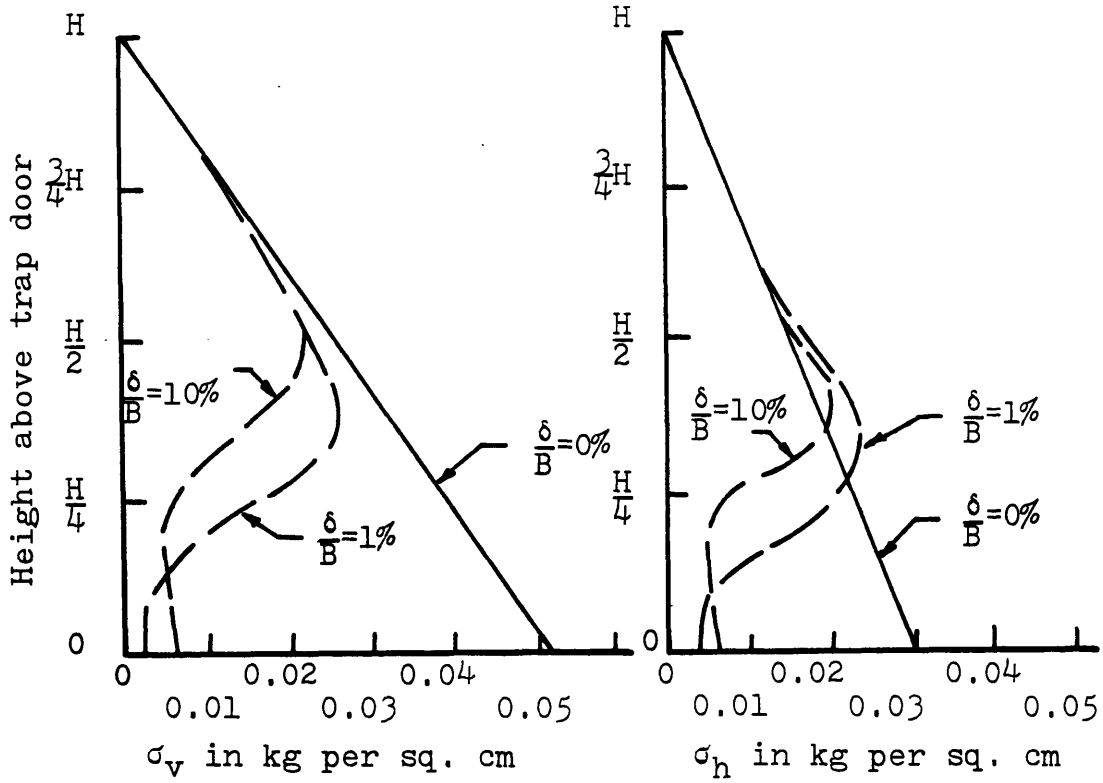

C. Vertical and horizontal stresses within sand body

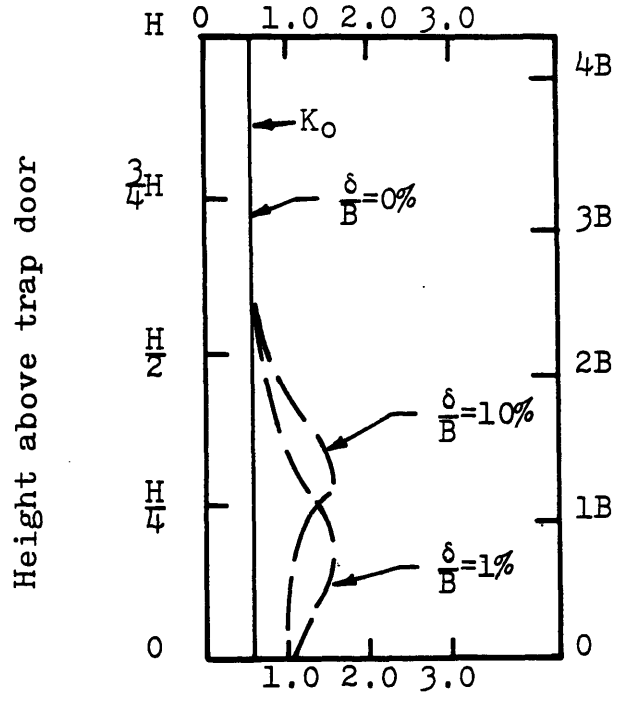

D. Coefficient of lateral earth pressure (K)

Figure 2.3(cont'd) Terzaghi's trap door experiment

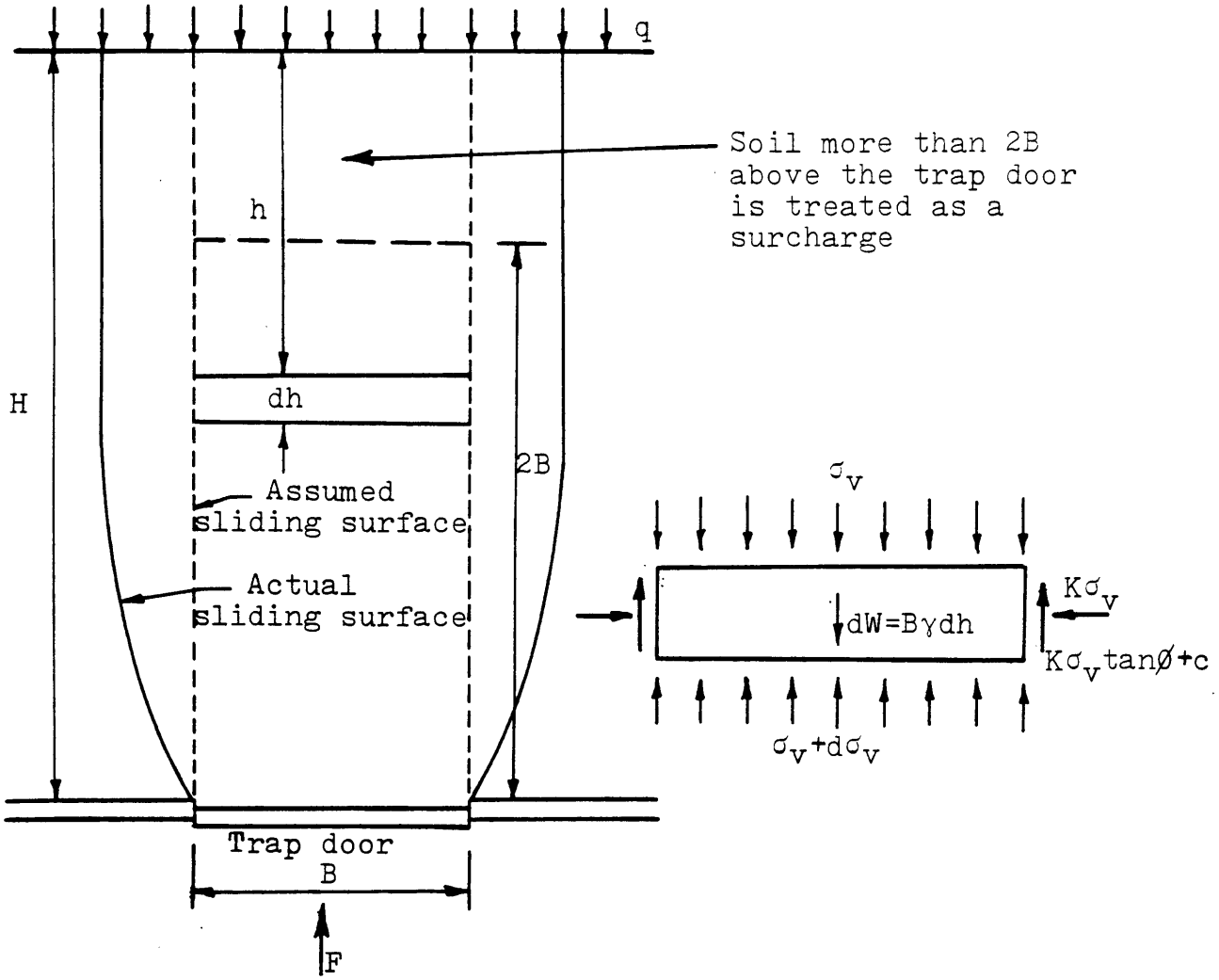

Figure 2.4 Arching above a yielding trap door

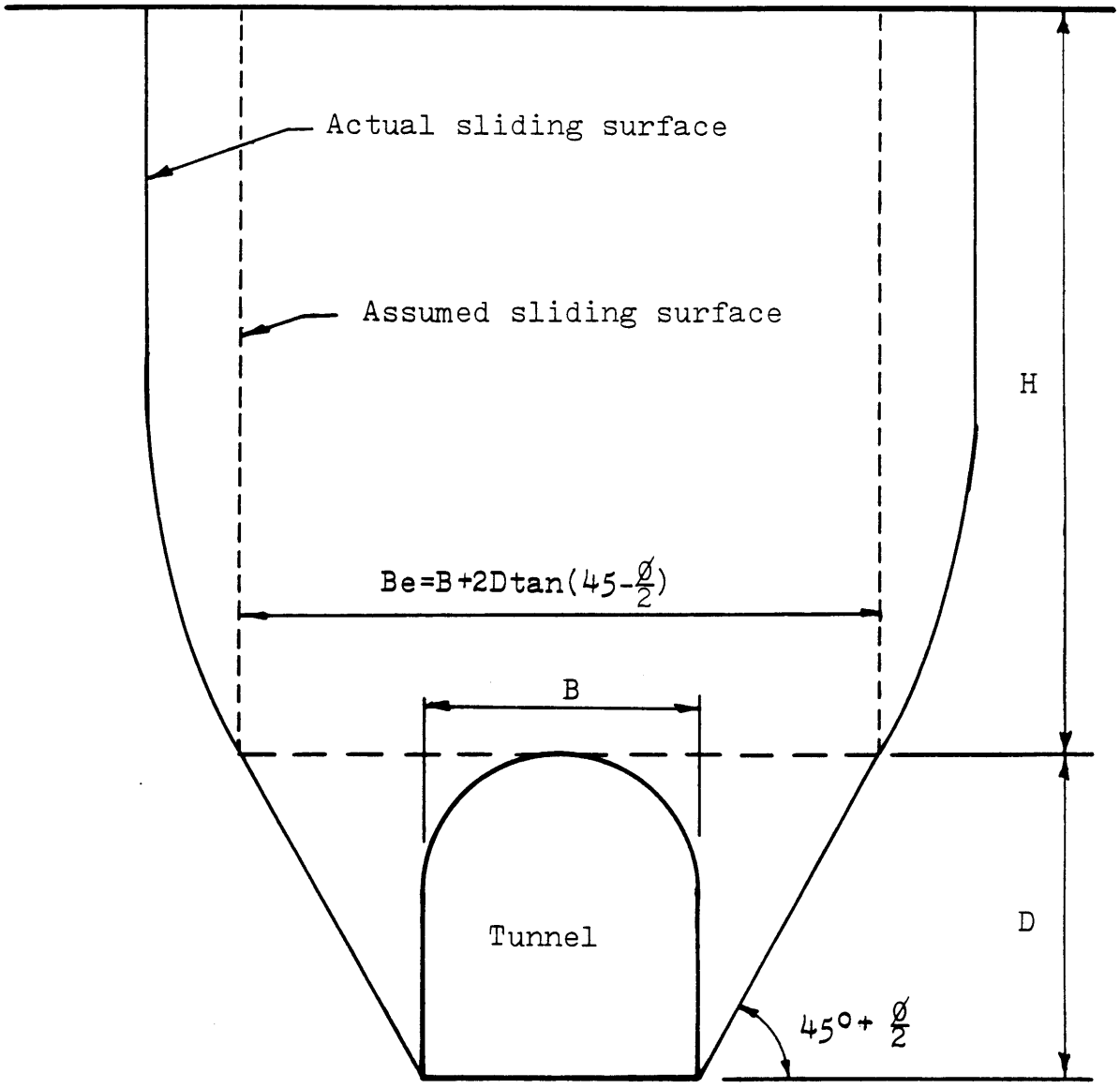

Figure 2.5 Determination of equivalent trap door width for a tunnel through sand

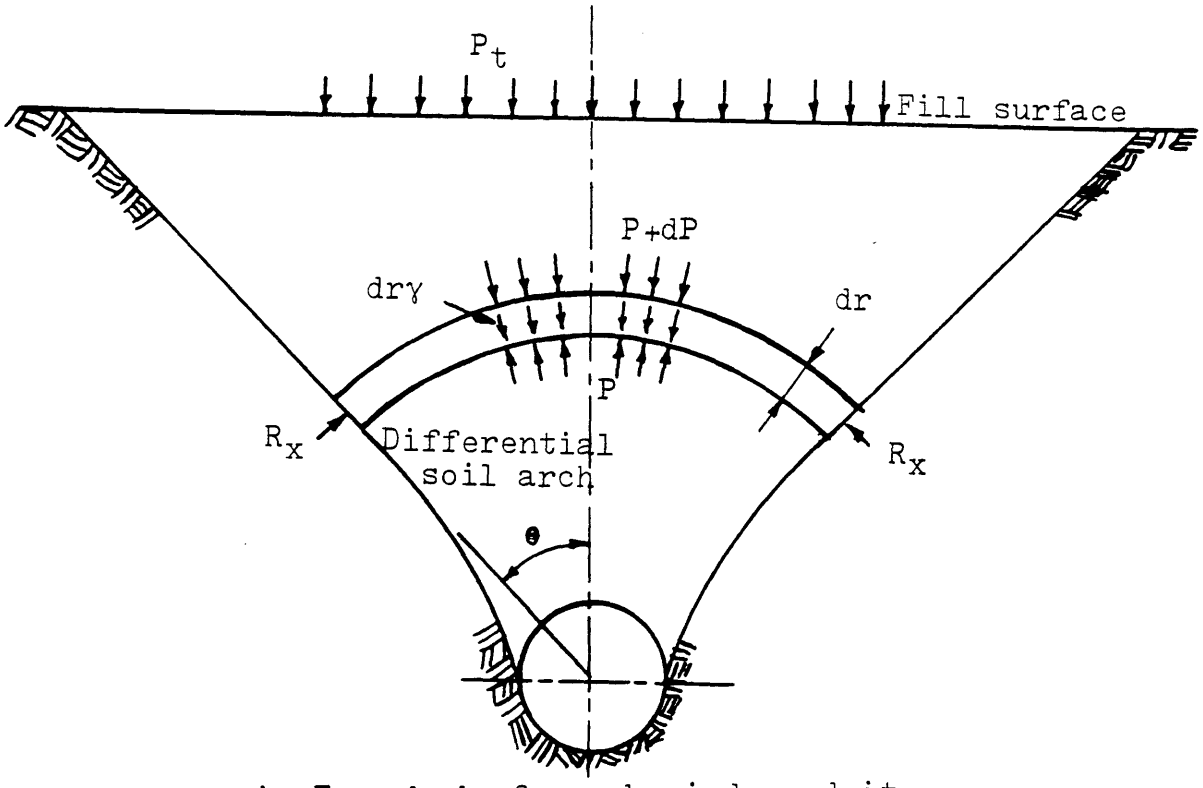

A. Free body for a buried conduit

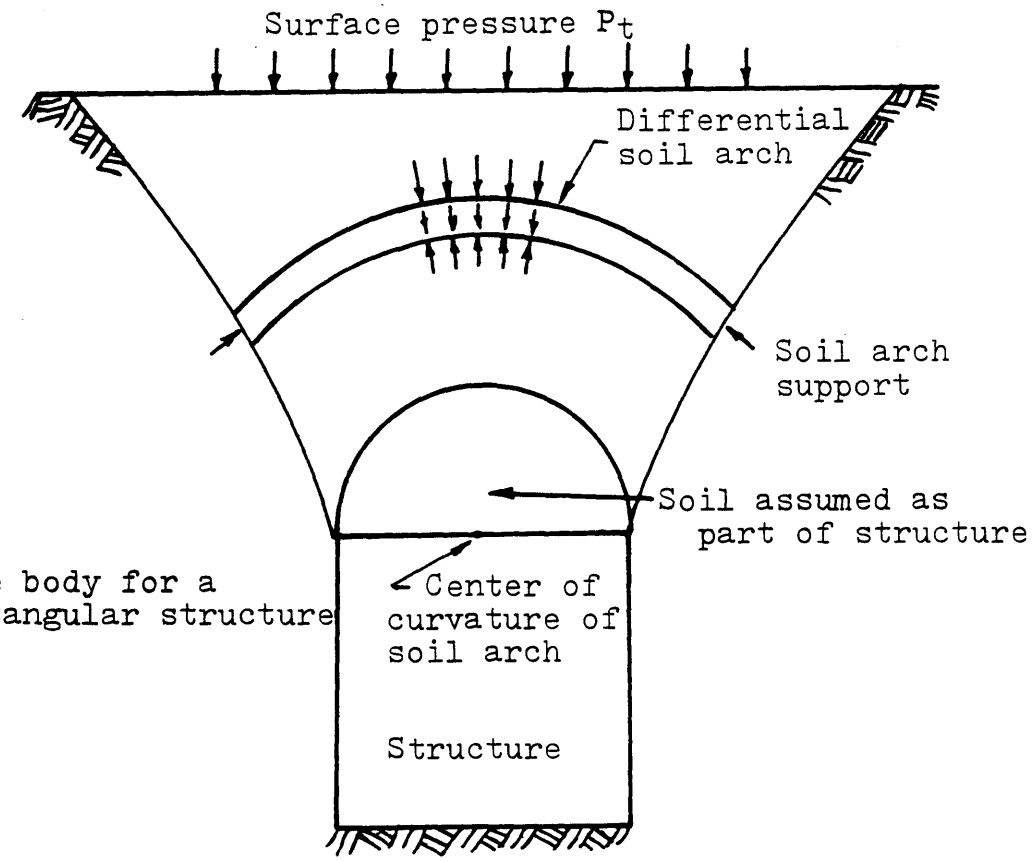

B. Free body for a rectangular structure

Figure 2.6 Free body diagrams for Nielson's arching analysis

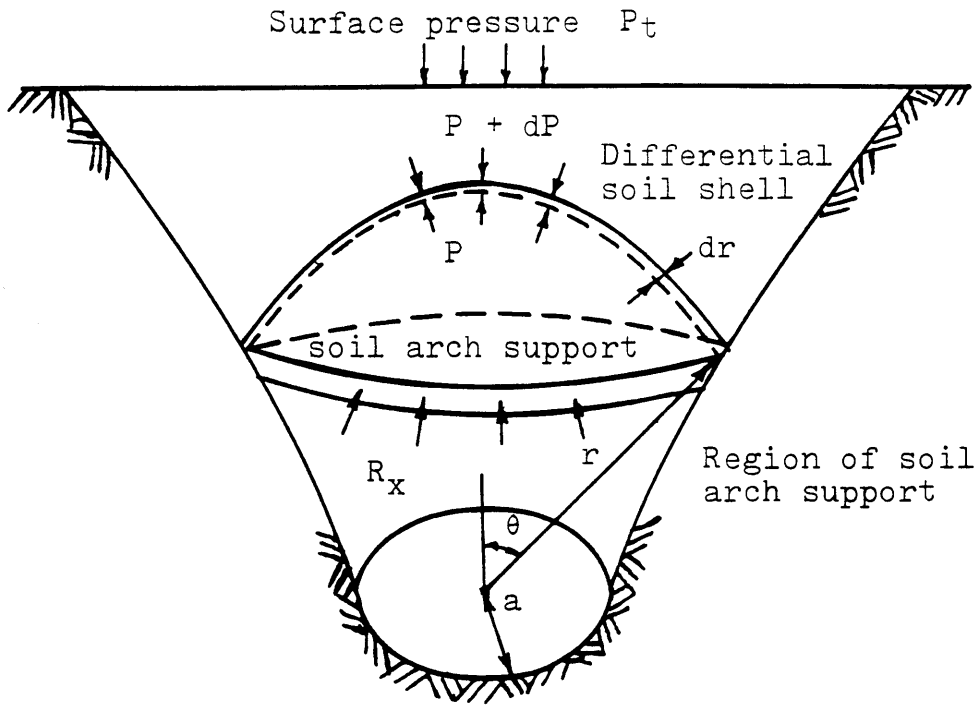

C. Free body for a three-dimensional structure

Figure 2.6 (cont'd) Free Body Diagrams for Nielson's Arching Analysis

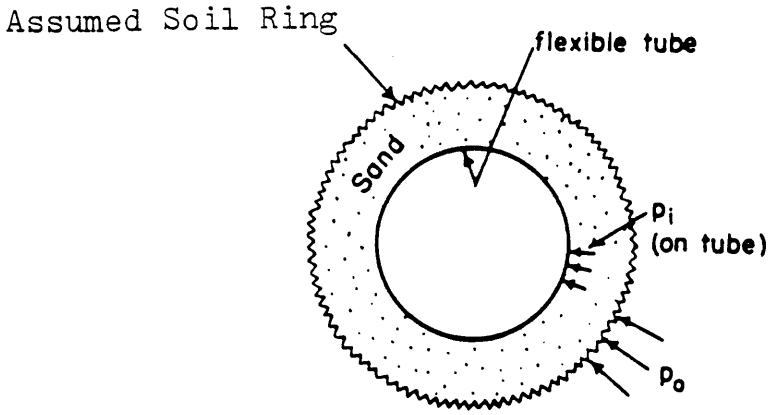

A. Soil Acting as Ring About Structure
(from Luscher and Höeg, 1964)

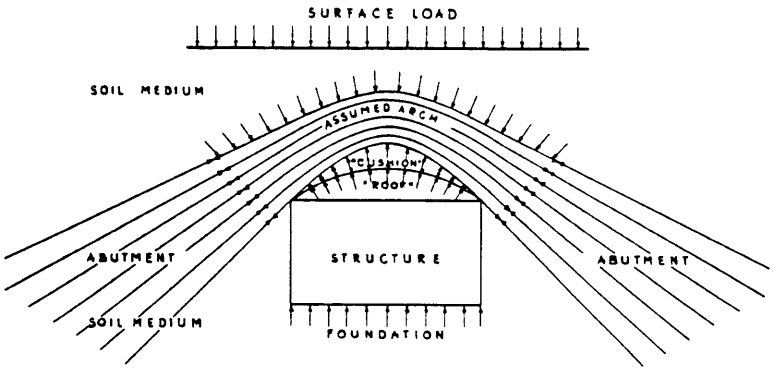

B. Soil Acting as Arch Above Structure
(from Getzler et. al., 1968)

Figure 2.7 Examples of Ground Arch/Ring Approaches

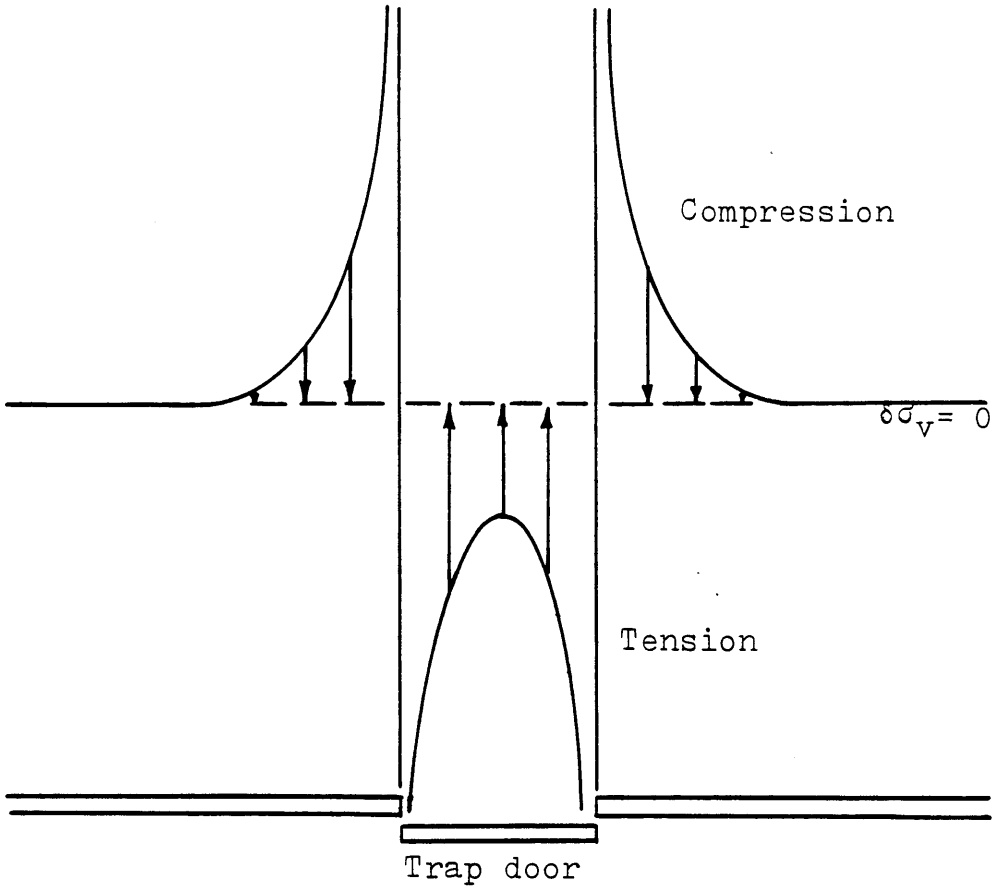

Figure 2.8 Typical Distribution of Change in Vertical Stress for Downward Translating Trap Door (after Finn, 1963)

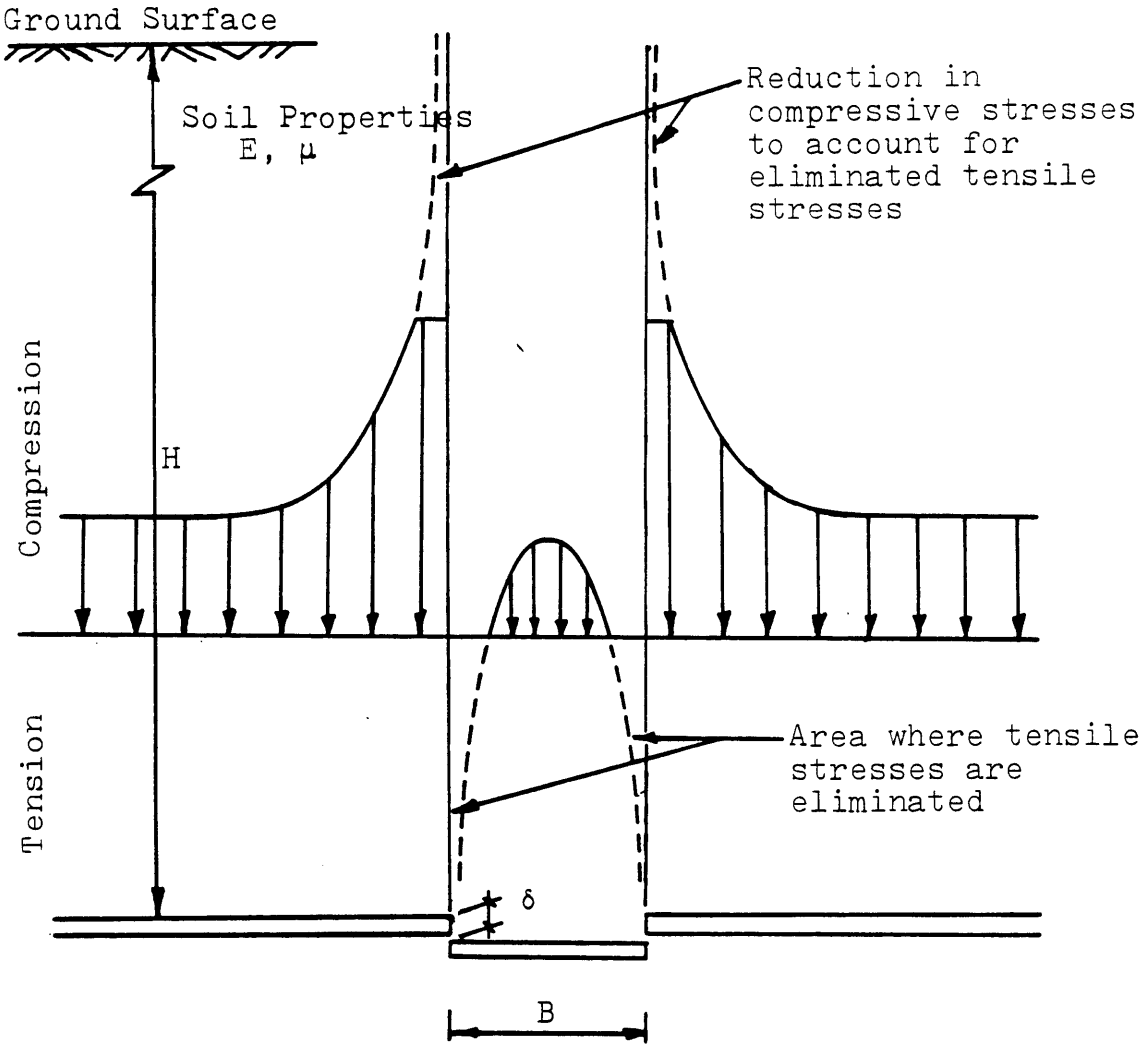

Figure 2.9 Chelapati's Technique for Elimination of Tensile Stresses in Elastic Solution for Arching

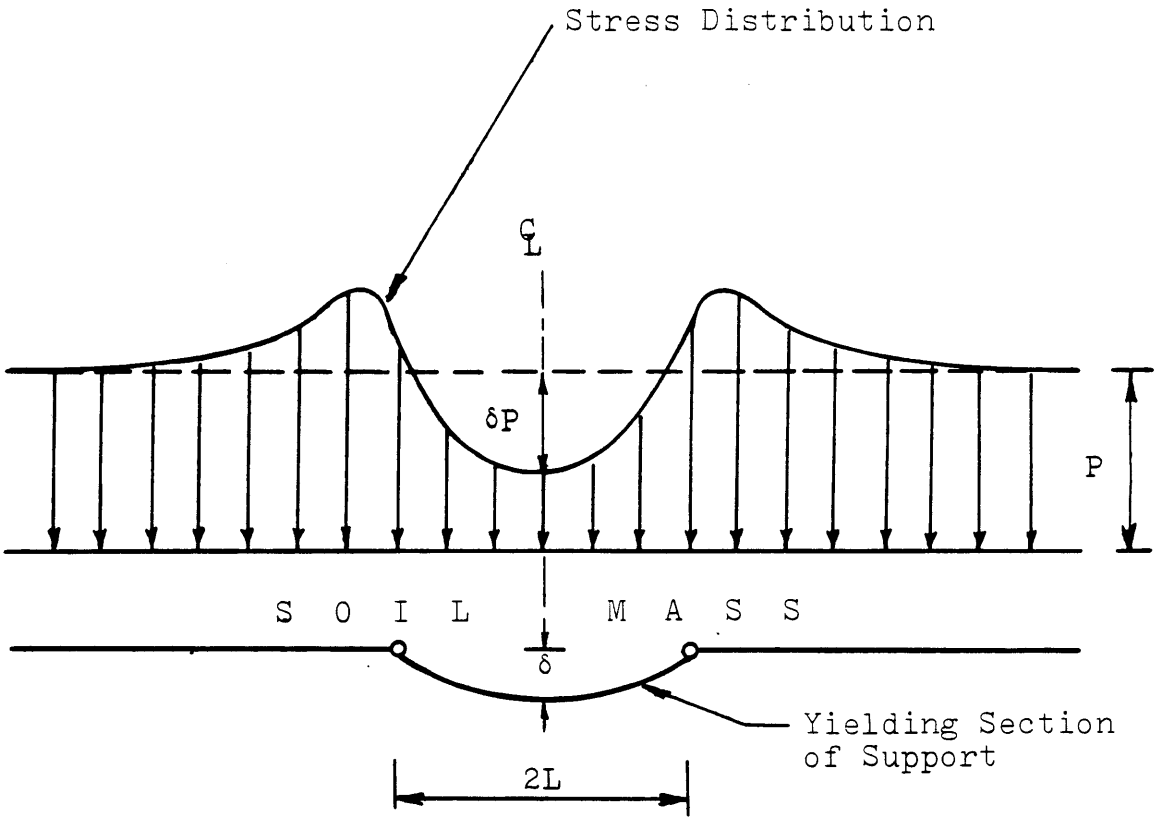

Figure 2.10 Stress Change at Center of Yielding Section (after Bjerrum, et.al, 1972)

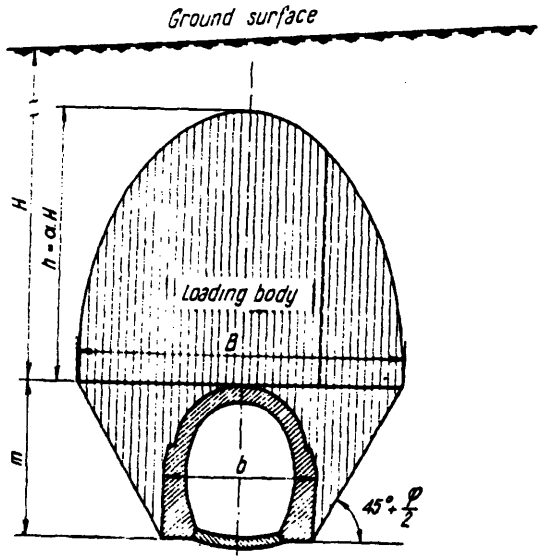

$$\alpha_1 = 1 - \frac{\tan\phi \cdot \tan^2(45° - \phi/2)H}{b + 2m \cdot \tan(45° - \phi/2)},$$

Total Force on Tunnel = $\gamma BH\alpha_1$

Figure 2.11 Empirical Approach to Determination of Forces on a Tunnel Lining (from Szechy, 1966)

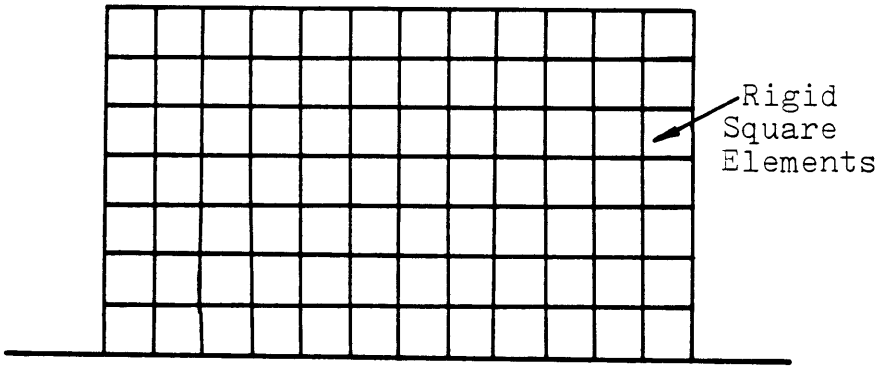

A. Initial Configuration

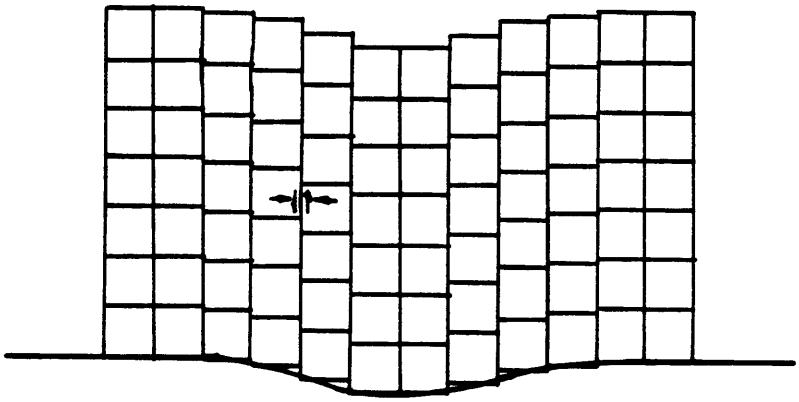

B. Following Yielding of Structure

Figure 2.12 Truesdale and Vey Analytical Model

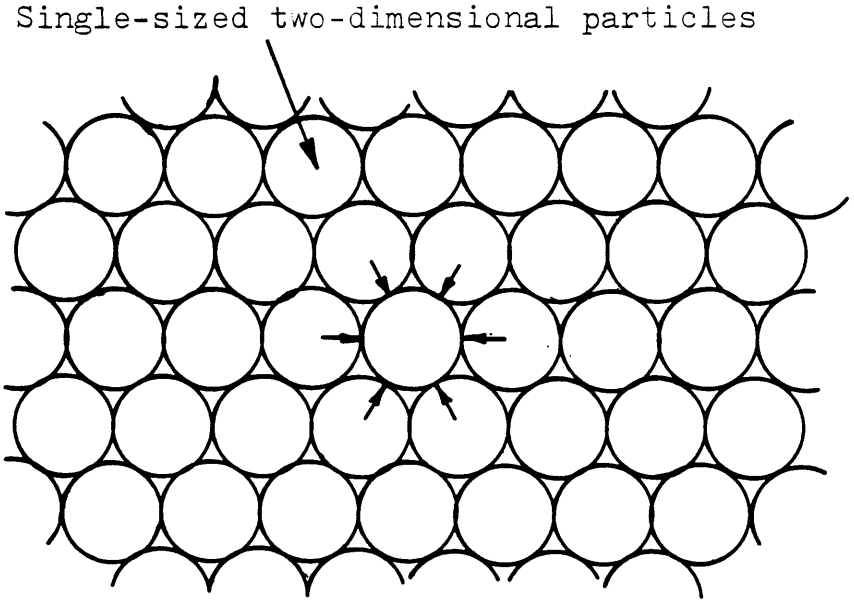

Figure 2.13 Model for Systematic Arching Theory
(after Trollope, 1957)

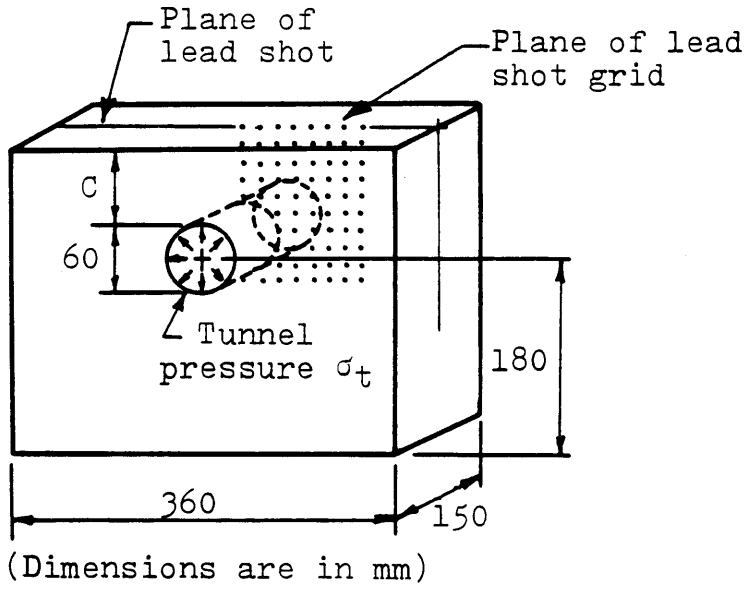

Figure 2.14 Model of Soft Ground Tunnel (from Atkinson et. al., 1977)

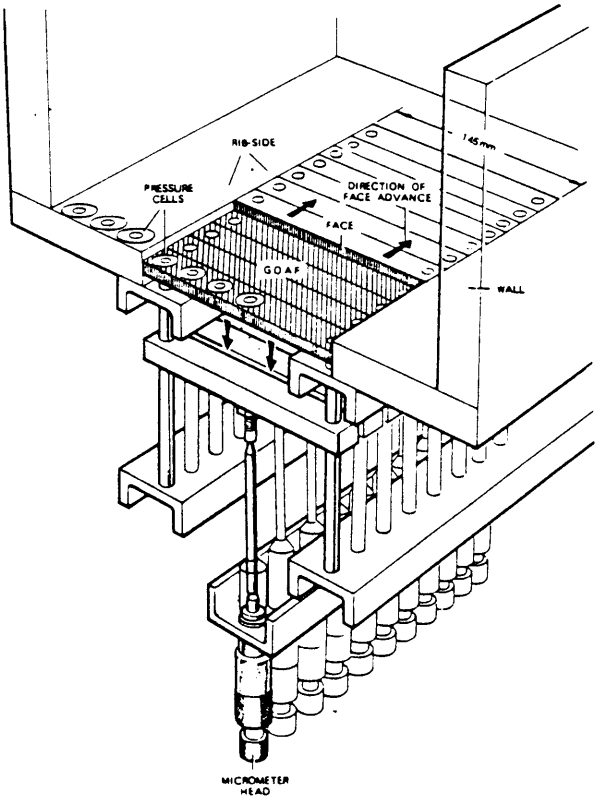

A. Apparatus

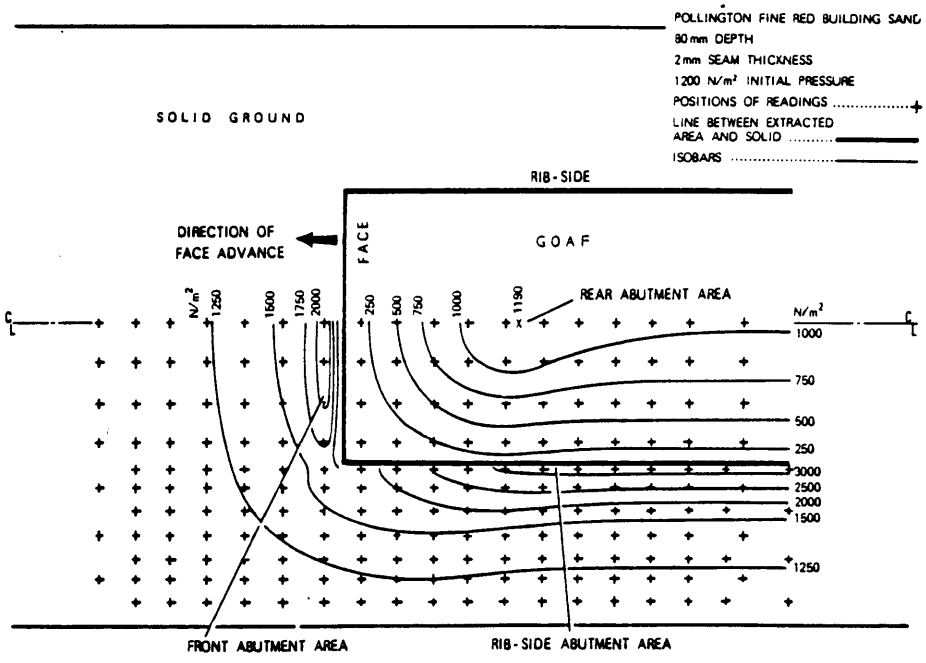

B. Vertical Stress Distribution

Figure 2.15 Harris' Experimental Investigation of Longwall Coal Mining

CHAPTER 3: APPROACH TO TRAP DOOR PROBLEM USING PLASTICITY THEORY

3.1 Introduction

Previous investigations have taken a number of approaches in formulating solutions to the problem of a translating trap door within a granular medium. Visual observations and pressure measurements clearly show that many of these approaches are not mechanistically correct. For example, the soil does not behave elastically, nor does it shear along vertical planes progressing from the trap door edges. Also, vertical stresses do not remain uniform across horizontal surfaces within the deforming zones. Assumptions such as these are commonly inserted to render the problem determinant; however, they introduce varying degrees of error into resulting solutions.

The author believes a more appropriate approach, one which closely resembles observed behavior in laboratory tests, is provided by plasticity theory. This chapter presents some basic fundamentals from plasticity theory which are necessary for formulating an approach to the trap door problem. It then goes on to derive solutions for the active (lowering trap door) and passive (rising trap door) cases. A more thorough treatment of plasticity theory can be found in Davis (1968), Lee and Herington (1974), or Lee (1975). Much of the material in the following sections is drawn from these references.

3.2 General Considerations

3.2.1 Idealized Model

Figure 3.1 shows the idealized model for this analysis. The soil is represented by a frictional granular material which is cohesionless, isotropic, and homogeneous. A layer of this material with finite thickness (H) and unlimited lateral extent rests on a base containing a trap door. This door, which may be raised or lowered, has width B and an infinite length perpendicular to the plane of the figure. This allows

for strains to only develop in the plane of Figure 3.1 when the trap door moves.

The assumption of plane strain is consistent with the testing procedures used by the author to observe development and locations of failure zones within the soil. It also readily permits one to apply two-dimensional plasticity theory. General extension of the results of this analysis to three-dimensional arching is discussed in Section 3.7.

3.2.2 Development of Elastic and Plastic Zones

As the trap door translates, equilibrium conditions and strain-displacement relationships must be satisfied throughout the deforming soil mass. In addition, any point within the mass will either be in an elastic or plastic state depending upon whether the strength of the material is exceeded along any plane through the point. By defining boundary conditions and constructing stress characteristics (as described in Section 3.3) one can locate the elastic and plastic zones within the mass. Traditional stress-strain equations from elasticity theory govern the soil's behavior in elastic zones, while the failure criteria and plastic flow rules define the behavior within plastic zones.

3.2.3 Failure Criterion

A number of failure criteria exist for granular materials. The most widely known and the one used here is that attributed to Coulomb for a c, ϕ material. Using this criterion and assuming a linear envelope with no cohesion (as shown in Figure 3.2) one defines upper limits for the relative magnitudes of shear and normal stresses which can exist at any point within the soil, as well as defining the onset of plastic behavior within the material. One should note at this juncture that planes whose stress states fall on the envelope must be located at angles of $\pm(45^{\circ} - \phi/2)$ to the major principal stress direction. This will be important to the construction of stress characteristics in Section 3.3.

3.2.4 Dilation

Granular material exhibits a volume increase, or dilation (against the confining stresses) during deformation. Typically granular soil will behave as a strain softening material as shown in an idealized form in Figure 3.3. The rate of dilation is high in the early stages of failure and gradually decreases as further yielding occurs. Eventually the material's volume becomes constant at a value corresponding to its critical state, or constant volume, void ratio.

The level of dilation will vary among different soils, as well as between samples of the same soil depending upon material properties and boundary conditions. The total magnitude will increase with increasing initial density, particle angularity, and uniformity as well as decreasing levels of normal stress and porosity (Rowe, 1962 and Mitchell, 1976).

Dilation is non-recoverable deformation and is therefore a manifestation of plastic behavior. In the context of plasticity theory, dilation can be defined as "the plastic volumetric strain increment ($\delta\epsilon_{vol}^{plastic}$) resulting from a given plastic shear strain increment ($\delta\epsilon_{shear}^{plastic}$)" (Roberds and Einstein, 1977). A mathematical expression relating these two strain increments is called a Plastic Flow Rule and is the subject of the next section.

3.2.5 Plastic Flow Rule

The purpose of this section is not to develop a plastic flow rule for granular soils, nor is it to comment on the correctness of any of the flow rules previously presented by others. Its purpose is rather to show what a flow rule represents, and to introduce a variable (called Angle of Dilation) which is commonly part of a flow rule expression and is important to the formulations contained in the remainder of this chapter. A detailed treatment of flow rules and the associated mathematics can be found in Davis (1968), Lee (1975), or Roberds and Einstein (1977).

Restating from the previous section, a flow rule can be

expressed as:

$$\text{Plastic Flow Rule} = \frac{(\delta \epsilon_{vol}^{plastic})}{(\delta \epsilon_{shear}^{plastic})} \qquad (3.1)$$

The flow rule therefore forms vectors in the $\delta \epsilon_{vol}^{plastic}$ - $\delta \epsilon_{shear}^{plastic}$ space. Three such vectors are shown in Figure 3.4. Also shown in this figure is a 'plastic potential' which is a line defined as being perpendicular to all plastic strain increment vectors. In addition, the variable, 'angle of dilation" (ν), is presented in Figure 3.4. This is simply the angle of the plastic potential with respect to the horizontal. Consequently, ν also defines the direction of the plastic strain increment vector and is therefore a convenient variable to use for expressing a flow rule. One can see that when $\nu > 0^{o}$ the material will expand (dilate) while for $\nu = 0^{o}$ no volume change occurs.

Atkinson and Potts (1975) show that ν must always be equal to or less than ϕ in order for the rate of plastic work to everywhere be zero or positive. For the case of $\nu = \phi$ the plastic potential (in $\delta \epsilon_{vol}^{plastic}$ - $\delta \epsilon_{shear}^{plastic}$ space) will be shaped identical to the failure surface (in σ - τ space) and therefore, the ratio of plastic strain increments (plastic deformation behavior) is defined by the failure criterion. This is called an 'Associated Flow Rule' and is an assumption commonly made. It is advantageous because it greatly simplifies the mathematics of the problem and, in addition, if one follows the approach set down by Drucker and Prager in work they did during the 1950's, it is possible to establish upper and lower bound solutions for some problems not having a closed form solution (Davis, 1968).

When the angle of dilation (ν) assumes values other than ϕ, a 'Non-associated Flow Rule' exists and the plastic potential is independent of the failure criterion. Problems with non-associated flow rules do not lend themselves to rigorous solution through plasticity theory, but may still be solved in a general form using fundamental principles of the theory.

Considerable theoretical work has been performed in the last decade aimed at developing the mathematics to solve non-associated flow rule problems. A list of references may be found in Anand (1983).

The literature contains little information as to appropriate values of ν for various problems. Davis (1968) found peak ν for a dense sand to be 17^{o}, but does not give details of the tests involved. Bransby and Blair-Fish (1975) performed silo type tests and obtained values up to 26^{o} and 35^{o} depending on the technique used to analyze results. For model tunnel tests in dense sand at low stress levels Atkinson, et.al. (1975) reference results indicating that initial values of ν attain magnitudes near ϕ.

From observations by others, combined with the author's own results, it may be concluded that dense sand possesses a non-associated flow rule with peak values of ν occurring at the onset of plastic behavior, and values steadily decreasing as the strain softening discussed in Section 3.2.4 develops. For the purposes of analysis a varying flow rule with the dilation angle essentially equal to ϕ initially and decreasing thereafter until $\nu = 0^{o}$, at large deformations, will be assumed. The special case of $\nu = 0^{o}$ applies when deformations are large and one assumes the material has reached its critical state (i.e. the rate of plastic volumetric strain equals zero).

A major element lacking in this representation is a method for relating the value of ν at any particular point, as the trap door is translating, to the displacement of the door at that instance. A theoretical approach to this could not be found in the literature; however, some observations made by the author at various stages during translation do provide approximate values of ν. It is felt that it is important to present these results here, however they will be restated and summarized in Chapter 6. Figure 3.5 and Table 3.1 present these values for a downward translating trap door (active arching) plotted against the normalized trap door displacement. Figure 3.6 and Table 3.2 give limited results for

an upward translating door (passive arching). Section 3.4.3 includes justification for relating the angle of dilation (ν) to the angle (α) at which discontinuities form.

3.3 Plastic Stress Fields and Stress Characteristics

As previously mentioned, the Coulomb expression defines two directions, located at $\pm(45^\circ - \phi/2)$ to the major principal stress at a point, along which the failure criterion is satisfied. These directions may vary between points within the stress field due to variations in the direction of major principal stress; however, these directions for all points form the loci of two families of curves, sometimes called α and β lines. These curves always intersect at $(90^\circ \pm \phi)$ and are termed stress characteristics. Figure 3.7 shows the development of α and β lines for a particular point from knowledge of the major principal stress direction.

For problems with simple geometry the stress characteristics can be constructed graphically from knowledge of the boundary conditions much as one constructs flow nets for seepage problems. A simple example is found in Figure 3.8. If the soil is loaded with σ_1 vertical the characteristics are those indicated. The solution to this problem is quite simple if boundary and large strain effects are neglected, leaving the σ_1 direction constant within the material. In zones of varying principal stress directions the characteristics will no longer be straight lines, but will assume the shape of logarithmic spirals. Characteristics must always be smooth continuous curves without breaks or sharp inflections. Where complicated stress states and boundary conditions exist, determination of characteristics requires incorporation of iterative numerical methods. Information on these may be found in Lee (1975).

Once the stress characteristics for a particular problem are located, one can determine the orientation of principal stresses at any point and how they vary across the plastic field.

It is important to keep in mind that stress characteristics are obtained without consideration of plastic flow and are, as the name implies, concerned with stress distribution. They should not be considered as slip lines for plastic flow.

3.4 Velocity Fields in Plastic Regions

3.4.1 Velocity and Strain Rates

Granular soils will generally exhibit behavior which is independent of time. Reactions to changes in boundary conditions will be instantaneous. Classical plasticity theory does not contain this assumption and the terms velocities and strain rates are used rather than displacements and strains respectively. For this discussion the convention of plasticity theory is adopted.

3.4.2 Velocity Characteristics

Through a procedure analogous to the construction of stress characteristics, one can determine velocity characteristics for a given problem. These are curves along which there is no extension during plastic flow. Their location is defined by the plastic flow rule as they are located at $\pm(45^\circ - \nu/2)$ to the direction of the major principal strain rate.

Incorporating the assumption that major principal strain rate direction is coincident with that for major principal stress, and returning to Figure 3.8, one sees that for an associated flow rule material ($\nu = \phi$) velocity and stress characteristics are identical. At the other extreme, with a no volume change material ($\nu = 0^\circ$), velocity characteristics are orthogonal to each other and at 45° to the principal stress direction. Intermediate values of ν give intermediate locations for the characteristics.

The normal procedure for deriving velocity characteristics is first to construct stress characteristics based on known boundary conditions and necessary assumptions. From these, one can obtain a complete pattern of velocity characteristics; starting at boundaries with known velocity conditions and

seeing that at all locations they intersect stress characteristics at $(\phi - \nu)/2$.

3.4.3 Discontinuities in Velocity

While a material is deforming it is common for discontinuities to develop within the velocity field with an associated velocity jump across each discontinuity. The terms 'slip lines' or 'slip planes', when used in soil mechanics, usually refer to these discontinuities because of the observed displacement or slip.

A discontinuity must, in fact, be a velocity characteristic and the direction of the change (jump) in velocity between the soil on either side of the discontinuity must be at the dilation angle (ν) to the plane of the discontinuity. Therefore, if one knows the velocity characteristics for a problem, the value of ν at a given displacement, and an anticipated direction for velocity change (jump) between two regions of soil, the location of the characteristic along which separation is likely to occur may be surmised. This is a major premise of the solution for the trap door problem contained in the remainder of this chapter. It also provides justification for the use, in Section 3.2.5, of slip lines experimentally observed as a tool in determining the approximate magnitude of ν and how it varies with displacement (Figures 3.5 and 3.6).

The Coulomb failure criterion is satisfied along stress characteristics, but not velocity characteristics. With the Mohr circle in Figure 3.9 one can show that the expression relating normal stress (σ_{nc}) to shear stress (τ_c) along velocity characteristics is:

$$\tau_c = \sigma_{nc} \left(\frac{\cos\nu \sin\phi}{1 - \sin\nu \sin\phi}\right) \qquad (3.2)$$

For the associated flow rule ($\nu = \phi$) this reduces to the more common Coulomb expression (with $c = 0$):

$$\tau_c = \sigma_{nc} \tan\phi \qquad (3.3)$$

This is as would be expected, since in this case stress and

velocity characteristics coincide.

3.5 Active Arching Over Trap Door

3.5.1 General

Returning to the idealized model in Figure 3.1, an active arching condition, characterized by reduced vertical stresses on the trap door, will be mobilized when the door translates downward with respect to the unyielding surrounding surface. The geometry of the problem requires the behavior to be symmetrical about the centerline of the door; therefore, for both active and passive cases, figures will only show stresses and velocities for the right half of the problem.

3.5.2 Observed Soil Behavior

Figure 3.10 and photographs A.7 - A.10 in Appendix A present the general behavior observed during active arching. A triangular shaped zone above the door expands vertically with noticeable dilation present. There is some lateral contraction, but it is largely compensated for by dilation. Stress measurements indicate that the major principal stress directly above the door is approximately horizontal.

Areas of soil on either side of the trap door act much as abutments, receiving stress transferred from the door itself. These zones undergo vertical contraction with some lateral expansion toward the door. The major principal stress is vertical.

3.5.3 Stress Characteristics

From the orientation of σ_1 above the trap door and side abutments, the stress characteristics shown in Figure 3.11.A were constructed. By analogy to traditional earth pressure theory an active stress state exists over the trap door (zone A in Figure 3.11.A) with passive zones at each edge (zone B) and transitional fields (zone C) connecting the two. Figure 3.12 gives the directions of major principal stress throughout the plastic field, which were derived from the stress characteristics.

3.5.4 Velocity Characteristics

By incorporating the flow rule developed in Section 3.2.5, velocity characteristics can be obtained from the stress characteristics. With ν initially equal to ϕ the velocity and stress characteristics are identical (Figure 3.11.A). As ν decreases, characteristics of velocity different than those for stress occur, with representative ones depicted in Figure 3.11.B (for $\nu = 20^{\circ}$). Once the constant volume condition ($\nu = 0^{\circ}$) is reached the characteristics achieve the configuration of Figure 3.13.

Imposing the condition that discontinuities develop in the soil at ν to the direction of velocity jump, surfaces of separation can now be obtained. From the insert in Figure 3.11.A one sees that the soil directly over the trap door moves downward with respect to that adjacent to the door (i.e. has a different velocity). This creates a vertical jump in velocity at the trap door's edges, requiring a velocity discontinuity to form as shown. Since a discontinuity is also a characteristic, it must be linear for compatibility with the characteristic field. By the symmetry of the problem a triangular prism develops above the door with sides inclined at ν to the vertical. This forms the free body found in Figure 3.14.A.

3.5.5 Force on Trap Door When $\nu = \phi$

The simplest solution for the free body occurs when $\nu = \phi$. This reduces the expression relating stresses along velocity characteristics (Section 3.4.3) to: $\tau = \sigma_n \tan\phi$ (3.4)
From Figure 3.14.A one can see that vertical components of shear (T) and normal (N) forces acting upon the edges of each differential element will be equal and opposite in magnitude, contributing no net vertical force. The force on the trap door will therefore only be the weight of material within the free body, yielding:

$$F = \gamma B^2/4\tan\nu \qquad \text{for } B/H \leq 2\tan\nu \qquad (3.5)$$

and $$F = \gamma BH\,(1 - (H/B)\tan\nu) \qquad \text{for } B/H > 2\tan\nu \qquad (3.6)$$

where F is force per unit length perpendicular to plane of

Figure 3.14.

3.5.6 Force on Trap Door When $0^o < \nu < \phi$

For the transitional case of ν, a free body diagram with trapezoidally shaped differential elements, as shown in Figure 3.14.A, can be constructed, but a solution is not readily apparent. For this case the stresses on the elements' side boundaries are related by the long form of the expression in Section 3.4.3; however, even if solution for the free body were possible it is not known what value for normal stress to use at these boundaries.

It may, however, be concluded that values of force on the trap door for $0^o < \nu < \phi$ lie within the limits set by $\nu = \phi$ in the previous section and $\nu = 0^o$ in the following section.

3.5.7 Force on Trap Door When $\nu = 0^o$

At the limiting case of $\nu = 0^o$ velocity discontinuities are vertical, originating from the trap door edges. The free body diagram (Figure 3.14.B) is identical to that from the silo theory Jaky (1948) with the exception that shear and normal stresses on the boundaries are related by:

$$\tau = \sigma_n \left(\frac{\cos\nu \sin\phi}{1 - \sin\nu \sin\phi}\right) = \sigma_n \sin\phi \qquad (3.7)$$

Again the question as to determination of appropriate values for normal stress on the discontinuities arises. Lacking better information, the commonly used assumption that normal stresses equal horizontal geostatic stresses is adopted. This yields the solution:

$$F = \frac{\gamma B^2}{2K\sin\phi}\left(1 - e^{-2K\frac{H}{B}\sin\phi}\right) \qquad (3.8)$$

Other variables being equal, one obtains values for F about 15 to 25% greater than from the silo theory over a typical range of ϕ values, because of the presence of the term $\sin\phi$ rather than $\tan\phi$ in the expression. The appropriate value of K to use in these equations is the source of much debate. This question is addressed in Chapter 6 when experimental results

are presented.

It is questionable whether shear resistance is mobilized over the entire height of the prism for large H, consequently one could modify this expression using Terzaghi's approach so as to treat soil more than 2B above the door as a surcharge. The resulting equation is:

$$F = \gamma B^2 \left(\frac{1 - e^{-4K\sin\phi}}{2K\sin\phi} + (H/B - 2)\, e^{-4K\sin\phi}\right) \quad (3.9)$$

3.6 Passive Arching Over Trap Door

3.6.1 General

Translating the trap door upward with respect to the unyielding surface in Figure 3.1 yields increased vertical stresses on the door and reduced stresses adjacent. This redistribution results from passive arching. As before, the problem is considered symmetric about the centerline, and much of the information presented in the following sections is analogous to that for the active case previously presented.

3.6.2 Observed Soil Behavior

Figure 3.15 and photographs A.11 and A.12 in Appendix A present the general behavior observed during passive arching. A trapezoidal prism of soil above the door moves upward with some vertical contraction and lateral expansion. Dilation may be observed near the prism's lateral edges. This is analogous to a passive earth pressure zone with σ_1 vertical.

The soil on either side of the trap door is in an active state with σ_1 horizontal. This is characterized by some vertical expansion, lateral contraction, and dilation near the boundaries with the central prism.

3.6.3 Stress Characteristics

From the orientation of major principal stress at the boundaries, presented in the last section, one can construct the stress characteristics for passive arching shown in Figure 3.16.A. The active (A), passive (B), and transitional (C) zones may be seen in this figure. Major principal stress directions throughout the field are depicted in Figure 3.17.

3.6.4 Velocity Characteristics

The initial velocity characteristics for $\nu = \phi$ are identical to stress characteristics in Figure 3.16.A. As angle of dilation decreases these velocity characteristics gradually move. For an intermediate value of ν the corresponding characteristics are presented in Figure 3.16.B. Upon reaching the constant volume state ($\nu = 0^{o}$), velocity characteristics are those previously presented in Figure 3.13 with orthogonal families of curves.

The insert in Figure 3.16.A shows the direction of velocity jump at the trap door edge to be vertical, leading to a discontinuity oriented as shown. The characteristic field requires this discontinuity to be planar and leads to the development of a trapezoidal prism of soil above the door bounded by discontinuities. The sides of the prism are inclined at ν to the vertical, as shown in the resulting free body (Figure 3.18.A). Horizontal forces on this free body are symmetric and, therefore, only vertical forces act on the trap door.

3.6.5 Force on Trap Door When $\nu = \phi$

For the case of $\nu = \phi$, normal and shear stresses along the discontinuities are related by:

$$\tau = \sigma_n \tan\phi \qquad (3.4)$$

As can be seen in Figure 3.18.A, this results in vertical components of shear (T) and normal (N) forces acting upon the edges of each differential element which are equal and opposite in magnitude, contributing no net vertical force. Consequently, the force on the trap door per unit length (F) is simply the weight of the material within the free body or:

$$F = \gamma H (B + H \tan\nu) \qquad (3.10)$$

3.6.6 Force on Trap Door When $0^{o} < \nu < \phi$

The free body diagram for this transitional case is also that shown in Figure 3.18.A. As with the active case, no solution for the force on the trap door is presented, because of a lack of information regarding magnitude of normal stress acting on the discontinuities, and the unavailability of a

solution for F from the free body diagram (Figure 3.18.A).

The true value of force (F) on the trap door for $0^{o}<\nu<\phi$ lies between limits established by the $\nu = 0^{o}$ values.

3.6.7 Force on Trap Door When $\nu = 0^{o}$

The free body diagram for passive arching and $\nu = 0^{o}$ (Figure 3.18.B) corresponds to that for the active case (Figure 3.14.B) except for shear forces (T) acting in the opposite direction along the elements' boundaries. Again shear and normal stresses along these boundaries are related by (Section 3.4.3):

$$\tau = \sigma_{n}\sin\phi \qquad (3.11)$$

If, as with the active case, the assumption of normal stresses on the discontinuities equalling horizontal geostatic values is introduced, the resulting solution will be:

$$F = \frac{\gamma B^{2}}{2K\sin\phi}\left(e^{2K\frac{H}{B}\sin\phi} - 1\right) \qquad (3.12)$$

Values from this equation will be slightly different than those given by the passive equation from the silo theory due to the presence of the term $\sin\phi$ rather than $\tan\phi$ relating shear and normal stresses. Comparitive values from both equations are offerred in Chapter 6 when experimental and theoretical results are presented.

3.7 Three-Dimensional Extension

3.7.1 General

The theory and solutions presented thus far all carry the assumption of plane strain behavior. If one assumes the trap door has infinite length, velocities only occur within planes parallel to that of Figure 3.1. For many real problems the plane strain assumption does not hold.

This section presents approximate solutions for active and passive arching over rectangular and circular trap doors for two limiting cases, $\nu = \phi$ and $\nu = 0^{o}$. For the purposes of these derivations it is assumed that behavior predicted by two-dimensional plasticity theory can be extended to three-dimensional geometries. Observations of the development of

sinks and heaves at the ground surface were made during raising and lowering of circular and rectangular trap doors. They indicate that prisms of soil with cross-sectional geometries similar to those inferred from two-dimensional theory do develop in three dimensions.

3.7.2 Circular Trap Door

The general shape of the free body for a lowering circular trap door is a cone as shown in Figure 3.19. As in the two-dimensional case the force on the door when $\nu = \phi$ is simply the weight of the free body or:

$$F = \frac{\pi B^3 \gamma}{24 \tan\nu} \qquad \text{for } B/H \leq 2\tan\nu \quad (3.13)$$

$$F = \frac{\pi B^3 \gamma}{24 \tan\nu} - \frac{\gamma \pi \tan^2\nu}{3} \left(\frac{B}{2\tan\nu} - H\right)^3 \qquad \text{for } B/H > 2\tan\nu \quad (3.14)$$

As further displacement occurs ν decreases until at the constant volume state ($\nu = 0^\circ$) the free body is a cylinder. This condition is analogous to the three-dimensional active silo problem. Using a solution given by McNulty (1965), which has been modified to incorporate the revised expression between τ and σ_n on discontinuities ($\tau = \sigma_n \sin\phi$), one obtains:

$$F = \frac{\pi \gamma B^3}{16 K \sin\phi} \left(1 - e^{-4K\frac{H}{B}\sin\phi}\right) \qquad (3.15)$$

where F is now total force on the circular trap door. Treating soil more than 2B above the door as a surcharge the equation becomes:

$$F = \frac{\pi \gamma B^3}{4} \left[\frac{\left(1 - e^{-8K\sin\phi}\right)}{4K\sin\phi} + (H/B - 2)\, e^{-8K\sin\phi}\right] \qquad (3.16)$$

Moving now to the passive arching case above the circular trap door, the resulting free body resembles an upside-down truncated cone (Figure 3.20). For $\nu = \phi$ the prisms weight and, therefore, force on the trap door is:

$$F = (1/3)\gamma\pi\tan^2\nu\left(\frac{B}{2\tan\nu} + H\right)^3 - \frac{\pi\gamma B^3}{24\tan\nu} \qquad (3.17)$$

The other limiting case, that of large deformations where $\nu = 0^\circ$, produces a cylindrical free body similar to

that from McNulty (1965) for a passive three-dimensional silo theory. Modifying this approach yields:

$$F = \frac{\pi\gamma B^3}{4}\left[\frac{(e^{8K\sin\phi} - 1)}{4K\sin\phi} + (H/B - 2)\, e^{8K\sin\phi}\right] \qquad (3.19)$$

3.7.3 Rectangular Trap Door

If the orientation of discontinuities in the two-dimensional active arching case is extended to a rectangular shaped trap door, the soil prism bounded by these discontinuities is that found in Figure 3.21. Discontinuities are oriented at ν to the vertical, with L being the longer dimension of the door. For $\nu = \phi$ vertical and horizontal external stresses, as before, do not contribute to the force on the trap door.

$$F = \frac{\gamma B^2}{4\tan\nu}(L - B/3) \qquad \text{for } B/H \leq 2\tan\nu \qquad (3.20)$$

$$F = \gamma\left[BLH - H^2\tan\nu\,(L + B - \tfrac{4}{3}H\tan\nu)\right] \qquad \text{for } B/H > 2\tan\nu \qquad (3.21)$$

In order to obtain a solution for the active $\nu = 0^o$ condition, the free body diagram in Figure 3.22 was constructed. Vertical forces acting on the element of thickness dh are those shown plus an upward acting shear force developed along the boundaries. Solving for the force on the trap door gives:

$$F = \gamma B^2 L^2 \frac{(1 - e^{-2K\sin\phi\,(H(L + B)/BL)}}{2K\sin\phi\,(L + B)} \qquad (3.22)$$

For an upward translating trap door (passive case) the soil prism bounded by discontinuities is shown in Figure 3.23 with a resulting trap door force when $\nu = \phi$ of:

$$F = \gamma[BHL + H^2\tan\nu\,(L + B + \tfrac{4}{3}H\tan\nu)] \qquad (3.23)$$

For the passive case with $\nu = 0^o$ the free body diagram in Figure 3.22 again applies with the shear force equal to that from the active case, but now downward acting. This gives a trap door force of:

$$F = \gamma B^2 L^2 \left[\frac{e^{2K\sin\phi\,(\frac{H(L + B)}{BL})} - 1}{2K\sin\phi\,(B + L)}\right] \qquad (3.24)$$

3.8 Summary and Potential Future Areas of Investigation

This chapter presented an approach to the trap door problem founded on fundamentals of classical plasticity theory and yielding predicted behavior closely resembling that actually observed by this author and others. Solutions presented are not necessarily rigorous, however they do provide insight into what is actually occurring within the soil when a trap door is lowered or raised. In Chapter 6 those solutions derived herein will be compared with experimental results.

This chapter has also helped identify some areas of study requiring further investigation before this approach can be readily applied to actual geotechnical problems. Several of these areas are outlined in the following paragraphs.

An effort to obtain solutions when $0^{o} < \nu < \phi$ would be most beneficial. This involves two major tasks; first, a solution of the free body diagrams (Figures 3.14.A and 3.18.A) is necessary, and second, the magnitude of stress at discontinuities within the soil is required. The orientation of principal stresses at the discontinuity is given by characteristics, but not their magnitude.

Model studies show that once a discontinuity is formed soil will tend to slip along it rather than forming other discontinuities indicated by plasticity theory (photographs A.13 - A.19 in Appendix A). This could have important implications for real problems such as parallel or intersecting tunnels constructed at different times.

In Section 3.4.2 it was assumed that major principal strain rate and major principal stress coincide in direction. This makes the determination of velocity characteristics from stress characteristics possible, an important step in the derivation. This is a common assumption in plasticity theory, whose application to the trap door problem is not certain. Figures 3.24 shows some information on this subject. Figure 3.24.A contains principal stress trajectories, for active arching, obtained from finite element analyses by Getzler, et. al. (1970), while Figure 3.24.B shows direction of major

principal strain rate for model tunnel experiments by Atkinson, et.al. (1977). Even with differing model geometries, the agreement between the directions of major principal stress and major principal strain rate is quite good, as is the agreement with principal stress directions shown in Figure 3.12.

Much of the theory in this chapter assumes plane strain behavior. The literature contains little information on the three-dimensional behavior of particulate matter. This makes it difficult to evaluate the appropriateness of extensions used to formulate solutions for the circular and rectangular trap doors. Consequently, application to more practical three-dimensional problems such as stresses about an underground cavity or an advancing tunnel shield are limited.

Actual problems where arching plays an important role seldom involve a uniformly yielding structure next to an unyielding horizontal surface. Instead, varying levels of ground movement occur all around the structure for reasons like: ground loss during construction, force equilibration between soil and structure, and stress-strain behavior of soil during mobilization of arching. At present, most attempts to incorporate these factors involve empirical rules whereby an equivalent trap door width, different than the actual, is used, or else large safety factors are applied to the results. In Chapter 4 this question of ground movement, particularly around tunnels, is addressed.

Other inherent assumptions requiring further examination include: ϕ being treated as constant throughout deformation, characteristics are constructed without consideration of material self weight within the plastic zone, and soil is given idealized properties.

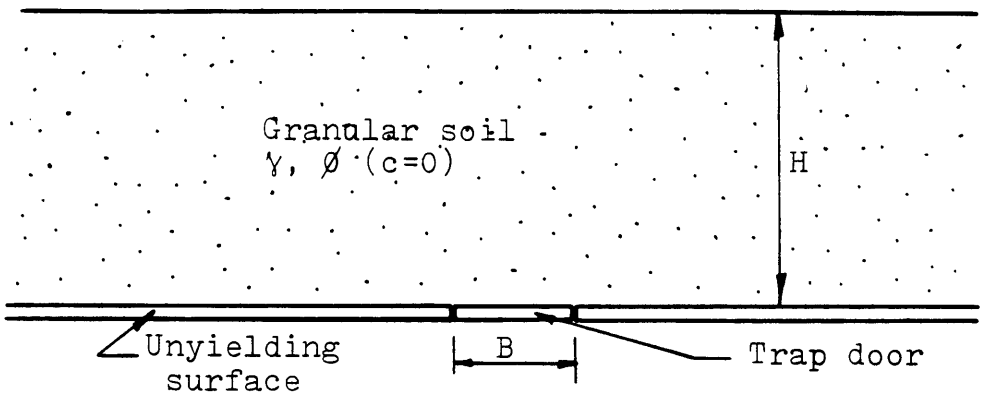

Figure 3.1 Idealized Model

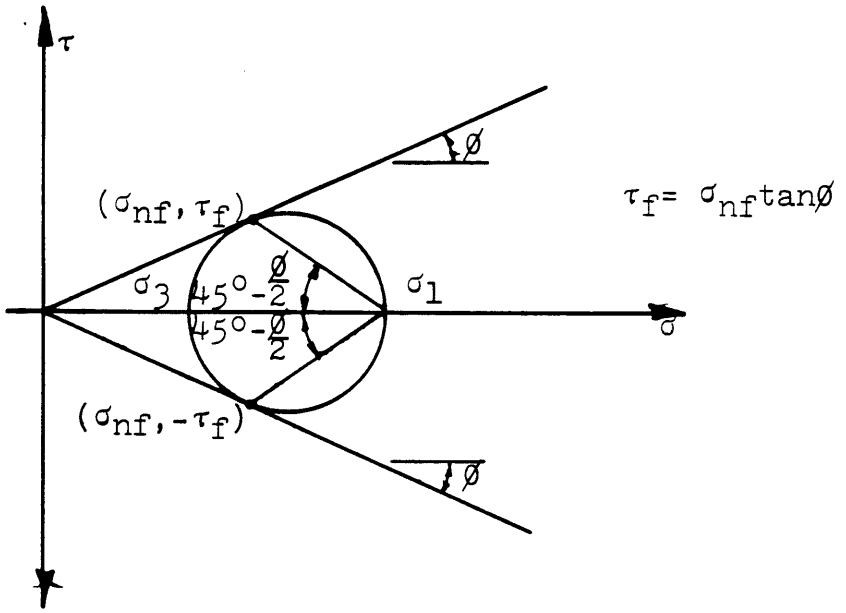

Figure 3.2 Coulomb Failure Criterion

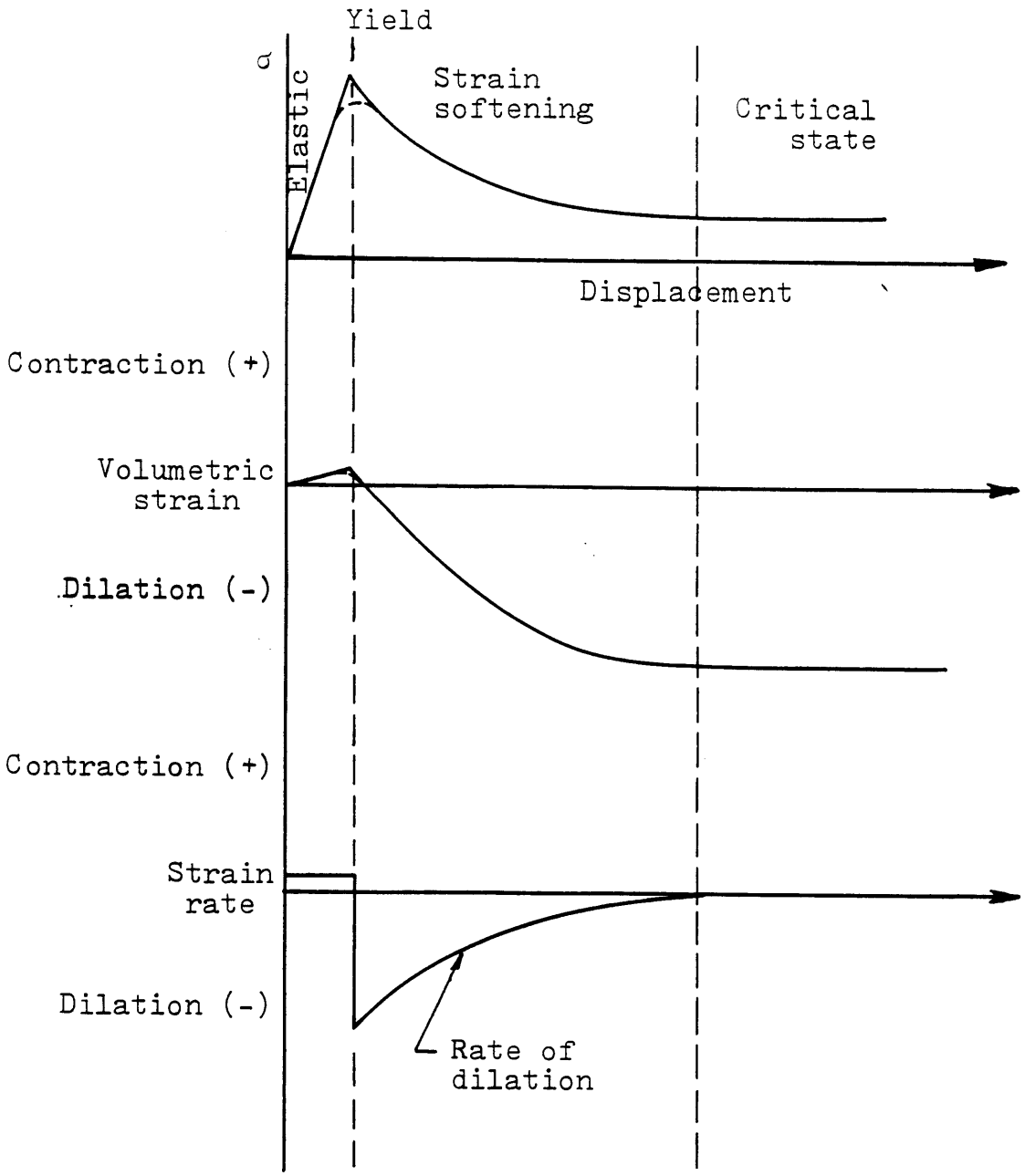

Figure 3.3 Strain Softening Behavior

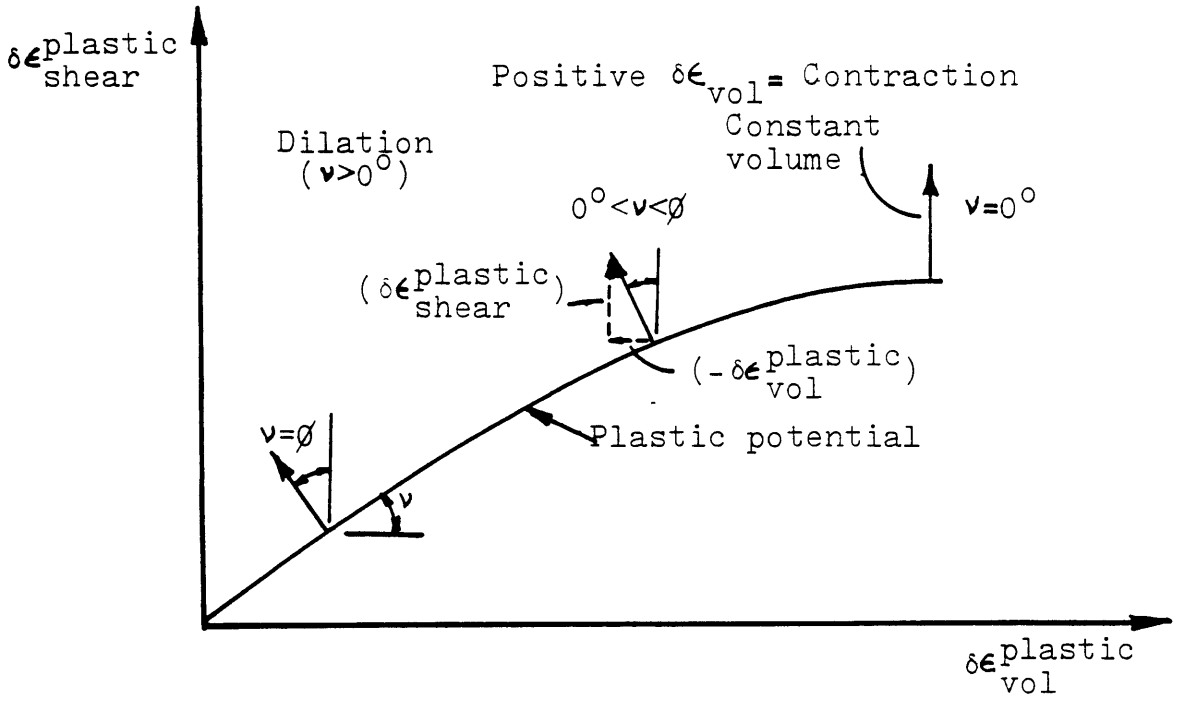

Figure 3.4 Plastic Flow Rule

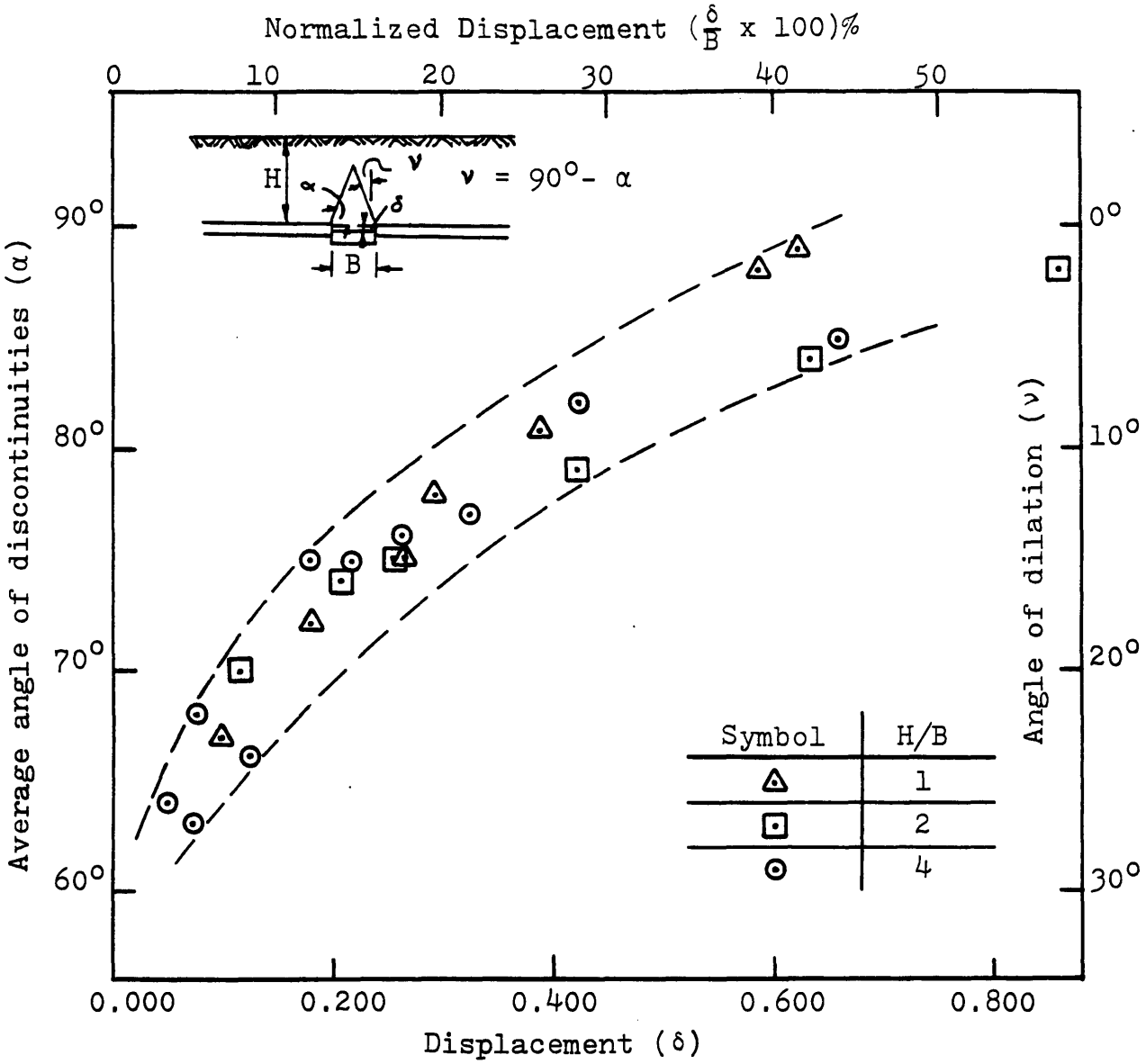

Figure 3.5 Variation of Angle of Dilation with Normalized Displacement for Active Arching Case

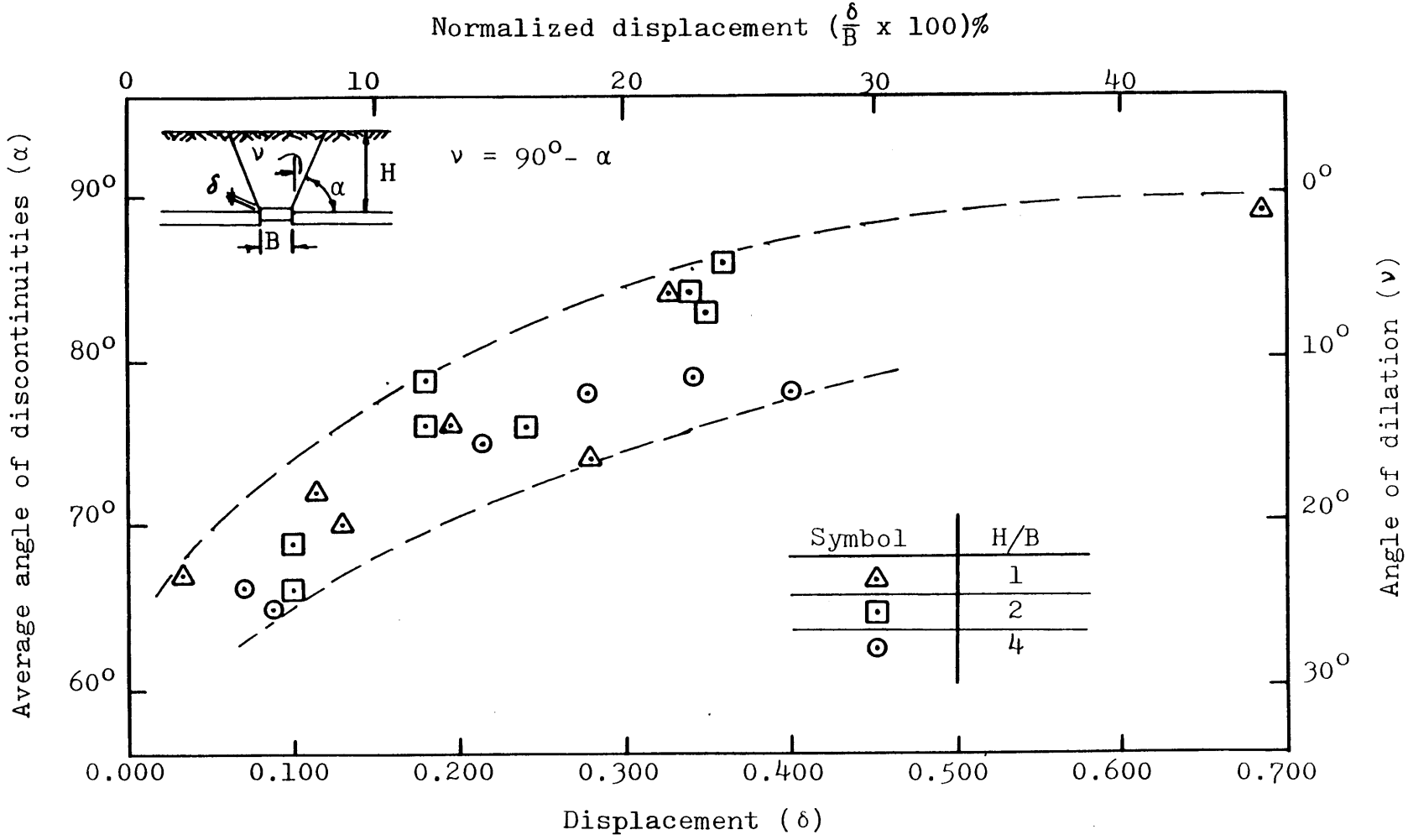

Figure 3.6 Variation of Angle of Dilation with Normalized Displacement for Passive Arching Case

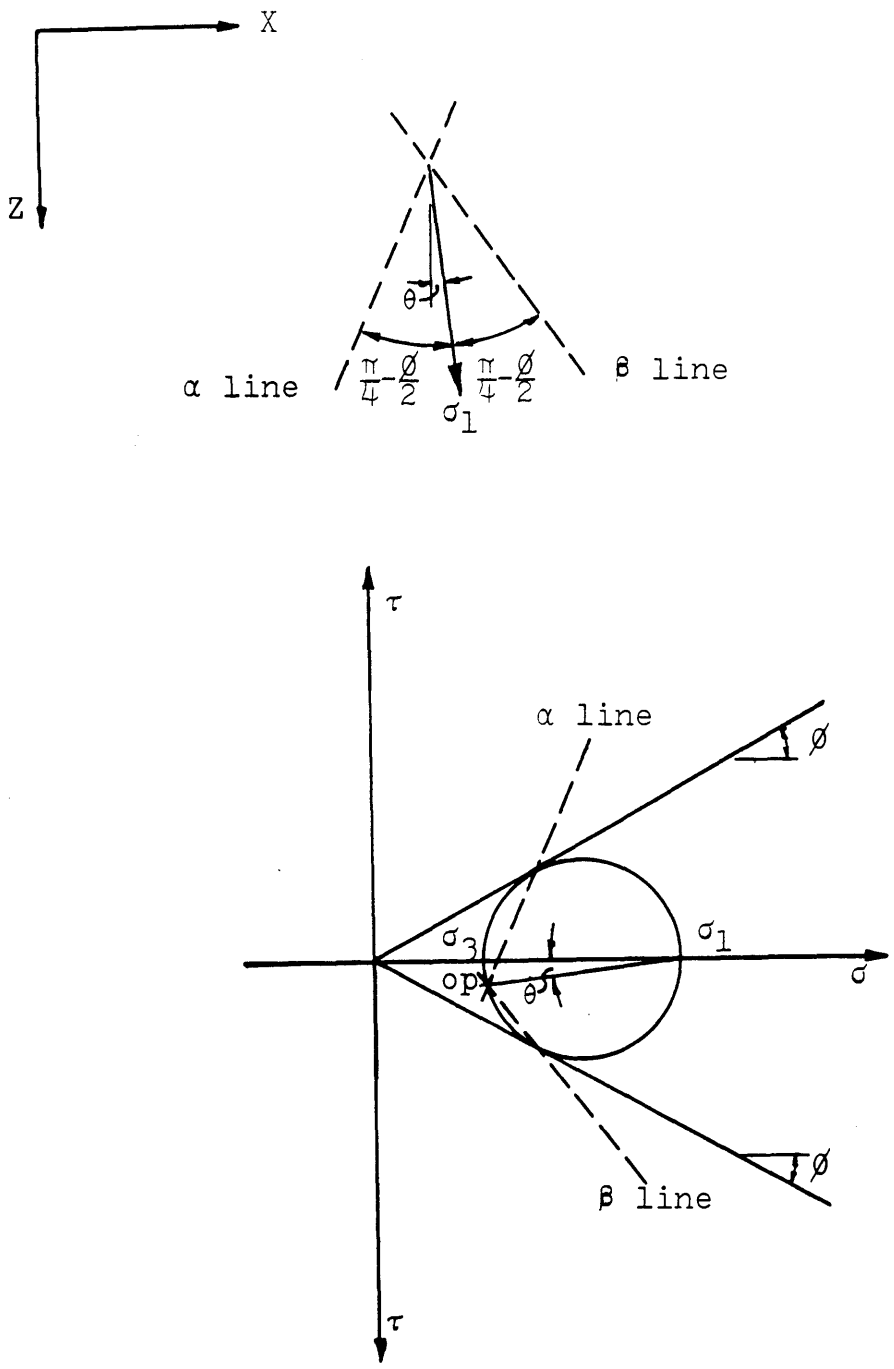

Figure 3.7 Locations of Stress Characteristics

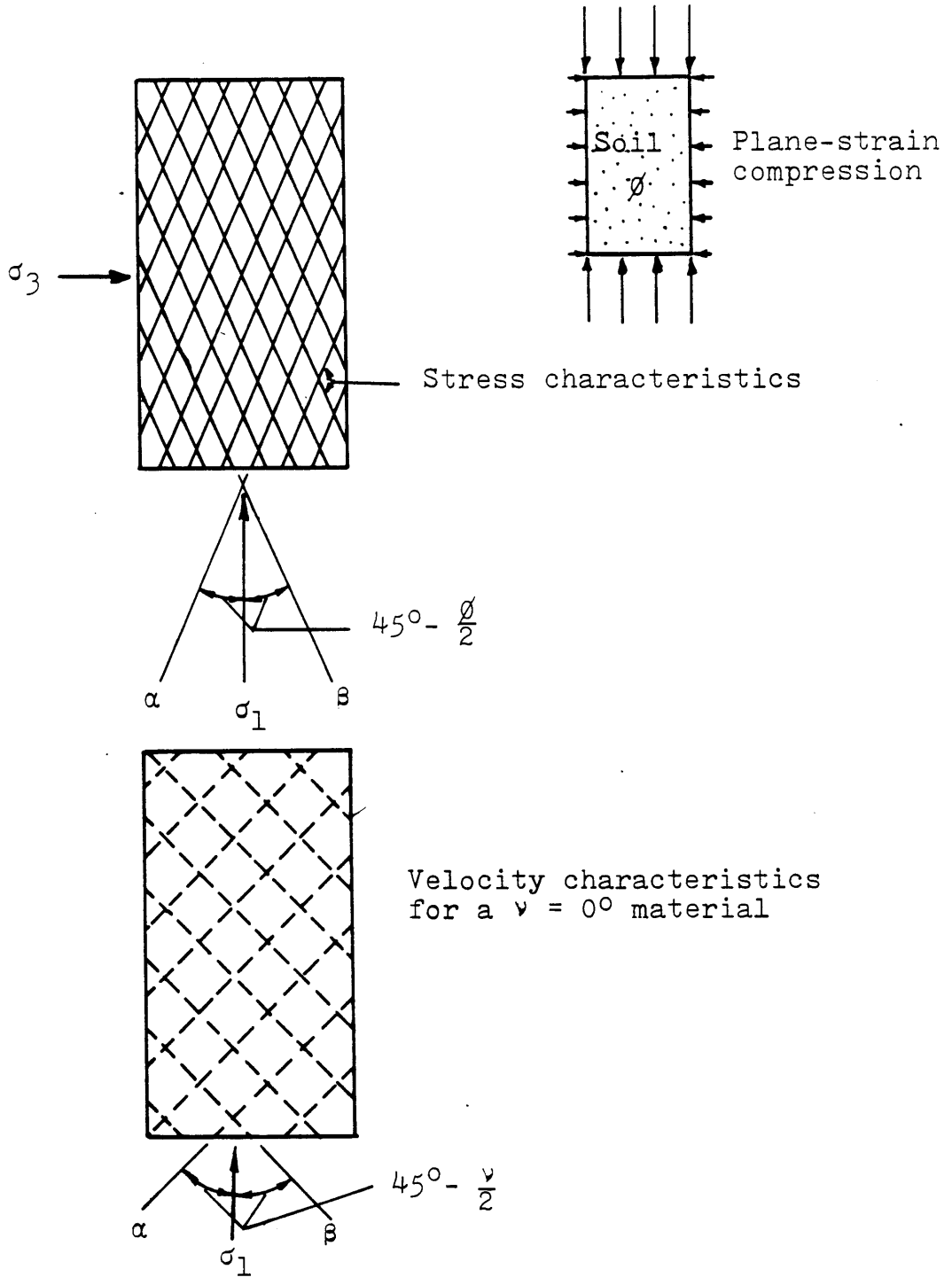

Figure 3.8 Example of Locations for Stress and Velocity Characteristics

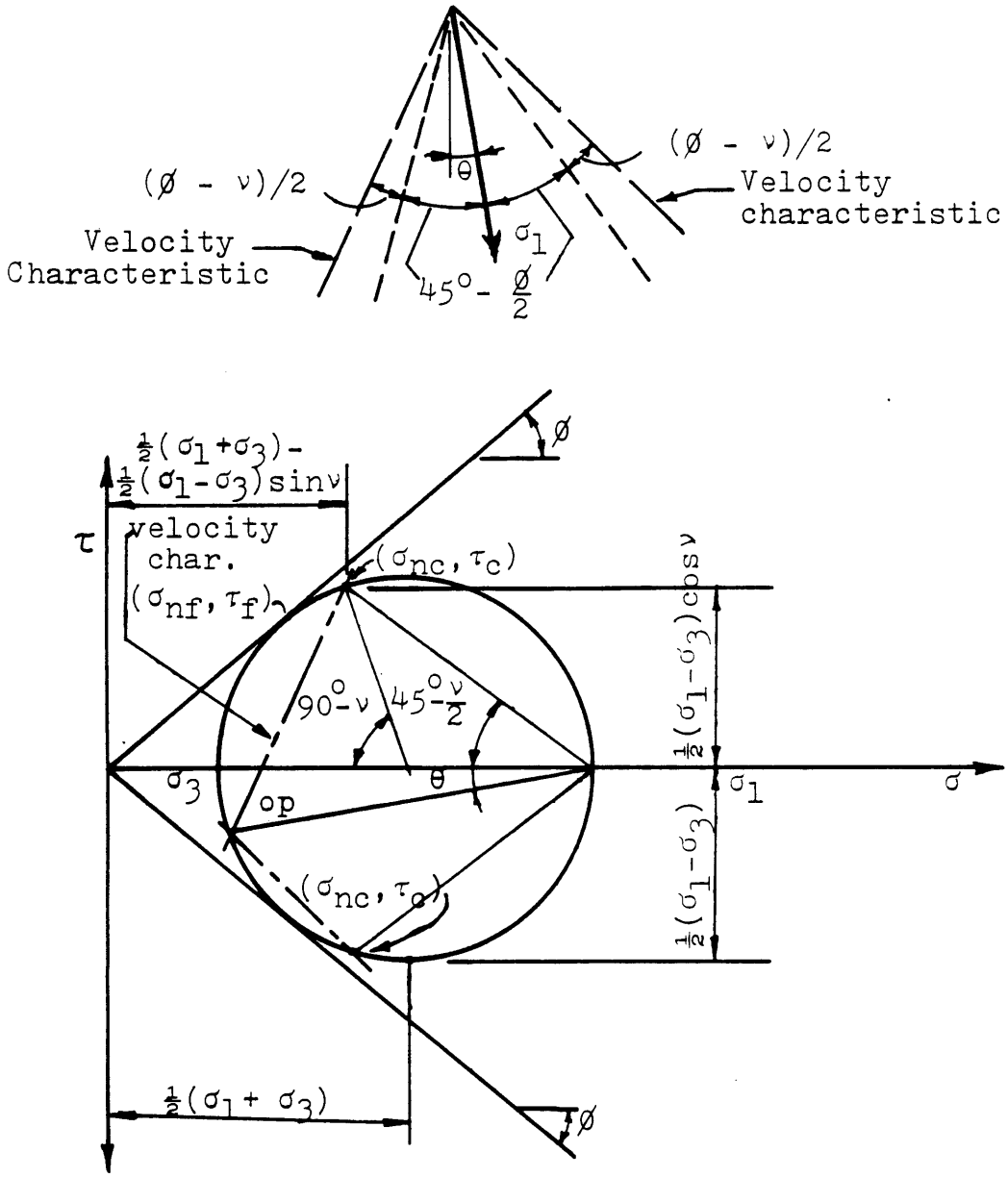

Figure 3.9 Mohr Circle for Stresses on Velocity Characteristics

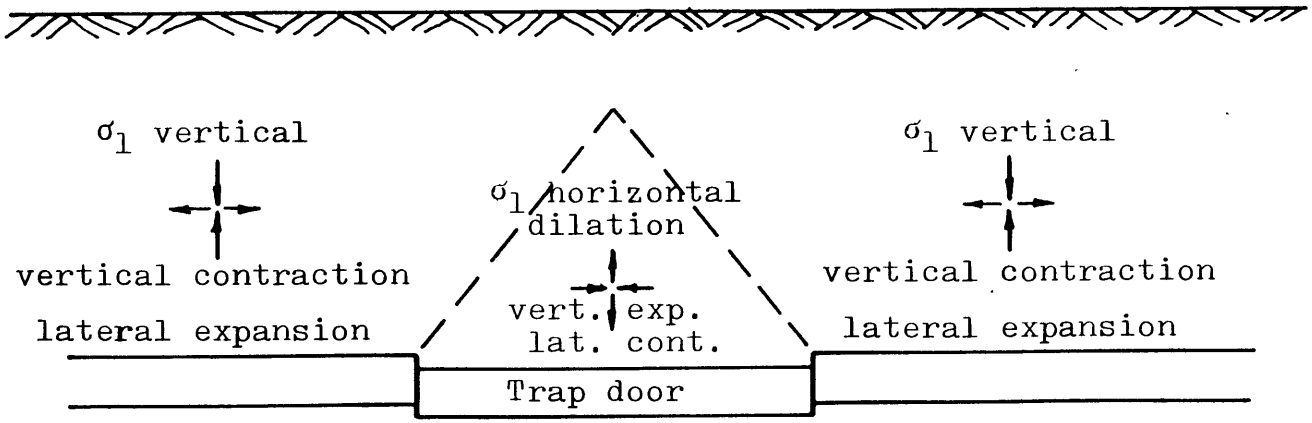

Figure 3.10 General Soil Behavior - Active Arching

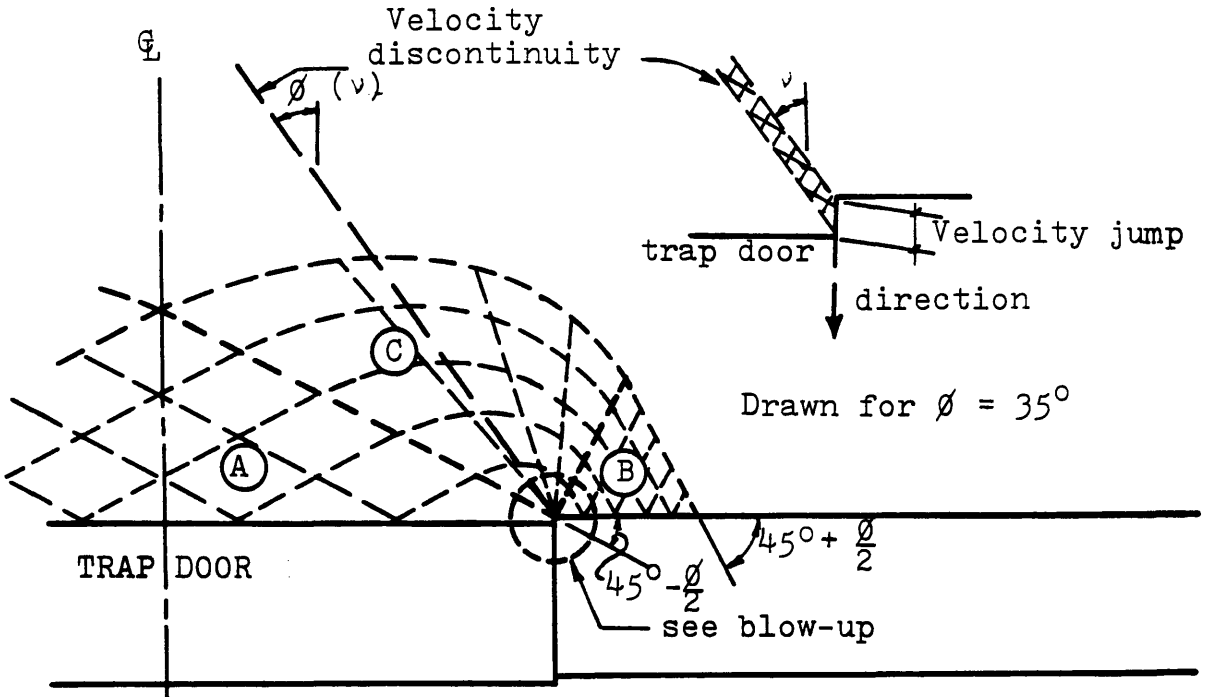

A. Stress Characteristics for Active Arching

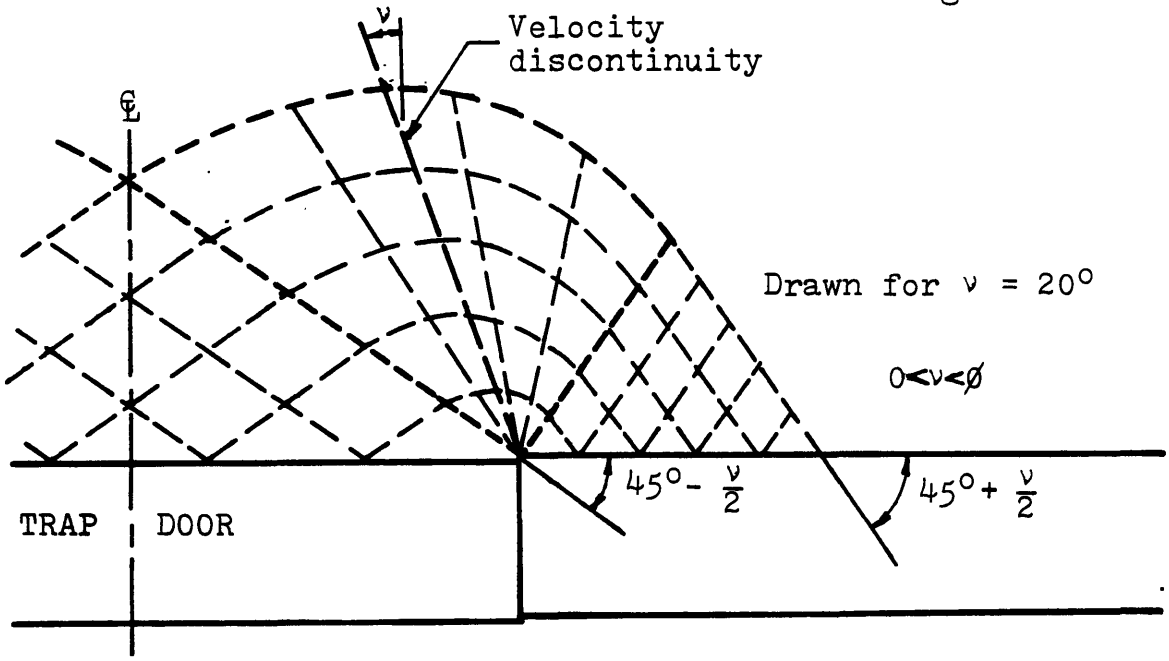

B. Velocity Characteristics for Active Arching

Figure 3.11Characteristics for Active Arching

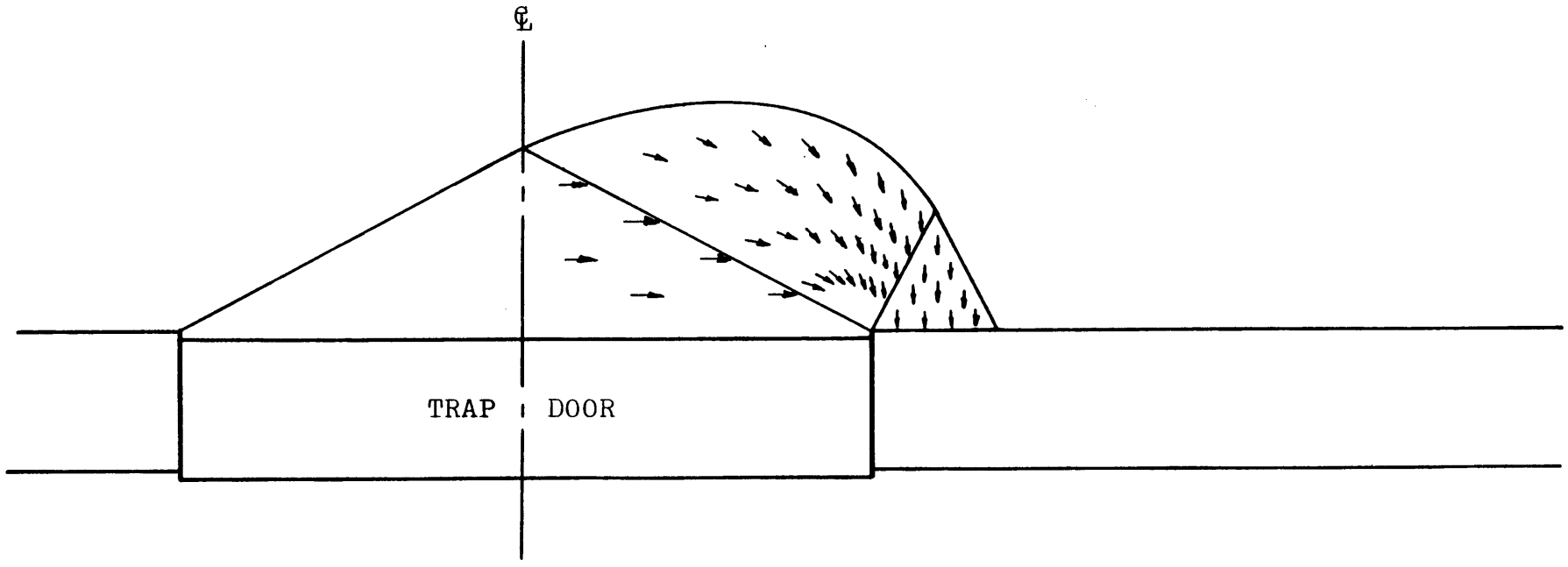

Figure 3.12 Direction of Major Principal Stress - Active Arching

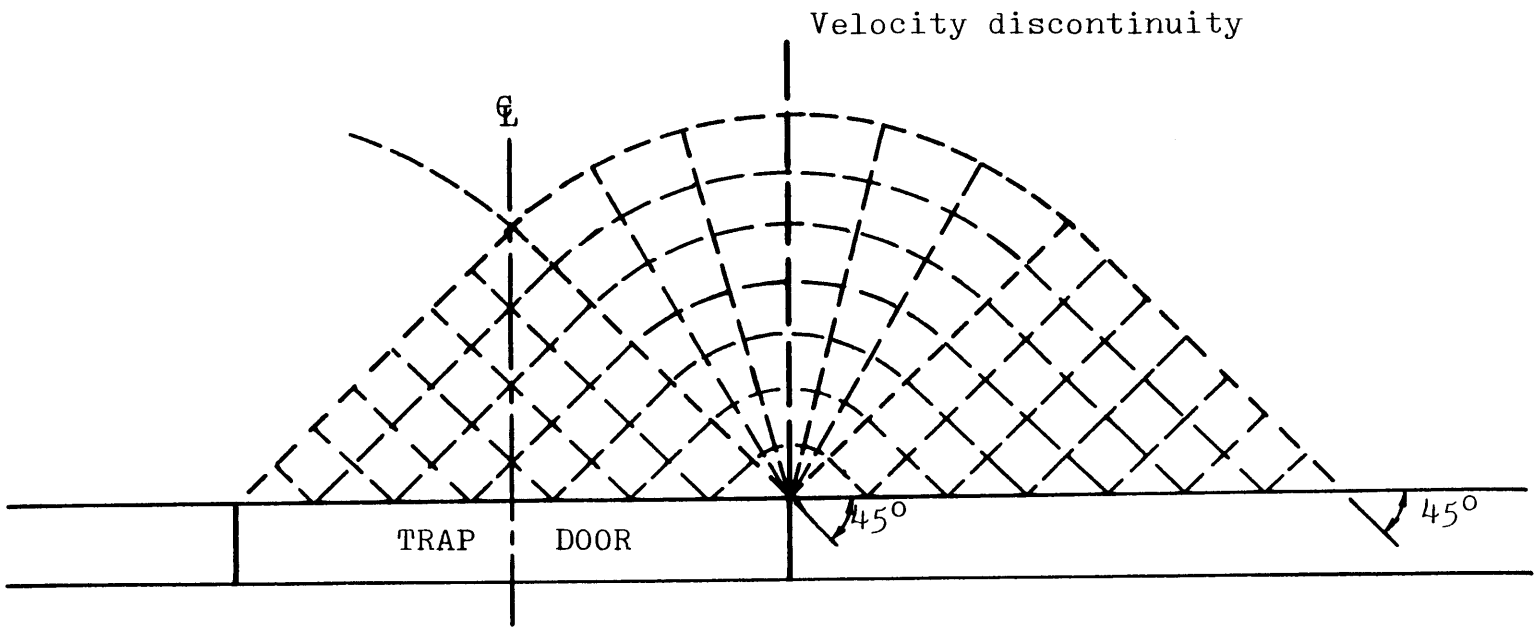

Figure 3.13 Velocity Characteristics and Discontinuities for $\nu = 0^{o}$; Applies for Active and Passive Cases

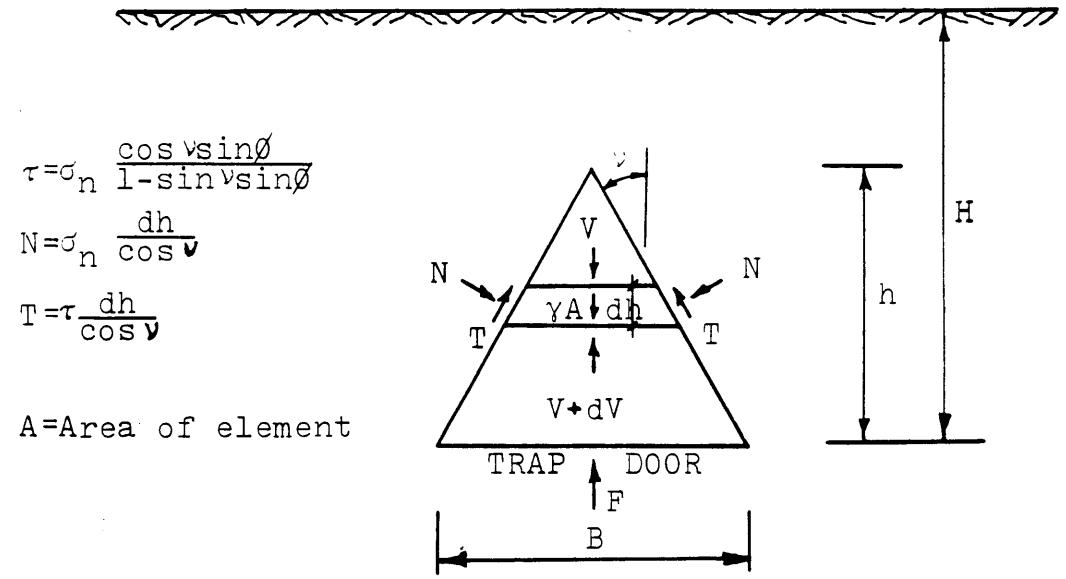

A. Free Body Diagram for $\nu>0^o$

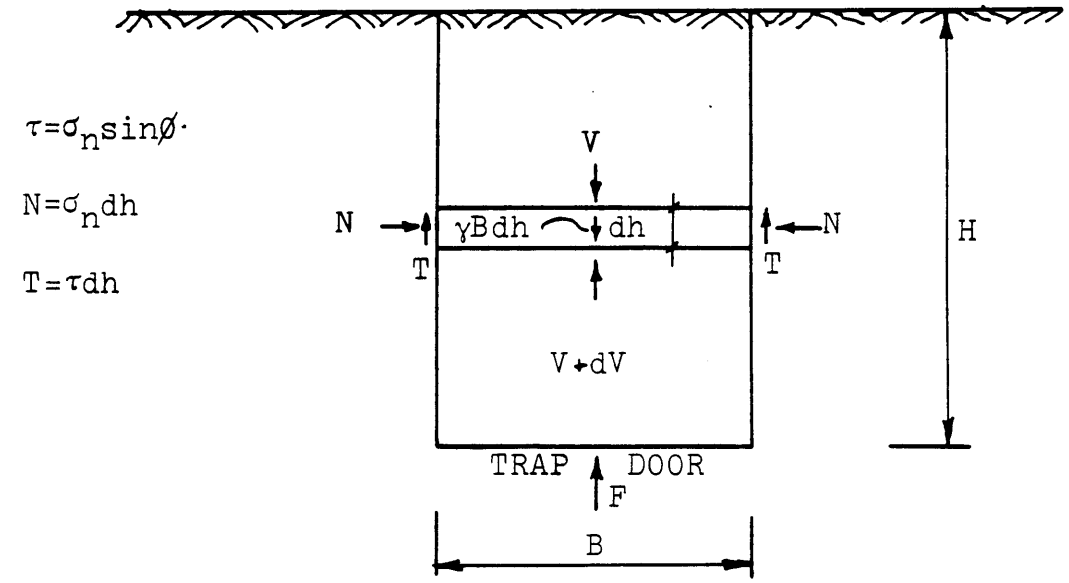

B. Free Body Diagram for $\nu=0^o$

Figure 3.14 Free Body Diagrams for Active Arching

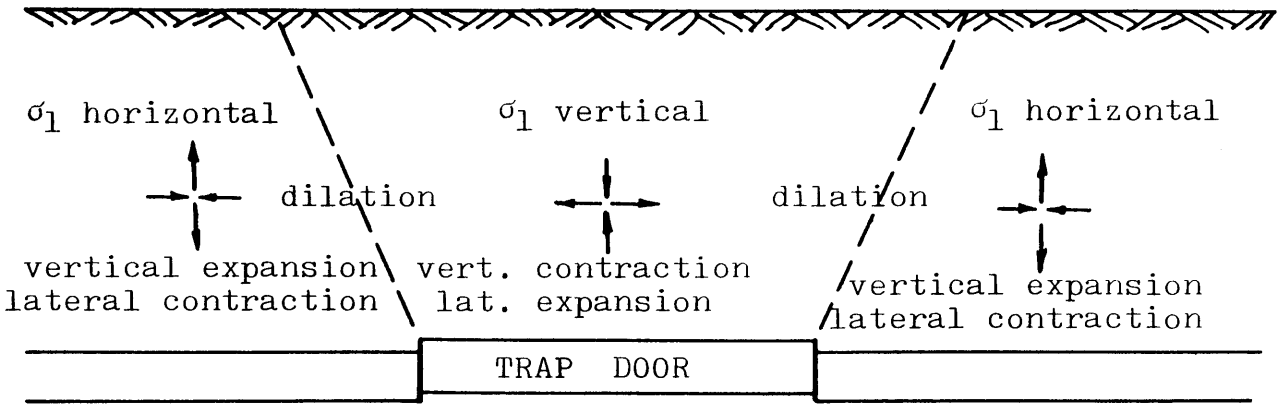

Figure 3.15 General Soil Behavior - Passive Arching

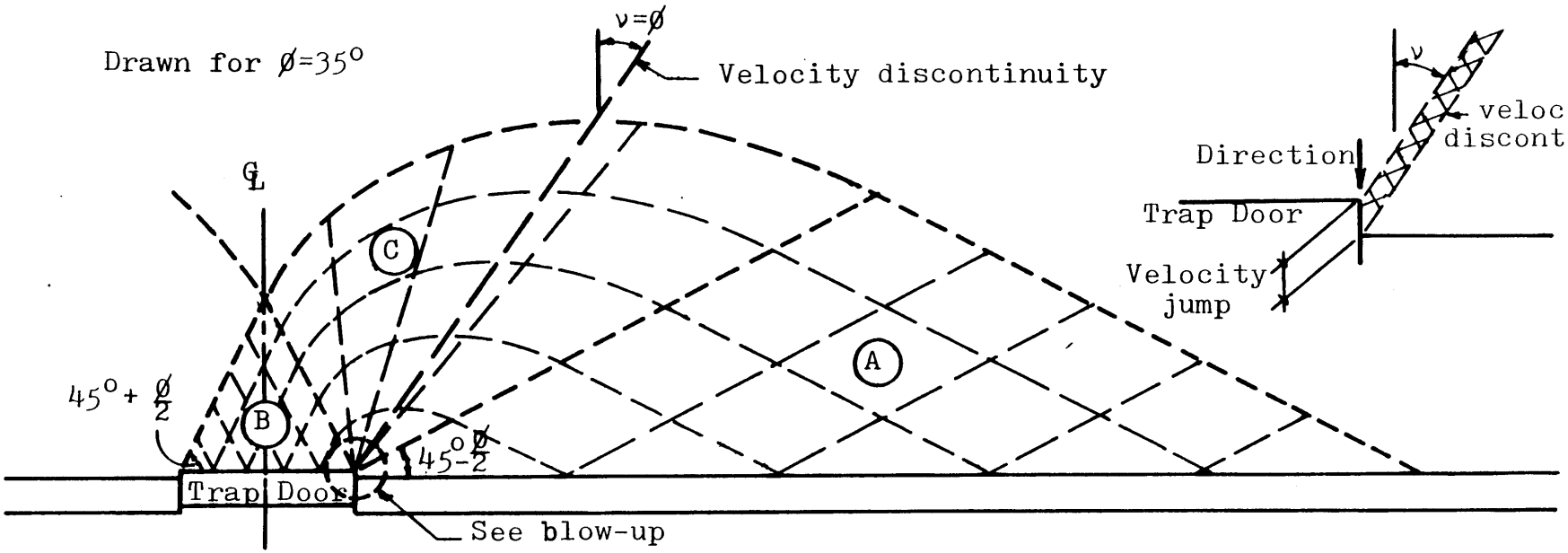

A. Stress Characteristics for Passive Arching

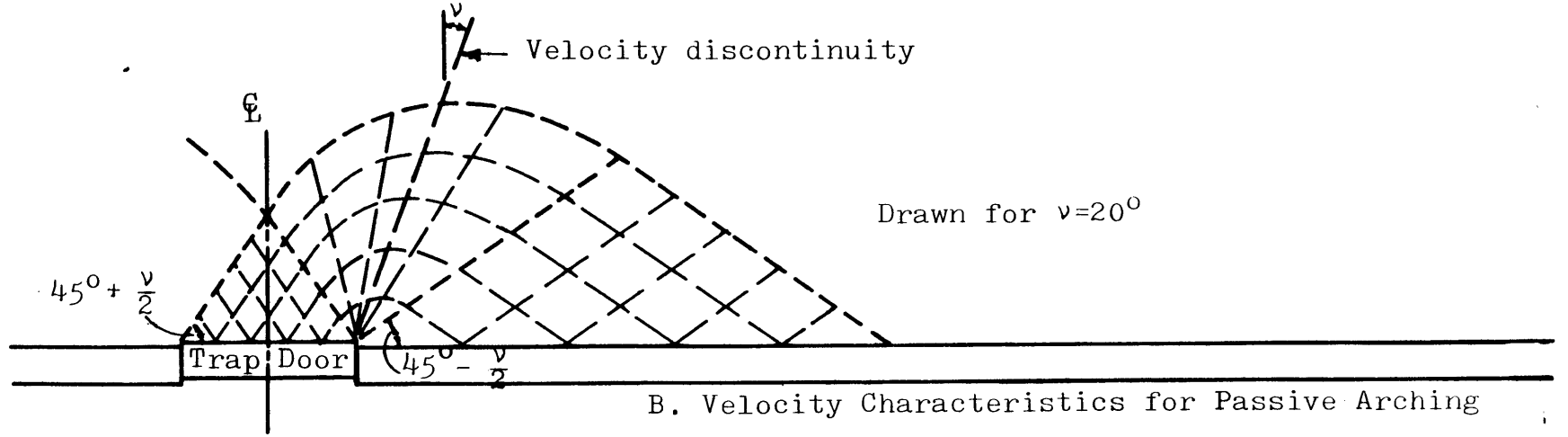

B. Velocity Characteristics for Passive Arching

Figure 3.16 Characteristics for Passive Arching

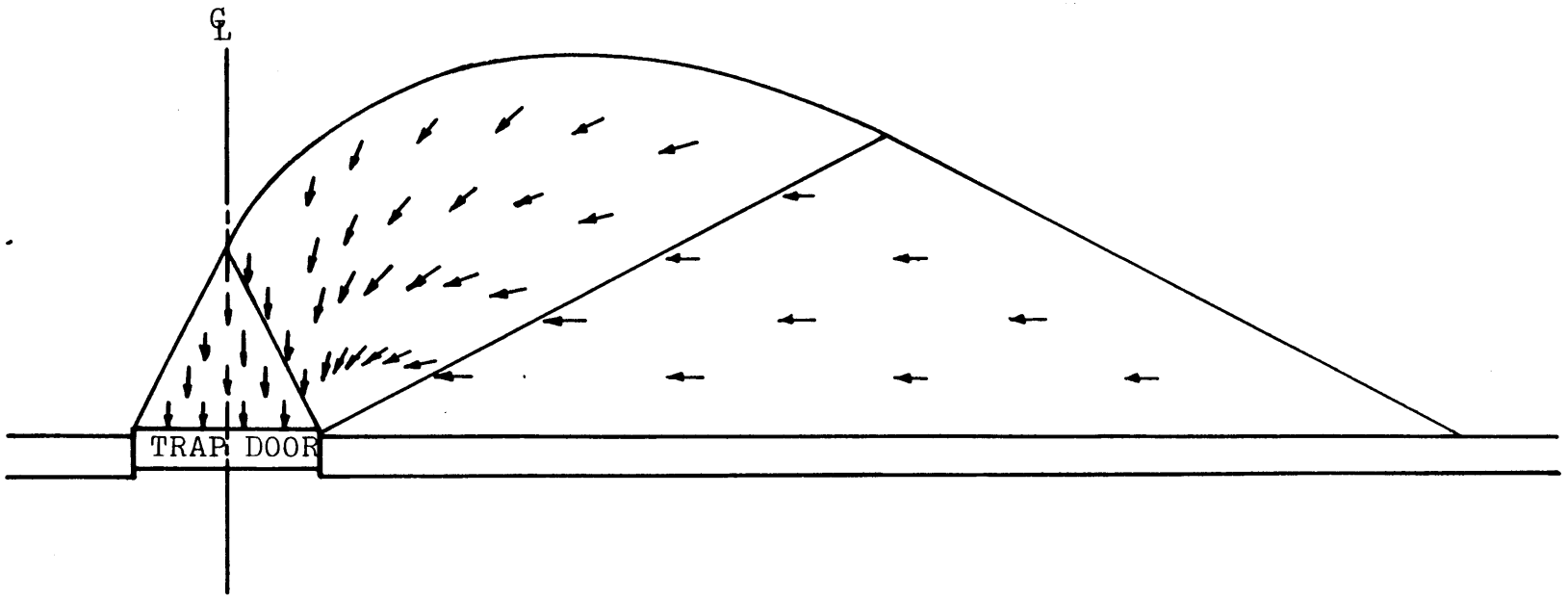

Figure 3.17 Direction of Major Principal Stress - Passive Arching

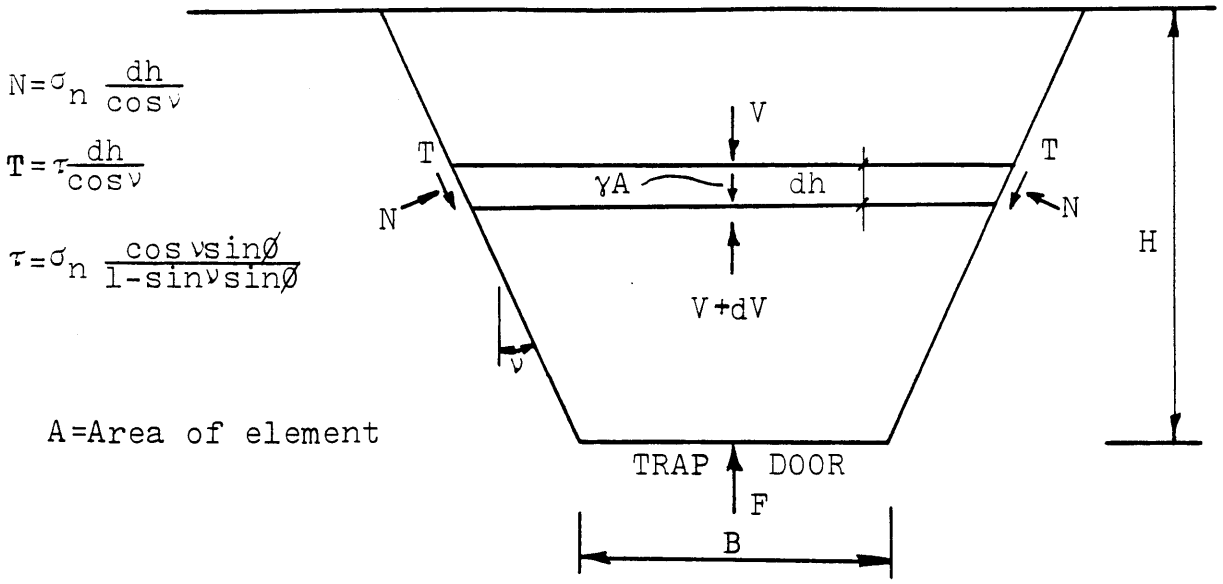

A. Free Body Diagram for $\nu>0^{\circ}$

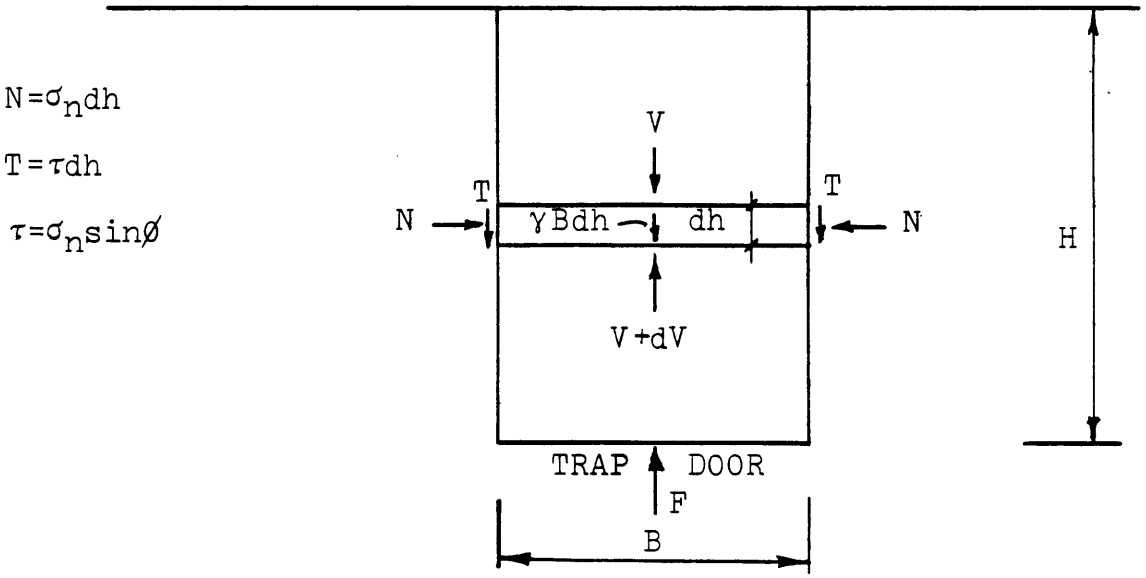

B. Free Body Diagram for $\nu=0^{\circ}$

Figure 3.18 Free Body Diagrams for Passive Arching

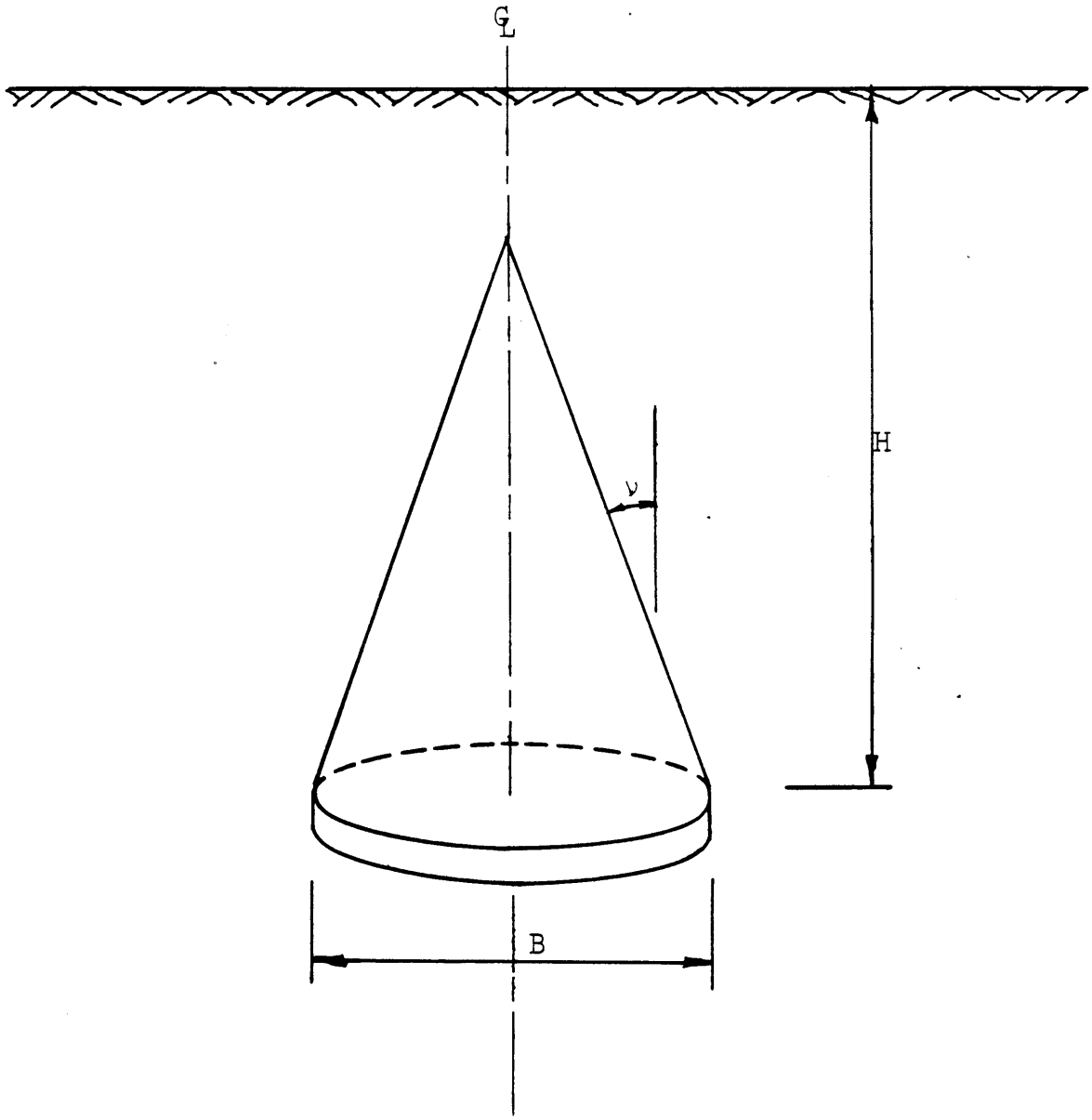

Figure 3.19 Prism of Soil for Active Arching Above a Circular Trap Door

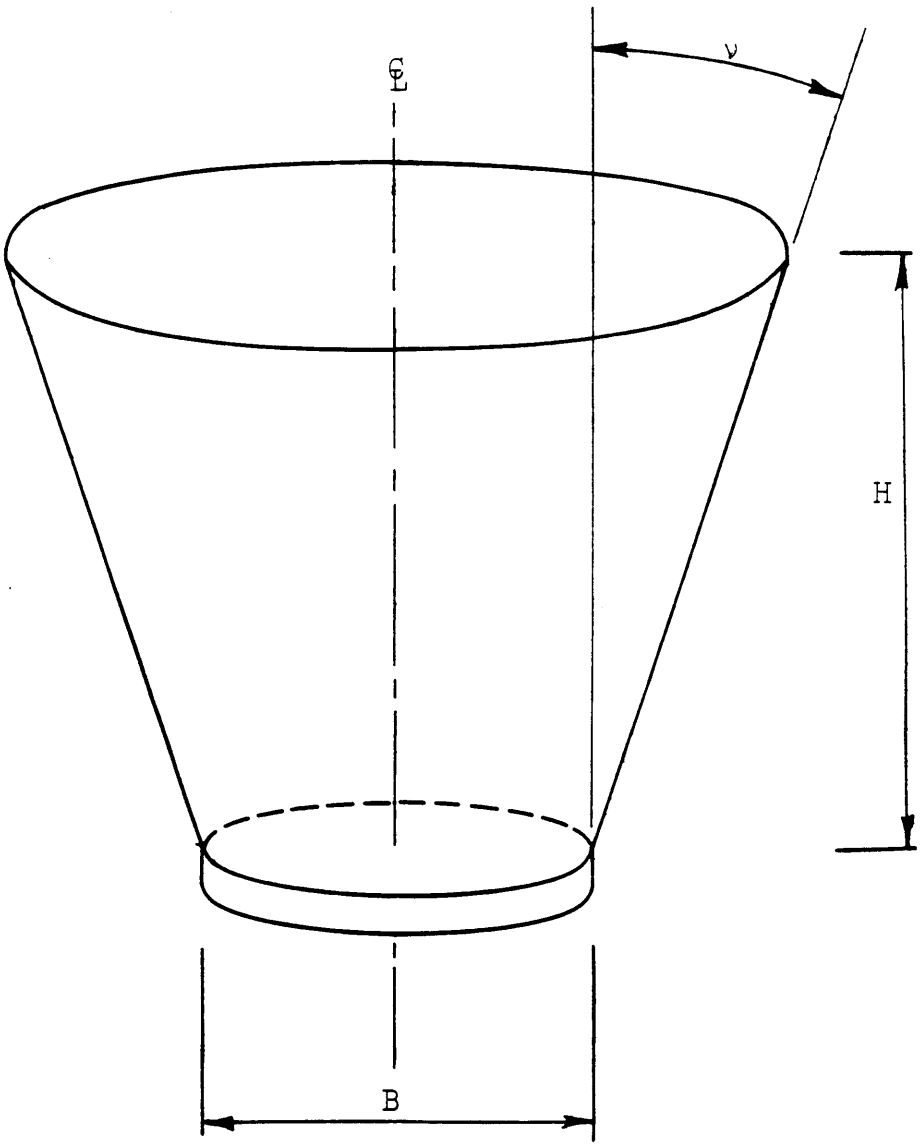

Figure 3.20 Prism of Soil for Passive Arching Above a Circular Trap Door

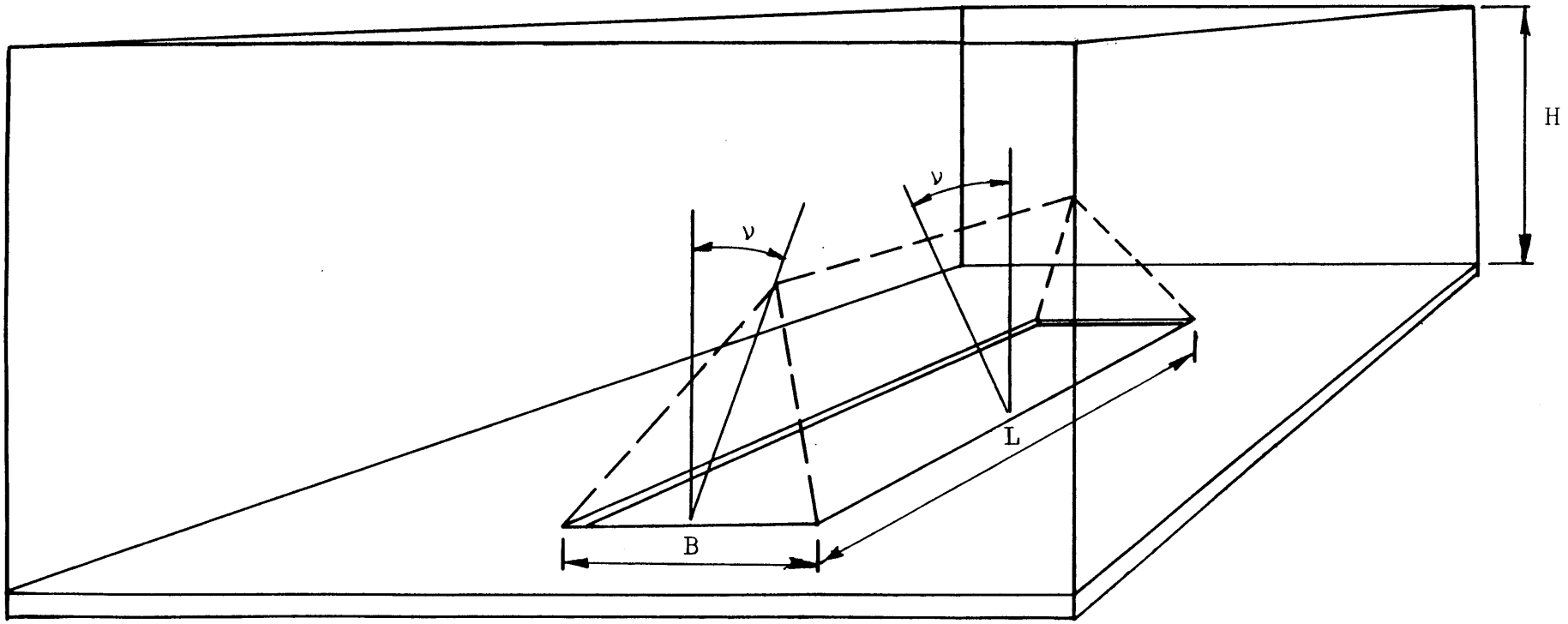

Figure 3.21 Prism of Soil for Active Arching Above a Rectangular Trap Door

$$F=\gamma B^2L^2\ \frac{1-e^{\mp 2K\sin\phi\ \frac{H(L+B)}{BL}}}{\pm 2K\sin\phi(L+B)}$$

Upper signs for active,
lower for passive

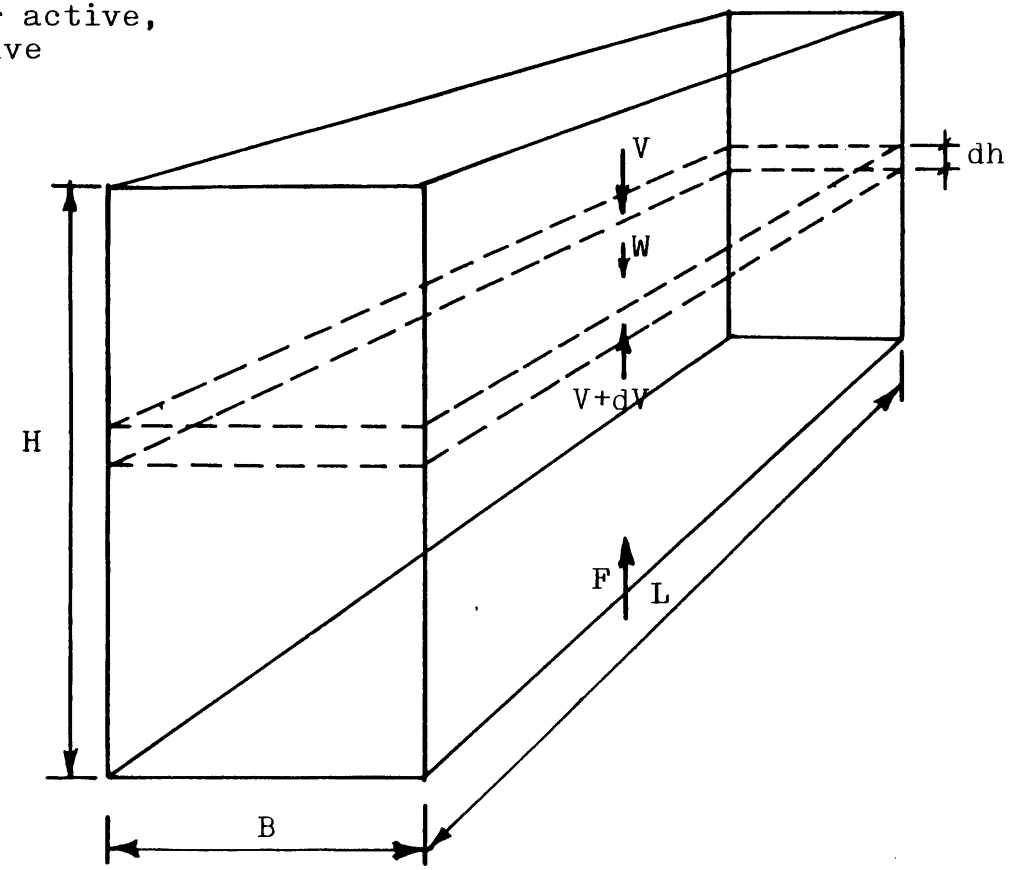

Figure 3.22 Free Body Diagram for Rectangular Trap Door (ν=0) - Active and Passive Cases

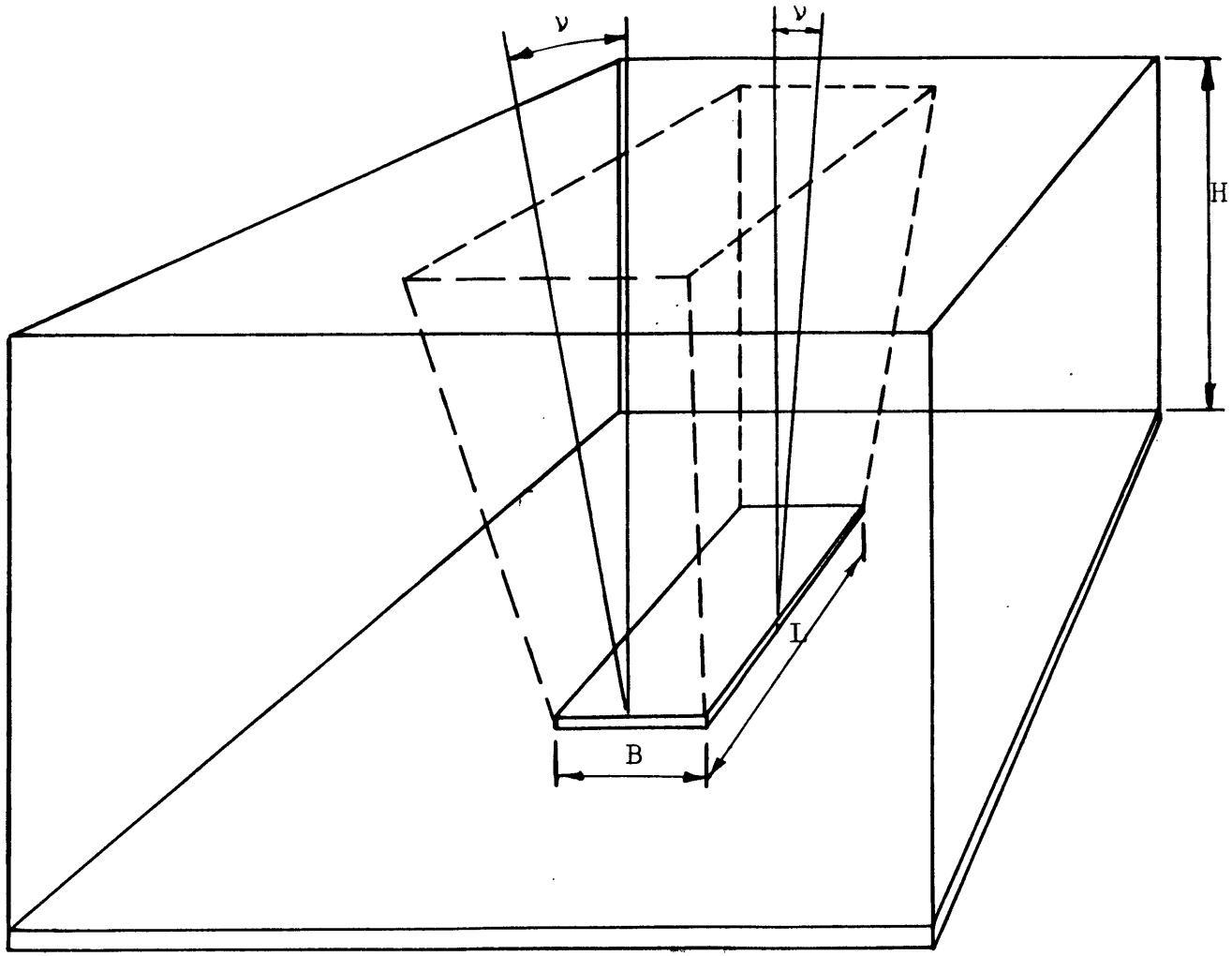

Figure 3.23 Prism of Soil for Passive Arching Above a Rectangular Trap Door

A. Principal Stress Trajectories (from Getzler, et al., 1970)

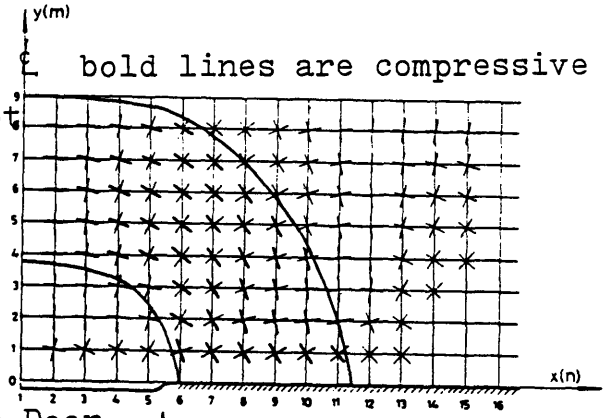

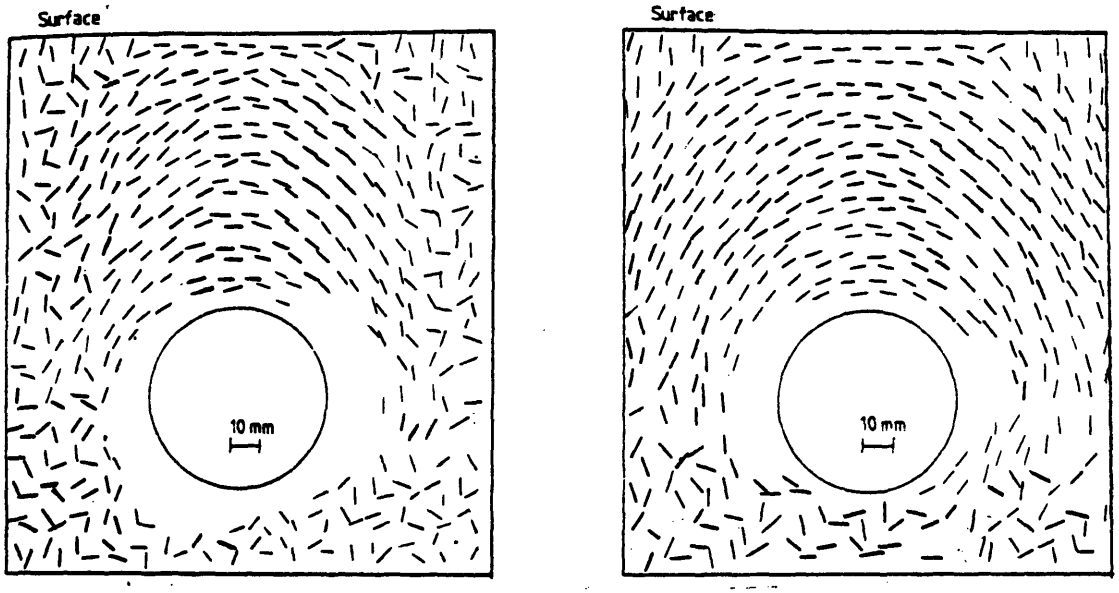

Dense Sand

Loose Sand

B. Direction of Major Principal Strain Rate (from Atkinson, et. al., 1977)

Figure 3.24 Directions of Major Principal Stress and Major Principal Strain Rate During Active Arching

H/B	Avg. Angle of Discontinuity (α)	Avg. Angle of Dilation (ν)	Displacement (δ)	Normalized Displacement ($\delta/B \times 100$)
4	64°	26°	0.048"	3.20%
4	63	27	0.077	5.13
4	66	24	0.123	8.20
4	74	16	0.221	14.73
4	76	14	0.324	21.60
4	68	22	0.078	5.20
4	75	15	0.181	12.07
4	76	14	0.264	17.60
4	82	8	0.425	28.33
4	81	9	0.425	28.33
4	84	6	0.664	44.27
4	85	5	0.664	44.27
2	70	20	0.119	7.93
2	70	20	0.119	7.93
2	75	15	0.260	17.33
2	79	11	0.423	28.20
2	84	6	0.637	42.47
2	88	2	0.859	57.27
2	74	16	0.211	14.07
1	66	24	0.104	6.93
1	78	12	0.292	19.47
1	88	2	0.587	39.13
1	72	18	0.185	12.33
1	75	15	0.266	17.73
1	82	8	0.389	25.93
1	89	1	0.623	41.53

Table 3.1 Approximate Values for Angle of Dilation for Lowering Trap Door

H/B	Avg. Angle of Discontinuity (α)	Avg. Angle of Dilation (ν)	Displacement (δ)	Normalized Displacement ($\delta/B \times 100$)
4	66°	24°	0.072"	4.80%
4	75	15	0.213	14.20
4	75	15	0.213	14.20
4	79	11	0.342	22.80
4	65	25	0.090	6.00
4	78	12	0.272	18.13
4	77	13	0.272	18.13
4	78	12	0.399	26.60
2	69	21	0.100	6.67
2	76	14	0.180	12.00
2	83	7	0.350	23.33
2	83	7	0.350	23.33
2	76	14	0.241	16.07
2	86	4	0.360	24.00
2	84	6	0.340	22.67
2	66	24	0.100	6.67
2	79	11	0.180	12.00
1	67	23	0.033	2.20
1	72	18	0.114	7.60
1	76	14	0.197	13.13
1	84	6	0.327	21.80
1	89	1	0.685	45.67
1	70	20	0.131	8.73
1	74	16	0.280	18.67

Table 3.2 Approximate Values for Angle of Dilation for Raising Trap Door

CHAPTER 4: GROUND MOVEMENTS AROUND STRUCTURES WITHIN GRANULAR SOILS

4.1 General

The main purpose of this chapter is not to give an in-depth study of the topic of ground movements associated with underground structures. Rather, it is intended to emphasize the interrelationship between ground movements and arching. One should keep in mind that without some relative ground movements between zones within the soil, no redistribution of stresses and thus no arching occurs. Assuming this relative movement is present, the associated redistributed stresses can cause further ground movement, again with changes in the stress field. Analytical approaches to relating ground movements to arching have not proven very successful, since ground movements are highly dependent upon the ground conditions encountered, and upon construction procedures and quality of construction.

The literature on this subject deals almost entirely with tunnelling, therefore it is this area on which emphasis is placed. However, many points can equally well apply to other underground facilities.

The following section presents results from this author's experiments and those by others which indicate the magnitudes of displacement which are generally required to mobilize arching around a buried structure. In subsequent sections information on the actual values of displacement normally experienced around tunnels is found, along with a brief review of the primary causes and patterns of displacements associated with tunnelling. In addition, a section addresses the question of how to adapt the approach presented in Chapter 3 (for obtaining the force on a yielding strip abutted by non-yielding horizontal surfaces) to determining the load which can be expected to act upon a buried structure. Finally, some experimental observations of surface displacements are given and compared with what would be anticipated from a frequently used empirical approach.

Several excellent papers are available which review

theoretical, laboratory, and field research relating to ground movements associated with soft ground tunnelling. These include: Butler and Hampton (1975), Cording and Hansmire (1975), Attewell (1977), Atkinson and Potts (1977), and Atkinson, Brown, and Potts (1977).

Two editorial points have to be made here:

1) At several points in this chapter (Sections 4.2 and 4.6) results of the experimental portion of this thesis are presented. It cannot be avoided that these are included here and again in Chapter 6, since it is felt that this information is important for the understanding of the general topic of ground movements.
2) An extension of the plasticity theory approach is presented in Section 4.5. Although this approach was treated in Chapter 3, its extension is largely dependent upon the level of ground movements occurring. Therefore, it was decided not to present it until after the topic of ground movements had been reviewed.

Surface displacements associated with tunnelling, while not directly related to arching, is a subject of major importance to designers. Since the experimental program did yield information on this topic, the decision was made to present these results under the general topic of gound movements and compare them with what would be predicted by commonly used theories.

4.2 Magnitudes of Displacement Necessary to Mobilize Arching

With few exceptions, construction of an underground structure causes displacements toward the structure within the surrounding soil. This process can be roughly represented by a lowering trap door. This results in the mobilization of active arching over the trap door (structure) with a reduction of stresses acting upon the door (structure).

This author conducted a series of trap door experiments

the details of which are presented and discussed further in Chapters 5 and 6. In general, it was found that the force on a lowering trap door decreased rapidly as displacement began. To give a quantitative picture the dimensionless 'displacement ratio' of trap door displacement to width (δ/B) will be used. For displacement ratios of 0.5 percent, 80 to 90 percent of the total stress reduction which would be obtained during an active arching test had already developed. The maximum arching (minimum force on the trap door, which ranged from 5 to 30% of the overburden) generally occurred at displacement ratios of 1.0 to 2.0 percent. At larger displacements the stresses on the trap door gradually increased until relatively constant values (generally 15 to 30% of the overburden, but can be higher as explained in Section 6.5.2) were obtained for δ/B greater than about 10 to 15 percent. This author's results are similar to those of Terzaghi (1936) previously presented in Section 2.4. He found that a displacement ratio of approximately 0.5 percent resulted in considerable active arching while maximum arching occurred at δ/B of about one percent.

Extending trap door results to actual tunnels, one can conclude from these experiments that better than 80 percent of the maximum possible load reduction on a tunnel due to arching can be expected when the ratio of ground displacement toward the tunnel to equivalent trap door width for the tunnel (δ/B_e) is approximately 0.5 percent. When this ratio is 1.0 to 2.0 percent, near maximum arching should exist. For larger displacements load reduction decreases, but still remains at better than 80 percent of that obtained at maximum arching. The concept of equivalent trap door width (B_e) was introduced in Chapter 2 and will be discussed further in Section 4.5. It ranges from the tunnel diameter for circular cross-sections to about two tunnel widths for square cross-sections.

4.3 Observed Magnitudes of Displacement Around Tunnels

A beneficial reduction in tunnel support design loads

resulting from active arching can only be realized if one is confident that displacements of sufficient magnitude do occur. Displacements around any particular tunnel are highly dependent upon the construction technique as well as upon local soil properties, and have not proven to be readily predictable with any degree of accuracy. However, data from instrumented sections of tunnels indicate that displacements of at least 1 to 2 percent of the tunnel diameter (or width for non-circular sections) can generally be expected when traditional design and tunnelling construction techniques are used with granular soils.

In the following discussion the term 'lost ground' will be used. This term is defined as "the volume of soil which displaces across the boundary defining the perimeter of the tunnel" and 'percentage of lost ground' is "the volume of lost ground expressed as percentage of total tunnel volume" (Cording and Hansmire, 1975). The terms exclude ground movements resulting from liner deflection. From these definitions it is clear that the "occurrence of lost ground" will contribute to the mobilization of arching around a tunnel. Summaries of lost ground and percentage of lost ground for a number of tunnelling projects are presented in Attewell (1977) and Cording and Hansmire (1975). The former indicates that lost ground alone creates soil displacements at the crown ranging from 0.8 to 3.0 percent of the tunnel's diameter (width) within granular soils. The latter show average displacements (attributable to lost ground) adjacent to tunnels, in granular soil, falling in the range of 0.7 to 4.5 percent.

Besides considering ground movements resulting from the construction process, one must look at those associated with deflection of the tunnel liner system after its installation. This involves the question of relative flexibilities of the soil and liner, which is a major design consideration, but will not be discussed here other than giving typical values for liner deflections. Peck, Hendron, and Mohraz (1972) presents an approach for qualifying these relative flexibilities.

Peck (1975) asserts that commonly used primary liners, such as steel ribs and timber or steel lagging, can be expected to deform 0.5 to 1.5 percent of the tunnel's diameter. Hansmire and Cording (1972) measured deflections of up to 1.2 percent of the tunnel diameter for a flexible primary lining in the Washington, D.C. Metro and described this as consistent with their past experiences. Cording and Hansmire (1975) summarize average liner deflections for a number of projects, finding that as a percent of tunnel diameter these displacements range from less than 0.5 to over 3.0 percent.

The information presented thus far leads one to conclude that displacements around most tunnels do in fact reach or exceed those levels (1 to 2 percent) necessary for mobilization of considerable shearing resistance with associated load redistribution (i.e. active arching does occur). Typical distributions of these displacements along with the general causes are presented in the next section.

4.4 Patterns of Displacements Around Tunnels

4.4.1 Sources of Ground Movement

As mentioned previously, ground movements associated with tunnelling in granular soil are attributable to the excavation process and to the deflection of the liner. The latter is reasonably predictable while the former can vary greatly depending upon soil conditions and the degree to which construction is controlled. Examples of construction practices impacting the degree of movement include: dewatering, grouting of voids, plowing and yawing of a shield, presence of internal pressure, degree of overcutting around liners, level of face support, and balancing of material removed with tunnel advance. Also, without care large quantities of ground may be lost quickly in non-cohesive sands due to limited or non-existent standup times.

4.4.2 Typical Cross-Sectional Displacements

Field and laboratory investigations exist which give insight into typical cross-sectional patterns of displacement

adjacent to tunnels. Hansmire and Cording (1972) present the results, reproduced in Figure 4.1, from an instrumented section of tunnel in granular soil. The figure shows contours of total displacement at the left and directions of displacement on the right. The largest magnitudes of total displacement occur within a near triangular wedge above the tunnel. This behavior is similar to what would be predicted by plasticity theory (Section 4.5). Some lateral displacement was observed at the sides of the tunnel, but there was little displacement near the invert. Figure 4.2 summarizes the volumetric behavior of the soil around this same section of tunnel. Dilation occurs above the tunnel while contraction is observed at the sides or abutments where arching causes increased stresses.

A laboratory investigation at Cambridge University (previously discussed in Section 2.11) yielded results agreeing well with those above. They used lead shot and radiographic techniques to monitor the displacement field as the pressure within a model tunnel was reduced. Typical displacements within dense and loose sands are given in Figure 4.3.A, while Figure 4.3.B shows values of volumetric strain at two instances during the tests. The negative signs in the latter figure indicate dilation above the tunnel, however due to the low stress level present in the test no contraction was observed at the sides.

4.4.3 Typical Longitudinal Pattern of Displacements

As a tunnel advances through a granular soil, displacements will develop several tunnel diameters in advance of the face and they will continue to increase until well after the face has passed. Figure 4.4 shows a typical distribution of the development of these displacements based upon information from Ranken and Ghaboussi (1975) and Katzenbach and Breth (1981). Displacements ahead of the tunnel are largely attributable to two sources. First, as arching develops around the tunnel, stresses increase ahead of the face with an associated compression of the soil. Second, the ground generally moves

three-dimensionally into the tunnel face, causing displacements and increasing the extent of stress redistribution due to arching. In the literature the percentage of total displacements occurring ahead of the face (relative to total displacements) ranges from less than 10 percent (Butler and Hampton, 1975) to approximately 50 percent (Attewell, 1975).

4.5 Adaptation of Plasticity Theory Approach to Tunnels

The approaches presented in Chapter 3 for the determination of the force acting on a trap door during active arching can be extended to provide approximate values of force on a tunnel liner (or other underground structure) in granular soil if an equivalent trap door width (B_e) is used to represent the tunnel (structure). Terzaghi (1943) first proposed this approach which was previously presented in Section 2.4 and Figure 2.5. Briefly reviewing, the equivalent trap door width for a circular tunnel is simply the tunnel diameter, while that for a rectangular or horseshoe cross-section is defined by Terzaghi as:

$$B_e = B + 2D \tan(45^\circ - \frac{\phi}{2}) \qquad (4.1)$$

where B is the tunnel width and D its height.

It is this author's opinion that Terzaghi's values for equivalent trap door width are oversimplified and that more research needs to be performed in this area. Plasticity theory requires that the slip lines (velocity discontinuities) correspond to velocity characteristics; therefore, ν should be used rather than ϕ in Terzaghi's equation. In addition, the equivalent trap door width would be largely dependent upon the level of lateral movement adjacent to the tunnel.

For model tests on circular tunnels Atkinson, et.al. (1975) obtained results which would indicate that the equivalent width was approximately the diameter. Their experiments (described in Section 2.11) did not, however, model construction of the tunnel, and it is then when most lateral movements occur; also, they note that almost the entire movement of the flexible liner in their experiments was vertical with maximum

values at the crown.

Assuming one could construct a circular tunnel so as to produce negligible lateral movements at the sides while still allowing sufficient vertical movements to occur above the tunnel (to mobilize active arching), velocity discontinuities as shown in Figure 4.5.A should develop. This produces an equivalent trap door width slightly smaller than the tunnel diameter (B). If sufficient lateral movement occurs during construction to create active earth pressure conditions at the sides of the tunnel, discontinuities develop which are tangent to the tunnel and inclined at $45^{o} + \nu/2$ to the horizontal. The extent of these discontinuities and therefore the equivalent trap door width for the tunnel depends upon the magnitude of these lateral movements. Figure 4.5.B shows this relationship.

Again assuming sufficient vertical movements develop to mobilize active arching, discontinuities similar to those for circular tunnels occur around tunnels with rectangular cross-sections (Figure 4.6). Equivalent trap door widths will thus range from the tunnel's width for no lateral movement to larger values if lateral movements do occur. Terzaghi's value is obtained if ϕ is substituted for ν in Figure 4.6.B (i.e. associated flow rule assumed) and the discontinuities at the sides of the tunnel are assumed to extend linearly to the elevation of the roof.

Once an equivalent trap door width is determined, the force per unit length (F) can be obtained using the approaches in Chapter 3. It is then commonly assumed that this force must be resisted entirely by the structure. This assumption generally overestimates the vertical liner load, since, as can be seen in the free body diagrams in Figure 4.7, some of the load may be resisted by the wedges of soil adjacent to the structure. The level of this resistance component is not easily obtained and it is, therefore, usually ignored. Some assumptions must also be made for the determination of design lateral loads on the sides of the structure. Readers are referred to

a popular approach to this in Proctor and White (1977).

4.6 Surface Displacements Above Shallow Tunnels

The mechanism for transfer of soil movements (associated with tunnelling) to the ground surface is not well understood. The volume of the trough observed at the surface is usually smaller than that measured at the tunnel, because of dilation of the soil above the tunnel; however, cases exist where contraction of the soil led to a volume of the trough at the surface exceeding that at the tunnel. While a few theoretical investigations of the formation of settlement troughs have been undertaken, their application is limited. The most widely quoted treatment is an empirical approach proposed by Peck (1969).

Attewell (1977) reviews several models for plane strain surface movements based on the migration of voids through an assemblage of spheres or discs. These are not directly adaptable to actual tunnelling problems, however they do predict that the settlement trough will assume a shape approximately described by a normal probability distribution function, provided movements are small with respect to the tunnel dimensions. For large displacements the trough becomes 'V' shaped with sides at the material's angle of repose. Attewell does not define what magnitudes of displacement are considered small and large. This author observed formation of 'V' shaped troughs above lowering trap door when experiments were conducted with small overburden ($H/B \leq 1$) and large displacements ($\delta/B \geq$ 30 percent).

Peck (1969) compiled information from a number of settlement troughs for tunnels in various soil conditions. He found that a normal probability distribution curve could typically be found which would closely resemble the trough. Figure 4.8.A shows the properties of such a curve. One needs only to specify the maximum displacement at the centerline (δ_{max}) and the distance from the centerline to the point of inflection (i) to define the curve. Once i was determined for the various

tunnel projects, Peck found that by plotting the ratio of overburden depth to tunnel width (H/B), versus the ratio of i to tunnel half-width (i/R), the projects fell into regions related to soil conditions (see Figure 4.8.B). Following from the assumption of a normal probability distribution approximating the trough's shape it is also possible to approximate the volume of displacement at the surface per unit length of trough through the expression:

$$V_s = 2.5 \times i \times \delta_{max} \qquad (4.2)$$

Cording and Hansmire (1975) use the same approach, but they introduce the term 'angle of draw' (β) which is defined as "the vertical angle from the edge of the excavated area to the edge of the subsidence trough" (see Figure 4.9). It is determined from:

$$\tan\beta = (2.5i - B/2)/H \qquad (4.3)$$

For 'sands above the groundwater level' the angle of draw ranges from approximately 11^o to 26^o.

Figures 4.9 and 4.10 show settlement troughs obtained by this author from trap door experiments with overburden to trap door width ratios (H/B) of 1.0 and 2.0 respectively (corresponding photographs are A.20 and A.21 in Appendix A). Due to the scale of the apparatus, displacement ratios (δ/B) larger than those typically associated with tunnelling were necessary. These figures also contain normal distribution curves chosen to closely fit the data. The properties of these curves when plotted on Peck's empirical graph (see Figure 4.8.B) indicate the soil conditions to be 'sand above the groundwater level'. Angles of draw for the two troughs are approximately 13.5^o and 12.6^o, which again corresponds to 'sand above the groundwater level'. The widths of these troughs do tend to be narrower than what one would anticipate from Peck's approach, but this can largely be attributed to the characteristics of the trap door apparatus (virtually all displacement is vertical and located directly above the door, whereas for actual tunnels lateral movement at the sides is also present, spreading

displacements over larger area and increasing the trough width). Comparing the volumes of the observed settlement troughs with the 'theoretical' volume created by the doors' displacement indicates that dilation occurred above the door, increasing the soil's volume by between 10 and 15 percent.

Throughout this section surface displacements have been treated as occurring two-dimensionally while these are, in fact, three-dimensional (just as are displacements adjacent to an advancing tunnel). Hansmire and Cording (1972) present an excellent representation of this fact constructed from data obtained for a section of the Washington, D.C. Metro (Figure 4.11). Contours of equal settlement are shown on the figure's left, while those for direction and magnitude of horizontal movements are found on the right. Attempts to model and better understand this three-dimensional behavior were made in the experimental portion of this research and will be presented in Chapter 6.

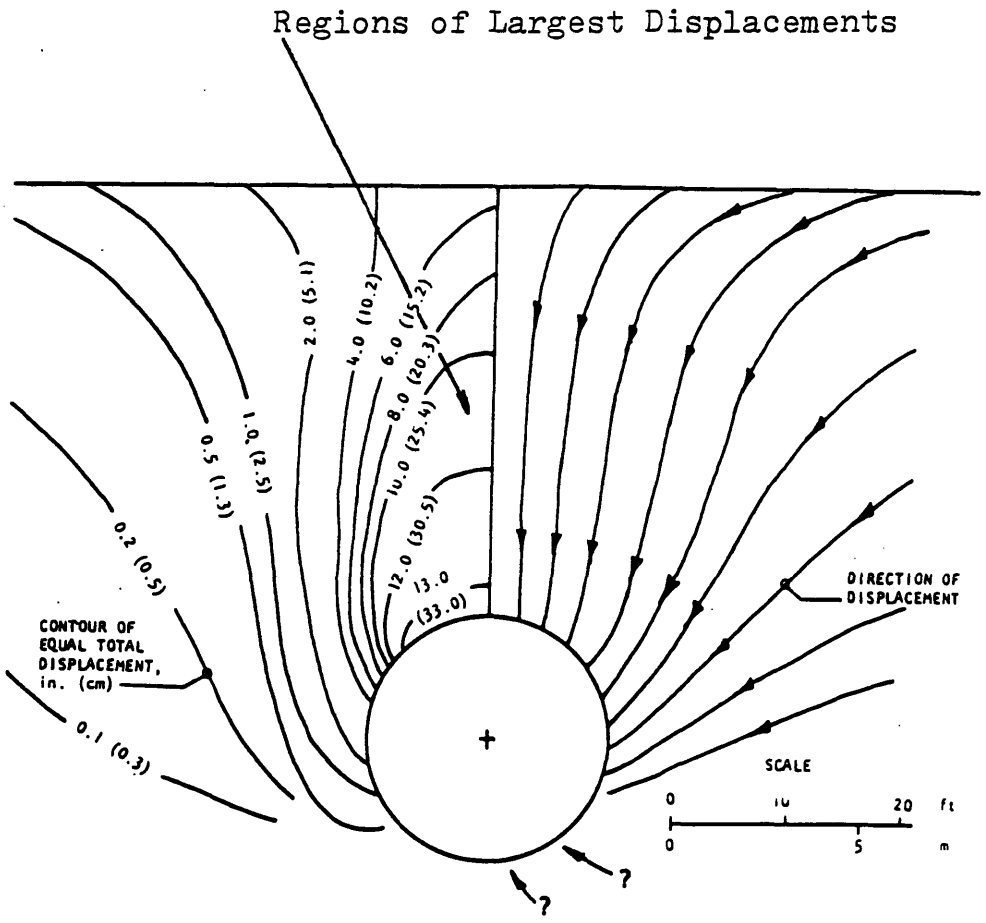

Figure 4.1 Total Displacement and Directions of Displacement Around a Tunnel (from Hansmire and Cording, 1972)

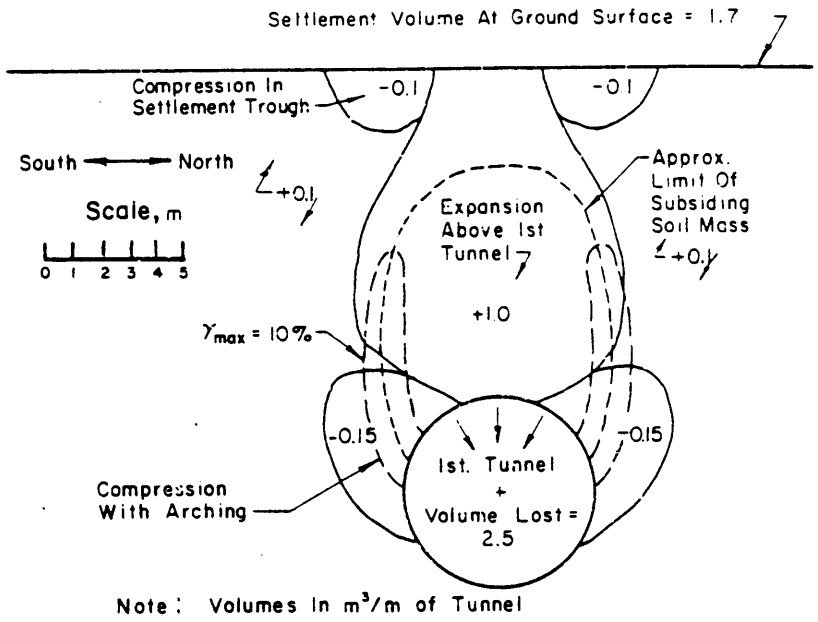

Figure 4.2 Volumetric Soil Behavior Around a Tunnel (from Cording and Hansmire, 1975)

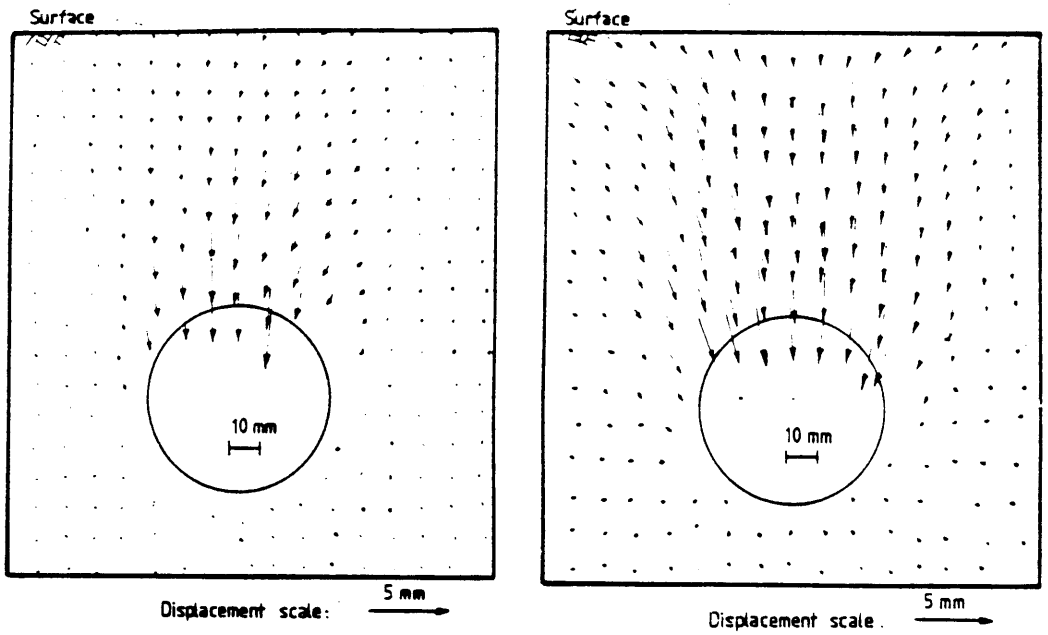

Dense Sand Loose Sand

A. Distribution of Soil Displacements Around Tunnels Near Collapse in Dense and Loose Sand

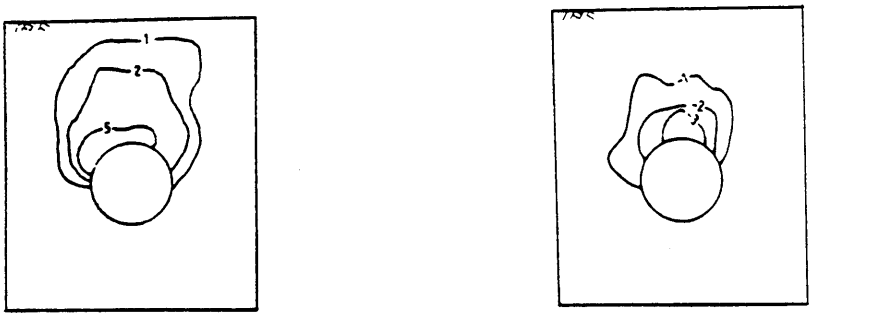

Shear Strain Volumetric Strain

B. Contours of Shear and Volumetric Strain (%) Around a Model Tunnel in Dense Sand

Figure 4.3 Soil Behavior Around a Model Tunnel (from Atkinson, et. al., 1977)

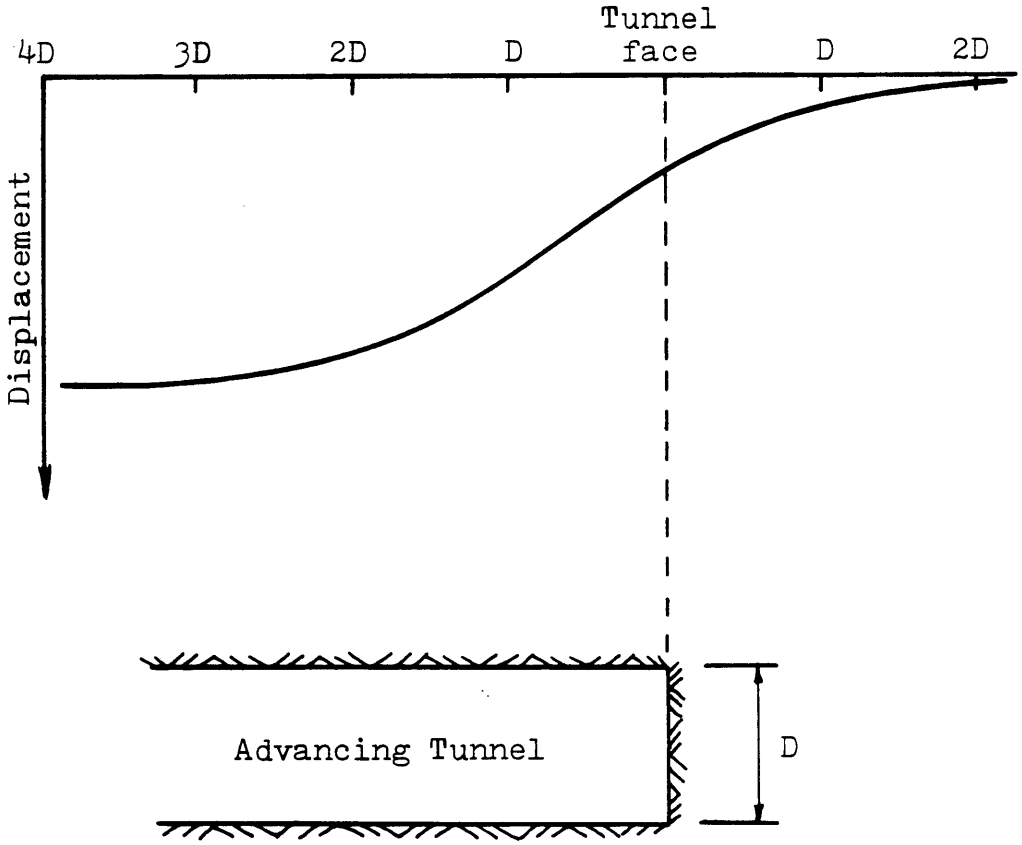

Figure 4.4 Typical Longitudinal Displacements Around a Tunnel

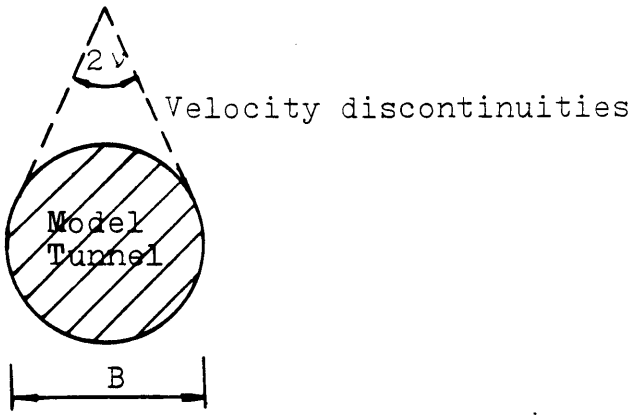

A. Small Lateral Movement

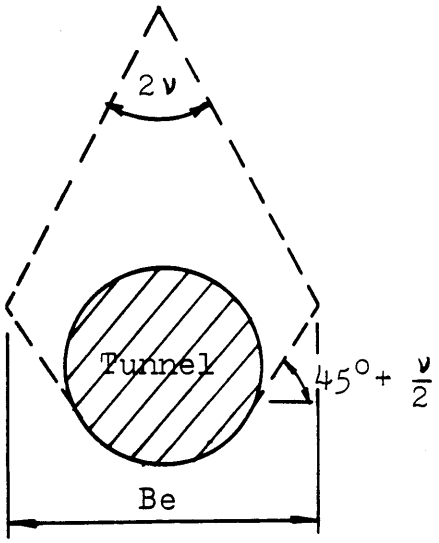

B. Moderate Lateral Movement

Figure 4.5 Relationship Between Equivalent Trap Door Width and Lateral Movement for Circular Cross-Section

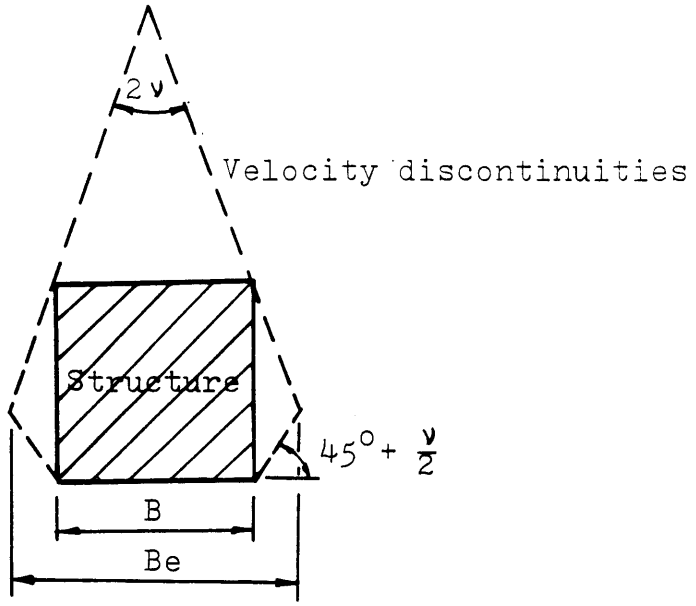

A. Small Lateral Movement

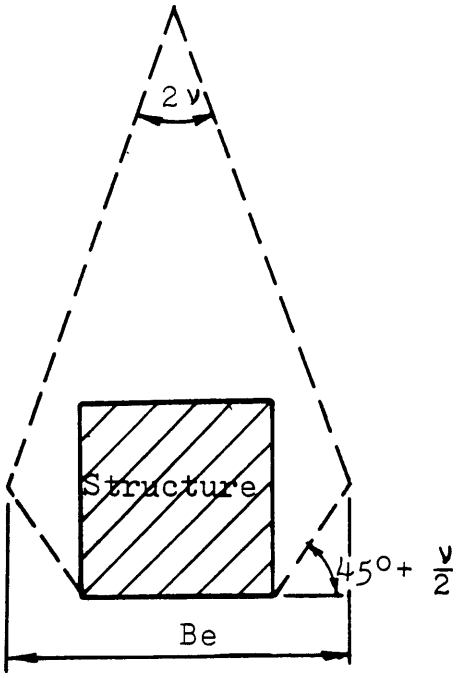

B. Moderate Lateral Movement

Figure 4.6 Relationship Between Equivalent Trap Door Width and Lateral Movements for Rectangular Cross-Section

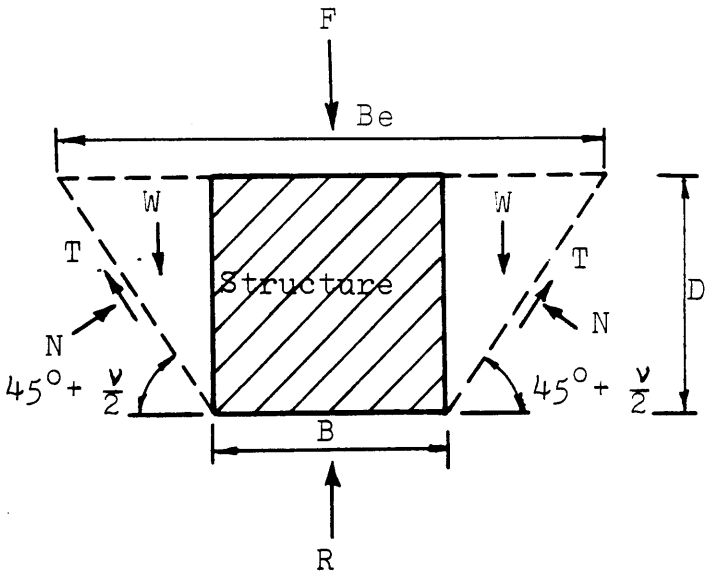

A. Rectangular Cross-Section

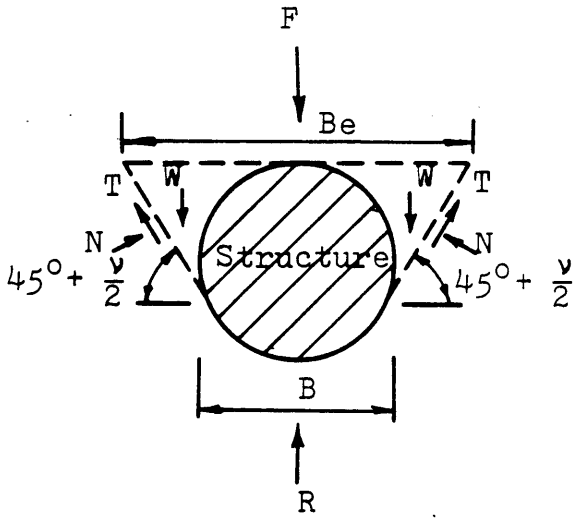

B. Circular Cross-Section

Figure 4.7 Typical Free Body Diagrams for Rectangular and Circular Cross-Sections

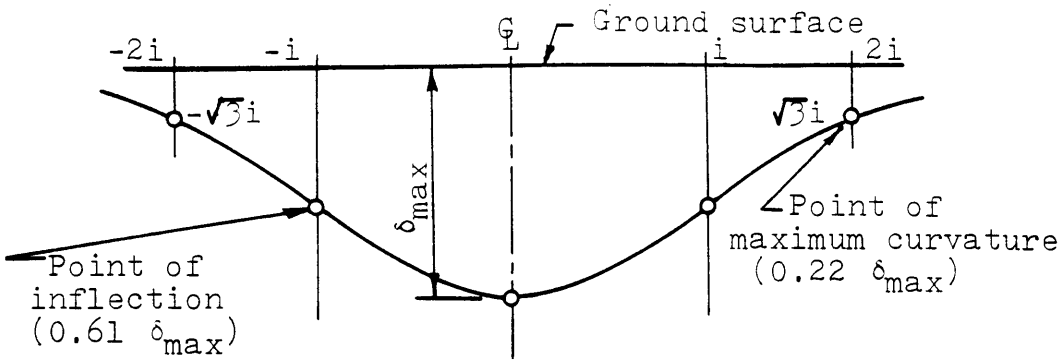

A. Properties of Normal Probability Curve

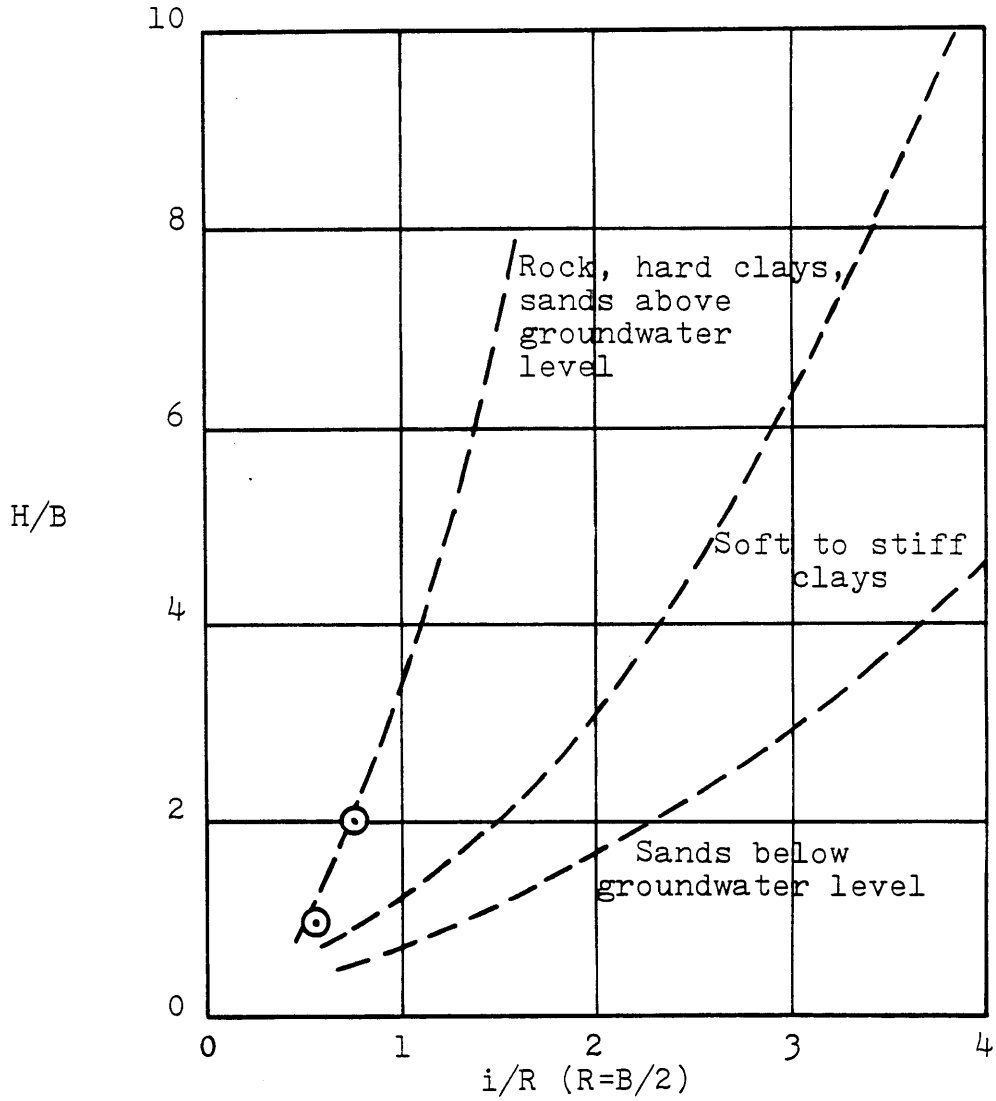

B. Classification by Soil Conditions

Figure 4.8 Peck's Approach for Predicting the Size of a Settlement Trough with Known Ground Conditions

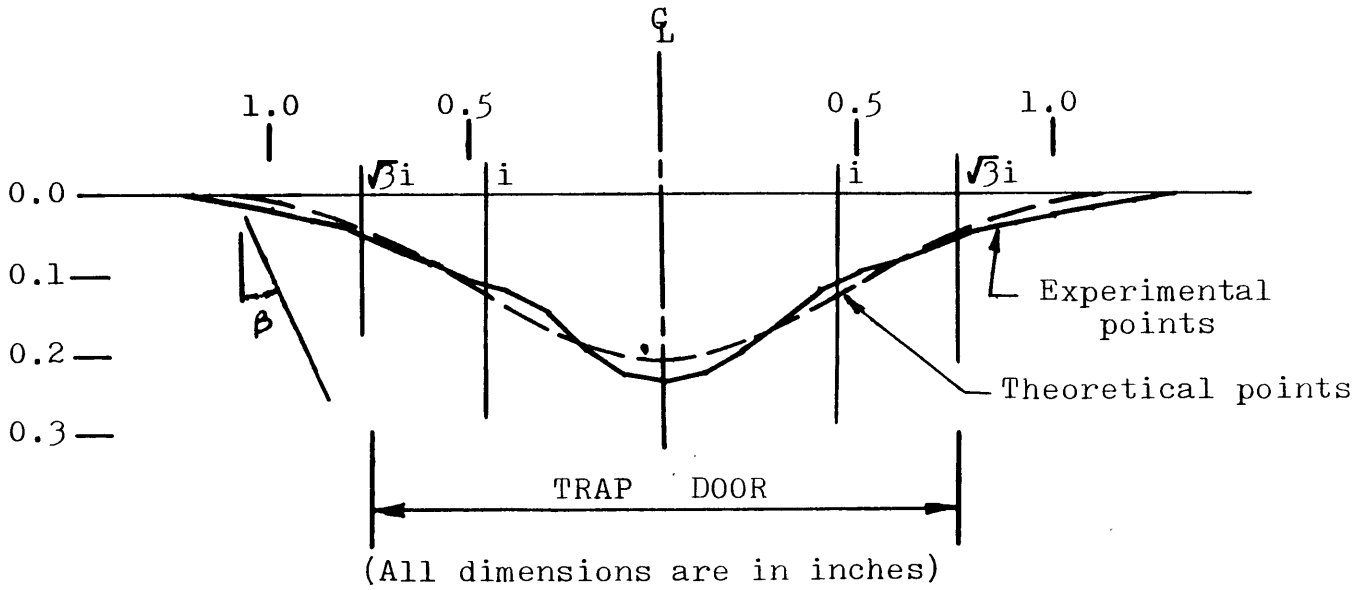

i=0.44 inches

β=13.5°

Figure 4.9 Observed Settlement Trough - Test Number 61

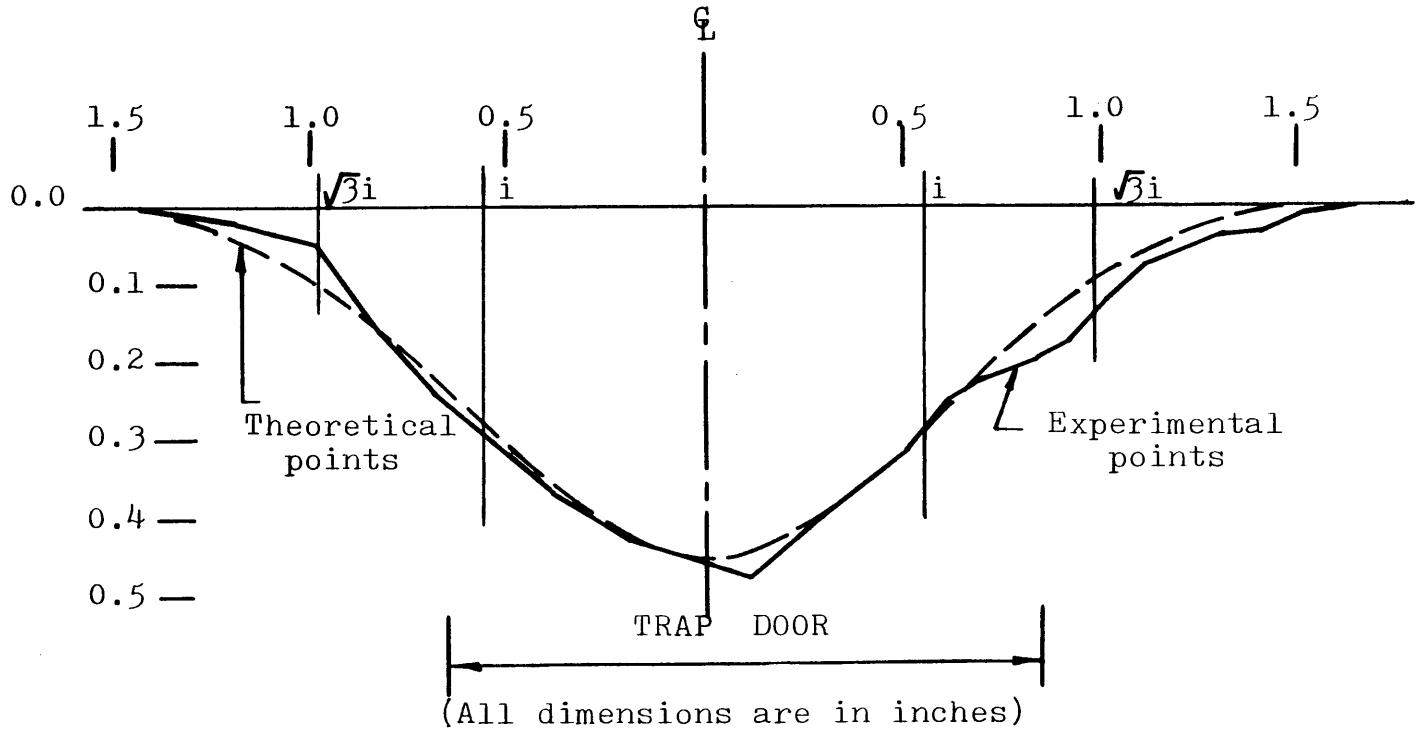

i=0.57 inches
β=12.6°

Figure 4.10 Observed Settlement Trough - Test Number 60

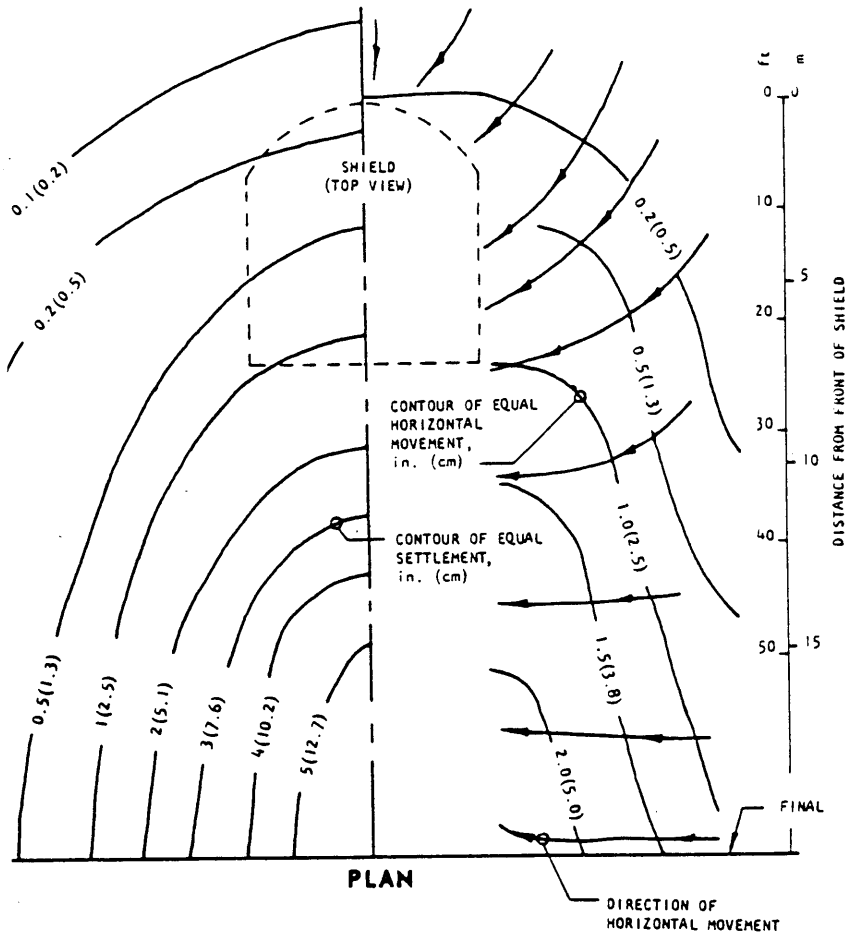

Figure 4.11 Surface Settlements Above an Advancing Tunnel (from Hansmire and Cording, 1972)

CHAPTER 5: EXPERIMENTAL EQUIPMENT, SOILS, AND PROCEDURES

5.1 General

After reviewing other research on arching, the decision was made to conduct an experimental investigation having several objectives. The first was to gain a better understanding of the mechanism by which arching develops. The second was to quantify the magnitude and pattern of stress redistribution around a deforming structure. Finally, by roughly simulating the advancing of a tunnel through the soil, insight into the three-dimensional behavior in the vicinity of the face can be obtained. Since no apparatus was available which would yield this information, it was necessary to design and construct such a device. The devices presented in this chapter are the results of in-depth examination of experimental devices used by other researchers, and have undergone considerable design evolution prior to being constructed. They were built at a minimal cost largely using readily available materials, and they generally satisfy the objectives presented above.

It was decided that rigid trap doors capable of translating uniformly up or down and initially flush within a horizontal base of similar material should be used. Having both the doors and surrounding base rigid provides better control over the system and knowledge as to what deformations are actually occurring at the soil-structure interface without considering the relative flexibilities of the two materials. Also, by controlling trap door displacements and measuring stresses at the interface the performance of the apparatus can be evaluated through comparison with results from some of the similar investigations reviewed in Chapter 2.

The scale for the apparatus was chosen so as to make installation of an instrumentation system possible and to facilitate visual observation of the soils' behavior. In addition, the scale had to be small enough such that the volume of sand necessary for a test is not excessive, while the lateral

boundaries are located at a sufficient distance from the doors such that their presence does not affect test results.

To represent a non-cohesive granular soil several types of dry sand were selected. Densities and moisture contents were checked periodically during the testing program. These materials have generally time-independent behavior allowing for rapid stabilization of stress readings. Whitman (1964) found the influence of strain rate (analogous to rate of trap door displacement) upon the strength of dry sand to be small, typically less than 15 percent when the time to achieve a specific displacement was varied between one minute and five thousands of a second.

The following sections present the apparatus developed for this investigation along with information on instrumentation, soils, test procedures, and data acquisition techniques adopted.

5.2 Initial Test Apparatus and Procedures

A preliminary apparatus was constructed for the purpose of determining whether the diaphragm type pressure transducers (Section 5.4) being considered for this investigation would give accurate results. A schematic of this apparatus is given in Figure 5.1. A 2.25 inch circular trap door with a flush mounted pressure transducer at its center, translates vertically with respect to the adjecent base through adjustment of the hand operated jack on which the trap door is mounted. Displacements are measured by two manually read dial gauges attached to the translating portion of the jack and in contact with the underside of the plywood base. The two gauges were located on opposite sides of the trap door and its displacement was considered to be the average of those indicated by the gauges.

A series of tests, summarized in Chapter 6 and Appendix B, were conducted which indicated that pressure transducers could be used in this research, and which also yielded information on arching around a circular trap door. In addition, several alternatives were explored for preventing sand from

entering the small gap between the trap door and adjacent base, with the placement of high vacuum silicone grease in this space prior to each test proving most successful.

Zero readings were taken before each test, followed by deposition of the sand using techniques described in Section 5.6. The volume of sand deposited and its depth were monitored during deposition along with the corresponding transducer reading. This information was used to compare actual and theoretical values of pressure on the transducer for various depths of sand so as to evaluate its performance. Following deposition the sand was initially left overnight to allow for dissipation of any static electrical charges it may have acquired (Harris, 1975). This period was later shortened to several hours to minimize drifts in pressure readings, attributed to variations in temperature within the laboratory. The trap door was then lowered or raised in stages, several thousands of an inch at a time. After each displacement the transducer reading was allowed to stabilize and then read simultaneously with both dial gauges. Following the test, the sand was removed and another transducer zero reading made. Data was reduced as described in Section 5.9.

5.3 Primary Test Apparatus

5.3.1 Configuration

After obtaining encouraging results from the initial test apparatus, it was decided to design and construct another apparatus (herein called primary test apparatus) which would be adaptable to a number of test configurations. Figure 5.2 contains a drawing of the resulting device, while photographs can be found in Appendix A (photographs A.1 - A.6). Nine $1\frac{1}{2}$ by $4\frac{1}{2}$ inch trap doors are located within a horizontal surface 24 inches square. Sand is deposited onto this surface and restrained by one of the two boxes described in Section 5.3.3. Individual trap doors can be lowered or raised while monitoring displacement and stresses.

A sheet of 3/4 inch plywood was located beneath the

plexiglas base to provide additional rigidity and thereby limit deflection during sand placement. Some deflection was found to occur at the unsupported plexiglas edge adjacent to the trap doors (see discussion in Section 6.7).

5.3.2 Trap Door System

The nine trap doors are arranged in a row each supported individually by the system shown in Figure 5.2; doors were machined to about 0.005 inch less than the nomimal horizontal dimensions to limit friction between adjoining surfaces. Individual trap doors are mounted on two $\frac{1}{4}$ inch aluminum rods which pass through a guide and are attached to a plexiglas crosspiece. One end of a $\frac{1}{4}$ inch by 4 inch bolt is fastened to this crosspiece while the other has a wingnut attached which rests on a bearing plate at the base of the apparatus. By manually turning this wingnut the trap door will move vertically up or down. One can control door displacements, using this system, to within approximately 5/10,000 of an inch.

The plexiglas trap door guide is made of two $\frac{1}{4}$ inch sheets, separated by $1\frac{1}{2}$ inches, with matching rod holes in each. It is attached to the underside of the plywood support and restrains the doors from moving horizontally. A dry lubricant placed on the rod hole sides before assembly reduces friction between the plexiglas and aluminum rod surfaces. In addition, all rods were mechanically buffed to limit surface roughness.

Trap doors can be lowered or raised approximately 0.4 inches in normal testing. By placing blocks, of the same size as the doors, on top or at their sides it is possible to increase the effective thickness of the doors and produce displacements of up to 0.9 inches.

5.3.3 Boundary Conditions

Two separate boxes were built to retain the sand during testing with the primary apparatus. Both are shown in Figure 5.3 and photographs A.1 and A.2 in Appendix A. They have no bottoms, but rather sit flat against the plexiglas surface.

The first box will be called the 'planar soil deformation tank'. It was designed to restrict movements of the soil such that they occur only within the plane parallel to the transparent face. This face, in turn, allows one to observe these deformations throughout a test. The interior face of the plexiglas walls are in the same plane as the planes of contact between the trap doors and adjacent fixed base.

The second sand retaining box is the 'three-dimensional soil deformation tank'. When placed on the apparatus, it provides an inner area 22½ inches square. With this tank in place the soil adjacent to the trap doors is free to deform three-dimensionally. The width was chosen based on an investigation by Getzler, et.al. (1970). They found that having a sand box at least four times as wide as the trap door (assuming the door is centered in the box) essentially eliminates any effects the boundary may have on deformations or stresses near the door.

5.3.4 Instrumentation

Vertical stresses at the base of the sand are measured using laboratory pressure transducers mounted at locations shown in Figure 5.2. These locations were selected to be both on and adjacent to trap doors, so as to provide an idea on the distribution of stresses. More information on these transducers is given in Section 5.4.

Displacement of each trap door is measured by dial gauges mounted on the trap door bearing plate (Figure 5.2) and in contact with the cross-piece of the trap door assembly. Two interchangable models of gauges were used (1: John Bull, Ltd. and 2: Soil Test, Inc.). The resolution was 1/10,000 inch and 5/10,000 inch respectively with travel ranges in excess of one inch.

5.4 Stress Measuring System

5.4.1 Rationale for Selection

A number of load measuring devices were considered for use in this investigation. Among these were load cells,

proving rings, pressure transducers, hydraulic pressure cells, and strain gauged compression elements. One of the objectives of this research was to study the distribution of stresses across the trap doors and adjacent rigid base; therefore, devices which would only measure total force on a stationary or translating trap door were less desirable.

Stress measuring cells belong to one of two categories depending on their location which can be either within the soil mass or at the soil-structure interface. The first type is typically difficult to install, since their presence alters the stress state which would have existed without the cell. They are very sensitive to differences in stiffness within the soil and between the soil and cell, and they often give false readings due to stresses other than those normal to the face. The boundary cells are commonly used in model studies. They are easier to install, more reliable, and more accurate providing the cell's stiffness is close to that of the material making up the boundary. They are, however, limited to only measuring stresses normal to the boundary.

A number of type AB, 25 psi pressure transducers manufactured by Data Instruments, Incorporated (formerly Tyco) of Lexington, Massachusetts were available to this author (see Figure 5.4). They are boundary stress cells with strain gauges mounted on a flat flexible diaphragm. For such a cell which is mounted flush with the boundary it is important to limit the deflection of the diaphragm to avoid the development of arching over the cell, with redistribution of stresses. Studies conducted at the Waterways Experiment Station during the 1940's and 1950's indicated that arching could be reduced to less than 5 percent if the ratio of diaphragm width (B_d) to centerline deflection (δ_d) is limited to approximately 2,000. Later studies by Mackey and Creighton (1965) and Harris and Seager (1973) recommended 100,000 for this ratio in order to have negligible arching, while Weiler and Kulhawy (1982) suggest keeping the ratio above 5,000. Based on data provided to this author by Data Instruments, Incorporated the plot

shown in Figure 5.5 was constructed. It shows the ratio of diaphragm diameter to centerline deflection (B_d/δ_d) plotted against applied pressure for a type AB, 25 psi pressure transducer. The curve is based on the diaphragm deflecting in a partial spherical shape with an active diameter of 0.705 inches and a volumetric displacement of 1.6×10^{-5} in.^{3}/psi (see insert in figure). Also indicated are the approximate points corresponding to the most common depths of sand used in the testing program. The diameter to centerline deflection ratios range from approximately 16,000 for 9 inches of sand overburden up to 94,000 for $1\frac{1}{2}$ inches of sand. The decision was made to proceed with these transducers since B_d/δ_d values were in the range necessary to limit arching. It was also felt that some experiments aimed at evaluating arching above these transducers were desirable. Results from such experiments are presented in Chapter 6.

5.4.2 Transducer Installation

In order to eliminate any bias in experimental results, it was decided that in performing sets of identical tests the individual pressure transducers would be rotated among the different locations available. This required a mounting system which facilitated easy removal of transducers while still providing sufficient rigidity to prevent any movement. Another consideration was the desire to have the sensitive face flush with the plexiglas surface even though dimensions vary slightly between transducers of identical type.

Figure 5.4 shows the transducer mounting system. The cell is held in place by a $\frac{1}{4}$ inch backplate and can be removed by unscrewing two bolts. The face is adjusted to be flush by varying the thickness of O-rings placed between the cell and base or trap door, and by adding paper washers as indicated. To prevent sand particles from lodging between the transducer and adjacent plexiglas surface and to provide additional rigidity, a bead of silicone rubber is placed in this space during mounting. Following installation of transducers, the apparatus is left overnight to allow the rubber to cure.

Care was taken to mount transducers flush, however McNulty (1965), using similar boundary cells concluded that, provided the projection is less than 1/25 of the diameter, the cell will register the same as if it were perfectly flush.

5.4.3 Impact of Transducer Performance on Selection of Soils

Since sand is a particulate material, the stress is transferred to the diaphragm of the transducer via many point loads. If the individual grains are too large with respect to the cell, these point loads will cause the transducer to indicate stress values different from those actually present in the soil. Weiler and Kulhawy (1982) recommend that the ratio of diaphragm diameter (B_d) to the sand's D_{50} be greater than 10 to avoid this problem.

All four sands selected for this investigation (Section 5.5) meet this criterion. Several preliminary tests with the Coarse Leighton Buzzard Sand (which has the largest grain size, B_d/D_{50}= 19) produced poor results which could not be attributed to any specific reason. It was, therefore, felt that localized arching might be the cause, leading to a decision not to use that sand in further tests. The next largest grain size was the Medium Tan Sand.

5.4.4 Calibration of Pressure Transducers

A calibration factor ranging from -0.1 to 1.1 psi was obtained for each transducer at the beginning of the experimental program by calibrating against a water column of varying height. This procedure was repeated near the end of the program with no appreciable changes occurring in calibration factors. To verify that the values obtained with water would also apply for sand, the transducer readings from a number of tests were plotted versus applied pressure (backcalculated from depth, density, and weight of material placed). A typical range of results for one transducer from many tests is shown in Figure 5.6. There is some scatter in the data, but they do generally fall near the line representing the water

calibration factor.

One transducer exhibited the peculiar behavior shown in Figure 5.7. Transducer readings are significantly higher than the corresponding overburden. No explanation has been found for this behavior; however, the results for this transducer are very reasonable if the indicated pressure is adjusted using the curve in Figure 5.8 which was obtained from the data presented in Figure 5.7.

5.5 Descriptions of Sands Used for Testing

Four sands were used at various points during this experimental investigation. They are (roundness classes from Lambe and Whitman (1969) in parentheses):

Fine Leighton Buzzard 120/200 (subangular)

Coarse Leighton Buzzard 20/30 (subangular to subrounded)

A Medium Tan Sand also called Bin 23 Sand (subangular to subrounded)

A Fine White Sand (angular to subangular)

Several dry sieve analyses were performed on each soil with the resulting grain size distributions shown in Figures 5.9 through 5.12. Table 5.1 presents information obtained according to ASTM D2487-69, 'Classification of Soils for Engineering Purposes', along with specific gravities (G) determined using the procedure described in Lambe (1951), as well as available friction angle information. All four sands are poorly graded (SP) according to the Unified Soil Classification System.

Sand densities (γ) were obtained by placing metal tares of known volume and weight within the soil during deposition. Following a test each tare was carefully removed, the soil leveled even with the tare's lip, and the sample's weight (and therefore density) determined. Approximate values of density were also obtained by monitoring the total weight of material placed and the corresponding depth at intervals during a test.

The water content (w) of each sand was checked periodically, with values never exceeding a fraction of a percent

(highest value 0.08%).

The type sand used for each test is noted in the summary which is contained in Appendix B. Since they performed well in early testing and a large supply was available, the Fine White Sand and Medium Tan Sand were used exclusively in later tests. Most testing was performed with the Medium Tan Sand, while those tests with the Fine White Sand were intended to investigate the effect of differences in sand type.

5.6 Soil Placement Procedure

Two different methods (Figure 5.13) were employed for depositing the sand into the testing apparatus in an effort to obtain a range of densities between tests while producing a uniform density throughout the mass within each test. Average values for each technique are presented in Table 5.2. The first method used a 3/8 inch inner diameter copper tube which was uniformly moved across the base, the tip being kept several inches above the sand's surface. This led to densities approximately 8 percent lower than the second technique, however this method was not employed in later tests after it was found that it did not produce densities as uniform as method 2.

The second method involved raining the sand continuously from one or two 16 ounce coffee cans suspended approximately 30 inches above the base for the initial test apparatus and 18 inches above the base for the primary apparatus (see photograph A.5 in Appendix A). The sand rained from approximately forty holes, each about 1.5 millimeters in diameter, placed in the bottom of each can. Slightly smaller holes were used for the Fine White and Fine Leighton Buzzard sands (those with smaller grain sizes) so as to maintain similar deposition rates among the different sands. Kolbuszewski (1958) found that this raining technique can produce very dense samples. Whitman, et.al. (1962) used it to obtain relative densities of 97 percent with deposition rates similar to those used here, and postulated as to why such high densities developed. They believed

that "when sand particles arrive more or less individually at an existing sand surface, it is possible for these particles to nestle down into the holes between existing sand particles in such a way as to give nearly optimum packing and maximum unit weight". Increasing the deposition rate raises the likelihood of several particles arriving at any hole simultaneously, thereby creating a looser packed arrangement.

Deposition rates with the copper tube were approximately 60 to 80 $in^3/min.$, while rates for the raining from cans varied from 6 to 11 $in^3/min.$ per can depending upon the sand used. For the three-dimensional tests where large volumes of sand were necessary, two cans were used simultaneously to increase the deposition rate. This made it possible to place a depth of $1\frac{1}{2}$ to 2 inches of sand per hour.

For tests where the plexiglas-sided tank was used to observe the soils' deformation behavior during trap door movement, sand was placed in layers with a thin band of contrasting color sand deposited between each later. Fine White Sand dyed blue was used for contrast in tests with the white sand, while for the other sand types the white sand (undyed) provided the contrasting layers. Shop vacuum connected to a 3/8 inch inner diameter plastic tube was used to produce a level surface for each layer. The tip of the tube was set a fixed distance above the apparatus' base and the tube was moved across the sand's surface removing a small amount of material, and leaving a level surface on which to place the contrasting sand.

5.7 Available Test Configurations

A number of different test configurations are possible using the primary testing apparatus. First, either the 'planar soil deformation tank' or the 'three-dimensional soil deformation tank' can be used; second, the 9 trap doors can be translated individually, simultaneously in groups, or in succession while measuring stresses on and/or adjacent to displacing door(s); and third, certain test characteristics can be varied. Among these characteristics are: sand type, depth

of sand (H), trap door displacement (δ), direction of trap door movement (developing active or passive arching), and sand density. As discussed in Section 5.6, no worthwhile results could be obtained by changing density, therefore it was not varied in subsequent tests.

5.8 Testing Procedures

The apparatus and instrumentation was inspected prior to each test. Power supplies and volt meters were warmed up and connected to pressure transducers at least one hour before starting a test. A bead of high vacuum silicone grease was placed on all adjoining surfaces between trap doors, and the doors were leveled using a straightedge. Generally, due to manufacturing imperfections, the trap doors do not sit perfectly flush with the base, but rather are adjusted to project slightly (0.001 to 0.005 inch) on one side and to be recessed about the same amount on the opposite side. One chooses the desired testing tank, places it on the base in the proper location, and reinspects all instrumentation. The operator records transducer and dial gauge readings throughout the test following procedures outlined in Section 5.9.

The test begins by depositing the desired quantity of sand following the procedures described in Section 5.6. Following the material's placement, the sand is carefully leveled with a straightedge (for three-dimensional soil deformation tank) or vacuum system (for planar soil deformation tank), and the filled apparatus is left for at least one hour before continuing with the test (to allow dissipation of any static electrical charges existing).

The prescribed number of trap doors were then lowered or raised the desired distances by rotating the wingnuts on the support assembly while checking magnitude of displacement on each door's individual dial gauge. Displacements were applied in steps of several thousandths of an inch at a time with smaller steps at the beginning where most stress

redistribution occurs. The step sizes increase at larger levels of total displacement. The rate of vertical movement was kept below about 0.01 in./min., however since the doors were lowered manually it was impossible to maintain a constant rate.

At the completion of a test the sand is carefully removed via scoops and the vacuum system, so as to avoid damaging the transducers. The tank is then removed, remaining sand is brushed from the base, and all trap door edges are cleaned well to remove silicone grease and sand. The used sand is kept separate from the source so that a different batch of the sand is used in the next test.

5.9 Recording and Reduction of Test Data

All test data were read and recorded manually. At the beginning of each test zero readings were taken for all dial gauges and pressure transducers. During deposition of sand the total weight and depth of material placed along with corresponding transducer readings were recorded at regular intervals. For the tests involving the removal of material by vacuum, the depth and pressure readings were recorded periodically.

Following soil placement, all instrumentation was read prior to beginning trap door displacement. During the displacement phase all instruments were allowed to stabilize at each interval, then a complete set of readings were made. Following a test all sand was removed and end zero values recorded for each transducer. For cases where beginning and end zeros differed appreciably, an average value was typically used for reduction of data unless one of the two readings was suspect for reasons such as voltage or temperature variations.

Each transducer output reading was accompanied by a record of the input voltage to make adjustments possible, accounting for any voltage variations during a test. Input voltage was recorded to the nearest millivolt and transducer output voltage to the hundredth of a millivolt. Values of actual stress normal to the diaphragm were obtained using these data

and the individual transducer's calibration factor determined as described in Section 5.4.

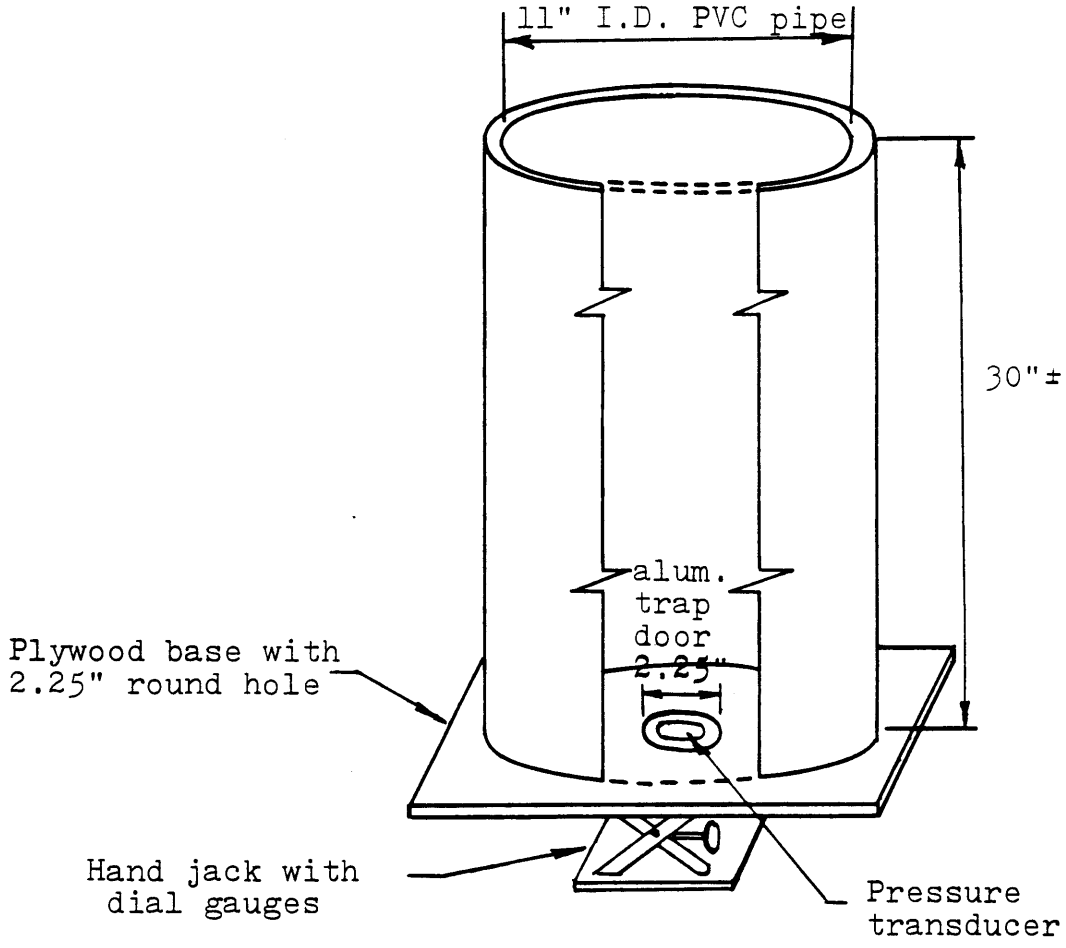

Figure 5.1 Initial Test Apparatus

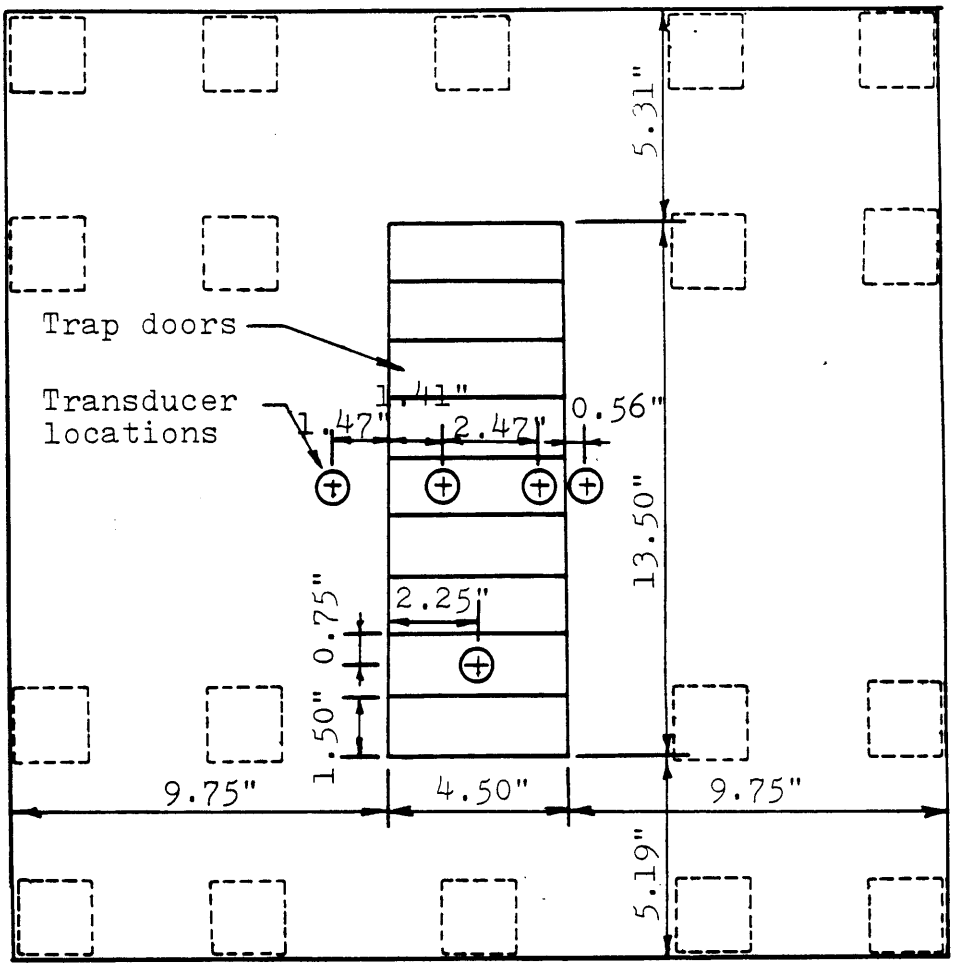

A. Plan

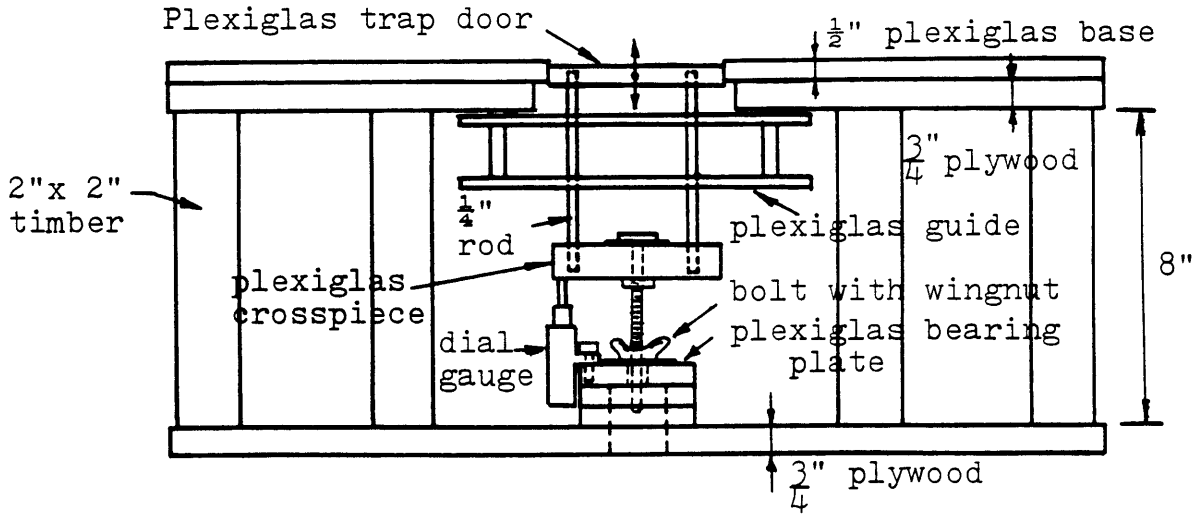

B. Profile

Figure 5.2 Primary Test Apparatus

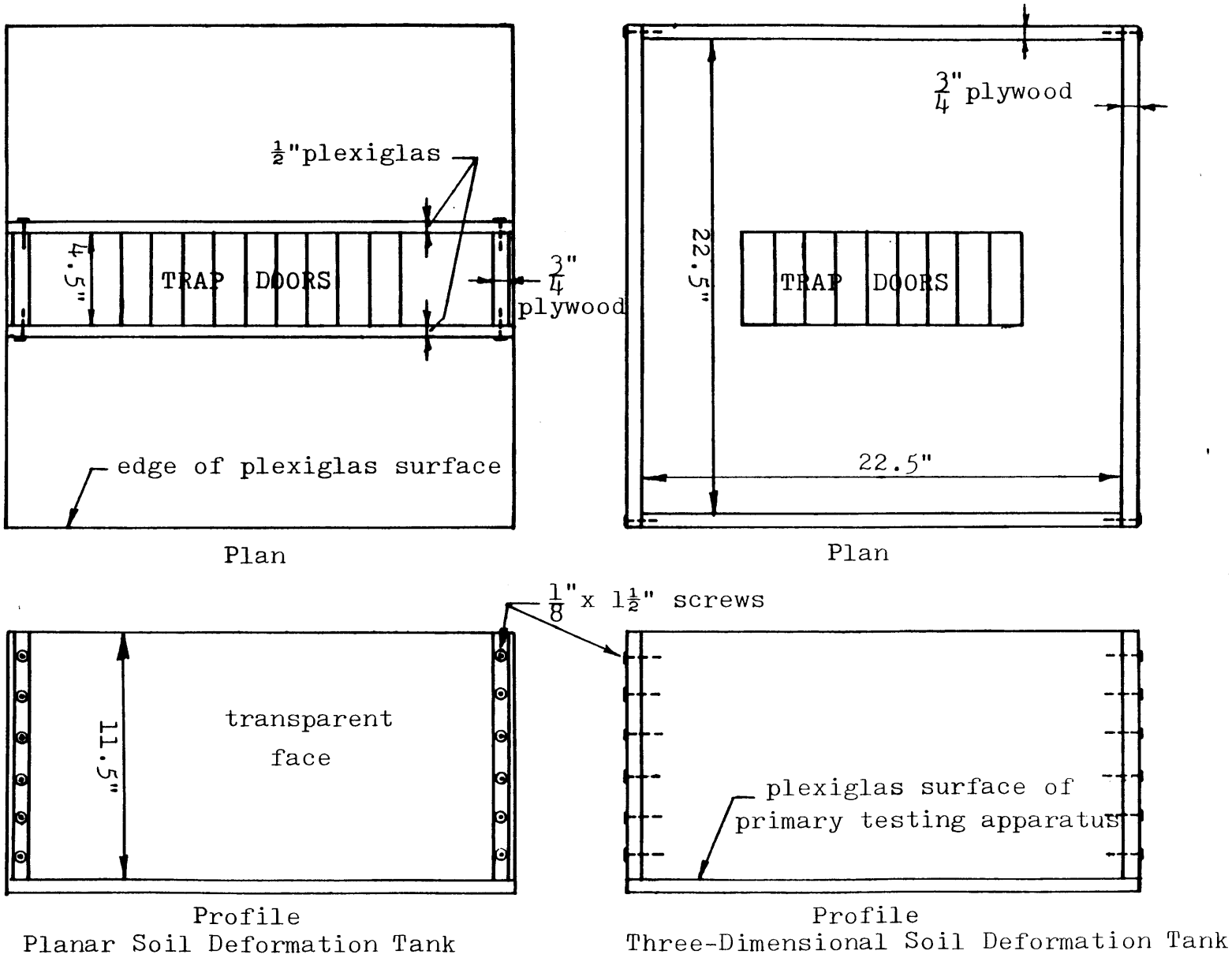

Figure 5.3 Sand Boxes from Primary Testing Apparatus

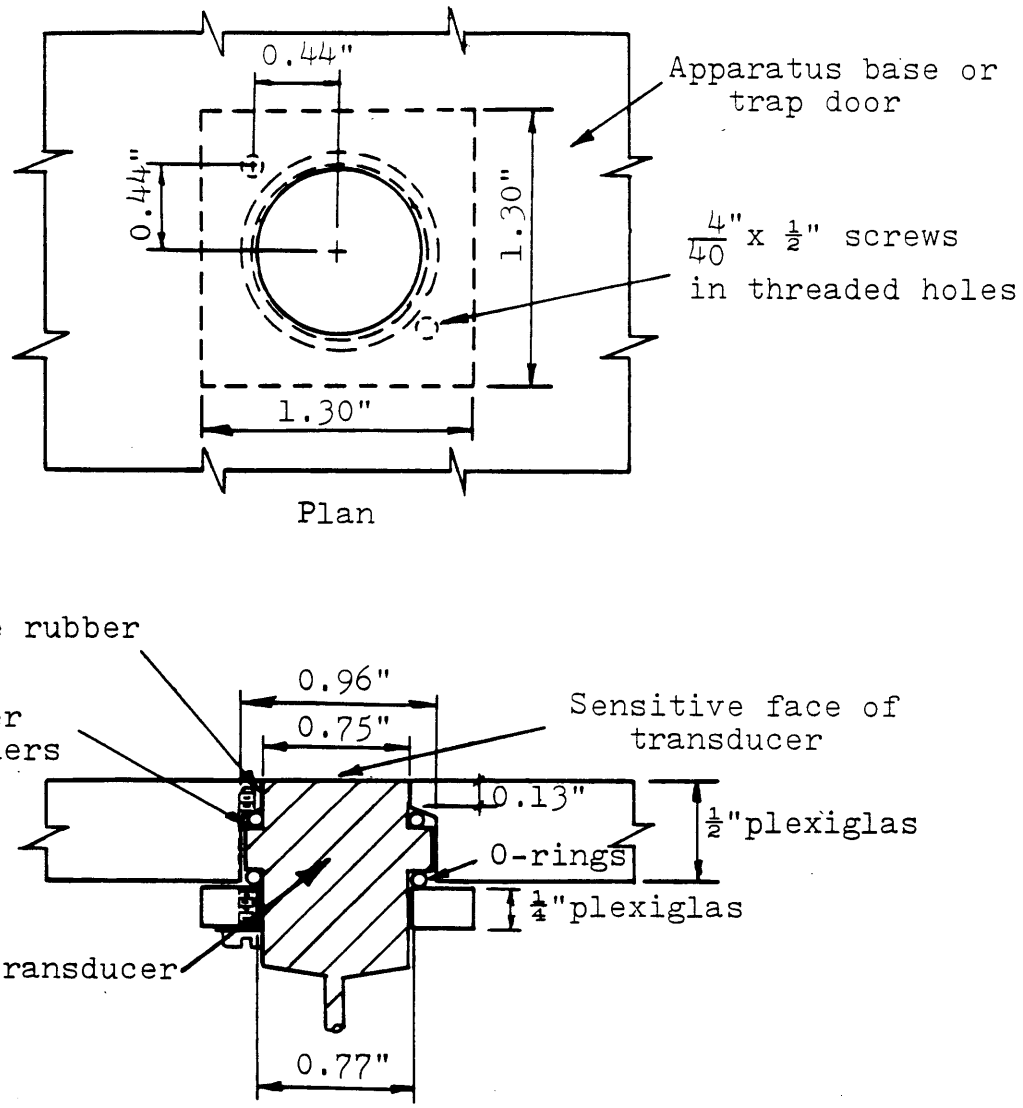

Figure 5.4 Mounting System for Pressure Transducers

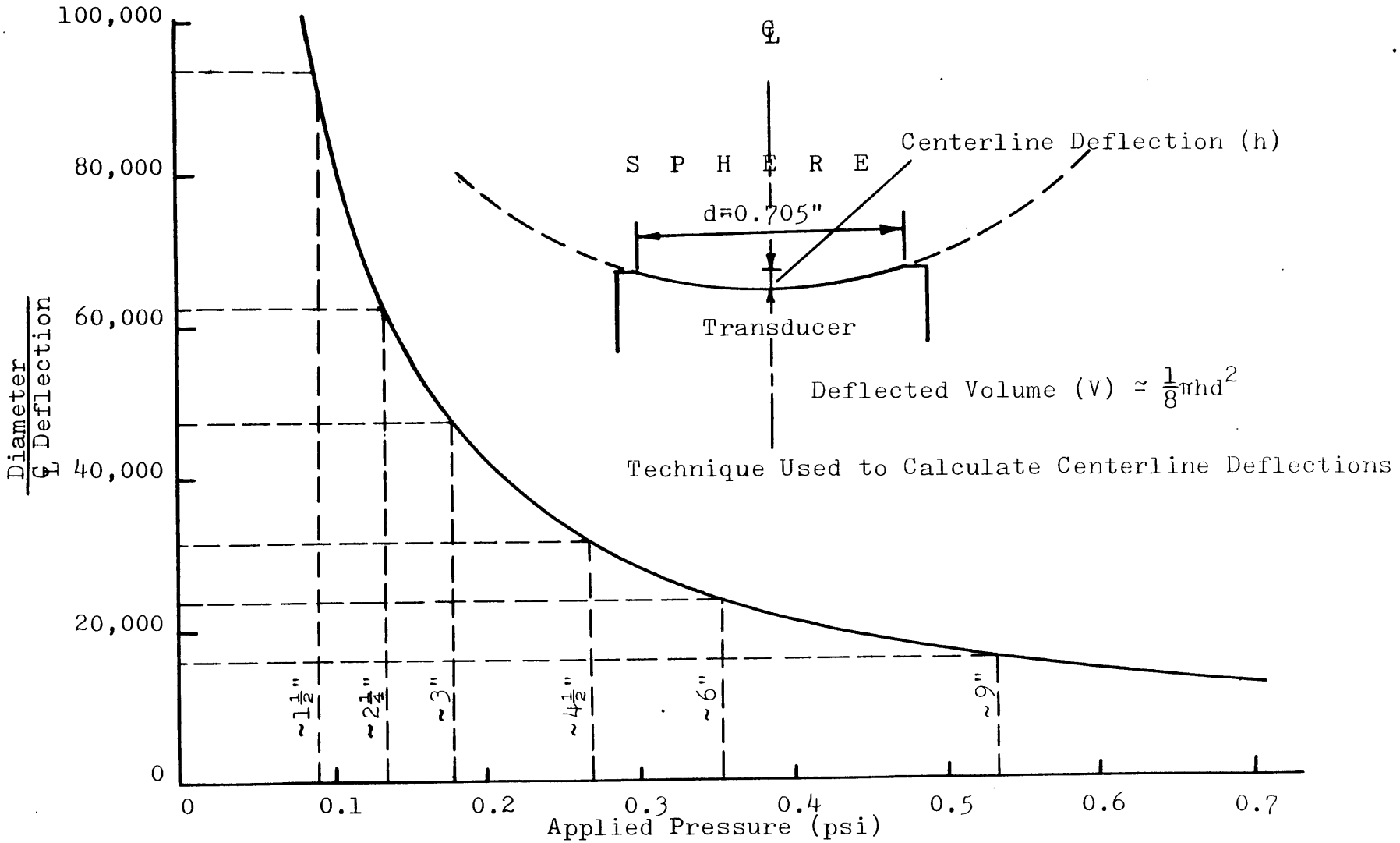

Figure 5.5 Typical Performance Tyco AB Transducer - 25 psi Capacity

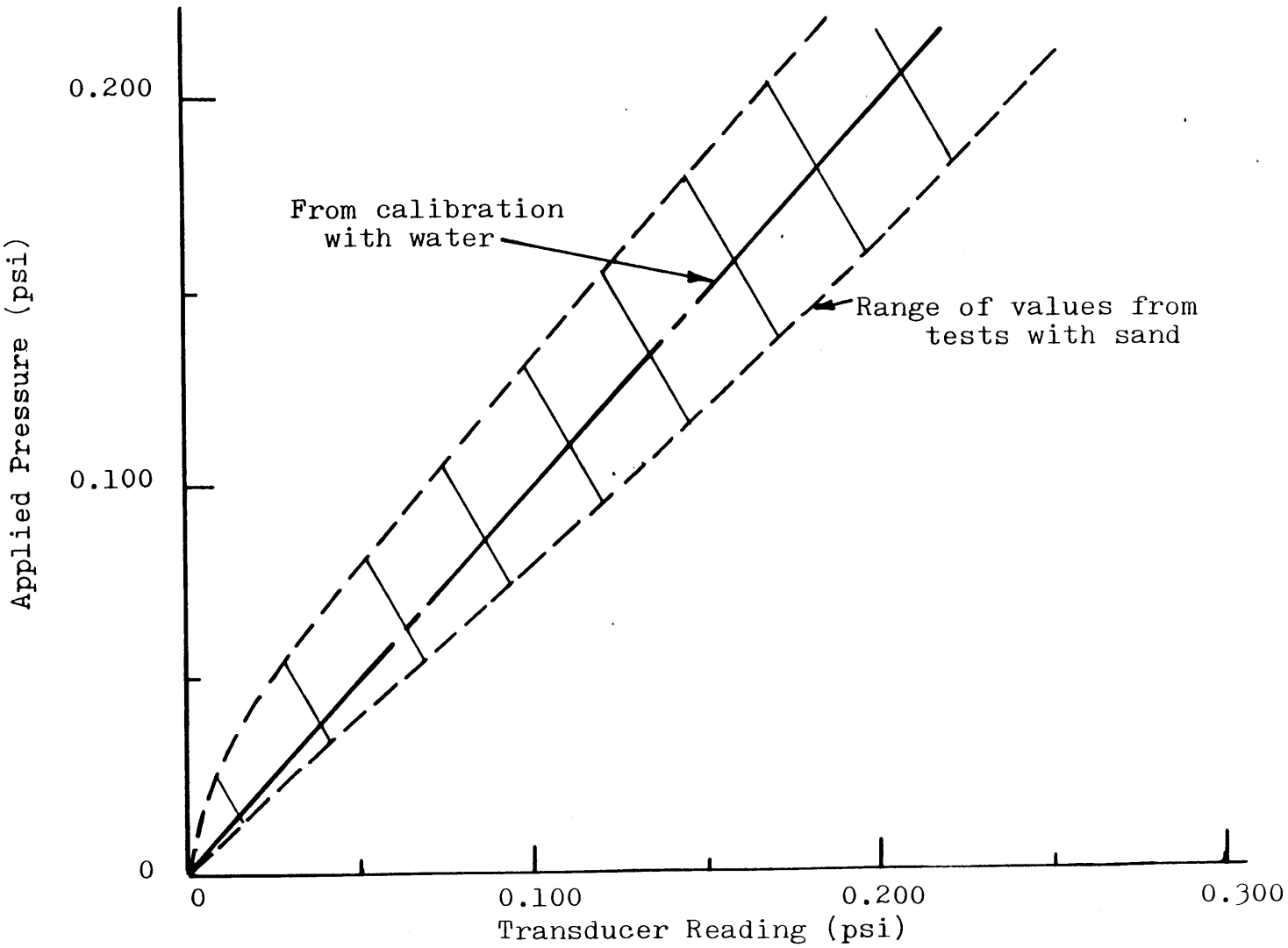

Figure 5.6 Typical Transducer Performance

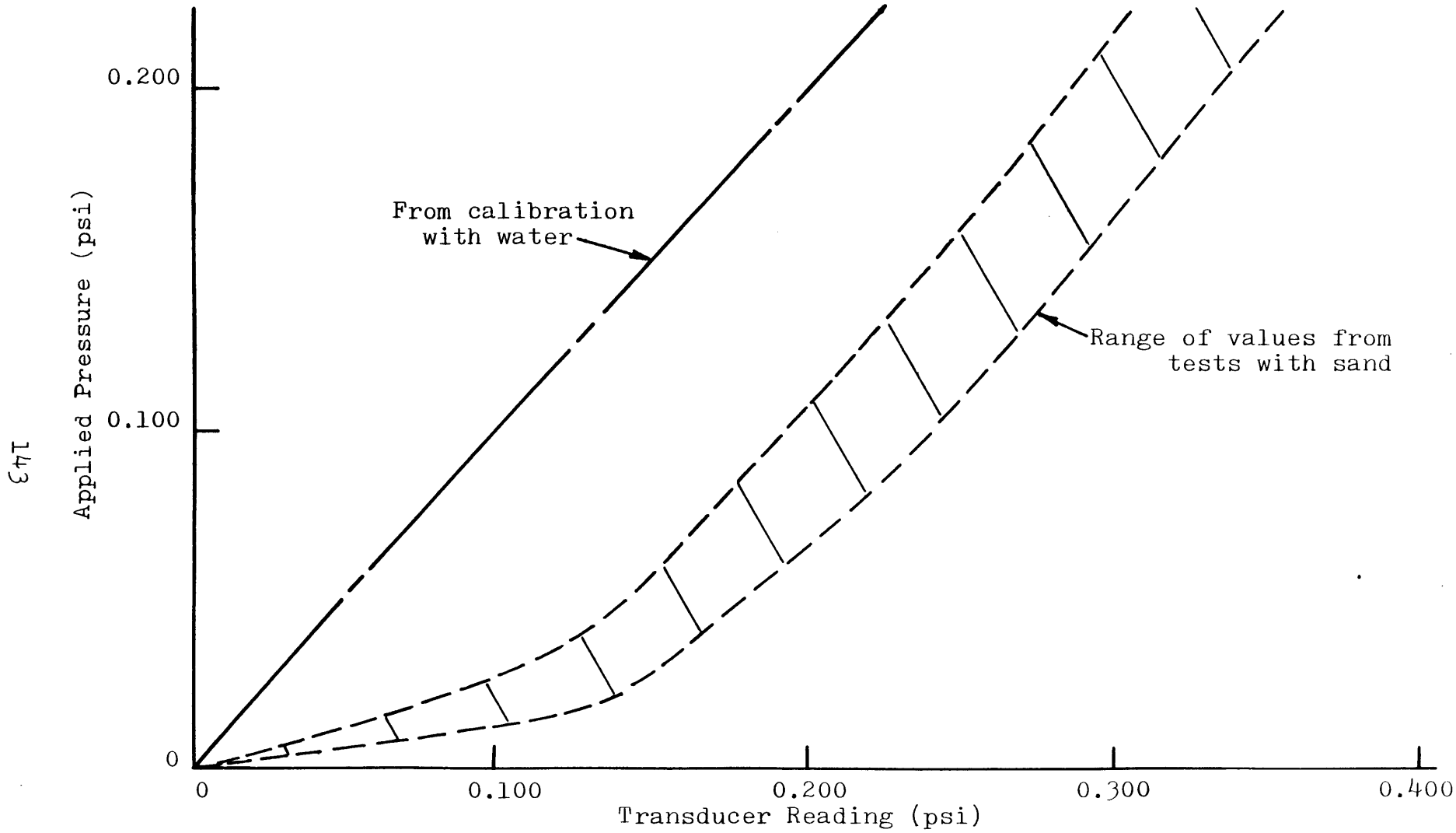

Figure 5.7 Performance of Transducer Number 85

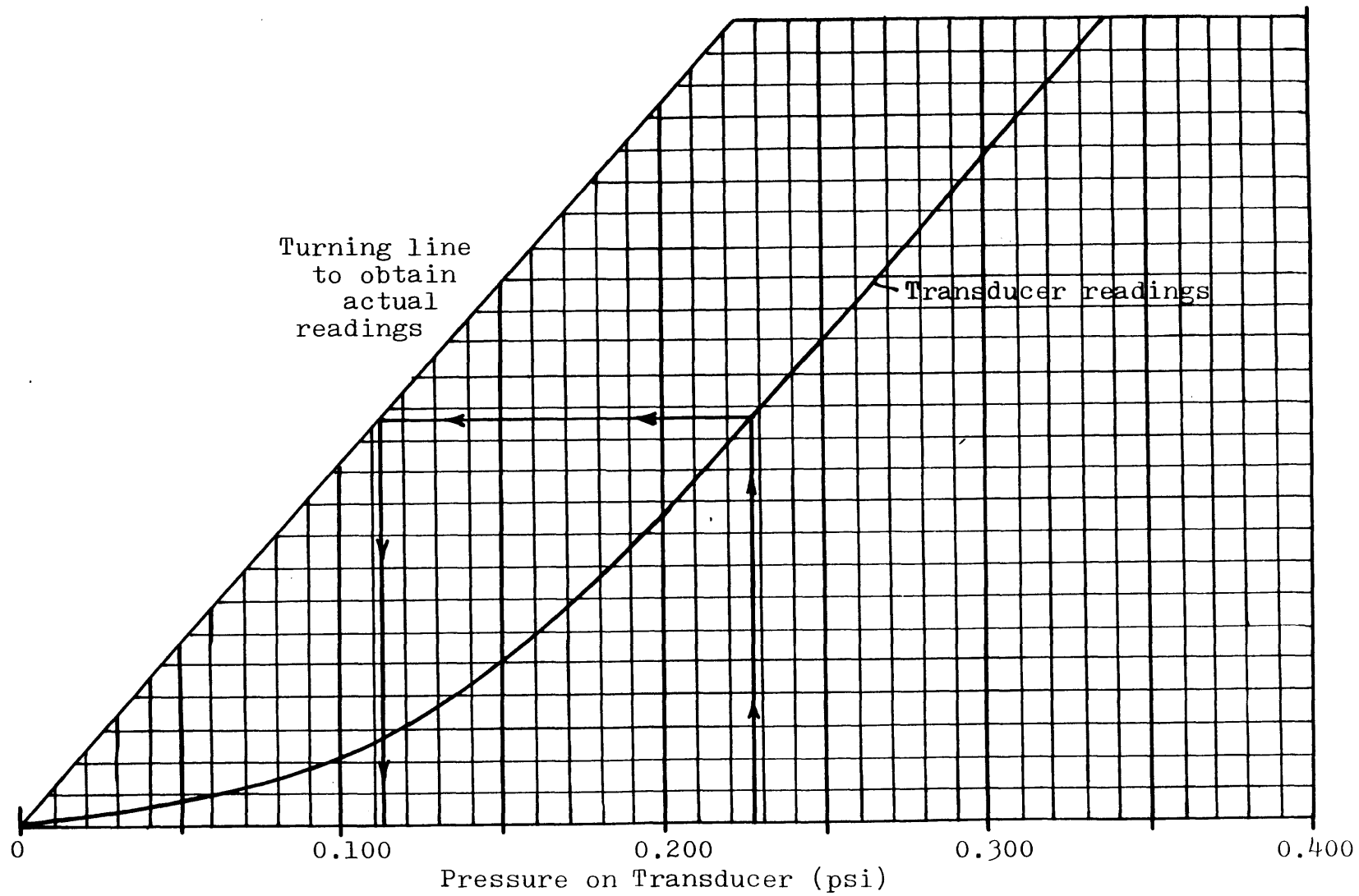

Figure 5.8 Adjustment Curve for Transducer Number 85 Readings

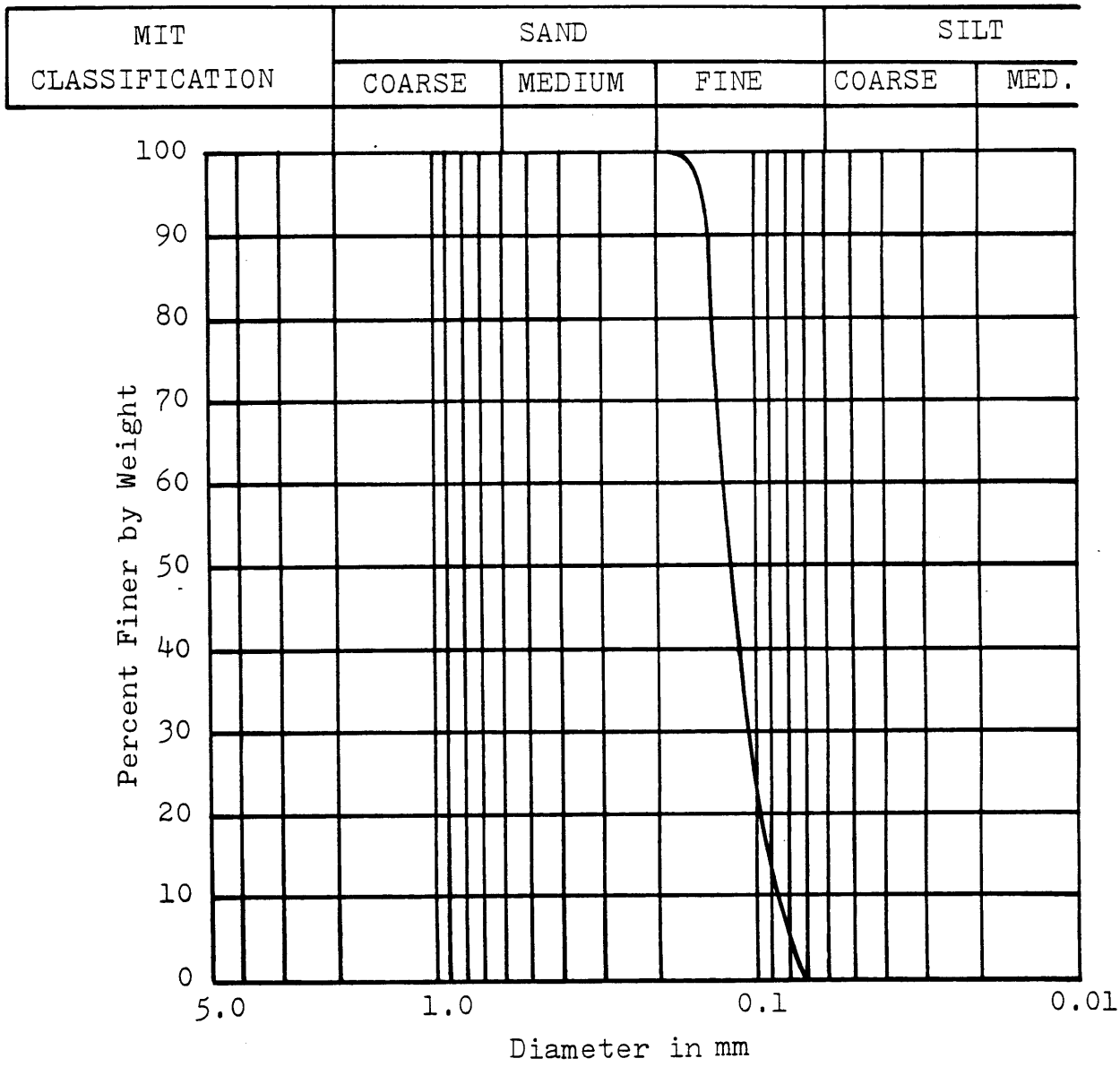

Figure 5.9 Grain Size Distribution --
Fine Leighton Buzzard Sand (120/200)

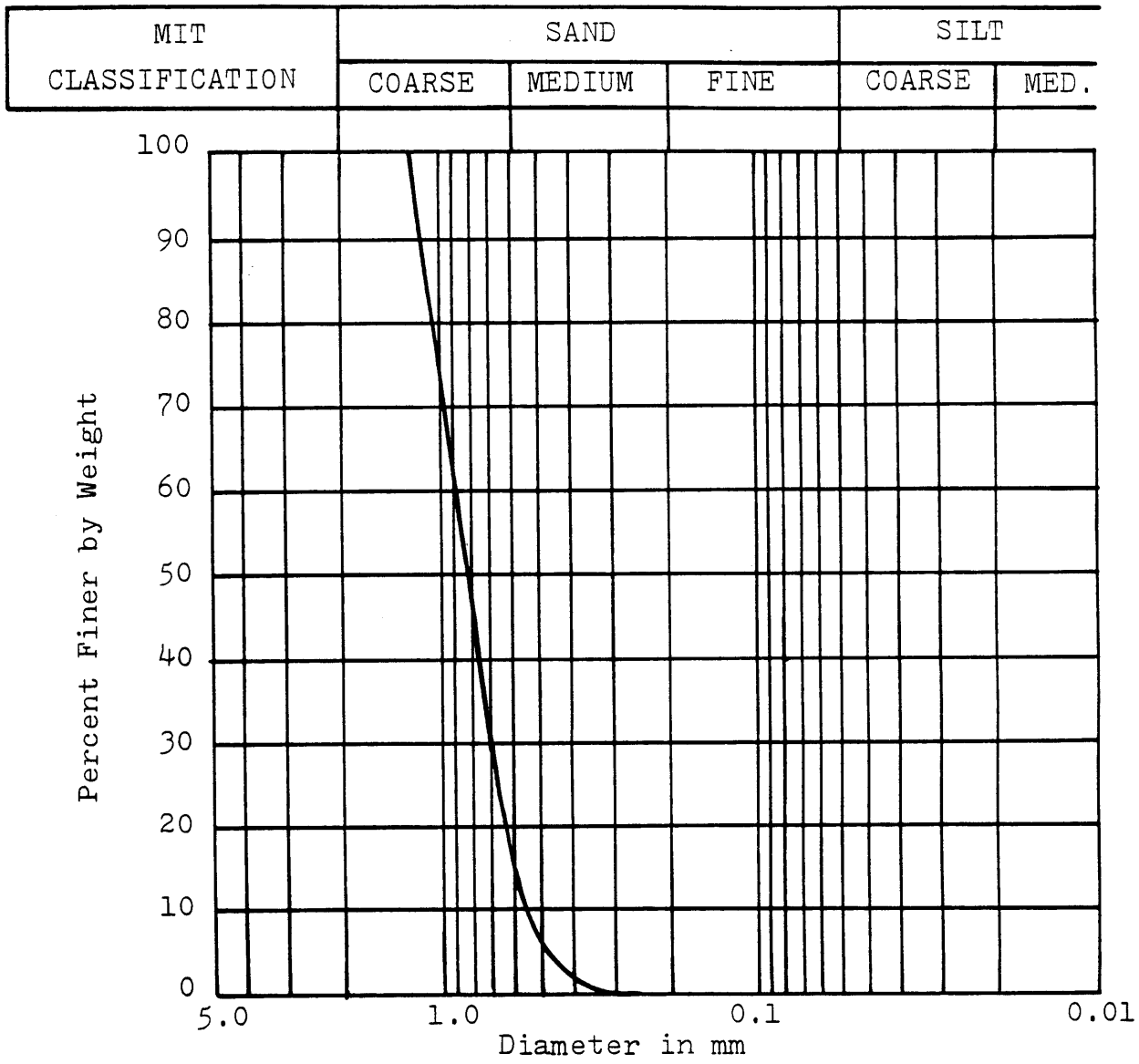

Figure 5.10 Grain Size Distribution --
Coarse Leighton Buzzard Sand (20/30)

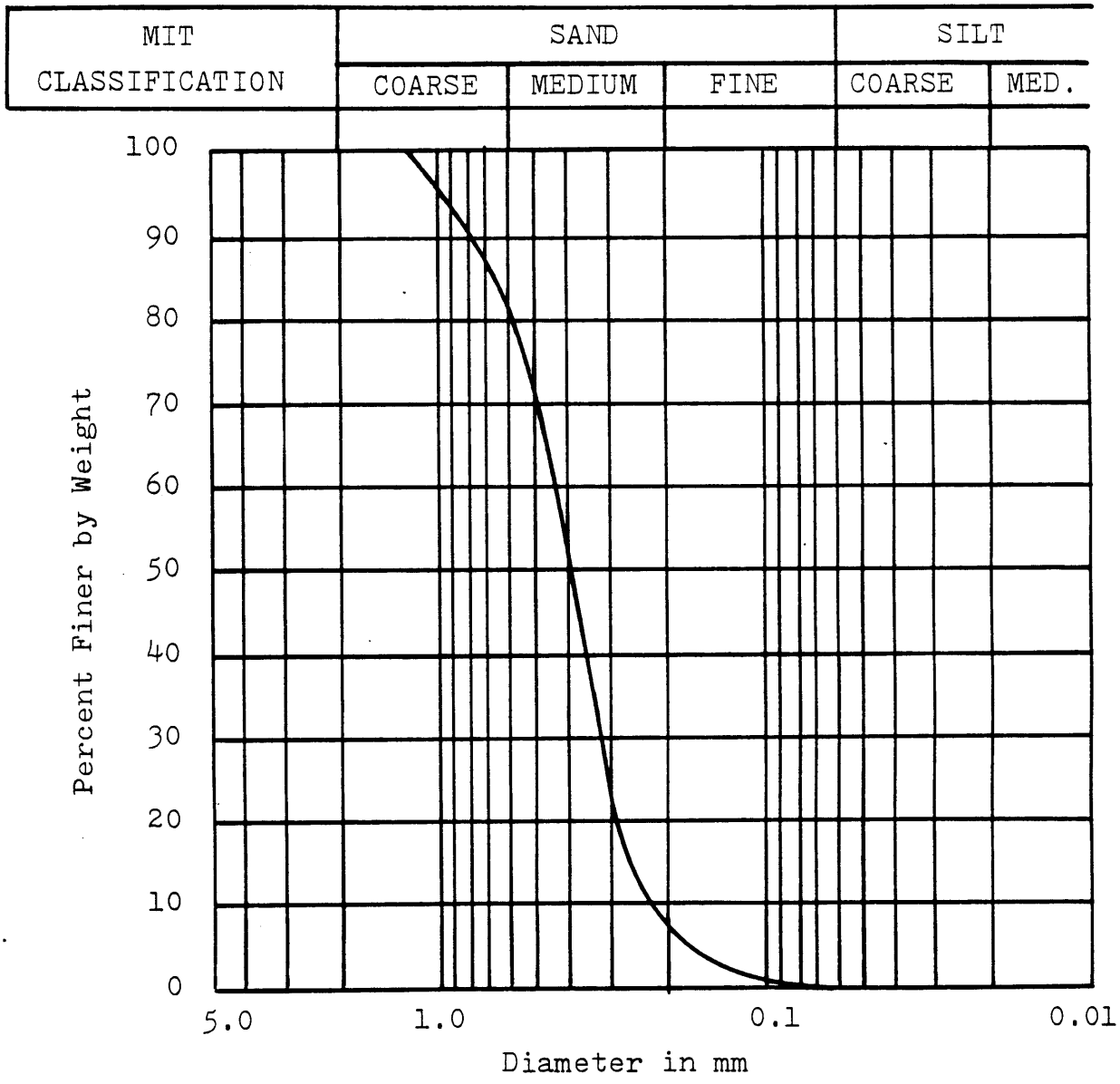

Figure 5.11 Grain Size Distribution -- Medium Tan Sand

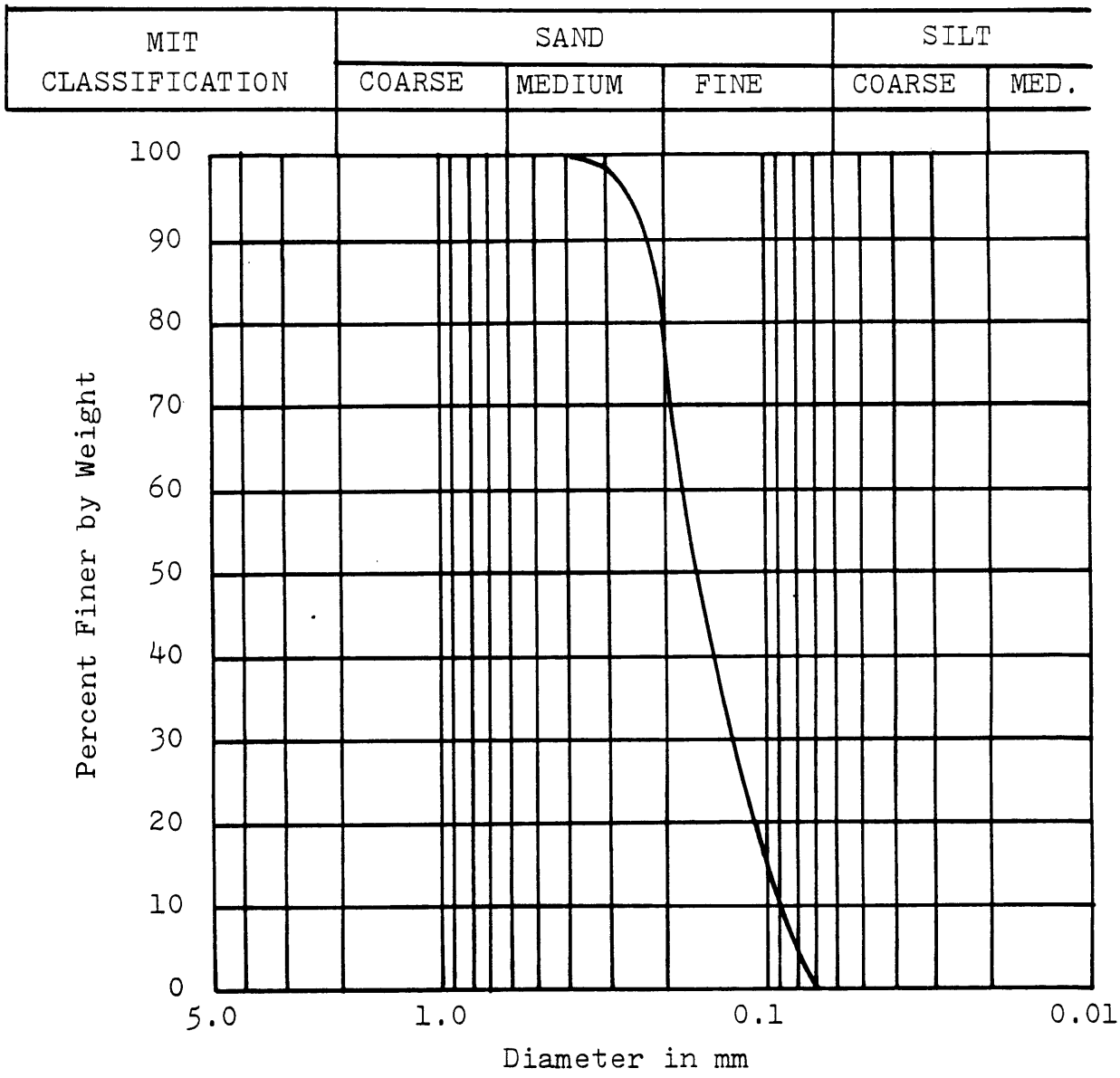

Figure 5.12 Grain Size Distribution --
Fine White Sand

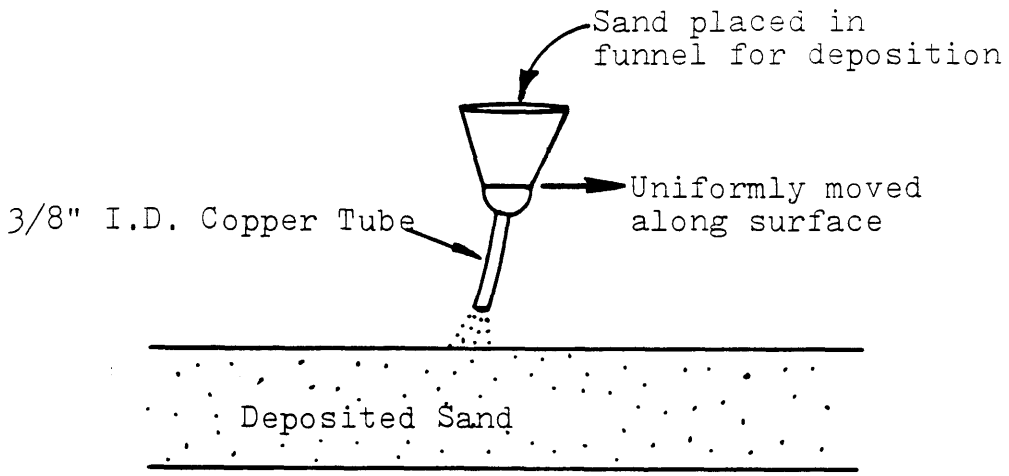

A. Deposition from a Copper Tube

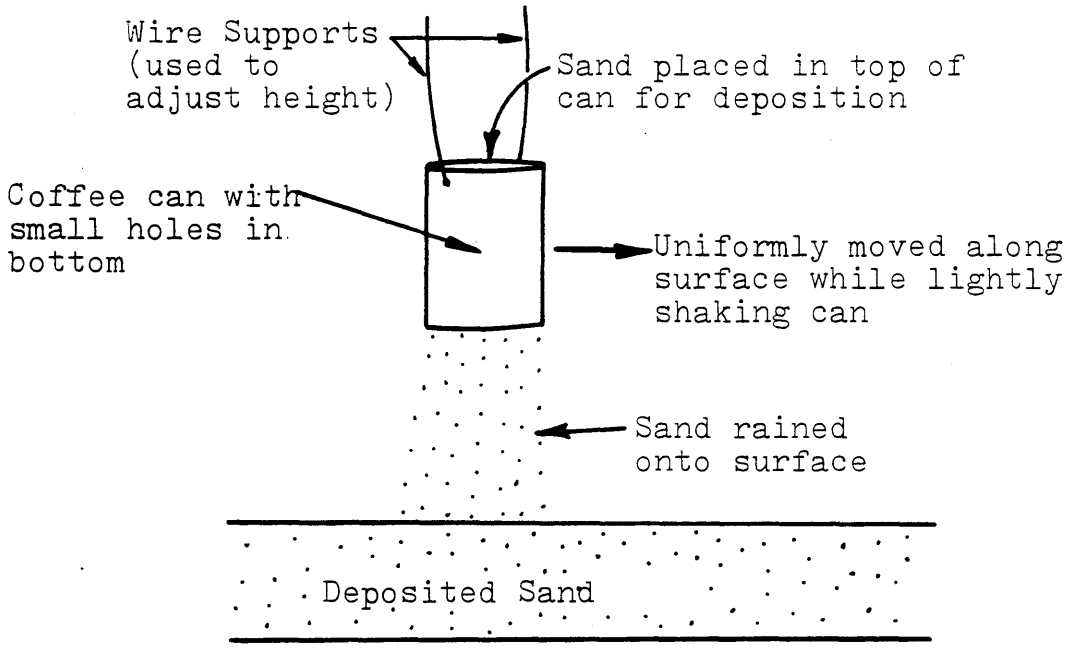

B. Deposition from a Can

Figure 5.13 Sand Deposition Techniques

Sand Type	Sieve Analysis					Specific Gravity (G)	Friction Angle (in degrees)
	D_{10}	D_{30}	D_{60}	C_u	C_z		
Fine Leighton Buzzard (120/200)	0.089	0.105	0.120	1.35	1.032	2.65 *	33^o from triaxial tests *
Coarse Leighton Buzzard (20/30)	0.605	0.705	0.905	1.50	0.910	2.65 **	34^o from triaxial tests **
Medium Tan Sand (also called Bin 23 sand)	0.215	0.320	0.445	2.07	1.070	2.66 ***	38^o from direct shear tests
Fine White Sand	0.091	0.127	0.165	1.81	1.074	2.66 ****	43^o from direct shear tests ****

(Dimensions in mm)

Coefficient of Uniformity (C_u) = D_{60}/D_{10}

Coefficient of Curvature (C_z) = $(D_{30})^2/D_{10} \times D_{60}$

Sources other than this thesis research:
* Bucknam, et. al. (1981)
** Bekenstein (1980)
*** Sien (1983)
**** Carrier (1969)

Table 5.1 Properties of Sand Used

Sand Type	Deposition Technique	
	via Copper Tube	Raining from Can
Fine Leighton Buzzard	95.1	100.2
Coarse Leighton Buzzard	99.4	108.1
Medium Tan Sand	98.4	106.2
Fine White Sand	97.8	104.1

(all densities in pounds per cubic foot)

Table 5.2 Average Densities Produced by Two Deposition Techniques

CHAPTER 6: TEST RESULTS AND COMPARISONS

6.1 General

The experimental program can be divided into three primary series of tests: 1) active arching above a circular trap door; 2) active and passive arching above a rectangular trap door with boundary conditions such that planar soil deformations occur; and 3) active arching above a series of trap doors lowered in succession so as to simulate an advancing tunnel. In addition, a number of tests were aimed at topics such as evaluating the transducer system's performance, measuring values for coefficient of lateral stress (K), and observing ground movements. A list of all tests performed, including the apparatus used, testing configuration, and characteristics of each test is found in Appendix B. Photographs of the primary testing apparatus and typical observed soil deformations during plane strain active and passive arching are found in Appendix A.

The considerable number of tests conducted generated a large quantity of data. For purposes of clarity not all data are presented here. Representative results are given from each set of tests, along with comparisons between actual and theoretical (from approaches presented in Chapters 2 and 3) values for maximim and ultimate arching loads for individual tests. A set of all data acquired can be found in a separate volume entitled "Laboratory Notes on Arching Tests, 1983".

6.2 Results Previously Presented

While most results from this experimental program are presented in this chapter, some information has already been included and discussed in previous chapters at points where this was necessary for understanding of the particular topics. A brief review of these items is presented here.

In defining a plastic flow rule for the sand used in this investigation (Section 3.2.5) the question as to appropriate values for the angle of dilation (ν) arose as well as

how this angle varies during trap door displacement. As explained in that section, ν can be approximately determined by observing the angles at which velocity discontinuities develop during trap door translation. To accomplish this the primary apparatus with the planar soil deformation tank was used. Thin bands of contrasting color sand made the locations of these discontinuities more apparent, and photographs were taken (some of which are reproduced in Appendix A) from which the angle of dilation was determined. The results are shown in Figure 3.5 and Table 3.1 for a lowering trap door (active arching) and Figure 3.6 and Table 3.2 for a rising door (passive arching). All results were obtained from tests using the Medium Tan Sand. Extrapolating from these results to obtain initial values for the angle of dilation, one finds that the maximum value of ν lies in the range of 35 ± 5 degrees. This is close to the friction angle (ϕ) for this material (38°), obtained from direct shear testing, and therefore supports the assumption used in Chapter 3 that initial values of ν approach the material's friction angle.

In Section 4.6 an approach was presented to predict the approximate size and shape of the settlement trough which will develop at the surface above a soft ground tunnel. In conjunction with that discussion results obtained from tests with the primary apparatus and the planar soil deformation tank were presented. The observed surface deformations, at the end of several tests, were plotted and compared with those predicted (Figures 4.10 and 4.11). Agreement was generally good with the troughs somewhat narrower and deeper than one would expect.

In evaluating the validity of the calibration technique used for the stress measuring system (Section 5.4.4), individual transducer readings, made during sand deposition, were combined for a number of tests. These readings were plotted against the corresponding theoretical pressure, calculated from knowledge of the total weight of material. Two such plots are shown in Figures 5.6 and 5.7. In addition, an investigation was made to determine whether localized arching occurs

above these transducers as a result of diaphragm deflection and, if so, to what extent it occurs. Results of this investigation are presented in the next section.

6.3 Arching Above Pressure Transducers

As mentioned previously (Section 5.4) it had to be established whether or not the transducer diaphragm displacement, associated with changes in the stress state within the soil, would lead to localized arching. Sufficiently large diaphragm displacements will cause the transducer to act as a yielding structure with rigid adjacent surfaces (as shown in Figure 2.9), and will lead to stress readings which bear little resemblance to the stress state without the transducer.

A series of tests was performed with the primary test apparatus and planar soil deformation tank in which sand was deposited into the tank in discrete quantities of known weight with transducer readings recorded after each quantity was placed. After the entire amount of sand was deposited, the material was removed via the vacuum system, this again in stages with periodic readings taken. Typical results for two transducers are shown in Figures 6.1 and 6.2. During the loading phase the readings are generally less than the theoretical stress based on the total weight of material placed, while for the unloading portion the readings tend to be larger than anticipated. This hysteretic behavior is as would be expected if some arching did occur. During loading the diaphragm deflects downward thereby reducing the load on the transducer and redistributing it to the sides (active arching). As unloading occurs the diaphragm moves upward developing passive arching with stresses on the transducer exceeding the actual stress state within the soil. The behavior shown near the end of the unloading phase, where readings actually indicate negative stresses, is not understood at the present time, but was observed in a number of calibration tests.

To further investigate the performance of the transducers, a test was performed following the procedures outlined above,

but having multiple load-unload cycles. Results from this test (using the same two transducers as Figures 6.1 and 6.2) can be found in Figures 6.3 and 6.4. It can be seen that smaller hysteretic loops are generally located within the limits of the larger ones. The behavior described here has been observed by other researchers when using similar boundary type pressure cells with sand (Trollope and Lee, 1961, and McNulty, 1965).

The actual and measured stresses were generally within 10 to 15 percent of each other, but on several occasions transducers were found to overestimate the stress by up to 30 percent during unloading cycles (this happened during tests with the highest maximum stresses, Tests 52 and 53). It was also observed that tests run at smaller stress levels exhibited less hysteresis (Figure 6.5). Until a better understanding of this arching behavior is obtained, no meaningful adjustment can be made to the measured stress values. The measured values are thus reported as such and are not corrected for diaphragm deflections. It can, however, be appreciated that any attempt to correct the results presented in this chapter so as to account for diaphragm deflection would increase the indicated magnitude of load reduction during active arching and similarly increase the magnitude of load increase occurring as a consequence of passive arching.

6.4 Distribution of Stresses Across a Trap Door

Much of the previous work on arching, particularly that involving vertical sliding surfaces, concentrates on providing solutions for the total force acting on the yielding structure without considering its distribution. Terzaghi (1943) assumed a uniform distribution for both active and passive arching, while Szechy (1966) proposes a triangular distribution for a translating rigid structure undergoing active arching. Since pressure transducers, as used in this investigation, measure the stresses at various points across the trap doors, they provide information on this distribution.

From Figures 6.18 through 6.23, which will be discussed in detail in Section 6.7, one can see that under active arching the vertical stress at the door's centerline is greater than that slightly to one side which, in turn, is greater than that near the edge. If one plots a cross-section of these stresses (Figure 6.6.A) a parabolic to triangular shaped distribution is obtained. Harris (1974) performed similar tests (see Figure 2.15) with more cells mounted on the trap doors, obtaining distributions again between triangular and parabolic in shape (see Figure 6.6.B). When the trap door undergoes passive arching the stresses across the door are nearly uniform with slightly higher values occurring near the door's edge (Figure 6.6.A).

The shapes of stress distributions observed in this experimental program closely agree with what one would predict based on plasticity theory. During active arching a triangular wedge of soil (Figure 3.14.A) develops above the door, while the trapezoidal mass shown in Figure 3.18.A develops during passive arching.

For the purpose of comparing results from this investigation with those from others, as well as with the various formulae proposed, it has been assumed that a triangular stress distribution exists on the trap door for active arching, and a uniform distribution for passive arching. With this assumption of uniform stresses during passive tests, the transducer reading is considered to be the mean stress on the door and the total trap door force can be obtained through multiplication by the door's area. During active arching transducers are assumed to be indicating the stresses due to the portion of the stress distribution directly above the diaphragm (see Figures 6.7 and 6.8). From this assumption combined with that of a triangular distribution (or conical distribution for a circular trap door) the approximate total force on the door can be determined by first multiplying transducer readings by the appropriate correction factor (given in Figures 6.7 and 6.8) and then multiplying by the door's area.

6.5 Plane Strain Arching

6.5.1 General

The results presented in this section are from tests with the primary test apparatus equipped with the planar soil deformation tank. This configuration models the condition of a translating rigid strip of width B and infinite length where all soil deformations are perpendicular to the infinite axis of the door. Tests were run with varying types and depths of sand, as well as with the doors lowering (active arching) and rising (passive arching). By changing the orientation of the tank it was also possible to obtain trap door widths of $1\frac{1}{2}$ or $4\frac{1}{2}$ inches.

Results are presented and compared with those predicted by this author and others. A dimensionless 'load factor' (C_c) is used for this comparison, which is defined as:

$$C_c = \frac{F}{\gamma B^2} \qquad (6.1)$$

where F is the force per unit length of door parallel to the infinite axis (i.e. $F = B(\sigma_v)_{avg}$), γ is the soil's unit weight, and B is the trap door width.

6.5.2 Active Arching Case

Nineteen tests were conducted from which active arching data was obtained. Figure 6.9 shows the typical behavior which was observed. Vertical stresses decrease rapidly as displacement begins until they reach a minimum value. This point will be referred to as that of 'maximum arching'. As further displacements occur the stresses increase somewhat with a relatively constant value obtained as displacements approach about 10 percent of the trap door width. This is referred to as the 'ultimate arching' state in this presentation. A summary of results from the tests in this series is found in Table 6.1. Four sand types were used with varying soil cover to trap door width ratios (H/B) ranging from 1.0 to 6.0. Tests numbered 66 and 67 had $4\frac{1}{2}$ inch trap doors while all others were $1\frac{1}{2}$ inch. Stress values given in the

table are those actually measured. To obtain the Trap Door Forces (F) and Load Factors (C_c) which are indicated, one must first adjust the given stresses by the appropriate correction factor (to account for the assumed triangular stress distribution across the trap door - Figure 6.7).

Defining load reduction on a trap door as the ratio of "decrease in force from the initial value" to "initial force due to the sand overburden" ($(F_o-F)/F_o$), one finds that for points of maximum arching, load reduction ranges from 68.1 percent for H/B = 1.0 to 93.4 percent with H/B = 6.0. The average for all tests was 87.6 percent. For the ultimate arching state load reduction ranges from essentially zero at H/B = 1.0 to 86.4 percent at H/B = 5.0. Some tests were not carried to large displacements, therefore results may overestimate the ultimate load reduction.

Figures 6.10 and 6.11 provide comparisons between experimental results and predicted values through plots of load factor (C_c) versus H/B. Figure 6.10 presents experimental results for the maximum arching points from tests conducted for this thesis and from Terzaghi (1936) and Harris (1974). Also shown are curves representing results predicted by the various theories reviewed in Chapter 2 and by the plasticity theory approach in Chapter 3. These expressions are summarized in Table 6.2. All curves are drawn for $\phi = 35^\circ$ and K = 1.2 (see Section 6.8). The plasticity theory solution is also shown for several other friction angles. Figure 6.11 shows results at the ultimate arching state, as well as curves for the corresponding plasticity theory solution at several friction angles.

Though there is scatter among data points in Figures 6.10 and 6.11, it is evident that the proposed plasticity theory solution provides: 1) better predictions of load factors at maximum arching than any of the existing theories and 2) reasonably good predictions of load factors at ultimate arching (for which it is the only approach available). It is especially encouraging to note that experimental results

obtained by other researchers (Terzaghi, 1936 and Harris, 1974) agree very well with values predicted by the proposed plasticity theory solutions.

6.5.3 Passive Arching Case

An examination of passive arching was not originally within the scope of this experimental program, however after reviewing papers by Matyas and Davis (1983a and 1983b) this author decided that the primary testing apparatus might provide the possibility for studying passive arching around buried culverts and ground anchors. Eight tests were thus included with two sand types and H/B ratios ranging from 1.0 to 4.0. Figure 6.12 presents the results from two of the tests representing the extreme H/B ratios. The curves are typical of the behavior observed. Stresses increase rapidly as displacement begins, eventually reaching a maximum value at the maximum arching point. With further displacement the stresses decrease gradually, but were not observed to obtain constant ultimate values for the range of displacements used (δ/B up to 30 percent). A summary of results from the tests in this series is found in Table 6.3. The ultimate values for stress and load factor, given in this table, are generally those corresponding to the maximum displacement for each test. The observed load increase on the trap door at the point of maximum arching ranged from 27 percent for H/B = 1.0 to 286 percent with H/B = 4.0.

Figures 6.13 and 6.14 provide a comparison between experimental results and predicted values, through plots of C_c versus H/B. Figure 6.13 shows experimental results for maximum arching from tests conducted for this thesis and from some tests by Matyas and Davis (1983b), as well as showing curves corresponding to the various theories. The experimental results and predicted curves for the ultimate state are in Figure 6.14. Expressions underlying the predicted curves are summarized in Table 6.4. Unless noted otherwise, curves are drawn for ϕ = 35 degrees and K = K_a where:

$$K_a = \frac{1 - \sin \phi}{1 + \sin \phi} \qquad (6.2)$$

The active value for coefficient of lateral stress is used to be consistent with work by Spangler (1973), however no experimental justification for this could be found.

At maximum arching (Figure 6.13) the experimental results of this investigation are consistent with those obtained by Matyas and Davis (1983) using an entirely different experimental approach. This fact supports the applicability of the primary test apparatus to investigations of passive arching around buried structures.

The proposed plasticity theory solution closely follows the general trend of experimental data points; it consistently overestimates the load factor (and thus trap door force), but only by about 5% when compared with Matyas' and Davis' (1983) data and approximately 10 to 15% when compared with data obtained by this author. It is believed that a part of this difference between predicted and observed values can be attributed to the procedure employed for data interpretation. For passive arching tests a uniform stress distribution is assumed to exist across the trap door with the transducer reading interpreted as being the mean vertical stress. The true distribution is, as was previously shown in Figure 6.6, higher at the edges and lower toward the center. Since the transducer is centered on the door, it will record a stress somewhat less than the actual mean value, and therefore the assumption of this being the mean vertical stress causes resulting load factors and trap door forces to be lower than actual values. Without further experimental work aimed at better determining the stress distribution across the door, no estimate can be made of the error that this assumption introduces nor can the data be corrected for the non-uniformity of the distribution.

There are clearly not enough data available to draw any strong conclusions regarding agreement with predicted values for ultimate arching. What data are presented in Figure 6.14 do lie near the proposed plasticity theory prediction, at low H/B ratios, which is encouraging (the results shown for

test number 63 (H/B = 4.0) are misleading since, as can be seen in Figure 6.2, the vertical stress was still decreasing (and with it C_c) when the maximum deformation was reached). Generally, the relative displacements associated with the ultimate state are well beyond what would be experienced adjacent to any real buried structure, thereby limiting practical applications of any solution for loads at ultimate passive arching.

6.6 Active Arching with a Circular Trap Door

A series of tests performed with the preliminary testing apparatus provided information on active arching above a circular trap door (due to the circular trap door's design--Figure 5.1--it could not be raised to investigate passive arching). Since these tests involve three-dimensional arching the dimensionless 'load factor' (C_c) had to be modified to:

$$C_c = \frac{F}{\gamma B^3} \qquad (6.3)$$

where F is now the total force acting upon the trap door attributable to the sand's presence, and the other terms are as defined previously.

Five tests were performed in this set with a summary of key results appearing in Table 6.5. Three types of sand were used with cover to diameter ratios (H/B) varying from 0.9 to 3.2. The general behavior was consistent with that for the plane strain active arching case, rapid stress reduction occurred with small displacements until a minimum value was obtained, $(\sigma_v)_{min}$, after which the vertical force gradually increased, reaching a fairly constant value, $(\sigma_v)_{max}$, at large displacements. This behavior was consistent for all tests (except number 16) with load reductions, after adjustment for the assumed conical stress distribution (Figure 6.8), ranging from 89.0 to 97.9 percent (average 93.5 percent) at the point of maximum arching and from 78.8 to 91.2 percent (average 85.7 percent) for the ultimate state (large displacements). Test number 16 exhibited a decrease in load reduction

between the maximum arching and ultimate arching which was approximately twice that for the other tests. The Medium Tan Sand used did not exhibit this behavior in subsequent arching tests, therefore this test's results are considered anomalous.

Figure 6.15 shows the load factors, corresponding to maximum arching, plotted against the cover to diameter ratios for the five tests. Also shown are the curves of predicted values (at several friction angles) for three-dimensional silo theory (Section 2.2) and plasticity theory ($\nu = \phi$) solution (Section 3.7.2). Figure 6.16 presents a C_c versus H/B plot for the ultimate state, with experimental results and curves for the plasticity theory (with $\nu = 0^o$).

One can see from Figure 6.15 that plasticity theory predicts load factors at maximum arching much better than three-dimensional silo theory. However, at both maximum and ultimate (Figure 6.16) arching plasticity theory consistently overestimates the load factor and thus trap door force by about 30 percent (based on $\phi = 35^o$ solution). Such an overprediction did not occur for plane strain active arching (Section 6.5.2) and it is thus felt that this overestimation is related to the many plane strain assumptions inherent in the plasticity theory formulation (Chapter 3). For reasons not fully understood at present, three-dimensional arching produces more significant load redistributions than can be predicted through simple extensions from plane strain arching.

6.7 Simulation of Arching Around an Advancing Tunnel

A program of eighteen tests was conducted aimed at exploring the pattern of vertical stress redistribution developing on and adjacent to a structure, such as a tunnel, as it advances through a soil mass. The primary testing device was used, equipped with the three-dimensional soil deformation tank.

Advancing of the tunnel heading was simulated by lowering each of the nine trap doors in succession by an equal amount. This is illustrated in Figure 6.17.A which presents

a series of profile sections along the common axis of the trap doors. Each successive section shows one additional trap door in the drop position. Also shown in this figure is a 'line of stress measurement'. This line represents the location of the pressure transducers mounted in the indicated trap door and adjacent base (see Figure 5.2 for exact transducer locations). Before lowering any trap doors and then following the lowering of each door, a set of stress readings was recorded. Each stress value recorded is assumed to be that present at the transducer's center. A set of readings therefore represents the stresses at points along a line perpendicular to the axis of the simulated tunnel. As successive trap doors are lowered the tunnel heading approaches this line and advances beyond it. This process leads to the pattern of effective recording locations for vertical stress which is shown in Figure 6.17.B. Each line of effective recording points corresponds to one of the profile sections in Figure 6.17.A (letters identify each). The direction of simulated tunnel advance and location of the face are as indicated. Effective recording points on the trap doors denoted as "in drop position" measure vertical stresses on the tunnel while all other locations record vertical stresses within the adjacent soil (actually at interface of base-soil or undropped trap door-soil).

Table 6.6 summarizes the sets of tests performed along with the key variables used. Two sands were employed, along with soil cover to trap door width ratios (H/B) ranging from 0.5 to 2.0. Based on the results presented in Chapter 4 for typical levels of ground movement around tunnels, a displacement ratio (δ/B) of one percent was considered appropriate for these tests. To explore the sensitivity of the observed stress distribution to changes in δ/B, the first two sets of tests were performed with all variables identical except δ/B (Figure 6.18 represents tests with $\delta/B = 0.01$ and Figure 6.19 tests with $\delta/B = 0.05$). Stronger stress redistribution occurred in the tests with the higher level of displacement. This

result is interesting in that it is inconsistent with previous experimental findings (Terzaghi, 1936 and Ladanyi and Hoyaux, 1969). At present, no explanation can be given for this behavior.

Figures 6.18 through 6.23 present normalized stress distributions obtained from each set of tests. The numerical values given for each effective recording point are the ratios between stress values at that point and the initial stress before any doors are lowered (this ratio is the average for all tests in a set). Also shown in these figures are approximate distributions of stress which are based on linear interpolation between recording points.

It should be noted here that (uncorrected) initial stress readings for the transducer position in the base immediately adjacent to the trap doors were consistently lower than the overburden. During a test this condition continued until the tunnel advanced to a point adjacent to the transducer (profile F in Figure 6.17.A). These lower stress values are believed to be the result of deflection of the plexiglas base's edge (adjacent to the trap doors) during sand placement, which leads to development of active arching above the transducer (see insert in Figure 6.17.B). To account for this stress reduction this position's readings in advance of the tunnel were adjusted upward by the difference between the overburden and initial stress reading.

The results clearly show that approaches which do not consider three-dimensional behavior will incorrectly model the stress redistribution in the vicinity of a tunnel's face. Even at shallow depths the presence of the structure affects stresses more than one diameter in advance, at least $\frac{1}{2}$ diameter to each side, and $1\frac{1}{2}$ diameters behind the face. Behind the line (noted in Figure 6.20) at about $1\frac{1}{2}$ diameters from the face, the stress distribution in all cases is essentially constant. Ahead of this line (toward the face) the shapes of stress distributions vary somewhat, with those from tests with the least overburden being much less gradual in their transitions and

having a region of near constant stress across much of the door (compare series of Figures 6.18 through 6.22). This results from a lower total magnitude of arching being mobilized at small overburdens with almost no load reduction indicated near the tunnel's centerline.

In all tests, zones of high stress, so called 'abutments', occurred ahead of and at the sides of the advancing structure. Stresses in excess of twice the overburden were measured at the side abutments, and of nearly $1\frac{1}{2}$ times the overburden were measured ahead of the face. Due to limitations as to how close to the trap doors one can mount the pressure transducers, the limit of stress increase in the soil adjacent to the structure could not be determined. The results also show that as the depth of cover increased, the zone of stress redistribution also increased somewhat in area (compare, for instance, Figures 6.18 (H/B = 0.5) and 6.21 (H/B = 2.0)).

Stress reduction over the lowered trap door was a maximum near the advancing face and at the sides, while it was a minimum along the centerline. Harris (1974) from similar experiments (Section 2.11) noted the formation of a rear abutment behind the face which was more pronounced and closer to the face for small depths of soil cover. The results of the tests presented here also show such an abutment at δ/B of 0.5 (Figures 6.18 and 6.22), but not at larger soil depths. The level of stress reduction over the trap doors increased with increasing soil depth (again compare Figures 6.18 (H/B = 0.5) and 6.21 (H/B = 2.0)).

Several comments can now be made relating this section's results to the proposed plasticity theory approach. The general pattern of stresses is in good agreement with the theory. Thinking of the tunnel as one end of a long rectangular trap door in the lowered position, one would expect the body of soil which applies the load to the tunnel to have a shape similar to that previously presented in Figure 3.21. A soil body of this shape would produce stresses similar to the observed distributions. In Figures 6.18 and 6.22 the flat region near

the tunnel centerline is where this mass penetrates the surface due to the low overburden. Stress concentrations or abutments form adjacent to all sides of the tunnel. What is difficult to understand is the disappearance of the rear abutment at higher H/B values. Finally, the increase in magnitude and area of load redistribution with increasing H/B is consistent with previous results and plasticity theory.

6.8 Approximate Values for K with Active Arching

The major uncertain variable in the arching theory presented in Chapter 3, as well as in those proposed by Terzaghi and by Spangler (Chapter 2), is the coefficient of lateral stress (K). This coefficient is defined at any point as the ratio between horizontal and vertical stress components present. As mentioned in Section 2.4 for active arching Terzaghi (see Figure 2.3) assumed K to be an empirical constant increasing from 1.0 immediately above the centerline of a downward translating trap door to about 1.6 at 1 to 1½ diameters above the door, and then decreasing to equal the coefficient of lateral stress at rest (K_o) above a height of 2½ trap door diameters where:

$$K_o = 1 - \sin\phi \qquad (6.4)$$

Whitman, et.al. (1962) backcalculated an average value for K of 1.2 above a structure undergoing active arching while Ang and Newmark (1963) obtained 1.5 from similar experiments. Other than these, few researchers have attempted to measure K during arching experiments. Other studies found in the literature have assigned values to this coefficient ranging from K_a to K_p where:

$$K_a = \frac{1 - \sin\phi}{1 + \sin\phi} \quad \text{and} \quad K_p = \frac{1 + \sin\phi}{1 - \sin\phi} \qquad (6.5)$$

Several tests in the present investigation were dedicated to examining whether the primary test apparatus could be used to examine values of K above the trap doors. The main problem to overcome is that the locations at which one wishes to

measure horizontal stresses do not lend themselves to placement of boundary type pressure cells. The configuration shown in Figure 6.24 and Appendix A, photograph A.6, was chosen as a simple approach for this examination. The planar soil deformation tank is placed at 90 degrees to its normal location such that only three trap doors fall within the tank. A piece of plexiglas identical in size to a trap door is covered with sandpaper on all sides in contact with sand, except for the area where a pressure transducer is mounted. The face of the transducer was brought flush with that of the adjacent sandpaper. With this device, located as shown in the figure, both horizontal and vertical stresses can be measured and thereby K determined. The three trap doors were carefully lowered together (acting as a single trap door $4\frac{1}{2}$ inches wide) while K values for a point 3/4 inch above the doors' centerline were measured (a photograph taken at the end of one such test is included in Appendix A). In determining vertical stresses the readings from the transducer mounted within the trap door are reduced to discount the 3/4 inch of sand directly above it. Figure 6.25 shows results from the most successful of these tests. K_o was found to be 0.51, which by using the formula previously presented indicates a friction angle for the soil of near 30 degrees (slightly smaller than indicated in Sections 5.5 and 6.3). As displacement begins, the vertical stress decreases rapidly while the horizontal stress remains nearly constant with only slight decreases. This causes K to increase to a maximum value of near 1.2, occurring at a displacement of approximately one percent of the trap door width (corresponding to the displacement at which stress reduction is generally a maximum in active arching tests). As displacements increase, vertical stresses increase somewhat and horizontal stresses decrease, yielding lower K values. At large displacements K becomes constant at a value larger than K_o.

The observed variation in K is consistent with the plasticity theory presented in Chapter 3. As the door initially

moves down, sufficient dilation occurs within the wedge of soil bounded by velocity characteristics at the initial angle of dilation, so as to maintain horizontal stresses at near initial values (and thus increase K). At a displacement of approximately one percent of the trap door width nearly maximum dilation has occurred and subsequent displacements lead to a decreasing angle of dilation and decreasing horizontal stresses.

The value of 1.2 for K at maximum active arching is in line with values from other researchers (which were presented at the beginning of this section), and is used throughout this chapter when comparing experimental results with those predicted by the various theories. This is not to say that this author is satisfied as to the correctness of this value. From reviewing the arching expressions presented (Table 6.2 and Chapters 2 and 3) one sees that the K value selected greatly affects the predicted results. In addition, the experimental results indicate that K varies depending upon the level of displacement present. It is therefore felt that more investigation is required on the subject of appropriate values for K.

6.9 Influence of Test Variables on Arching

The test variables studied in this experimental program were: sand type, density, depth of sand, trap door width, displacement, and three-dimensional versus planar soil deformation. The four sands used produced similar results with the only noticable difference being found in the tests simulating an advancing tunnel. Here the Fine White Sand showed less stress redistribution than did the Medium Tan Sand in identical sets of tests. This author knows of no explanation for this behavior. The Fine White Sand actually has a slightly higher friction angle (43° versus 38°) in direct shear tests (Table 5.2) and therefore, if anything, should produce more stress redistribution.

By comparison of tests with varying soil depths (H) and

trap door widths (B) one finds that for shallow depths of sand it is the ratio H/B that affects the level of arching obtained, not the independent magnitude of either variable. Active arching tests with two different trap door widths, but the ratio H/B equal, led to near identical values for load reduction. For a lowering trap door, load reduction increases with increasing H/B, but for H/B larger than about 2 the load on the door at maximum active arching changes little with increasing overburden. This is consistent with the proposed plasticity theory, where at maximum arching the trap door force is the weight of a triangular soil body (see Figure 3.14.A) above the door. With small H/B this body penetrates the sand's surface making force dependent upon depth, while at larger H/B (greater than 2) the body does not reach the sand's surface and force is independent of depth. At ultimate arching the plasticity theory approach assumes sand more than 2B above the door to act only as a surcharge on the arching body presented in Figure 3.14.B, which results in only a small increase in trap door force with increasing depth of sand (test results bear out this assumption).

For a rising trap door the percentage increase in the passive arching load increased as H/B did over the entire range used in these tests. Again, this is consistent with proposed plasticity theory where for maximum arching (δ/B approximately 1 to 2 percent) the trap door force is now the weight of the soil body in Figure 3.18.A and for ultimate arching (large displacements) the force is as determined from the free body in Figure 3.18.B (both solutions increasing with increasing H/B).

For both active and passive plane strain tests the normalized displacement (δ/B) necessary to mobilize maximum arching was approximately the same (1.8 percent average for active and 2.3 percent for passive). The magnitude of normalized displacement necessary to mobilize ultimate arching was not the same in these two types of tests. Active tests reached the ultimate state at δ/B values of approximately 10 percent,

while the ultimate state was not reached in passive tests having δ/B in excess of 30 percent.

Finally, in comparing results from planar and three-dimensional displacement tests one observes that the level of displacement necessary to mobilize full active arching is generally larger in the three-dimensional tests. For circular trap door tests δ/B averages 3.5 percent at maximum arching compared with the 1.8 percent for plane strain arching. On the other hand, in experiments simulating an advancing tunnel (Section 6.7) larger load redistribution was observed at δ/B of 5 percent compared with results at 1 percent (the reason for this apparent behavior is not presently known).

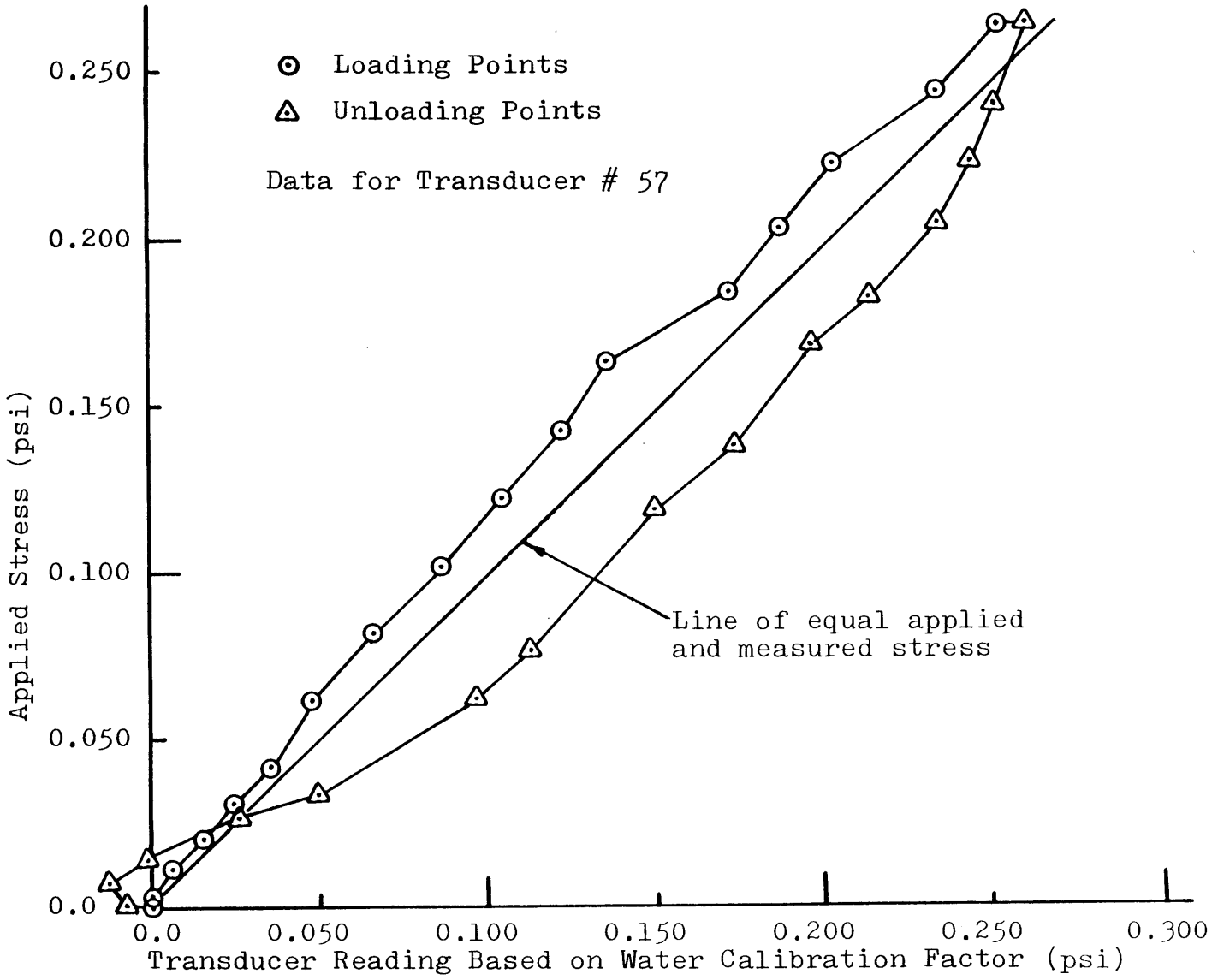

Figure 6.1 Load-Unload Cycle for Transducer

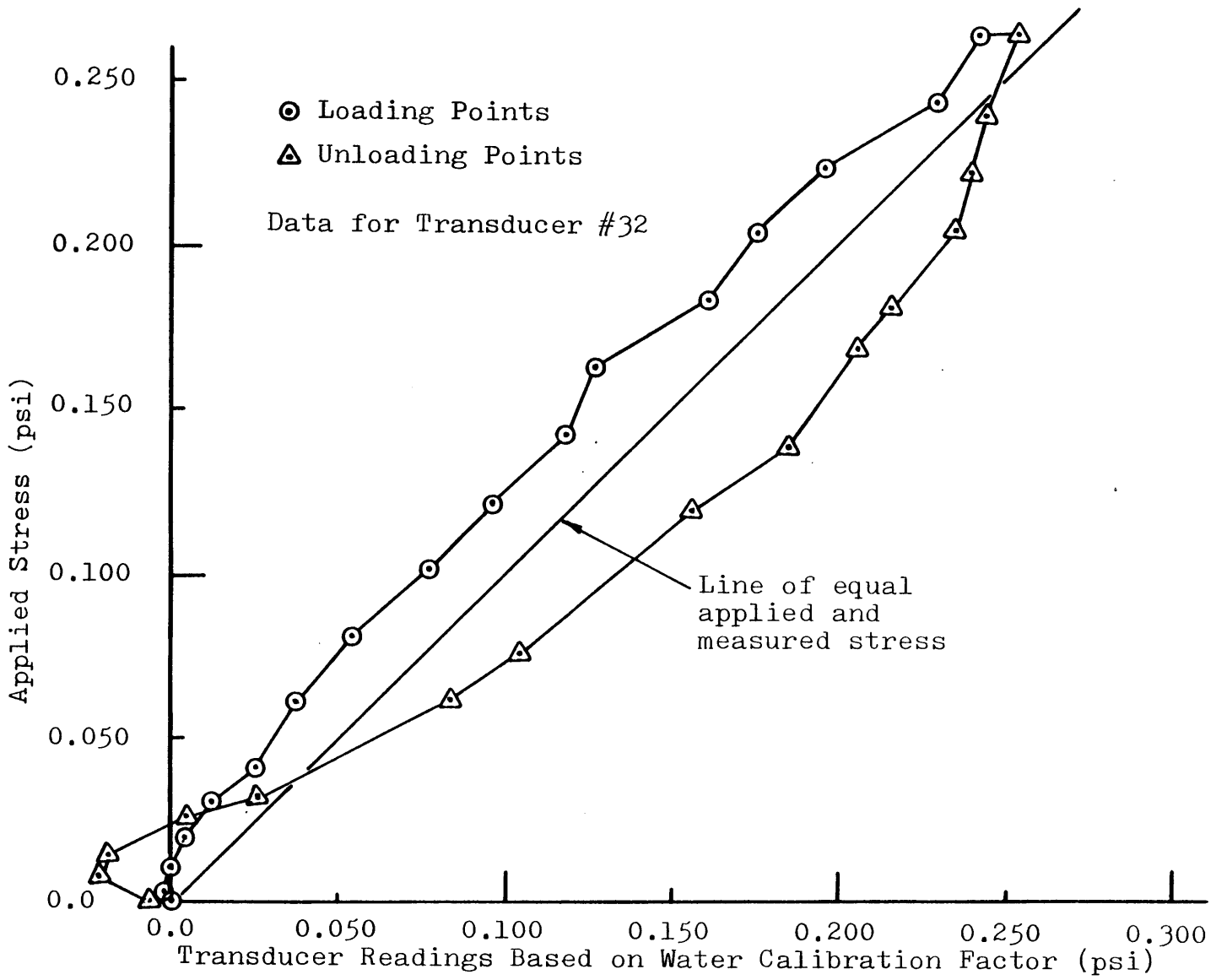

Figure 6.2 Load-Unload Cycle for Transducer

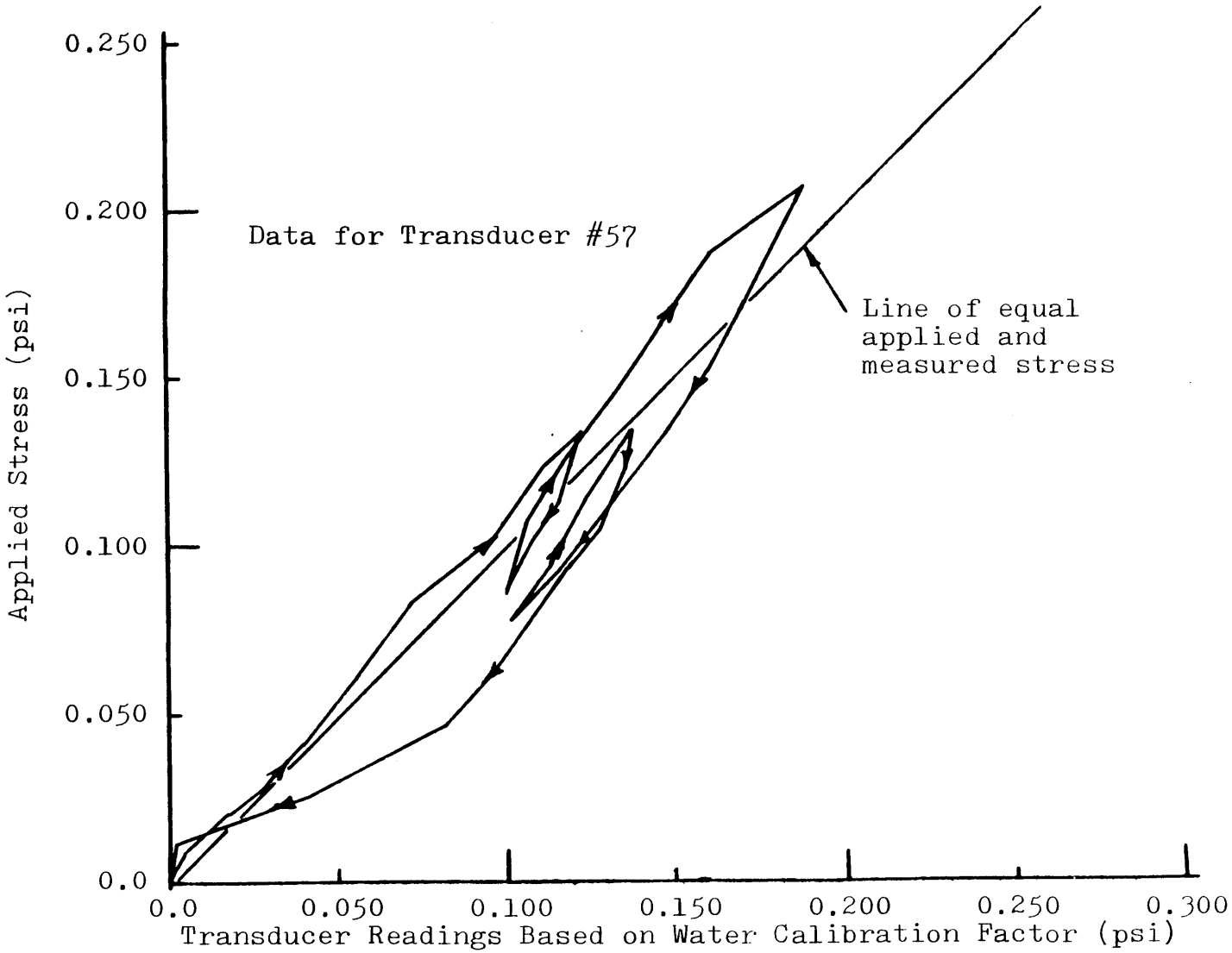

Figure 6.3 Successive Load-Unload Cycles for a Transducer

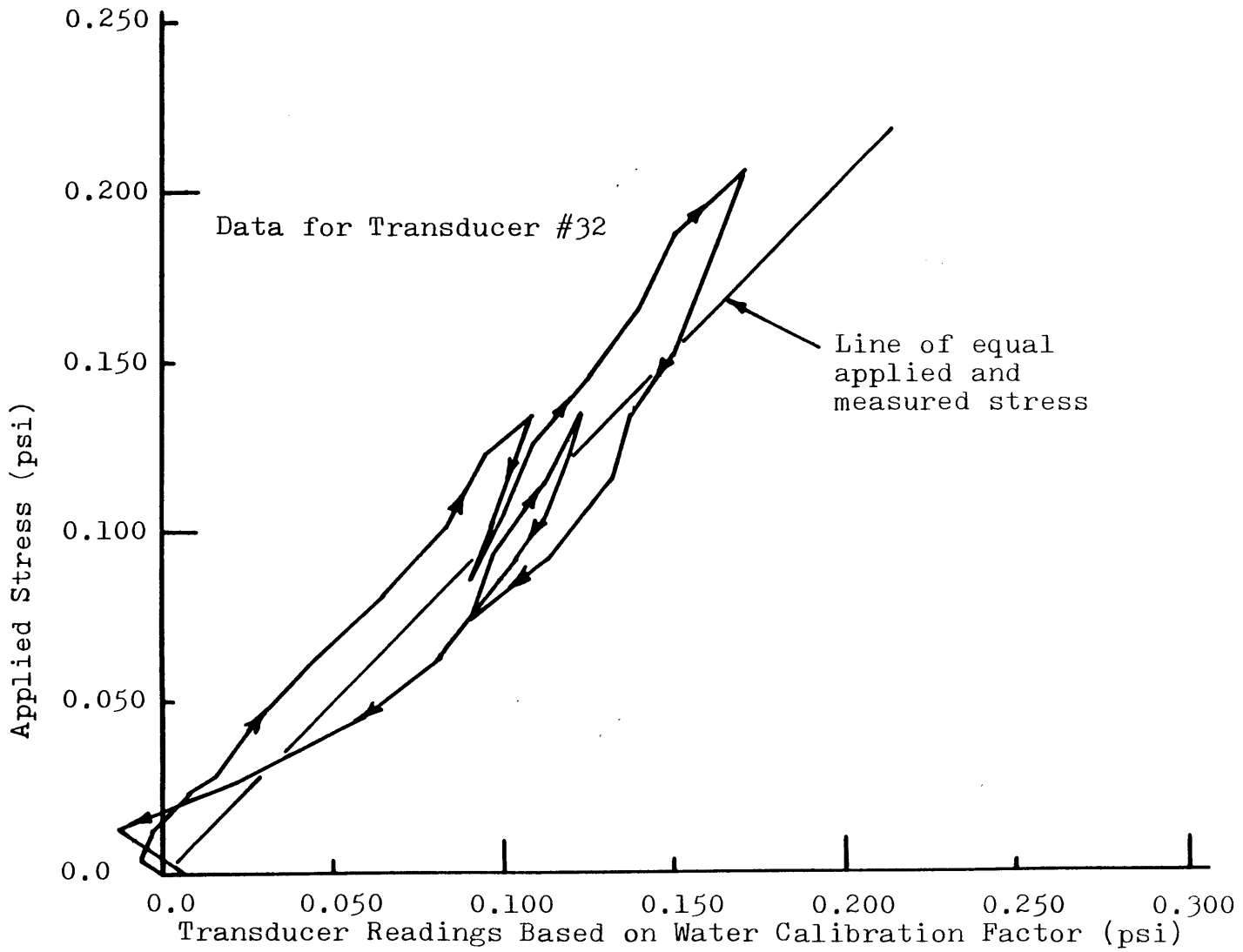

Figure 6.4 Successive Load-Unload Cycles for a Transducer

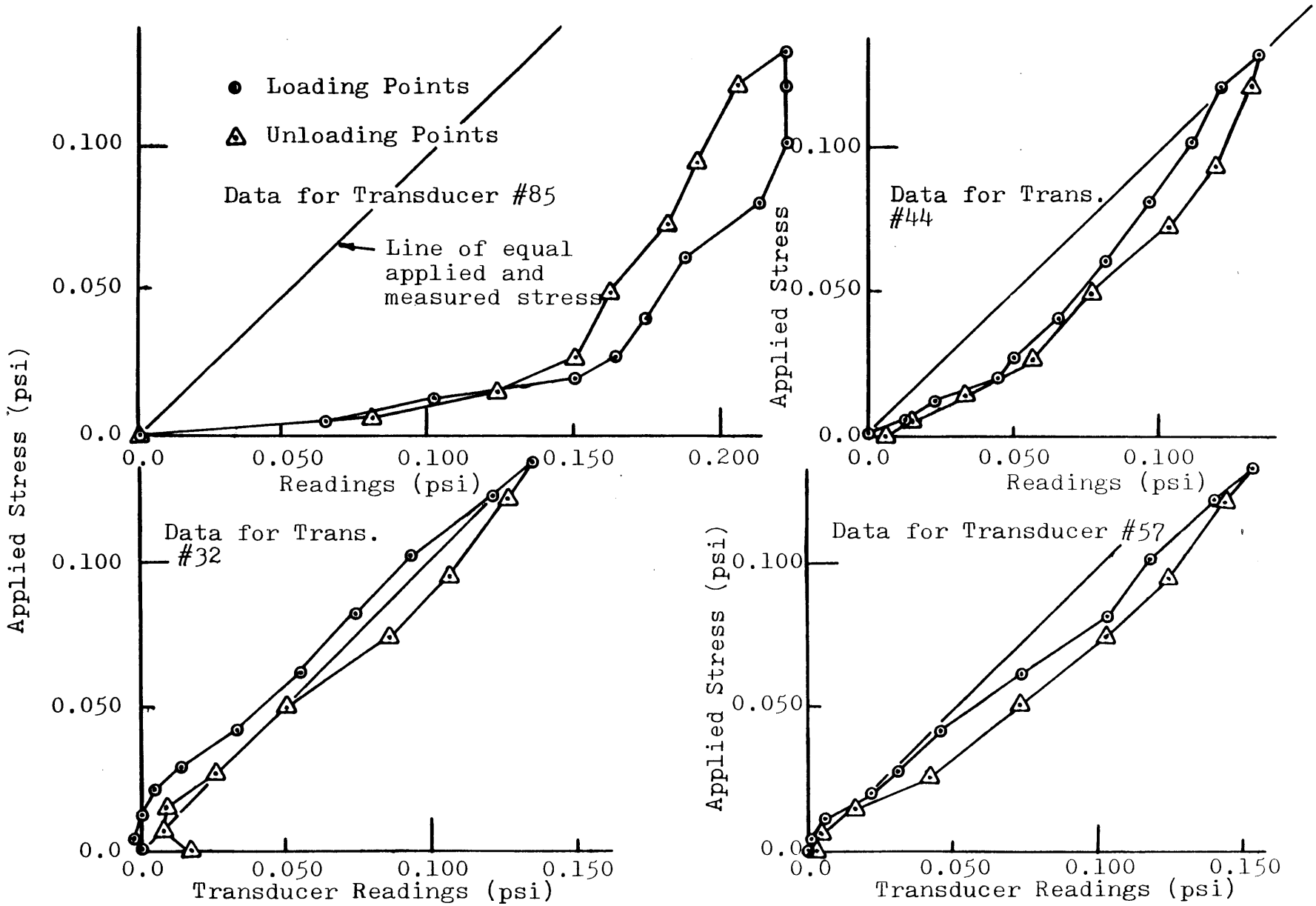

Figure 6.5 Load-Unload Cycles for Transducers

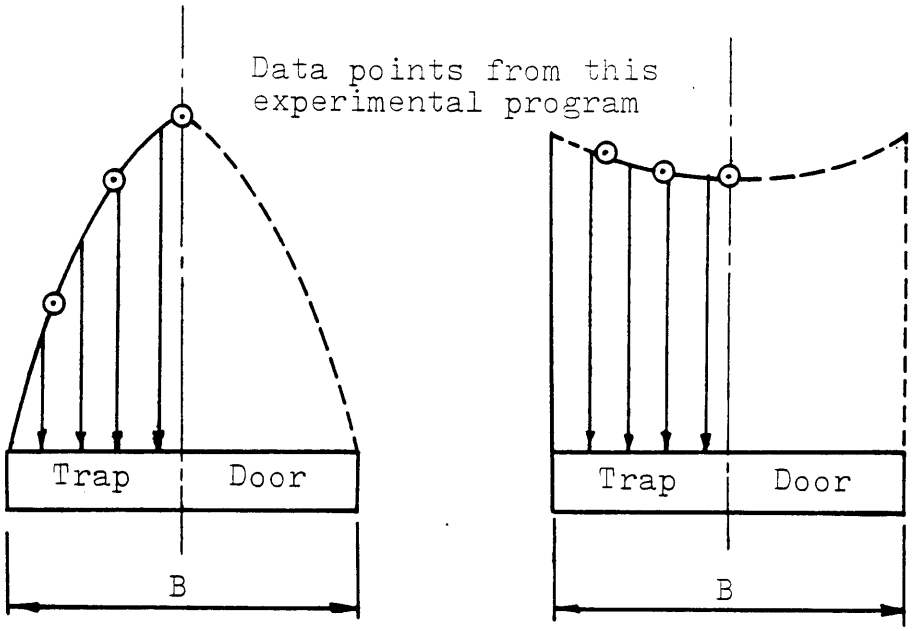

A. Observed Shapes of Stress Distributions (this thesis research)

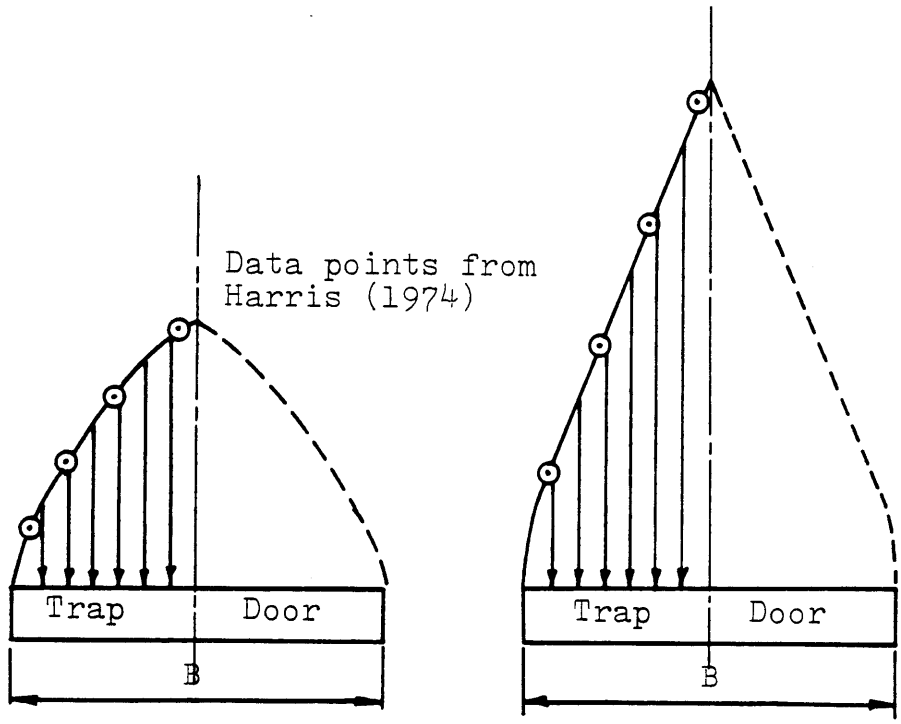

B. Harris' Observed Active Arching Distributions

Figure 6.6 Observed Shapes of Stress Distributions Across Trap Doors During Active and Passive Arching

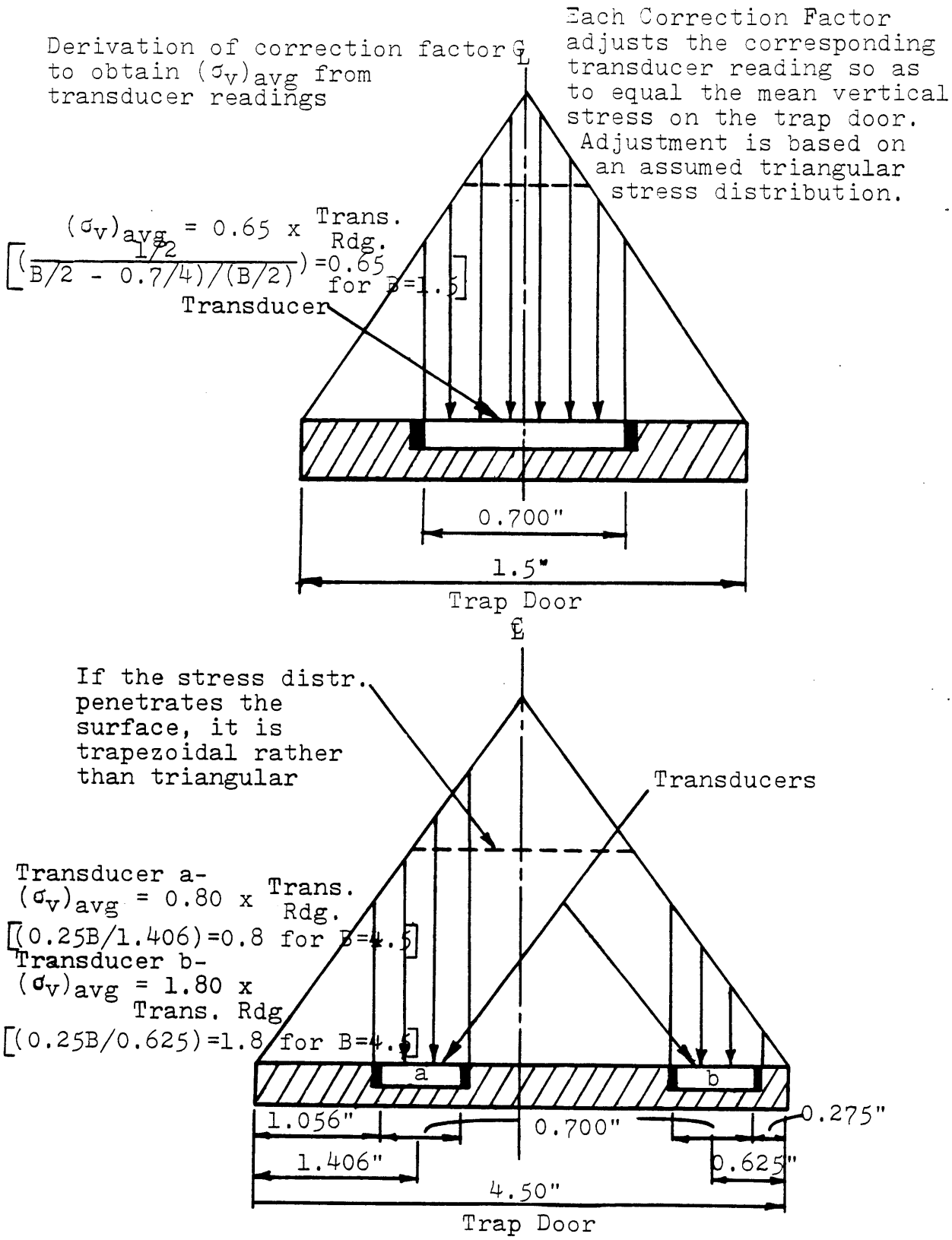

Figure 6.7 Assumed Distribution of Stresses Above a Rectangular Trap Door

Derivation of correction factor to obtain $(\sigma_v)_{avg}$ from transducer readings.

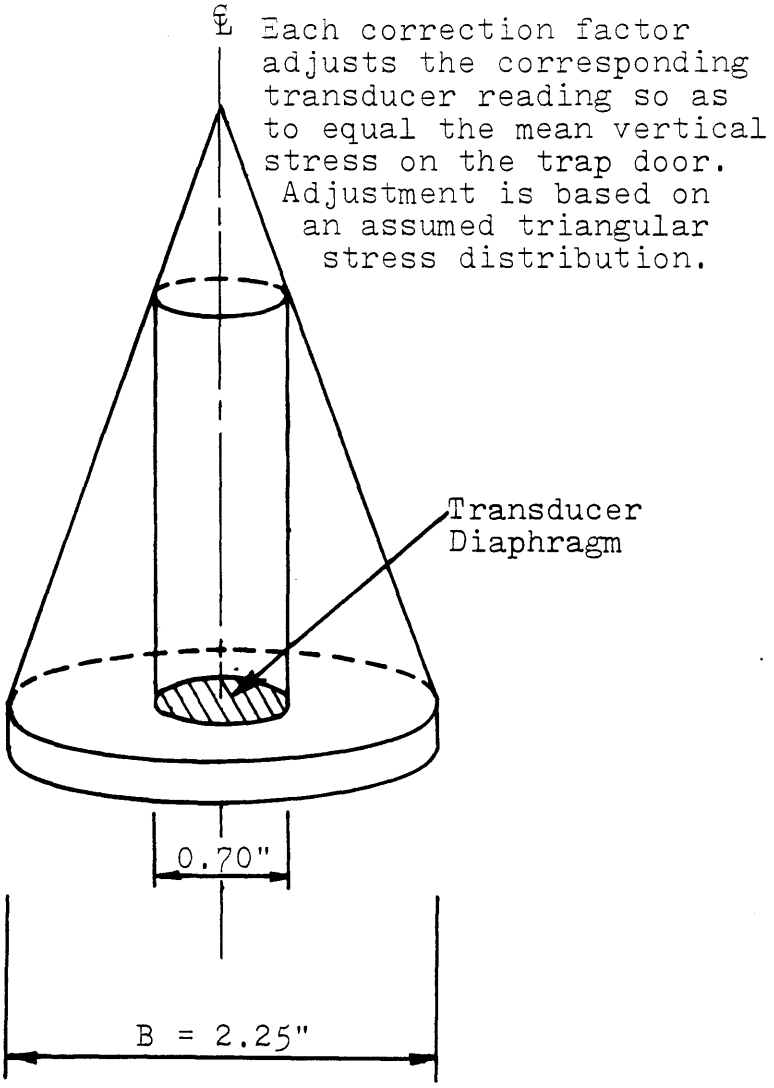

$$(\sigma_v)_{avg} = 0.42 \times \text{Transducer Reading}$$

$$\left[\left(\frac{B/3}{B - 2(0.70)/3}\right) = 0.42 \text{ for } B=2.25"\right]$$

Figure 6.8 Assumed Distribution of Stresses Above a Circular Trap Door

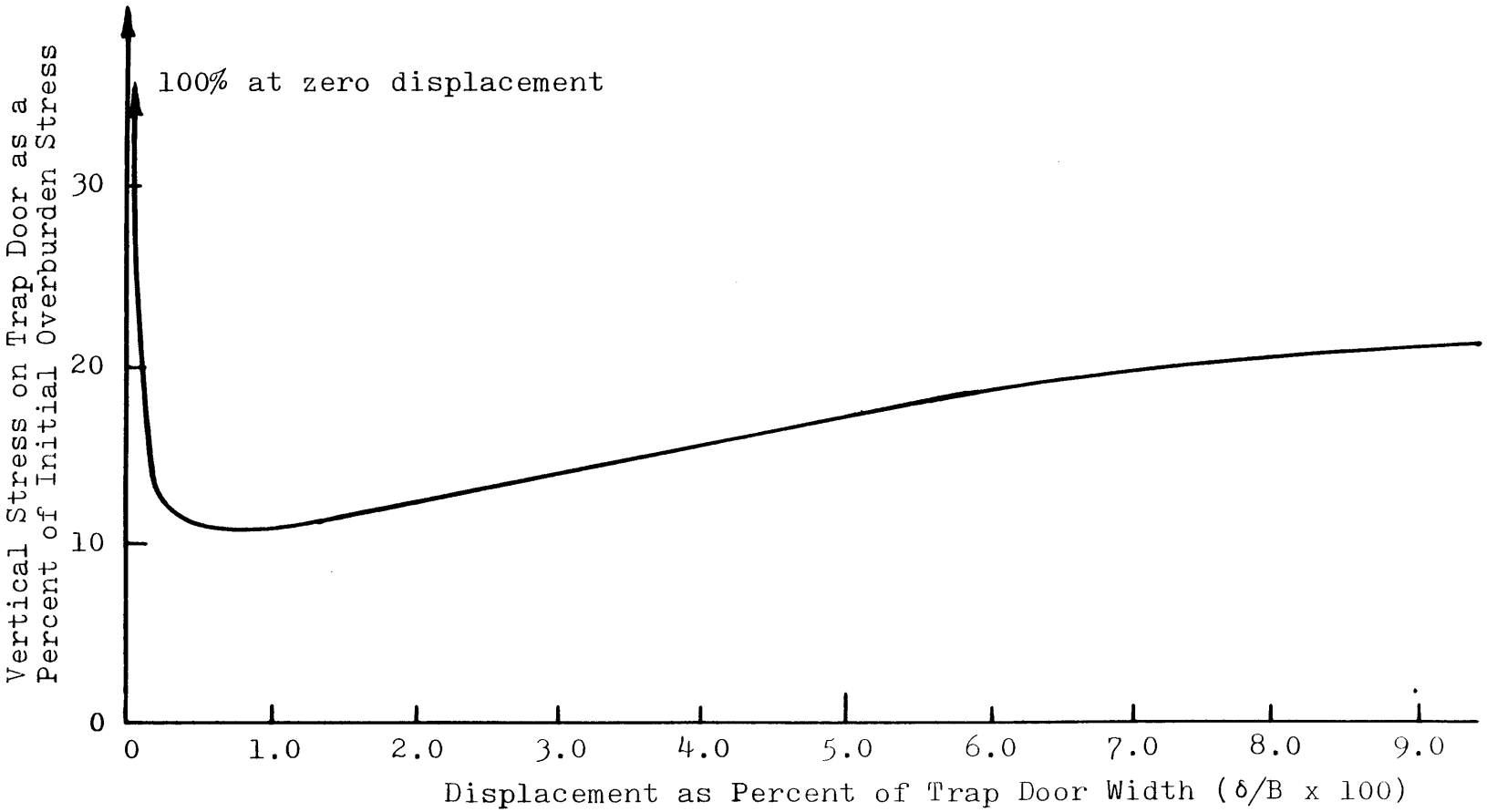

Figure 6.9 **Normalized Stress Versus Displacement Plot for Test Number 18**

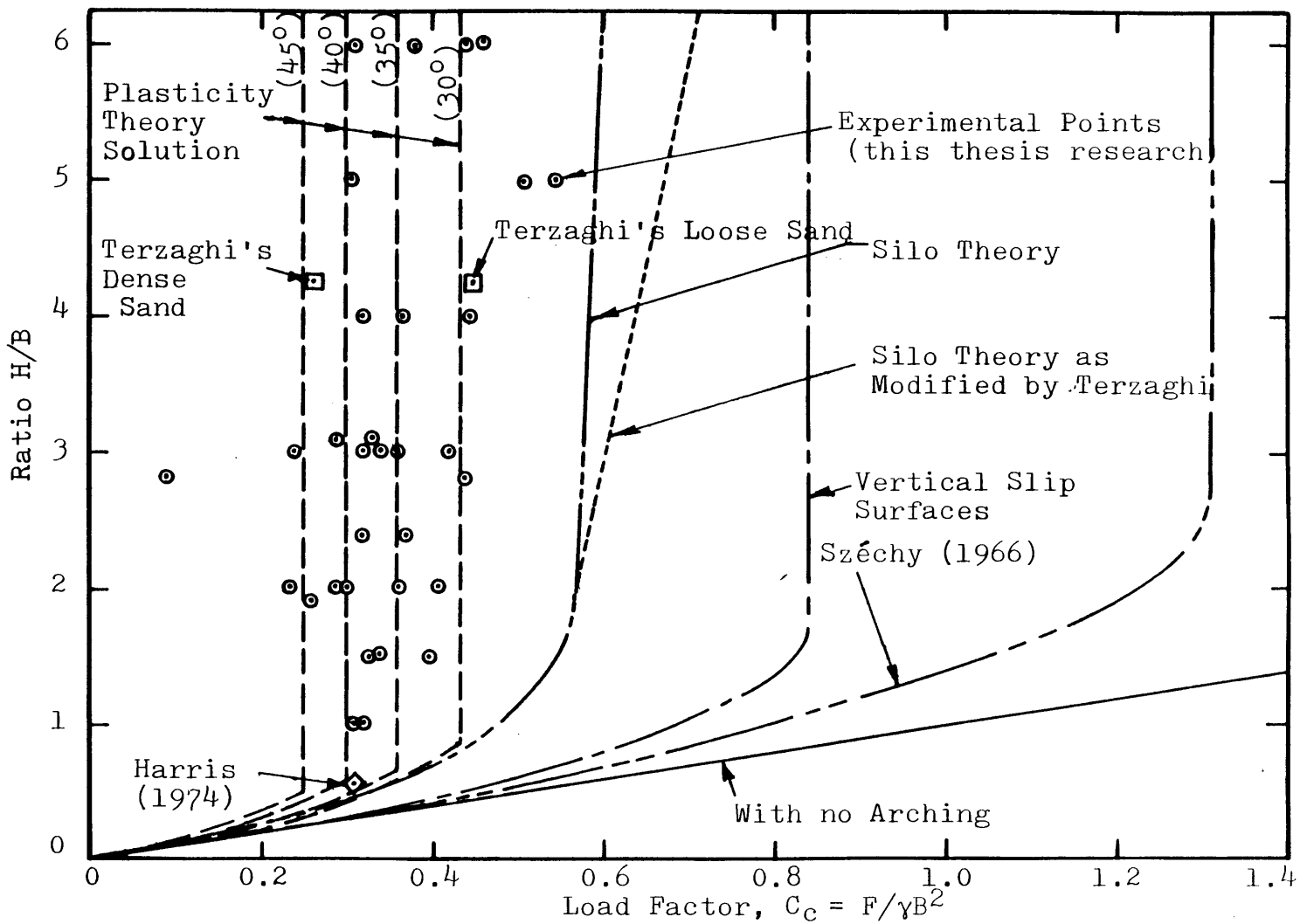

Figure 6.10 Comparison of Experimental Results with Those Predicted for Plane Strain Active Arching at the Maximum Arching State

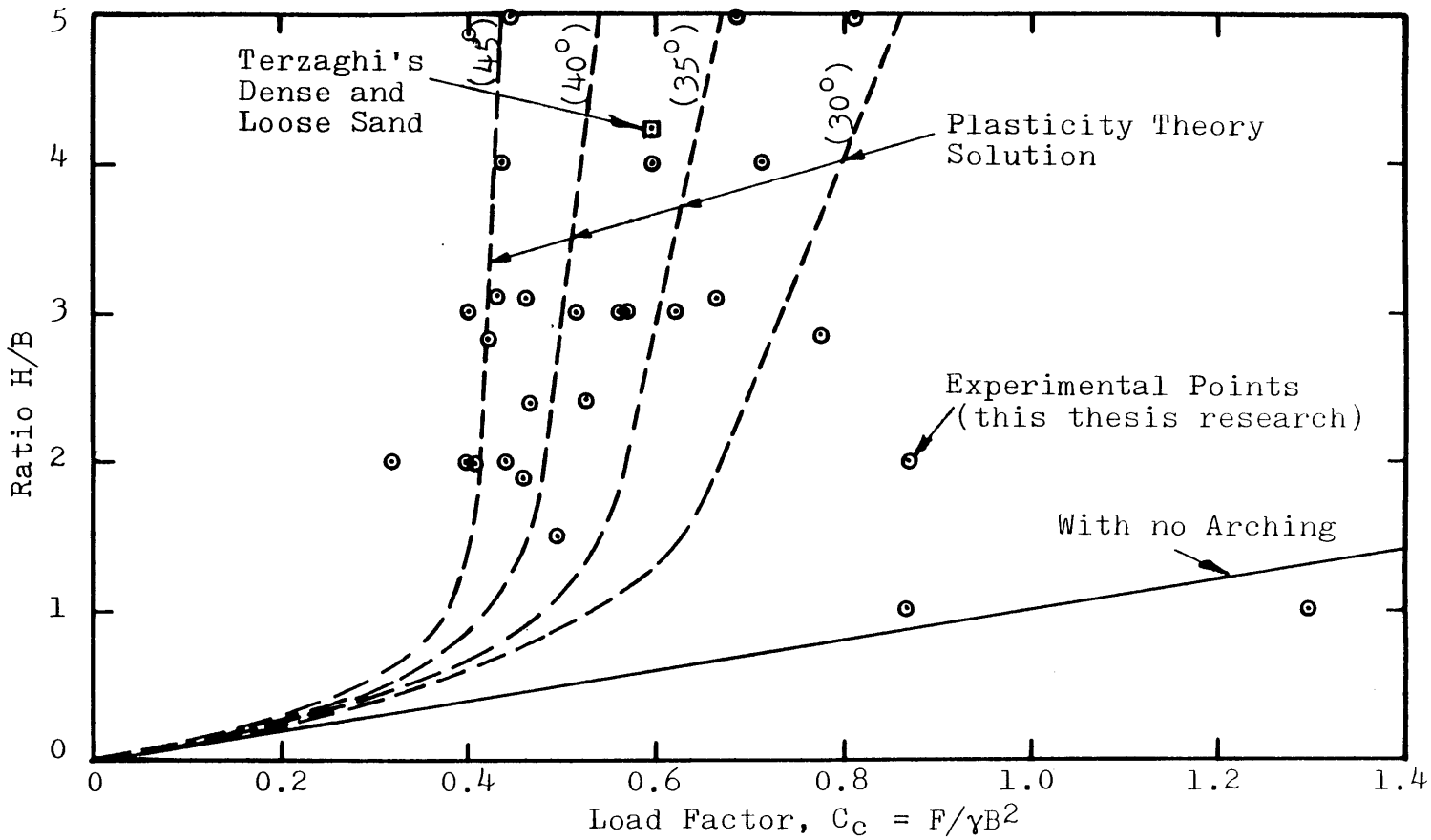

Figure 6.11 Comparison of Experimental Results with Those Predicted for Plane Strain Active Arching at the Ultimate Arching State

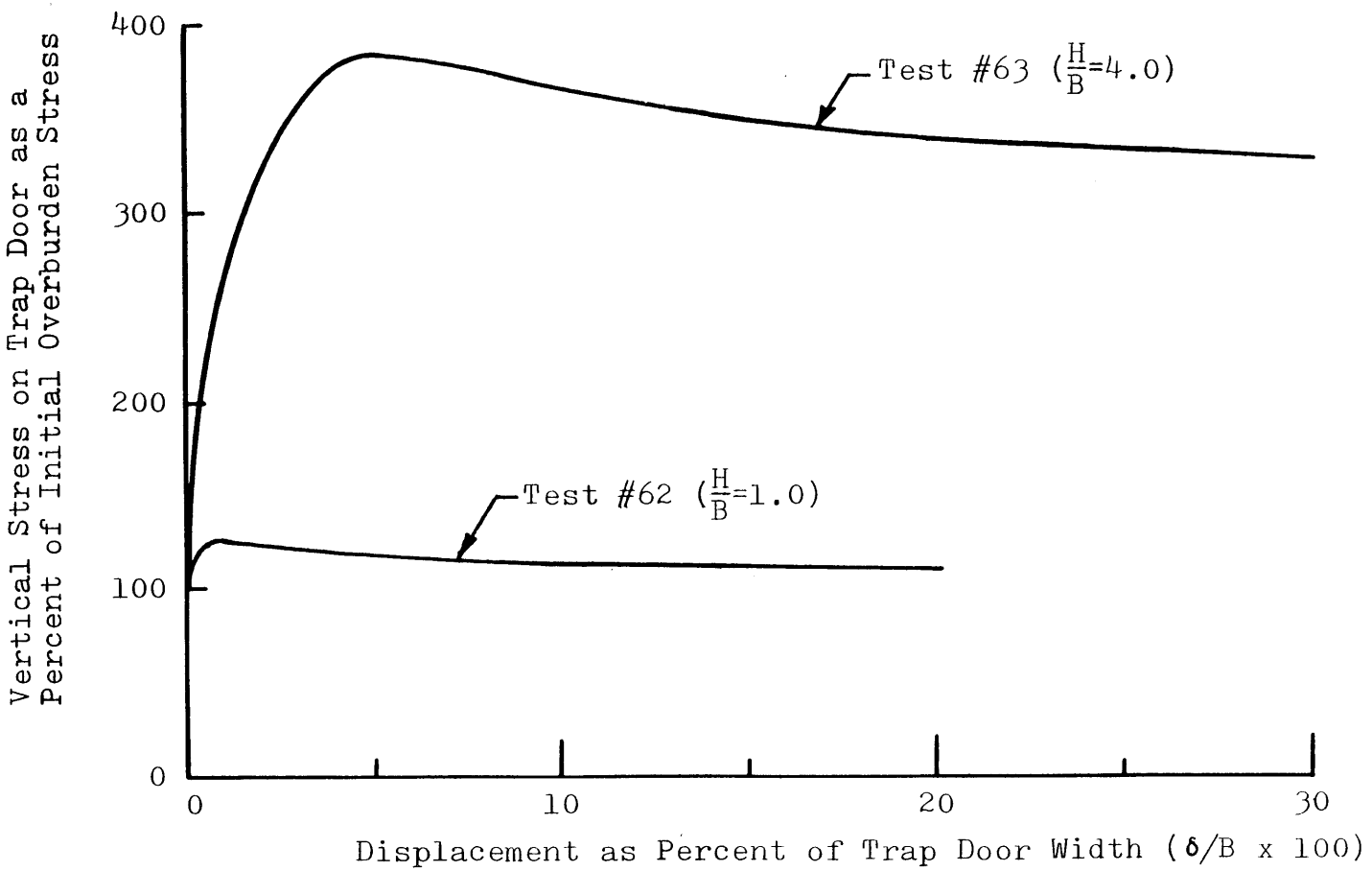

Figure 6.12 Normalized Stress Versus Displacement Plot for Tests Number 62 and 63

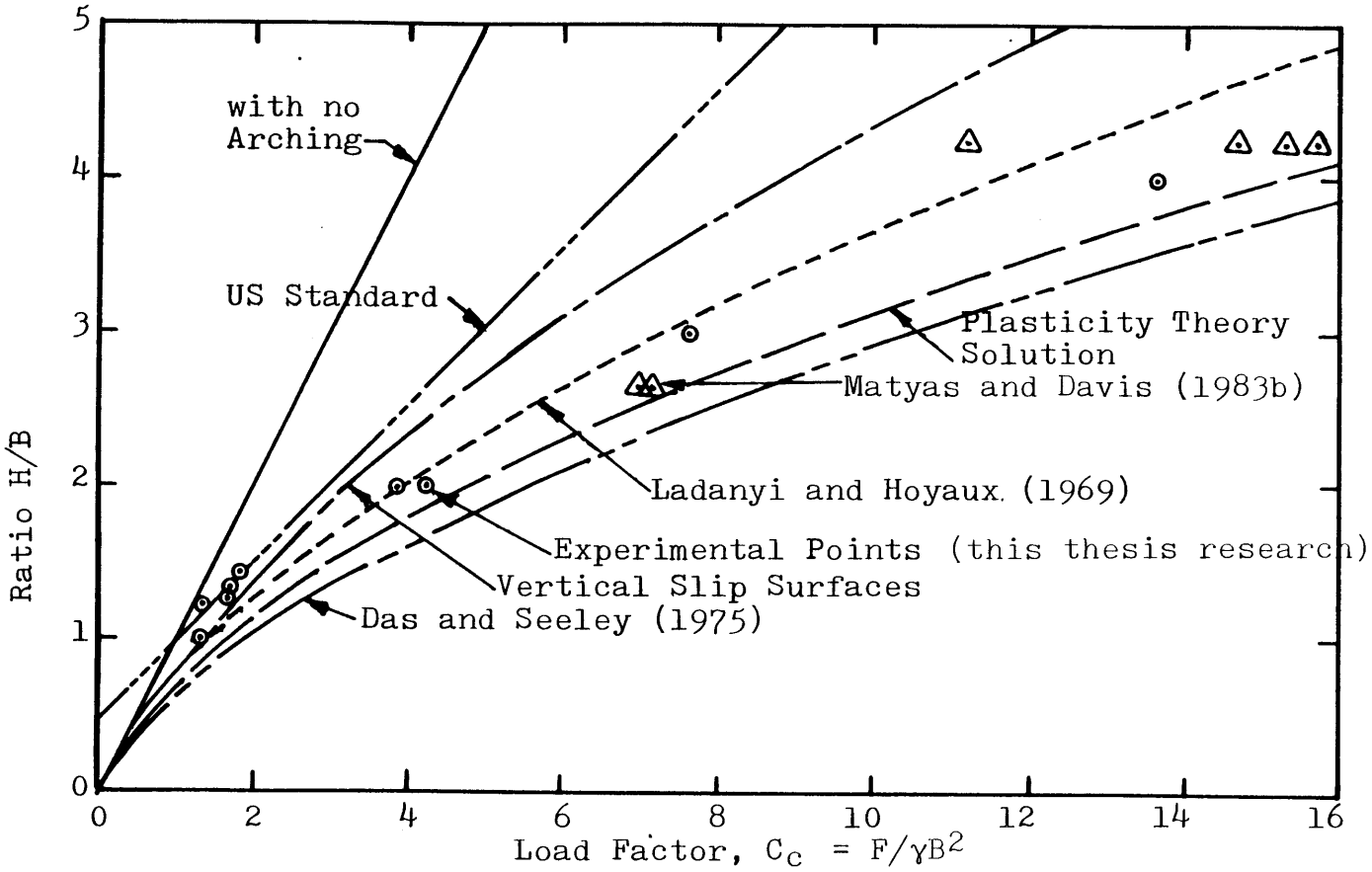

Figure 6.13 Comparison of Experimental Results with Those Predicted for Plane Strain Passive Arching at the Maximum Arching State

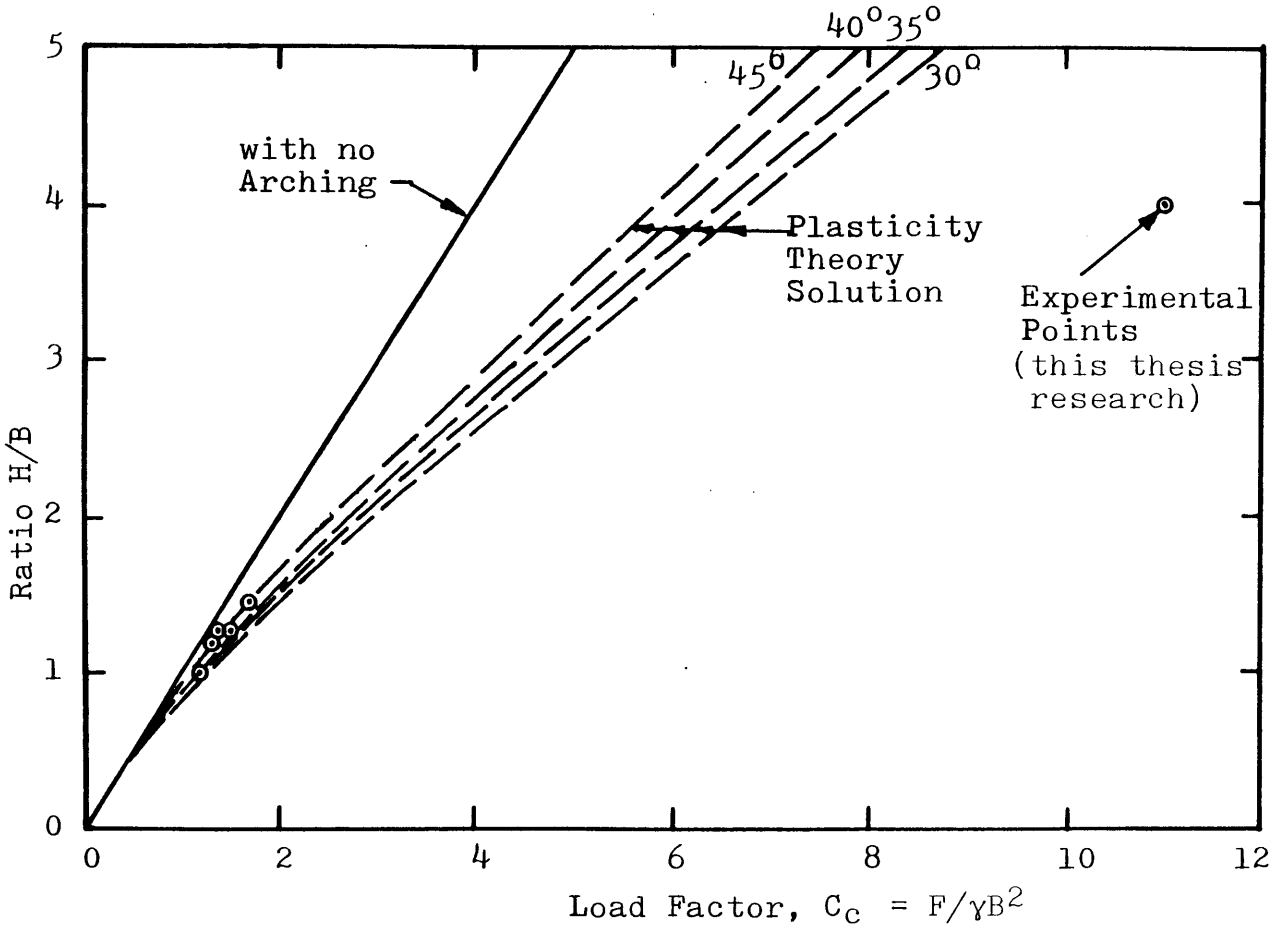

Figure 6.14 Comparison of Experimental Results with Those Predicted for Plane Strain Passive Arching at the Ultimate Arching State

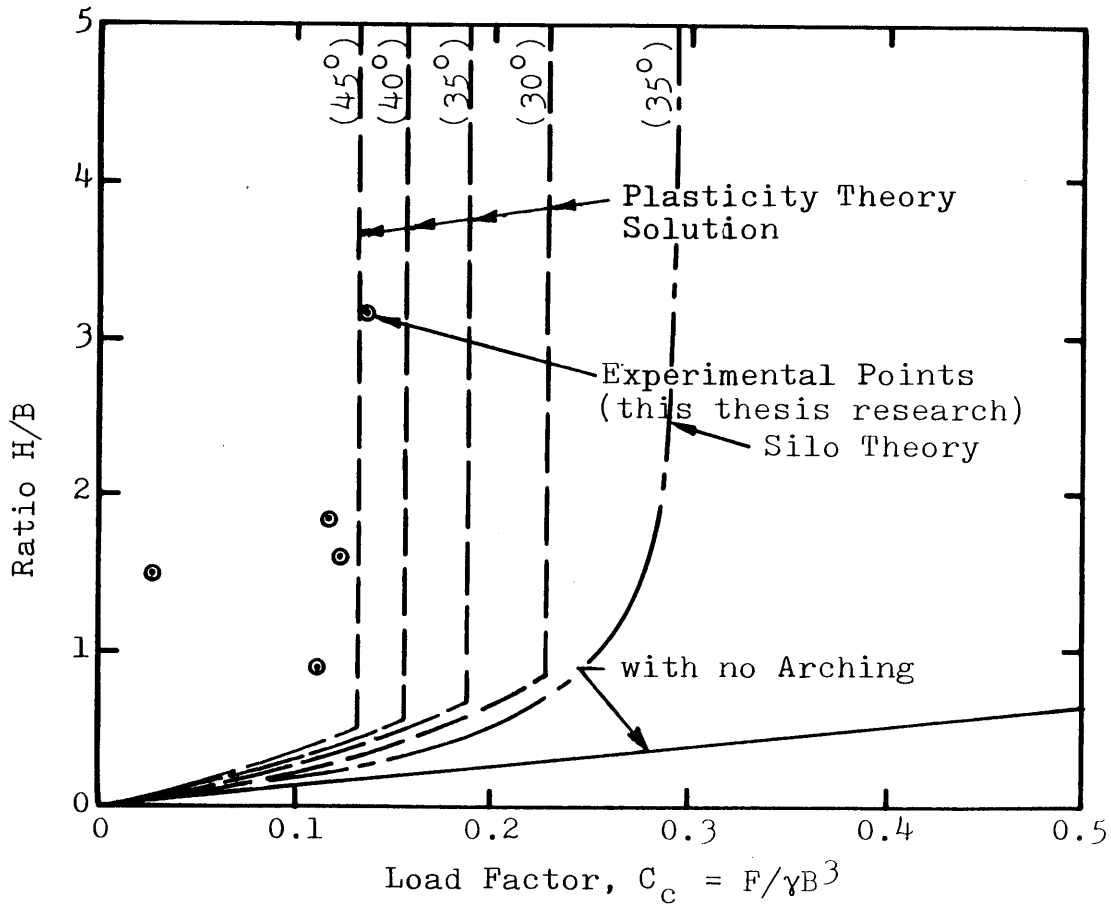

Figure 6.15 Comparison of Experimental Results with Those Predicted for Three-Dimensional Active Arching at the Maximum Arching State

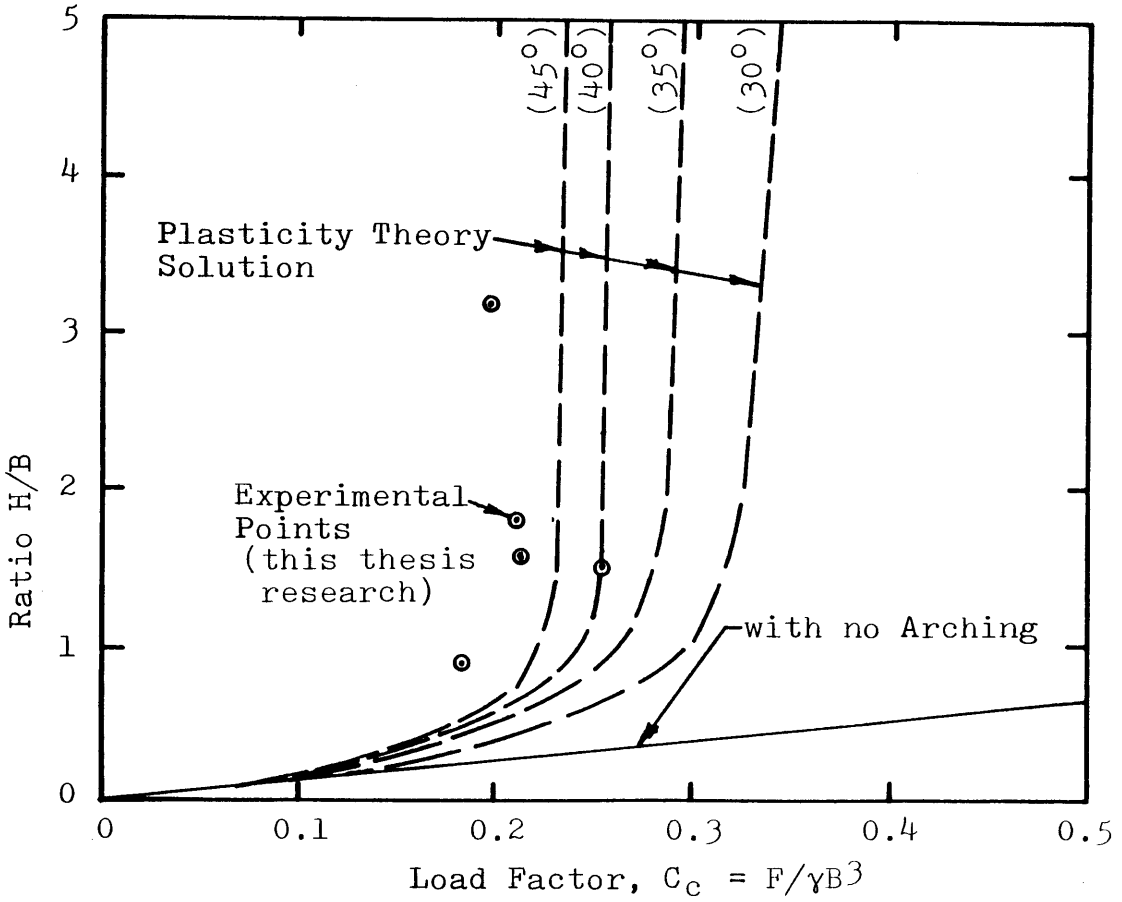

Figure 6.16 Comparison of Experimental Results with Those Predicted for Three-Dimensional Active Arching at the Ultimate Arching State

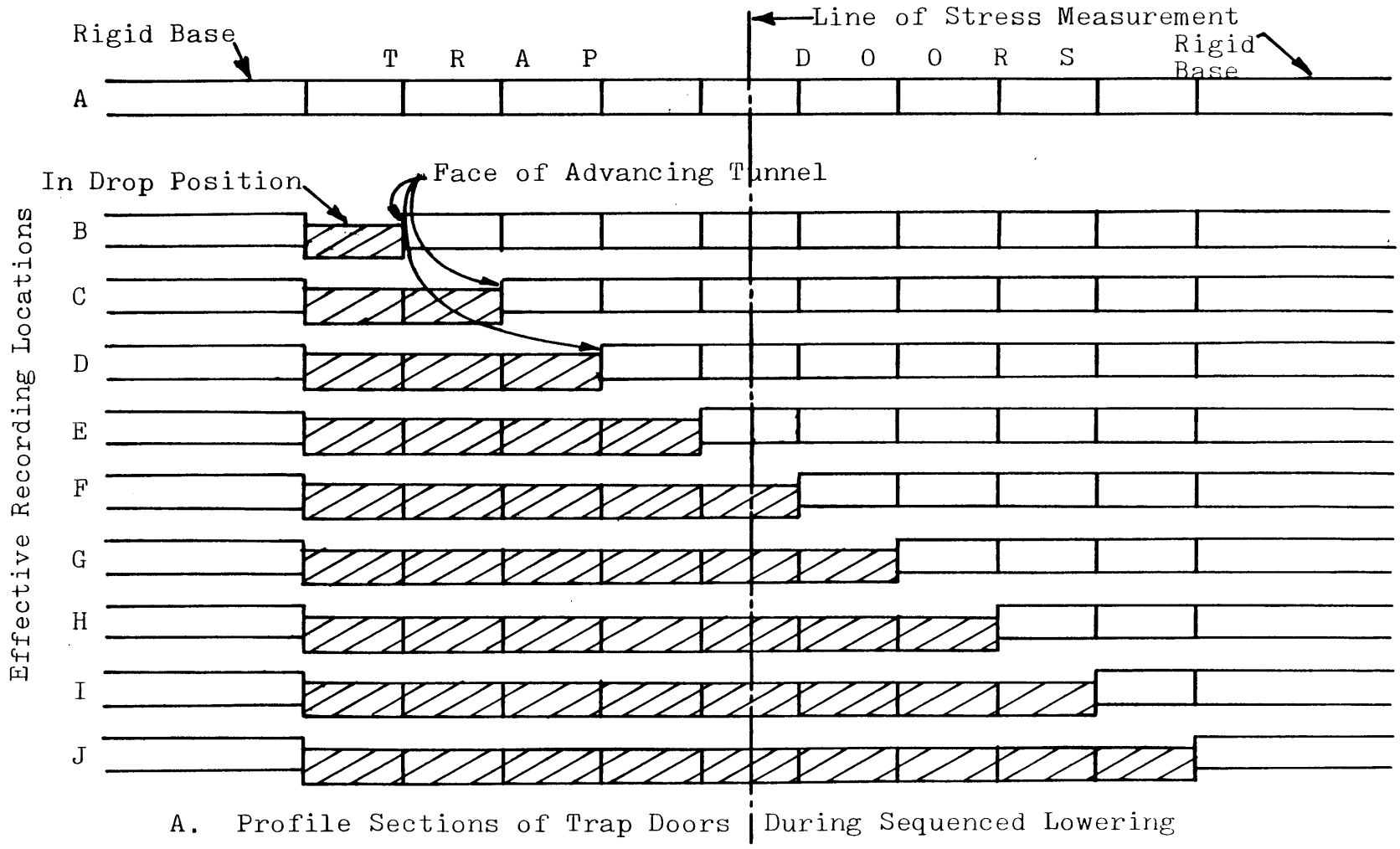

Figure 6.17 Effective Recording Locations for Vertical Stresses Advancing Tunnel Heading Tests

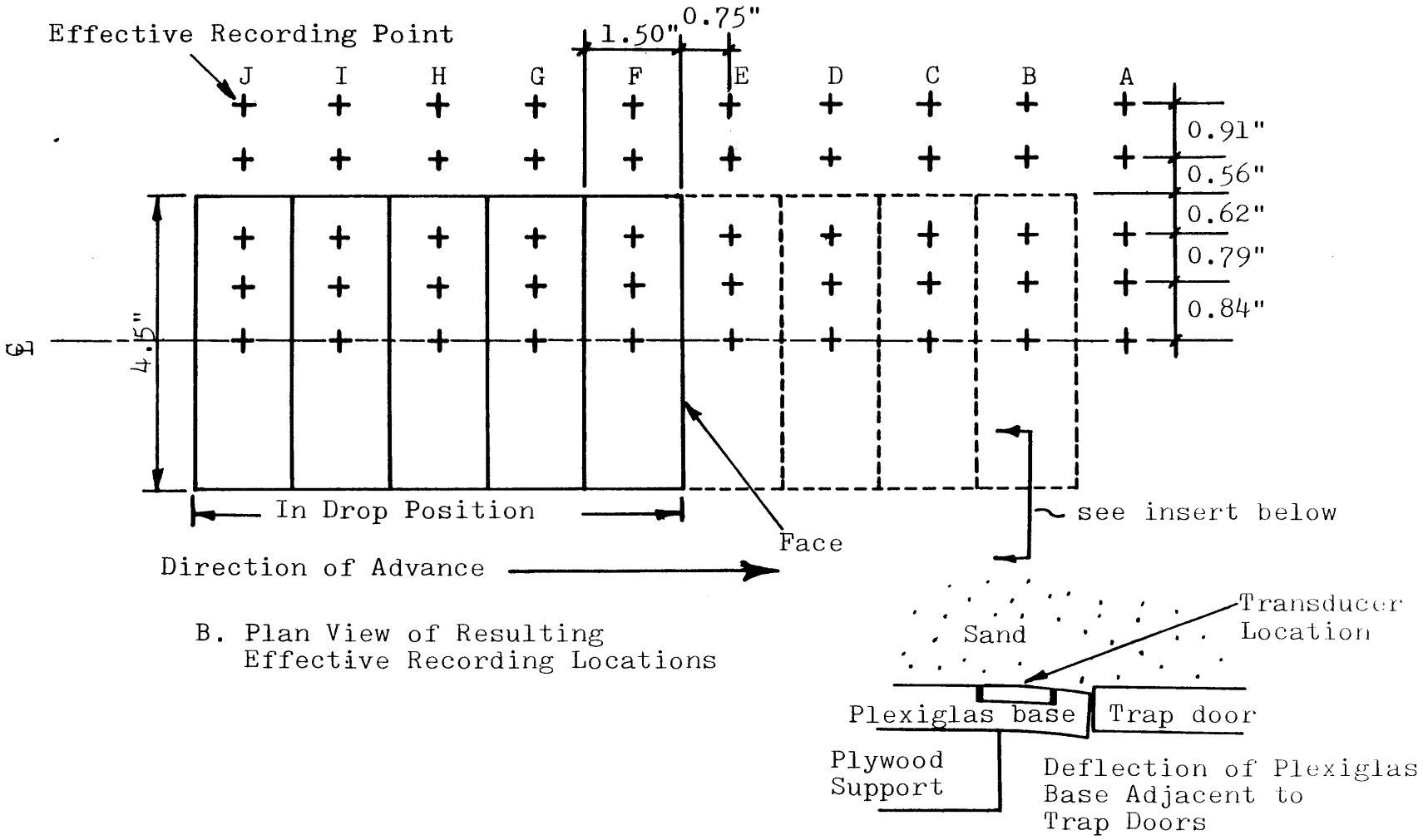

Figure 6.17 Effective Recording Locations for Vertical Stresses
Advancing Tunnel Heading Tests

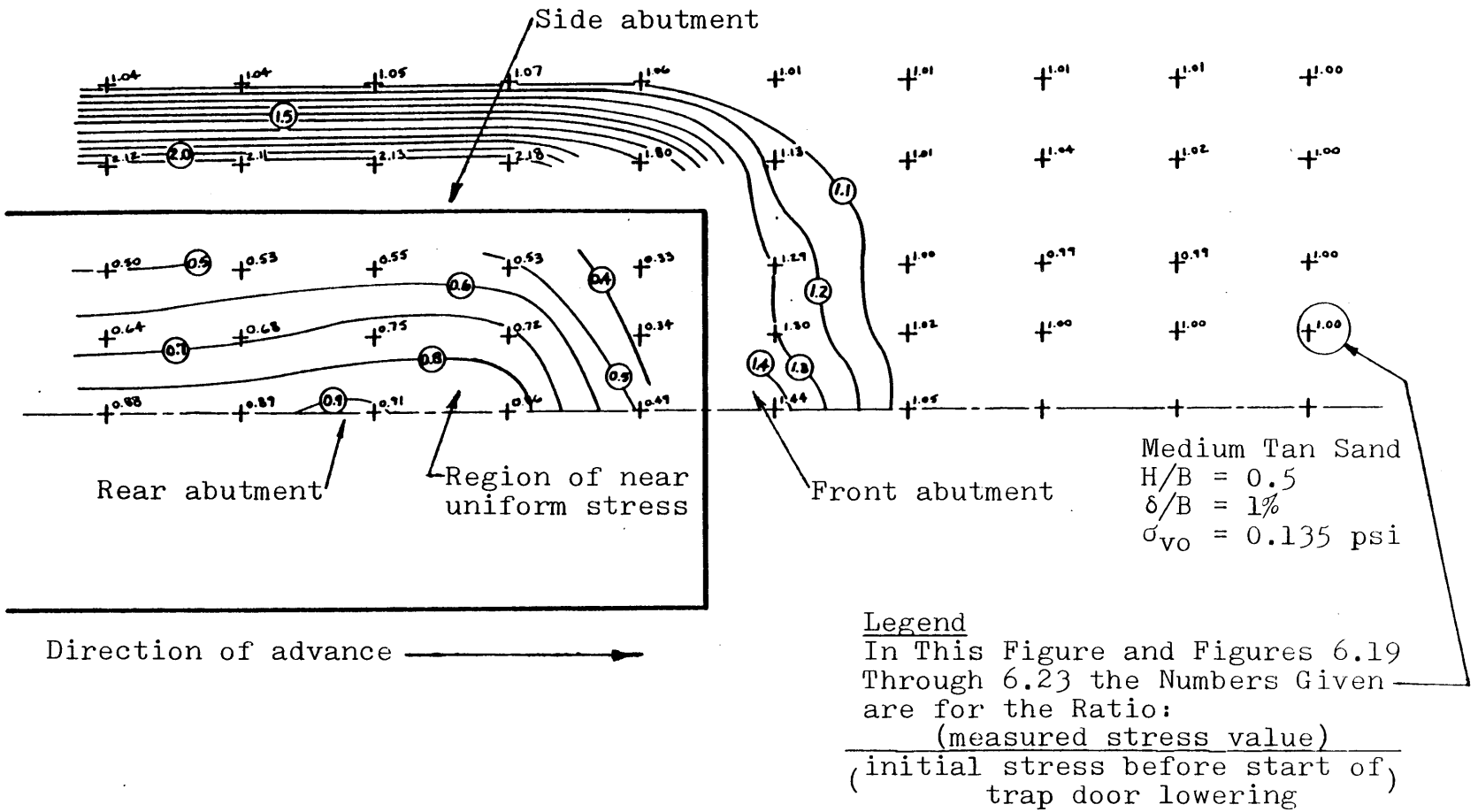

Figure 6.18 Results from Tests 34, 35, 36, 37, and 38
Vertical Stresses Around a Simulated Advancing Tunnel

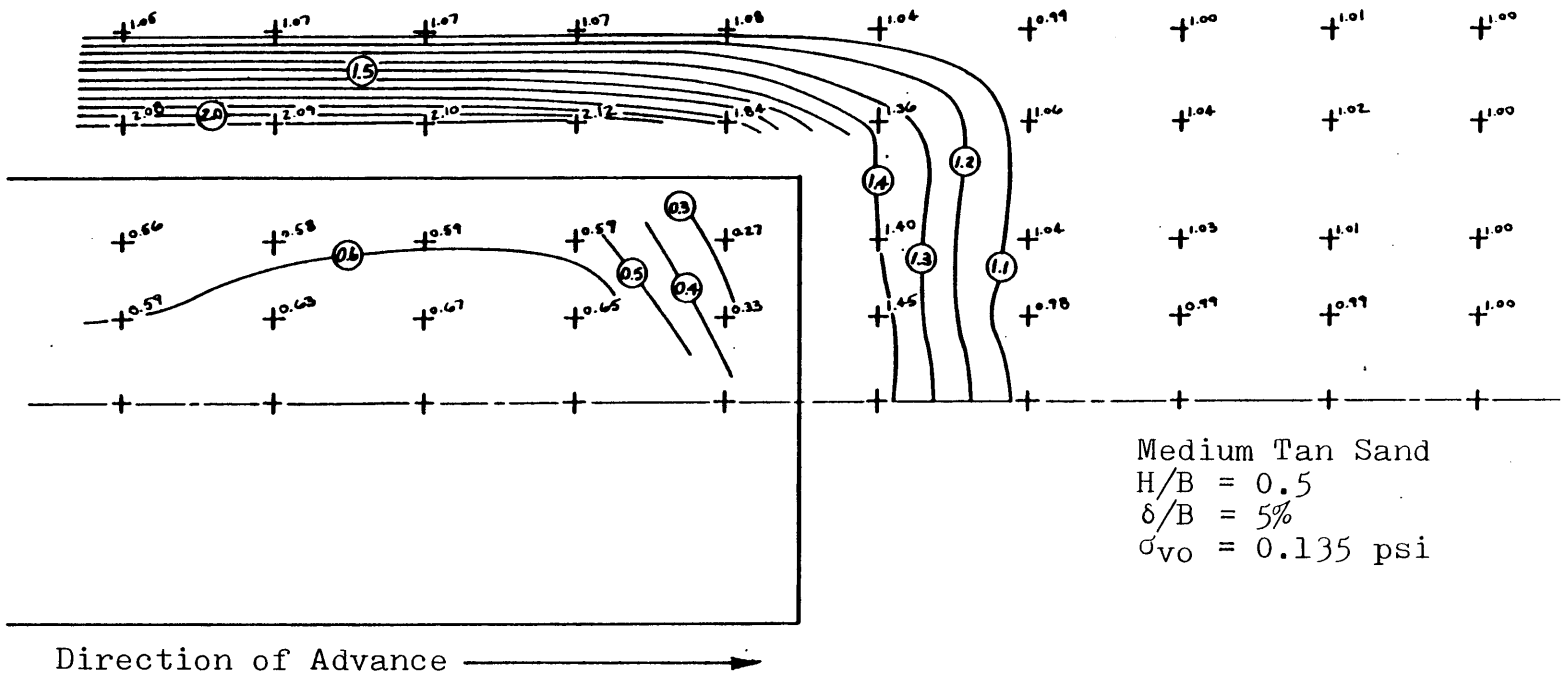

Figure 6.19 Results from Tests 41, 42, 44, and 46
Vertical Stresses Around A Simulated Advancing Tunnel

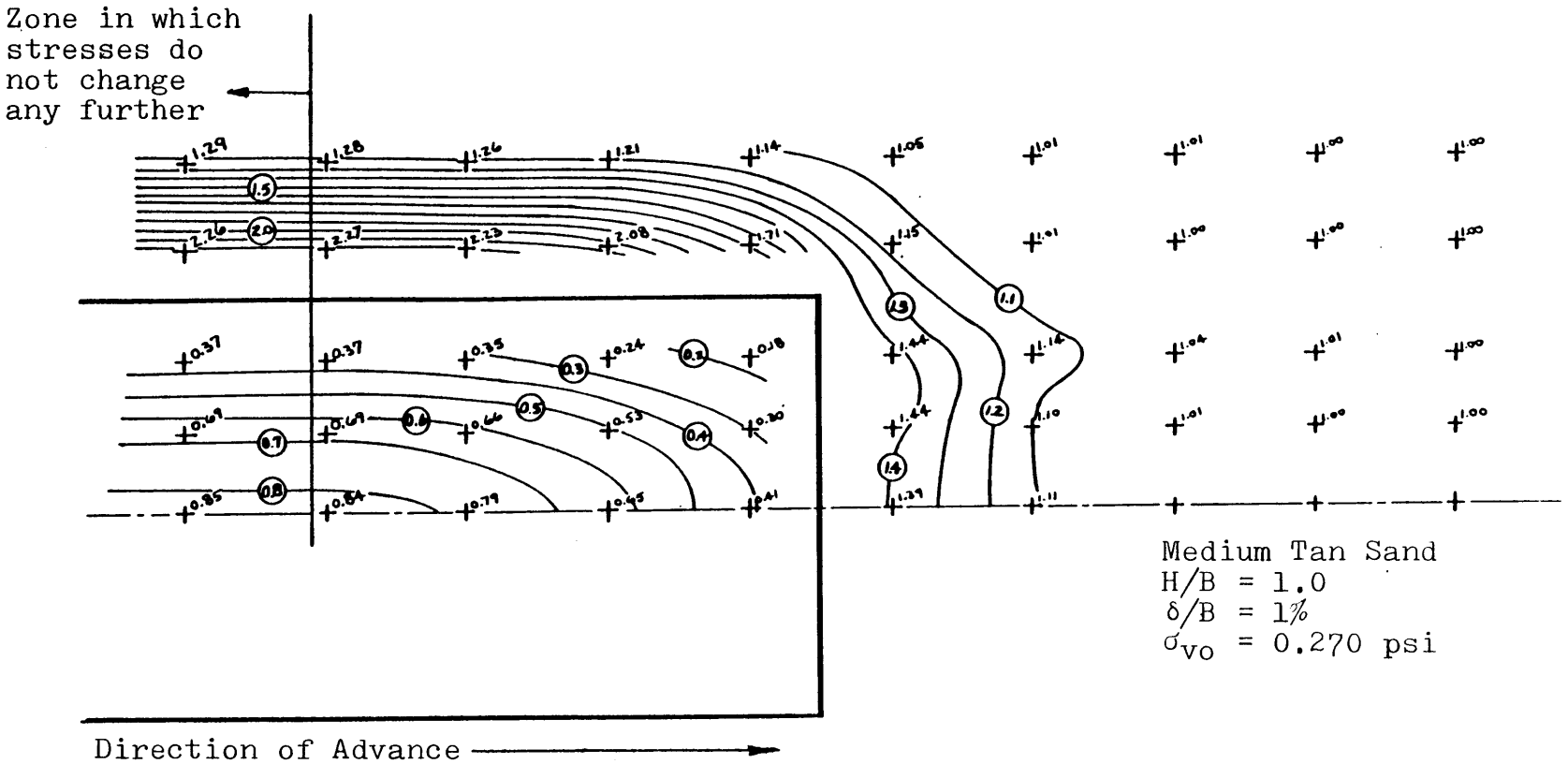

Figure 6.20 Results from Tests 39, 40, 43, and 45
Vertical Stresses Around a Simulated Advancing Tunnel

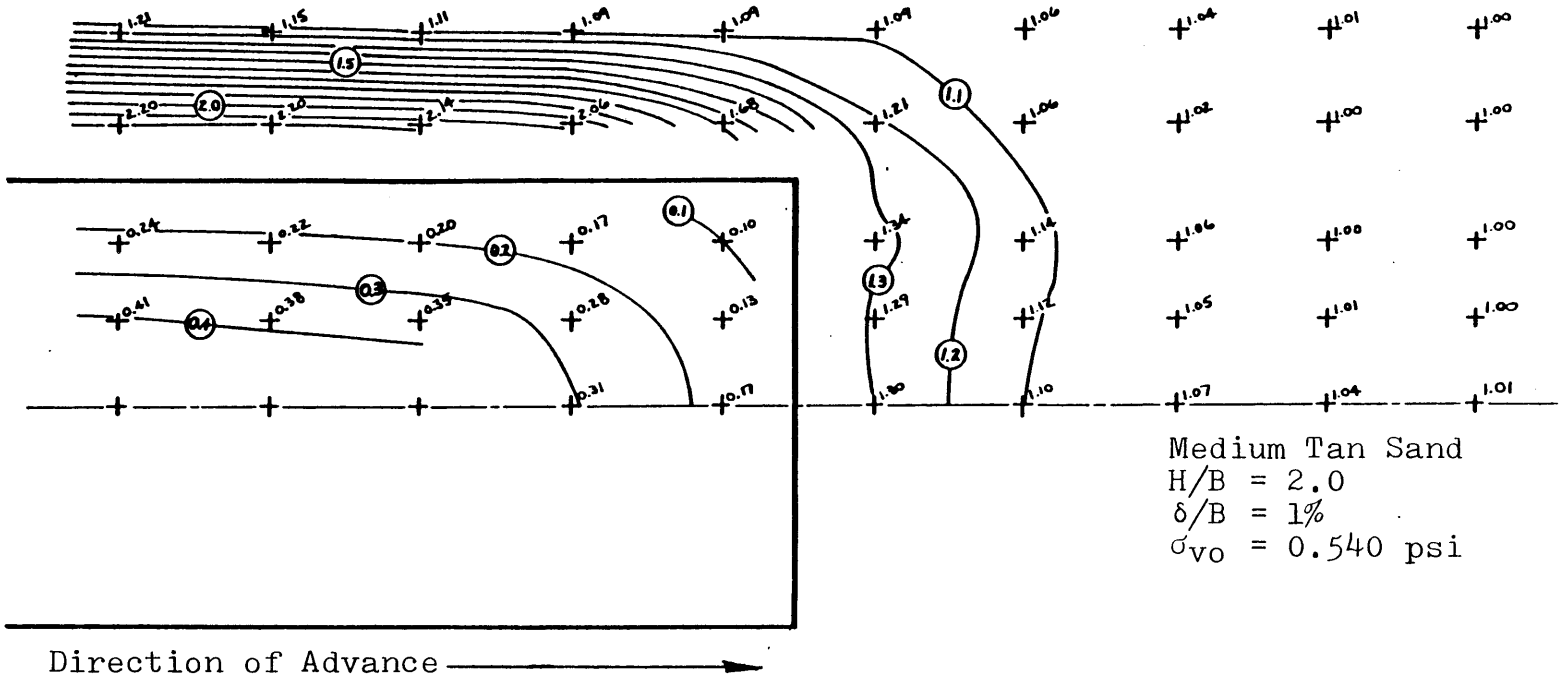

Figure 6.21 Results from Test 52
Vertical Stresses Around a Simulated Advancing Tunnel

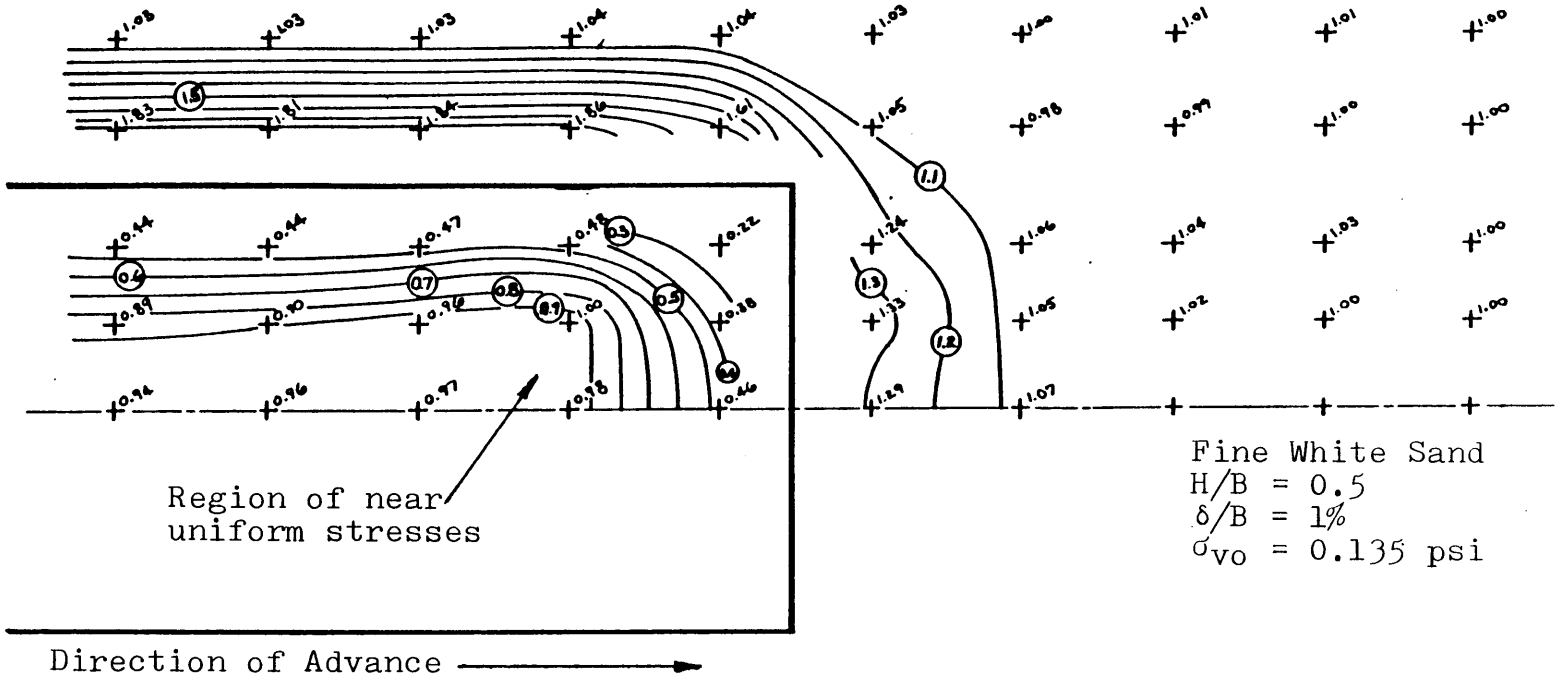

Figure 6.22 Results from Tests 48 and 49
Vertical Stresses Around a Simulated Advancing Tunnel

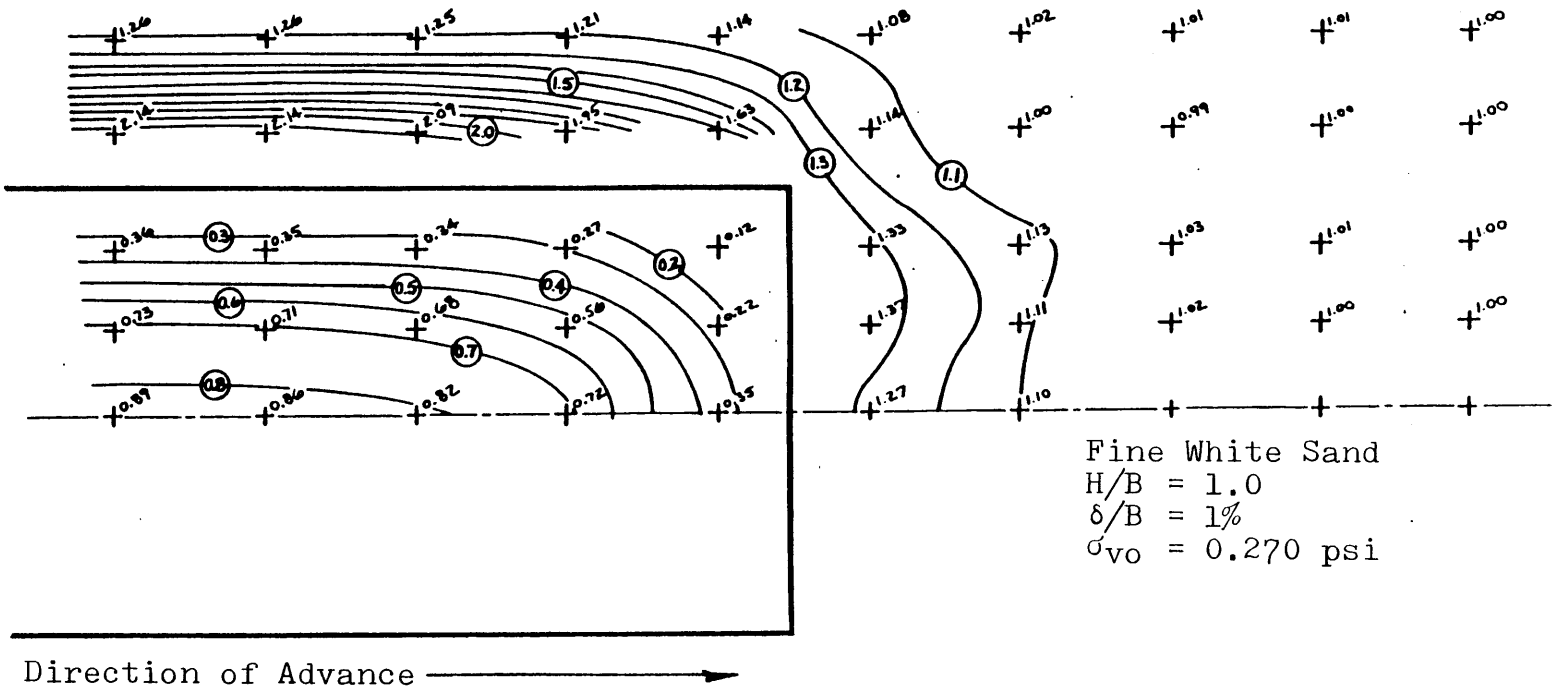

Figure 6.23 Results from Tests 47 and 50
Vertical Stresses Around a Simulated Advancing Tunnel

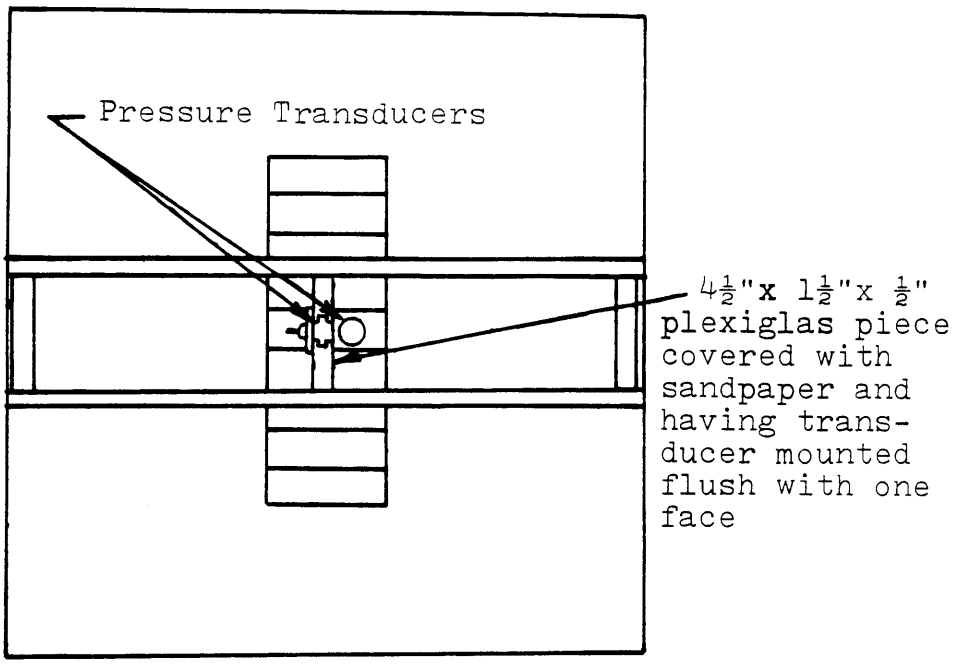

Figure 6.24 Test Configuration for Measuring K Value Above a Downward Translating Trap Door

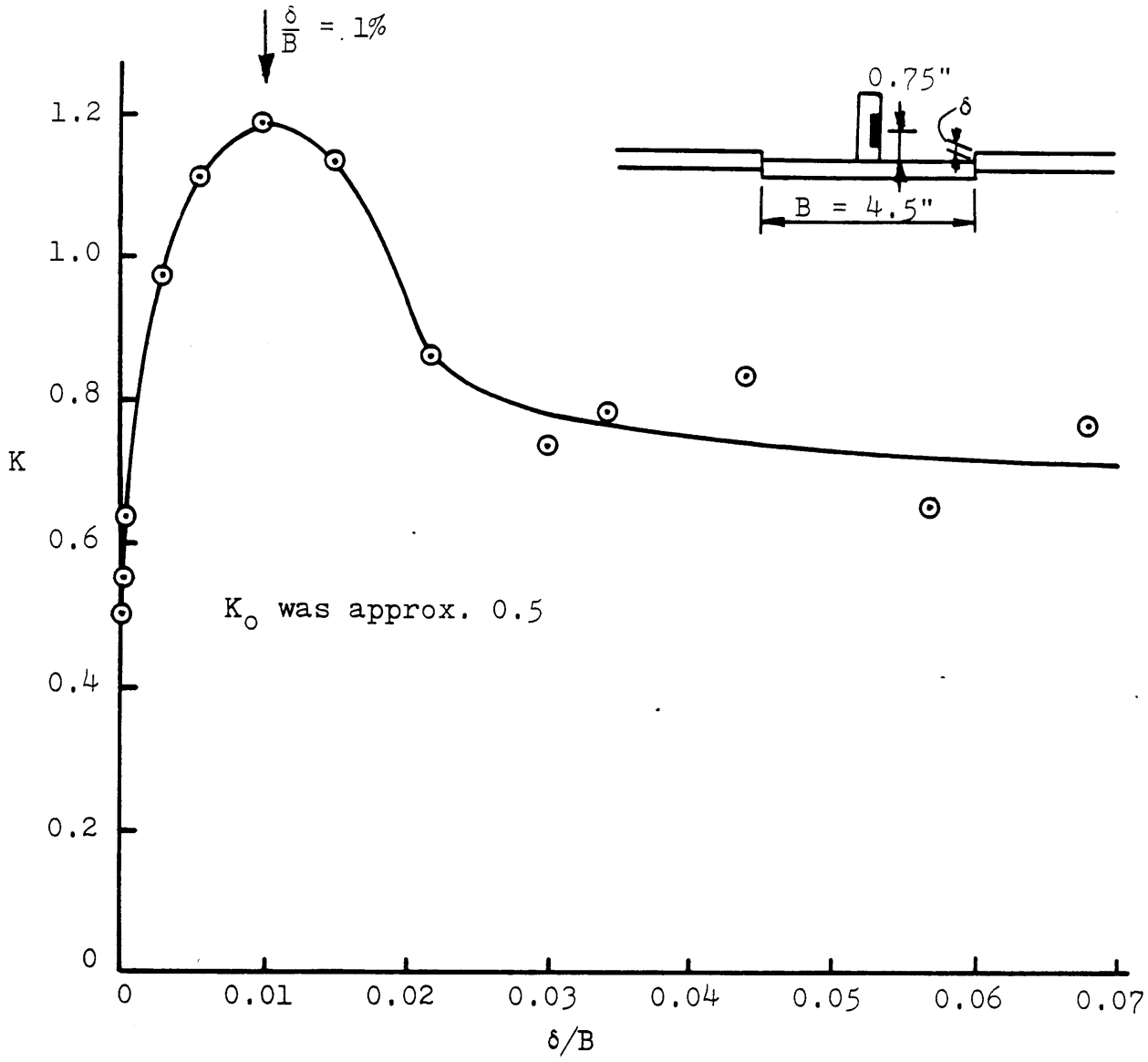

Figure 6.25 Experimentally Determined Values of K Above a Downward Translating Trap Door

Test Number	Sand Type	H/B	σ_{vo} (psi)	Values at Maximum Arching			Ultimate Values	
				(σ_v)min	δ/B	(C_c)min	(σ_v)max	(C_c)max
17	M.T.S.	2.8	0.204	0.014	0.018	0.11	0.049	0.385
18	M.T.S.	3.1	0.261	0.027	0.027	0.29	0.088	0.672
19	M.T.S.	1.9	0.143	0.024	0.095	0.26	0.058	0.457
21	C.L.B.S.	2.8	0.284	0.061	0.008	0.44	0.108	0.779
22	M.T.S.	3.0	0.199	0.047	NA	0.36	0.074	0.567
23	F.W.S.	3.1	0.207	0.042	NA	0.33	0.059	0.464
24	F.L.B.S.	3.0	0.206	0.043	NA	0.34	0.051	0.403
25	M.T.S.	3.0	0.215	0.042	NA	0.32	0.075	0.571
26	M.T.S.	1.5	0.095	0.044	NA	0.34	0.064	0.495
27	F.W.S.	3.1	0.192	0.041	NA	0.33	0.054	0.435
32	M.T.S.	2.4	0.187	0.049	0.012	0.37	0.070	0.529
			0.195	0.042	0.021	0.32	0.062	0.472
33	M.T.S.	3.0	0.320	0.057	0.013	0.42	0.085	0.626
			0.260	0.033	0.013	0.24	0.071	0.516
34	M.T.S.	1.5	0.302	0.045	0.030	0.33	NA	NA
			0.273	0.055	0.030	0.40	NA	NA
51	M.T.S.	6.0	0.506	0.062	0.030	0.46	NA	NA
			0.586	0.052	0.030	0.38	NA	NA
			0.519	0.060	0.030	0.44	NA	NA
			0.519	0.041	0.051	0.31	NA	NA
57	M.T.S.	2.0	0.160	0.039	0.005	0.29	0.043	0.320
			0.166	0.040	0.006	0.30	0.055	0.413
			0.175	0.049	0.004	0.36	0.056	0.411

Table 6.1 Summary of Data from Active Arching Tests with a Rectangular Trap Door in the Planar Soil Deformation Tank

Test Number	Sand Type	H/B	σ_{vo} (psi)	Values at Maximum Arching			Ultimate Values		
				$(\sigma_v)_{min}$	δ/B	$(C_c)_{min}$	$(\sigma_v)_{max}$	$(C_c)_{max}$	
66	M.T.S.	1.0	0.309	0.047	0.001	0.32	0.190	1.294	**
			0.224	0.102	0.001	0.31	0.286	0.869	*
67	M.T.S.	2.0	0.428	0.075	0.010	0.23	0.144	0.442	*
			0.515	0.061	0.015	0.41	0.130	0.874	**
68	M.T.S.	5.0	0.431	0.070	0.026	0.51	0.094	0.685	
			0.427	0.042	0.032	0.31	0.061	0.450	
			0.420	0.075	0.024	0.55	0.111	0.814	
69	M.T.S.	4.0	0.312	0.050	0.012	0.37	0.081	0.599	
			0.295	0.043	0.028	0.32	0.059	0.439	
			0.299	0.061	0.015	0.45	0.097	0.716	

All stresses are expressed in pounds per square inch (psi).

F.L.B.S. -- Fine Leighton Buzzard Sand
C.L.B.S. -- Coarse Leighton Buzzard Sand
M.T.S. -- Medium Tan Sand
F.W.S. -- Fine White Sand

Correction Factor for Triangular Stress Distribution -- * = 0.80, ** = 1.80, all others 0.65

Table 6.1 (cont'd) Summary of Data from Active Arching Tests with a Rectangular Trap Door in the Planar Soil Deformation Tank

Széchy (1966)

$$C_c = \frac{H}{B}\left(1 - \frac{H}{B}\tan\phi\tan^2\left(45^\circ - \frac{\phi}{2}\right)\right) \qquad \text{for } \frac{H}{B} < 5$$

$$C_c = \frac{H}{B}\left(\tan^4\left(45^\circ - \frac{\phi}{2}\right)\right) \qquad \text{for } \frac{H}{B} \geq 5$$

Vertical Slip Surfaces (from Matyas and Davis, 1983a)

$$C_c = \frac{H}{B}\left(1 - K_0\frac{H}{B}\tan\phi\right) \qquad \text{with } K_0 = 1 - \sin\phi$$

Silo Theory

$$C_c = \frac{1}{2K\tan\phi}\left(1 - e^{-2K\frac{H}{B}\tan\phi}\right)$$

Silo Theory as Modified by Terzaghi (1943)

$$C_c = \frac{1}{2K\tan\phi}\left(1 - e^{-2K\frac{H}{B}\tan\phi}\right) \qquad \text{for } \frac{H}{B} \leq 2$$

$$C_c = \frac{1}{2K\tan\phi}\left(1 - e^{-4K\tan\phi}\right) + \left(\frac{H}{B} - 2\right)e^{-4K\tan\phi} \qquad \text{for } \frac{H}{B} > 2$$

Plasticity Theory Solutions:

For Maximum Arching Point

$$C_c = \frac{H}{B}\left(1 - \frac{H}{B}\tan\phi\right) \qquad \text{for } \frac{H}{B} < \frac{1}{2\tan\phi}$$

$$C_c = \frac{1}{4\tan\phi} \qquad \text{for } \frac{H}{B} \geq \frac{1}{2\tan\phi}$$

For Ultimate Arching State

$$C_c = \frac{\left(1 - e^{-2K\frac{H}{B}\sin\phi}\right)}{2K\sin\phi} \qquad \text{for } \frac{H}{B} \leq 2$$

$$C_c = \frac{\left(1 - e^{-4K\sin\phi}\right)}{2K\sin\phi} + \left(\frac{H}{B} - 2\right)e^{-4K\sin\phi} \qquad \text{for } \frac{H}{B} > 2$$

Table 6.2 Summary of Plane Strain Active Arching Formulae

Test Number	Sand Type	H/B	σ_{vo} (psi)	Values at Maximum Arching			Ultimate Values	
				$(\sigma_v)max$	δ/B	$(C_c)max$	$(\sigma_v)min$	$(C_c)min$
28	M.T.S.	1.3	0.093	0.133	0.011	1.65	0.118	1.46
29	M.T.S.	1.2	0.078	0.124	0.004	1.37	0.107	1.29
30	F.L.B.S.	1.3	0.107	0.140	0.005	1.61	0.113	1.40
31	F.L.B.S.	1.4	0.104	0.140	0.001	1.79	0.127	1.63
62	M.T.S.	1.0	0.093	0.118	0.012	1.33	0.104	1.17
63	M.T.S.	4.0	0.314	1.211	0.048	13.68	0.976	11.02
64	M.T.S.	3.0	0.278	0.677	0.050	7.65	NA	NA
65	M.T.S.	2.0	0.174	0.338	0.040	3.82	NA	NA
		2.0	0.174	0.373	0.047	4.21	NA	NA

All stresses are expressed in pounds per square inch (psi).

F.L.B.S. -- Fine Leighton Buzzard Sand
C.L.B.S. -- Coarse Leighton Buzzard Sand
M.T.S. -- Medium Tan Sand
F.W.S. -- Fine White Sand

Table 6.3 Summary of Data from Passive Arching Tests with a Rectangular Trap Door in the Planar Soil Deformation Tank

U.S. Standard for Rigid Pipe (from Matyas and Davis, 1983a)

$$C_c = 1.961 \frac{H}{B} - 0.934$$

Vertical Slip Surfaces (from Matyas and Davis, 1983a)

$$C_c = \frac{H}{B}\left(K_o \frac{H}{B} \tan\phi + 1\right) \qquad \text{with } K_o = 1 - \sin\phi$$

Ladanyi and Hoyaux (1969)

$$C_c = \frac{H}{B}\left(1 + \frac{H \sin 2\phi}{2B}\right)$$

Das and Seeley (1975)

$$C_c = \frac{H}{B}\left(\frac{H}{B} K_a \tan\phi + 1\right)$$

Plasticity Theory Solutions --

For Maximum Arching State

$$C_c = \frac{H}{B}\left(1 + \frac{H}{B} \tan\phi\right)$$

For Ultimate Arching State

$$C_c = \frac{1}{2K_a \sin\phi}\left(e^{2K_a \frac{H}{B} \sin\phi} - 1\right) \qquad \text{for } \frac{H}{B} \leq 2$$

$$C_c = \frac{1}{2K_a \sin\phi}\left(e^{4K_a \sin\phi} - 1\right) + \left(\frac{H}{B} - 2\right) e^{4K_a \sin\phi}$$

where $K_a = \frac{1 - \sin\phi}{1 + \sin\phi}$ for $\frac{H}{B} > 2$

Table 6.4 Summary of Plane Stain Passive Arching Formulae

Test Number	Sand Type	H/B	σ_{vo} (psi)	Values at Maximum Arching			Ultimate Values	
				(σ_v)min	δ/B	(C_c)min	(σ_v)max	(C_c)max
11	F.W.S.	3.2	0.349	0.050	0.044	0.135	0.073	0.197
13	F.W.S.	1.8	0.295	0.043	0.087	0.116	0.078	0.210
14	F.L.B.S.	1.6	0.269	0.046	0.032	0.121	0.081	0.213
15	F.L.B.S.	0.9	0.161	0.042	0.030	0.111	0.069	0.182
16	M.T.S.	1.5	0.202	0.010	0.003	0.025	0.102	0.255

All stresses are expressed in pounds per square inch (psi).

F.L.B.S. -- Fine Leighton Buzzard Sand
C.L.B.S. -- Coarse Leighton Buzzard Sand
M.T.S. -- Medium Tan Sand
F.W.S. -- Fine White Sand

Correction Factor for Conical Stress Distribution -- 0.42

Table 6.5 Summary of Data from Active Arching Tests with a Circular Trap Door

Set of Tests	Sand Type	Depth of Sand (in.)	H/B	σ_{vo} (psi)	δ/B
34, 35, 36, 37, 38	M.T.S.	2.25	0.5	0.135	0.01
41, 42, 44, 46	M.T.S.	2.25	0.5	0.135	0.05
39, 40, 43, 45	M.T.S.	4.50	1.0	0.270	0.01
51	M.T.S.	9.00	2.0	0.540	0.01
48, 49	F.W.S.	2.25	0.5	0.135	0.01
47, 50	F.W.S.	4.50	1.0	0.270	0.01

M.T.S. -- Medium Tan Sand
F.W.S. -- Fine White Sand

Table 6.6 Summary of Tests Exploring Arching Around an Advancing Tunnel

CHAPTER 7: CONCLUSIONS AND SUGGESTIONS FOR FURTHER RESEARCH

7.1 Conclusions

Starting with a review of the present state-of-the-art knowledge about 'arching', theoretical and experimental work has been performed in this thesis research and has led to promising advances.

A new theoretical approach has been developed, founded on elementary plasticity theory, which predicts patterns of displacements and forces on rectangular and circular rigid structures undergoing either active or passive arching. Additionally, techniques have been suggested for extending these formulations to actual buried structures such as tunnels or culverts.

This approach has been verified by the experimental results of this research as well as some obtained by others. It was shown that it models actual arching behavior more correctly than any of the other existing approaches.

The experimental work is interesting by itself, including the design and construction of devices, and development of techniques for the quantitative investigation of arching under a variety of testing configurations. The devices made it possible to investigate both active and passive arching with soil deformations either restricted to being planar, or free to be three-dimensional. Additionally, the simulation of an advancing tunnel heading through a soil mass was accomplished, with stresses measured both on the tunnel and in the adjacent ground.

More details on these conclusions are now provided. First will be those relating to the plasticity theory, and second, those on the arching phenomenon in general.

Conclusions on Plasticity Theory Approach

Much work remains to be done before the proposed plasticity theory approach can become a reliable analytical tool for designers of underground structures, however a number of conclusions relating to the validity of this approach can be drawn from the experimental results presented in Chapter 6 and from the observations of ground movements (both field and laboratory) which were reported in Chapter 4. Specifically, the validity of this approach is shown by:

* Plasticity theory accurately predicts the ground deformation behavior adjacent to a yielding structure, including: locations and shape of discontinuities, patterns of deformation and volumetric behavior (both dilation and contraction).

* The shape of stress distributions developing above a rigid structure experiencing arching can be predicted with reasonable accuracy.

* For active plane strain arching (Section 6.5.2) the proposed plasticity theory provides: 1) a better prediction of trap door (structure) forces at maximum arching (maximum mobilization of stress redistribution; i.e. the minimum (active arching) or maximum (passive arching) force on the trap door) than any of the existing theories, and 2) reasonably good predictions of forces at ultimate arching (corresponding to large displacements) for which it is the only approach available.

* For passive plane strain arching (Section 6.5.3) the proposed theory again provides the best prediction of forces at maximum arching, however it consistently overestimates the magnitude by 10 to 15%. Some or all of this overestimation can be attributed to the test interpretation in which the assumption is made that uniform stresses across a trap door exist during passive arching, which results in measured trap door forces being somewhat

less than those actually existing. At ultimate arching, where plasticity theory provides the only available solution, the limited data obtained in this research lie near the predicted values at H/B ratios less than $1\frac{1}{2}$. More results are needed from tests with H/B > $1\frac{1}{2}$ before any conclusions can be drawn.

* For active three-dimensional arching (Section 6.6) plasticity theory predicts forces at maximum arching much better than the other available solution (three-dimensional silo theory), but still overpredicts trap door force by about 30%. Similar comments can be made for ultimate arching. It is felt that this overprediction may be related to the fact that the approach is based on the assumption of plane strain.

* Results of experiments simulating an advancing tunnel heading (Section 6.7) illustrate that plasticity theory is appropriate for predicting the general magnitude and distribution of stresses on and adjacent to such a structure.

* Experimental results from other sources (relating to both active and passive arching) all tend to be consistent with plasticity theory.

Briefly summarizing, one can conclude that the proposed plasticity theory approach provides predictions for forces on a rigid displacing structure at maximum arching, which (for the active and passive cases investigated) more closely agree with measured values than do predictions from any other available approach. Additionally, the plasticity theory is the only approach to address ultimate arching and to provide separate solutions for this state. Finally, for cases where the plasticity theory did not agree with experimental results it can be noted that the predicted force was always larger than the measured force (by up to 30%), which from a design standpoint is preferable.

Conclusions on Arching Phenomenon in General

It is possible to draw, from this thesis' research, a number of general conclusions on the phenomenon of arching.

* Active arching can reduce the loads on a buried structure by as much as 95 percent, while passive arching can increase these loads by several hundred percent. The magnitude of load reduction/increase depends on displacement and soil depth.

* Displacements of as little as 0.0005 times the width of the displacing structure can change the total load on the structure by as much as 50 percent (with active or passive arching). This indicates that considerable beneficial arching action can be developed at magnitudes of structural deformation well below those which could impair the structure's usefulness.

* For ranges of the ration "soil cover" to "trap door width" (H/B) of 0.5 to 6.0, load redistribution (for both active and passive arching) increased with increasing H/B.

* Beneficial load reduction (active arching) can exist even at very shallow depths of burial (H/B = 0.5). At larger depths of burial (H/B > 2.0) the arching mechanism leads to loads (for the active case) which are virtually independent of the depth of material above the structure.

* From the literature on observed ground deformations adjacent to tunnels, it can be concluded that deformations of sufficient magnitude (1 to 2 percent of the structure's width) to mobilize considerable arching and the associated stress redistribution do typically occur. It is, therefore, appropriate to consider this beneficial load reduction when designing the support system for a tunnel in granular soil.

* The levels of displacement necessary to reach ultimate arching (10 to > 30 percent of a structure's width) are well beyond those typically observed in the field, thereby limiting application of results for ultimate arching.

* Since the size of the trap door was not found to influence observed behavior, it is reasonable to assume that the experimental results can be extrapolated to larger structures.

7.2 Suggestions for Further Research

There are a number of areas in which further beneficial research on arching can be performed. Some of these will be summarized here, grouped into the categories "theoretical", "instrumentation", and "experimental".

In the area of theoretical formulation, the plasticity theory approach presented in Chapter 3 contained a number of simplifications and assumptions which were necessary to obtain solutions for the plane strain and three-dimensional trap door problems. Section 3.8 summarizes these simplifications and assumptions and it proposes a number of areas requiring further investigation including:

* Solutions for the case of $0^{o} < \nu < \phi$

* Effect of an existing velocity discontinuity on the formation of new discontinuities (this is important for a new structure placed adjacent to an existing structure).

* Appropriateness of the assumption that directions of major principal stress and major principal strain rate coincide.

* More rigorous extension of the plasticity theory approach (which is largely based on assumption of plane strain behavior) to problems involving three-dimensional ground deformations.

* Examination of results from actual tunnels to develop a better understanding of appropriate values for equivalent trap door width (as used in Section 4.5).

Generally, it is important that techniques be devised for applying plasticity theory to more complicated arching problems than just the translating rigid trap door. This requires extension of this approach to commonly encountered problem geometries (i.e. circular and rectangular structures) and inclusion in the analysis of the load-deformation behavior of the buried structure (so as to provide solutions for flexible yielding surfaces).

In the area of instrumentation, a stress measuring cell is needed which lacks some of the detrimental characteristics of the pressure transducers used in this investigation. Of particular concern is the hysteretic behavior observed during load-unload cycles with the transducers in contact with sand, as well as the general fact that pressure transducers are boundary-type cells and therefore unable to measure stresses within the soil mass. In addition, difficulties were encountered because of the low stress levels (small depths of sand) in the experimental program. These problems could be reduced either through use of cells with better readability and less temperature sensitivity or by raising the stress level through surcharging (such as with a pressure bag) on the sand's surface.

Finally, further experimentation, with the primary test apparatus, should be performed to clarify questions raised in this research, such as the following:

* Why are similar magnitudes of normalized displacement (δ/B) necessary to mobilize maximum active or passive arching, while for ultimate arching far more displacement is required in the passive case?

* Why did the normalized displacement (δ/B) at which maximum arching occurred tend to be higher in tests with three-dimensional soil deformations?

* Several tests showed somewhat different arching behavior when the sand type was varied, but no clear trend was observed. Does the sand type (and density at which it is deposited) have a perceptible impact on arching behavior?

* Plasticity theory would predict that structures having peaked or arched roofs experience greater active arching load reduction than those with flat roofs. Trap door experiments could show whether this in fact occurs.

* How does the value of K (coefficient of lateral stress) vary with distance above a yielding structure and with the magnitude of displacement?

* Do values for angle of dilation (ν) extrapolated from test results agree with those obtained from other testing techniques?

BIBLIOGRAPHY

Abbott, Phillip A., (1967), "Arching for Vertically Buried Prismatic Structures", Journal of the Soil Mechanics and Foundations Division, ASCE, Vol. 93, SM5, pp. 233-255.

Allgood, Jay R., (1964), "The Behavior of Shallow-Buried Cylinders", Proceedings, Symposium on Soil-Structure Interaction, University of Arizona, pp. 189-210.

Allgood, J.R. and J.B. Ciani, (1968), "The Influence of Soil Modules on the Behavior of Cylinders in Sand", Highway Research Record, No. 29, "Retaining Walls and Culverts", pp. 1-13.

Anand, L., (1983), "Plane Deformations of Ideal Granular Materials", Journal of the Mechanics and Physics of Solids, Vol. 31, No. 2, pp. 105-122.

Atkinson, J.H., E.T. Brown, and D.M. Potts, (1975), "Collapse of Shallow Unlined Tunnels in Dense Sand", Tunnels and Tunnelling, May 1975, pp. 82-87.

Atkinson, J.H., E.T. Brown, and D.M. Potts, (1977), "Ground Movements Near Shallow Model Tunnels in Sand", Proceedings, Large Ground Movements and Structures, The University of Wales Institute of Science and Technology, John Wiley and Sons, Inc., New York, pp. 372-386.

Atkinson, J.H. and A.M. Cairncross, (1973), "Collapse of a Shallow Tunnel in a Mohr-Coulomb Material", Proceedings of the Symposium on the Role of Plasticity in Soil Mechanics, Cambridge, 13-15 September 1973, pp. 202-206.

Atkinson, J.H., A.M. Cairncross, and R.G. James, (1974), "Model Tests on Shallow Tunnels in Sand and Clay", Tunnels and Tunnelling, July 1974, pp. 28-32.

Atkinson, J.H. and T.L.L. Orr, (1976), "Experiments on Model Tunnels in Stiff Clay", Proceedings, Sixth European Conference on Soil Mechanics and Foundation Engineering, Vienna, Vol. 1, pp. 277-280.

Atkinson, J.H. and D.M. Potts, (1975), "A Note on Associated Field Solutions for Boundary Value Problems in a Variable ϕ - Variable ν Soil", Geotechnique, Vol. 25, pp. 379-384.

Atkinson, J.H. and D.M. Potts, (1977), "Subsidence Above Shallow Tunnels in Soft Ground", Journal of the Geotechnical Engineering Division, ASCE, Vol. 103, GT4, pp. 307-325.

Atkinson, J.H., D.M. Potts, and A.N. Schofield, (1977), "Centrifugal Model Tests on Shallow Tunnels in Sand", Tunnels and Tunnelling, January 1977, pp. 59-62.

Attewell, Peter, (1977), "Ground Movements Caused by Tunnelling in Soil", Proceedings, Large Ground Movements and Structures, The University of Wales Institute of Science and Technology, John Wiley and Sons, Inc., New York, pp. 812-948.

Baus, R.L. and M.C. Wang, (1983), "Bearing Capacity of Strip Footing Above Void", Journal of Geotechnical Engineering, ASCE, Vol. 109, No. 1, pp. 1-14.

Bekenstein, Stefanie, (1980), Directional Shear Tests on Leighton Buzzard Sand, Master of Science Thesis in Civil Engineering, Massachusetts Institute of Technology.

Bello, Arturo A., (1977), "Simplified Method for Stability Analysis of Underground Openings", Proceedings, First International Symposium on Storage in Excavated Rock Caverns, Rockstore '77, Stockholm, Sweden, Vol. 2, pp. 289-294.

Bjerrum, L., C.J. Frimann Clausen, and J.M. Duncan, (1972), "Earth Pressures on Flexible Structures -- A State-of-the-Art Report", Proceedings, Fifth European Conference on Soil Mechanics and Foundation Engineering, Madrid, Spain, pp. 169-196.

Bransby, P.L. and P.M. Blair-Fish, (1975), "Deformations Near Rupture Surfaces in Flowing Sand", Geotechnique, The Institution of Civil Engineers, London, Vol. 25, pp. 384-389.

Bucknam, M.D., R.V. Whitman, and P.C. Lambe, (1981), Densification and Cyclic Triaxial Testing of Leighton Buzzard 120/200 Sand, Massachusetts Institute of Technology Research Report R82-15.

Burghignoli, A., (1981), "Soil Interaction in Buried Structures", Proceedings, Tenth International Conference on Soil Mechanics and Foundation Engineering, Stockholm, Sweden, Vol. 2, pp. 69-74.

Butler, R.A. and D. Hampton, (1975), "Subsidence Over Soft Ground Tunnel", Journal of the Geotechnical Engineering Division, ASCE, Vol. 101, GT1, pp. 35-49.

Butterfield, R., (1969), "A Theoretical Study of the Pressures Developed in a Silo Containing Single-Sized Particles in a Regular Packing", International Journal of Rock Mechanics and Mining Sciences, Pergamon Press, Vol. 6, pp. 227-247.

Butterfield, R., R.M. Harkness, and K.Z. Andrawes, (1973), "Idealized Granular Materials", Proceedings of the Symposium on the Role of Plasticity in Soil Mechanics, Cambridge, 13-15 September 1973, pp. 174-187.

Canizo, L., (1973), "Soil Pressure in the Vicinity of a Tunnel Face", Proceedings of the Symposium on the Role of Plasticity in Soil Mechanics, Cambridge, 13-15 September 1973, pp. 206-211.

Carrier, W.D., (1969), Lunar Soil Mechanics: Distribution of Contact Stress Beneath a Rigid Plate Resting on Sand, Doctor of Science Thesis in Civil Engineering, Massachusetts Institute of Technology.

Chadwick, W.L., (1976), Failure of Teton Dam, Report to U.S. Department of Interior and State of Idaho, Independent Panel to Review Cause of Teton Dam Failure, Wallace L. Chadwick, Chairman, U.S. Government Printing Office, Washington.

Chelapati, Chunduri V., (1964), "Arching in Soil Due to the Deflection of a Rigid Horizontal Strip", Proceedings, Symposium on Soil-Structure Interaction, University of Arizona, pp. 356-377.

Cording, E.J. and W.H. Hansmire, (1975), "Displacements Around Soft Ground Tunnels", Proceedings, Fifth Panamerican Conference on Soil Mechanics and Foundation Engineering, Buenos Aires, Vol. 4, pp. 571-633.

Davis, E.H., (1968), "Theories of Plasticity and the Failure of Soil Masses", Chapter Six from Soil Mechanics, Selected Topics, edited by I.K. Lee, American Elsevier Publishing Company, Inc., New York, pp. 341-380.

Davis, R.E. and A.E. Bacher, (1968), "California's Culvert Research Program -- Description, Current Status, and Observed Peripheral Pressures", Highway Research Record, No. 249, pp. 14-23.

Eadie, H.S., (1977), "Settlements Observed Above a Tunnel in Sand", Tunnels and Tunnelling, September 1977, pp. 93-95.

Einstein, H.H., C.W. Schwartz, W. Steiner, M.M. Baligh, and R.E. Levitt, (1980), "Improved Design for Tunnel Supports: Analysis Method and Ground Structure Behavior: A Review - Volume II", Massachusetts Institute of Technology, DOT-05-60136.

Eisenstein, Z., F. El-Nahhis, and S. Thomson, (1981), "Strain Field Around a Tunnel in Stiff Soil", Proceedings, Tenth International Conference on Soil Mechanics and Foundation Engineering, Stockholm, Sweden, Vol. 1, pp. 283-288.

Evans, I., (1977), "Face Support Requirements -- A Problem in Arching", International Journal of Rock Mechanics and Mining Sciences Geomechanics Abstracts, Pergamon Press, Vol. 14, pp. 1-5.

Feld, Jacob, (1948), "Early History and Bibliography of Soil Mechanics", Proceedings, Second International Conference on Soil Mechanics and Foundation Engineering, Rotterdam, Vol. 1, pp. 1-7.

Finn, W.D.L., (1963), "Boundary Value Problems of Soil Mechanics", Journal of the Soil Mechanics and Foundation Division, ASCE, Vol. 89, No. SM5, pp. 39-72.

Getzler, Z., M. Gellert, and R. Eitan, (1970), "Analysis of Arching Pressures in Ideal Elastic Soil", Journal of the Soil Mechanics and Foundations Division, ASCE, Vol. 96, SM4, pp. 1357-1372.

Getzler, Z., A. Komornik, and A. Mazurik, (1968), "Model Study on Arching Above Buried Structures", Journal of the Soil Mechanics and Foundations Division, ASCE, Vol. 94, SM5, pp. 1123-1141.

Hampton, D. and W.B. Truesdale, (1968), "Stress and Strain Gauges for Use in Soil Dynamic Research", Instrument Society of America, Vol. 7, No. 3, pp. 242-251.

Hansmire, W.H. and E.J. Cording, (1972), "Performance of a Soft Ground on the Washington Metro", Proceedings, North American Rapid Excavation and Tunnelling Conference, Chicago, Illinois, Vol. 1, pp. 371-389.

Harris, G.W., (1974), "A Sandbox Model Used to Examine the Stress Distribution Around a Simulated Longwall Coal-Face", International Journal of Rock Mechanics, Mining Sciences and Geomechanical Abstracts, Pergamon Press, Vol. 11, pp. 325-335.

Harris, G.W. and J.S. Seager, (1973), "Pressure Measurement in Sand Model Experiments and the Use of Pressure-Sensitive Transistors", International Journal of Rock Mechanics, Mining Sciences and Geomechanical Abstracts, Pergamon Press, Vol. 10, pp. 613-622.

Highway Research Board, (1971), "Structural Analysis and Design of Pipe Culverts", National Cooperative Highway, Research Report 116.

Jakobson, Bernt, (1958), "On Pressure in Silos", Proceedings, Conference on Earth Pressure Problems, Brussels, Vol. 1, pp. 49-54.

Jaky, J., (1948), "Pressure in Silos", Proceedings, Second International Conference on Soil Mechanics and Foundations Engineering, Rotterdam, Vol. 1, pp. 103-107.

Katzenbach, R. and H. Breth, (1981), "Non-linear 3-D Analysis for NATM in Frankfurt Clay", Proceedings, Tenth International Conference on Soil Mechanics and Foundation Engineering, Stockholm, Sweden, Vol. 1, pp. 315-318.

Kolbuszewski, J., (1958), "Fundamental Factors Affecting Experimental Procedures Dealing with Pressure Distribution in Sands", Proceedings, Brussels Conference on Earth Pressure Problems, Vol. 1, pp. 71-83.

Krizek, R.J. and J. Neil Kay, (1972), "Material Properties Affecting Soil-Structure Interaction of Underground Conduits", Highway Research Record, No. 413, pp. 13-29.

Ladanyi, B. and B. Hoyaux, (1969), "A Study of the Trap-Door Problem in a Granular Mass", Canadian Geotechnical Journal, Vol. 6, No. 1, pp. 1-15.

Lambe, T.W. and R.V. Whitman, (1969), Soil Mechanics, John Wiley and Sons, Inc., New York.

Lee, I.K.,)1975), "Application of Plasticity Theory to the Prediction of Earth Pressures", Chapter Two from: Soil Mechanics: Recent Developments, Edited by S. Valliappan, S. Hain, and I.K. Lee, William H. Sellen Pty. Ltd., Zetland, N.S.W. Australia.

Lee, I.K. and J.R. Herington, (1974), "Stability and Earth Pressures", Chapter Six from Soil Mechanics - New Horizons, Edited by I.K. Lee, American Elsevier Publishing Company, Inc., New York, pp. 205-236.

Linger, Don A., (1972), "Historic Development of the Soil-Structure Interaction Problem", Highway Research Record, No. 413, pp. 5-12.

Linger, D.A. and P. Fernandez, (1968), "Soil Pressure Distribution on Buried Structures", Highway Research Record, Number 249, "Retaining Walls and Culverts", pp. 24-36.

Luscher, U. and K. Höeg, (1964), "The Beneficial Action of the Surrounding Soil on the Load-Carrying Capacity of Buried Tubes", Proceedings, Symposium on Soil-Structure Interaction, University of Arizona, pp. 393-402.

Luscher, U. and K. Höeg, (1965), "The Action of Soil Around Buried Tubes", Proceedings, Sixth International Conference on Soil Mechanics and Foundation Engineering, Montreal, Canada, Vol. 2, pp. 396-400.

Mackey, R.D. and P. Creighton, (1965), "Pressure Cell Using Semiconductor Gauges", Engineering, 16 April 1965, pp. 513-514.

Markovic, O. and B. Popovic, (1970), "A Comparison of the Loading of a Tunnel Lining as Measured In Situ and Calculated by Analytical Methods", Proceedings, Second Congress of the International Society for Rock Mechanics, Belgrade, Vol. 2, pp. 883-889.

Matyas, E.L. and J.B. Davis, (1983a), "Prediction of Vertical Earth Loads on Rigid Pipes", Journal of Geotechnical Engineering, ASCE, Vol. 109, No. 2, pp. 190-201.

Matyas, E.L. and J.B. Davis, (1983b), "Experimental Study of Earth Loads on Rigid Pipes", Journal of Geotechnical Engineering, ASCE, Vol. 109, No. 2, pp. 202-209.

McNulty, J.W., (1965), An Experimental Study of Arching in Sand, Ph.D. Thesis in Civil Engineering, University of Illinois.

Mitchell, James K., (1976), Fundamentals of Soil Behavior, John Wiley and Sons, Inc., New York.

Morgan, J.R. and P.J. Moore, (1968), "Experimental Techniques", Chapter Five from Soil Mechanics, Selected Topics, edited by I.K. Lee, American Elsevier Publishing Company, Inc., New York, pp. 295-340.

Muir Wood, A.M., (1975), "The Circular Tunnel in Elastic Ground", Geotechnique, Vol. 25, No. 1, pp. 115-127.

Newmark, N.M., (1964), "The Basis of Current Criteria for the Design of Underground Protective Construction", Proceedings, Symposium on Soil-Structure Interaction, University of Arizona, pp. 1-24.

Nielson, Farrel D., (1966), Soil-Structure-Arching Analysis of Buried Flexible Structures, Ph.D. Thesis in Civil Engineering, University of Arizona.

Nielson, F.D., (1967), "Soil Structure Arching Analysis of Buried Flexible Structures", Highway Research Record, No. 185, pp. 36-50.

Peck, R.B., (1969), "Deep Excavation and Tunnelling in Soft Ground", Proceedings, Seventh International Conference on Soil Mechanics and Foundation Engineering, Mexico City, Vol. 1, pp. 225-258.

Peck, R.B., (1975), "Lateral Pressures Against Tunnels", Seminar on Lateral Soil Pressures Generated by Pipes, Piles, Tunnels, and Caissons, Dayton Section ASCE, 14 p.

Poulos, H.G. and E.H. Davis, (1974), Elastic Solutions for Soil and Rock Mechanics, John Wiley and Sons, Inc., New York.

Proctor, R.V. and T.L. White, (1946), Rock Tunnelling with Steel Supports, Commercial Shearing, Inc.

Proctor, R.V. and T.L. White, (1977), Earth Tunnelling with Steel Supports, Commercial Shearing, Inc.

Ranken, R.E. and J. Ghaboussi, (1975), Tunnel Design Considerations: Analysis of Stresses and Deformations Around Advancing Tunnels, Department of Transportation, Report No. FRA-OR and D 75-84.

Riley, William F., (1964), "Stresses at Tunnel Intersections", Journal of the Engineering Mechanics Division, ASCE, Vol. 90, EM2, pp. 167-179.

Roberds, W.J. and H.H. Einstein, (1977), A General Purpose Elasto Visco Plastic Critical State Behavioral Model, M.I.T. Department of Civil Engineering Research Report R77-8, March.

Rohmaller, P.L., (1968), Arching Effect for Underground Rectangular Structures Subjected to High Static Pressure, Ph.D. Thesis in Civil Engineering, University of Illinois.

Rowe, P.W., (1962), "The Stress-Dilatancy Relation for Static Equilibrium of an Assembly of Particles in Contact", Proceedings of the Royal Society of London; Series A, Mathematical and Physical Sciences, Vol. 269, pp. 500-527.

Rowe, P.W., (1963), "Stress-Dilatancy, Earth Pressures, and Slopes", Journal of the Soil Mechanics and Foundation Division, ASCE, Vol. 89, SM3, pp. 37-61.

Rude, Lawrence C., (1982), "Measured Performance of a Laboratory Culvert", Journal of the Geotechnical Engineering Division, ASCE, Vol. 108, No. GT12, pp. 1624-1641.

Rude, Lawrence C., (1983), "Load Reduction on Buried Rigid Pipe", Journal of Transportation Engineering, ASCE, Vol. 109, No. 1, pp. 107-123.

Selig, E.T., (1972), "Subsurface Soil-Structure Interaction: A Synopsis", Highway Research Record, No. 413, pp. 1-4.

Selig, E.T., (1975), "Stresses and Deflections Around Large Corrugated-Metal, Buried Structures", Seminar on Lateral Soil Pressures Generated by Pipes, Piles, Tunnels and Caissons, Dayton Section ASCE, 36 p.

Shakhunyants, G.M., (1958), "To the Problem of Earth Pressure", Proceedings, Conference on Earth Pressure Problems, Brussels, Vol. 3, pp. 80-84.

Smoltczyk, U. and P. Holzmann, (1969), "Earth Pressure Reduction in Front of a Tunnel Shield", Proceedings, Seventh International Conference on Soil Mechanics and Foundation Engineering, Mexico City, Mexico, Vol. 2, pp. 473-481.

Spangler, M.G. and R.L. Handy, (1973), Soil Engineering, 3rd Edition, Intext Educational Publishers, New York.

Szechy, Karoly, (1966), The Art of Tunnelling, Akademiai Kiado, Budapest.

Szwedzicki, Tadeusz, (1981), "FEM Calculation of Stress Around Underground Opening", Proceedings of the Seventh Plenary Scientific Session of the International Bureau of Rock Mechanics, World Mining Congress, Katowice, Poland, pp. 143-149.

Terzaghi, Karl, (1936), "Stress Distribution in Dry and in Saturated Sand Above a Yielding Trap-Door", Proceedings, First International Conference on Soil Mechanics and Foundation Engineering, Cambridge, Massachusetts, pp. 307-311.

Terzaghi, Karl, (1943), Theoretical Soil Mechanics, John Wiley and Sons, New York.

Triandafilidis, G.E., D. Hampton, and M. Spanovich, (1964), "An Experimental Evaluation of Soil Arching", Proceedings, Symposium on Soil-Structure Interaction, University of Arizona, pp. 403-420.

Trollope, D.H., (1957), "The Systematic Arching Theory Applied to the Stability Analysis of Embankments", Proceedings, Fourth International Conference on Soil Mechanics and Foundation Engineering, Vol. 2, pp. 382-388.

Trollope, D.H. and I.K. Lee, (1961), "The Measurement of Soil Pressures", Proceedings, Fifth International Conference on Soil Mechanics and Foundation Engineering, Paris, Vol. 2.

Trollope, D.H., M.G. Speedie, and I.K. Lee, (1963), "Pressure Measurements on Tullaroop Dam Culvert", Fourth Australia-New Zealand Conference on Soil Mechanics and Foundation Engineering, pp. 81-92.

Truesdale, W.B. and E. Vey, (1964), "An Investigation of Panel-Arching Effects in Noncohesive Soil", Proceedings, Symposium on Soil-Structure Interaction, University of Arizona, pp. 349-355.

Van Horn, D.A., (1964), "A Study of Loads on Underground Structures", Proceedings, Symposium on Soil-Structure Interaction, University of Arizona, pp. 256-282.

Vardoulakis, I., B. Graf, and G. Gudehus, (1981), "Trap-Door Problem with Dry Sand: A Statical Approach Based Upon Model Test Kinematics", International Journal for Numerical and Analytical Methods in Geomechanics, John Wiley and Sons, Ltd., Vol. 5, pp. 57-78.

Weiler, W.A. and F.H. Kulhawy, (1982), "Factors Affecting Stress Cell Measurements in Soil", Journal of the Geotechnical Engineering Division, ASCE, Vol. 108, No. GT12, pp. 1529-1548.

Whitman, R.V., Z. Getzler, and K. Höeg, (1962), "Static Tests Upon Thin Domes Buried in Sand", M.I.T. Research Project Report No. R62-41, December.

Whitman, R.V., Z. Getzler, and K. Höeg, (1963), "Tests Upon Thin Domes Buried in Sand", Journal of the Boston Society of Civil Engineers, January, pp. 1-22.

Wiehle, Carl K., (1964), "Review of Soil-Structure Interaction", Proceedings, Symposium on Soil-Structure Interaction, University of Arizona, pp. 239-245.

Crandall, S. H. and N. C. Dahl (1959), An Introduction to the Mechanics of Solids, McGraw Hill Book Company; New York.

Sien, P. C. (1983), Personal Communication.

APPENDIX A

Photographs of Testing Program

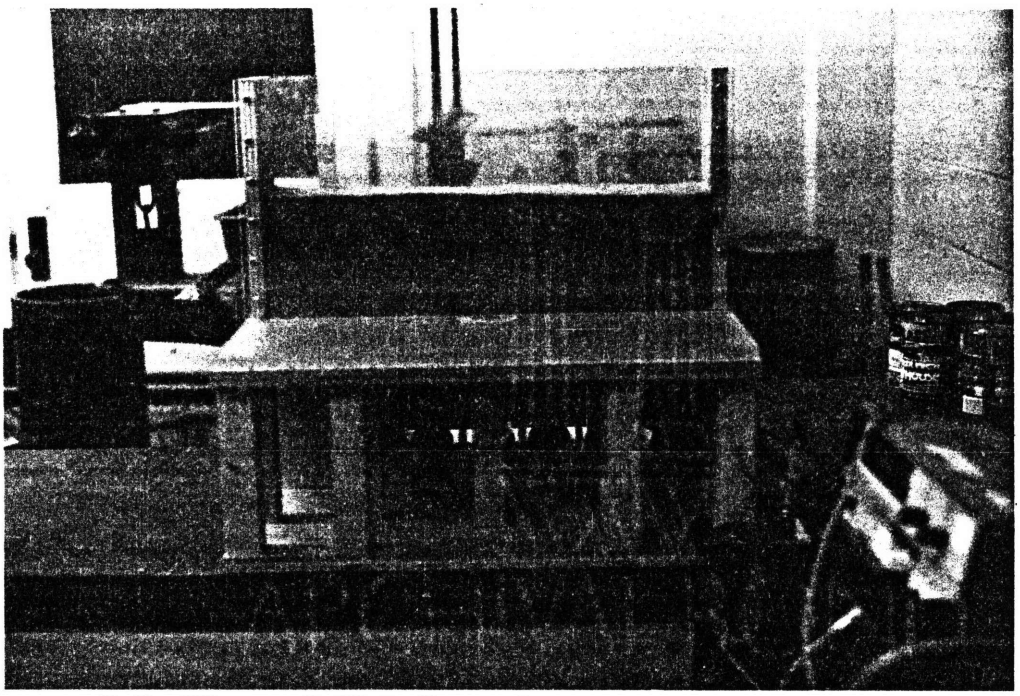

A.1 Planar Soil Deformation Tank

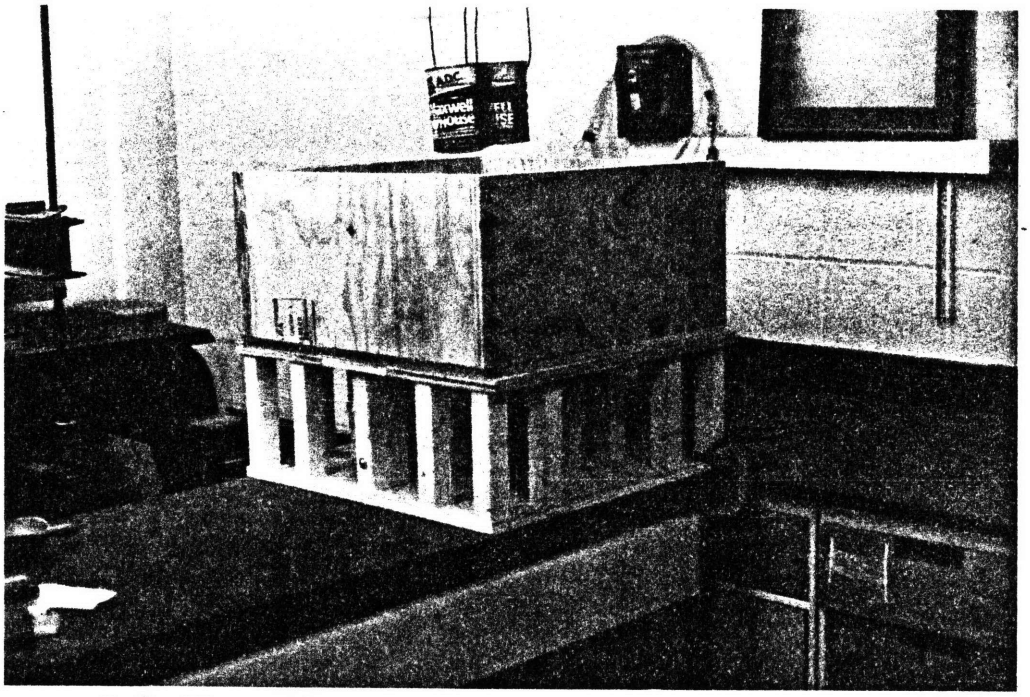

A.2 Three-Dimensional Soil Deformation Tank

Primary Test Apparatus with Soil Containment Tanks in Place

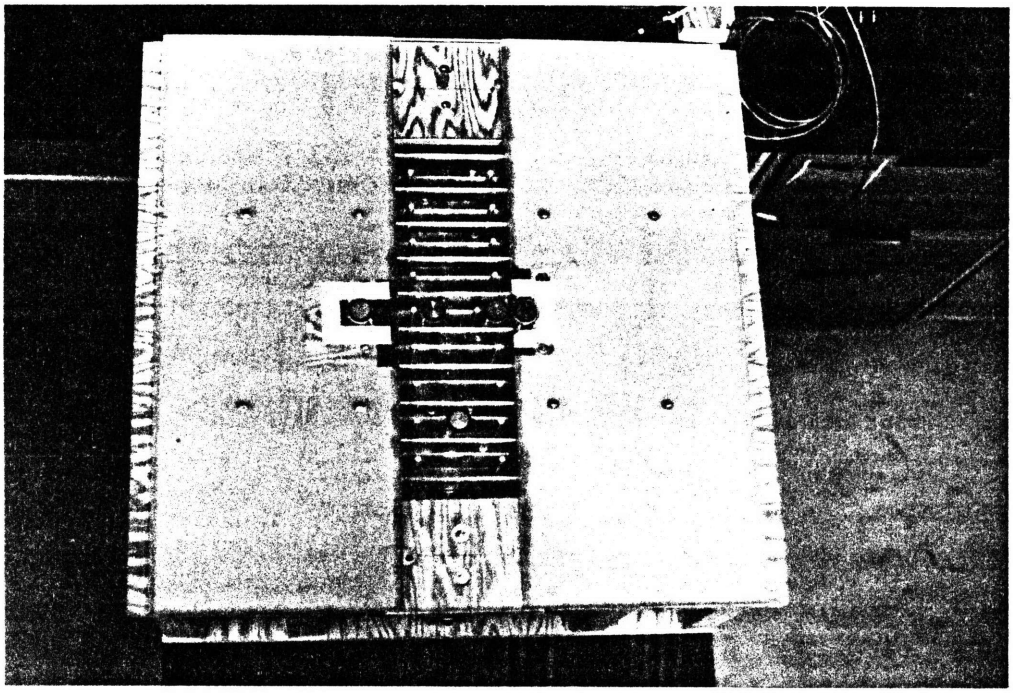

A.3 Top View without Containment Tank in Place; Primary Test Apparatus

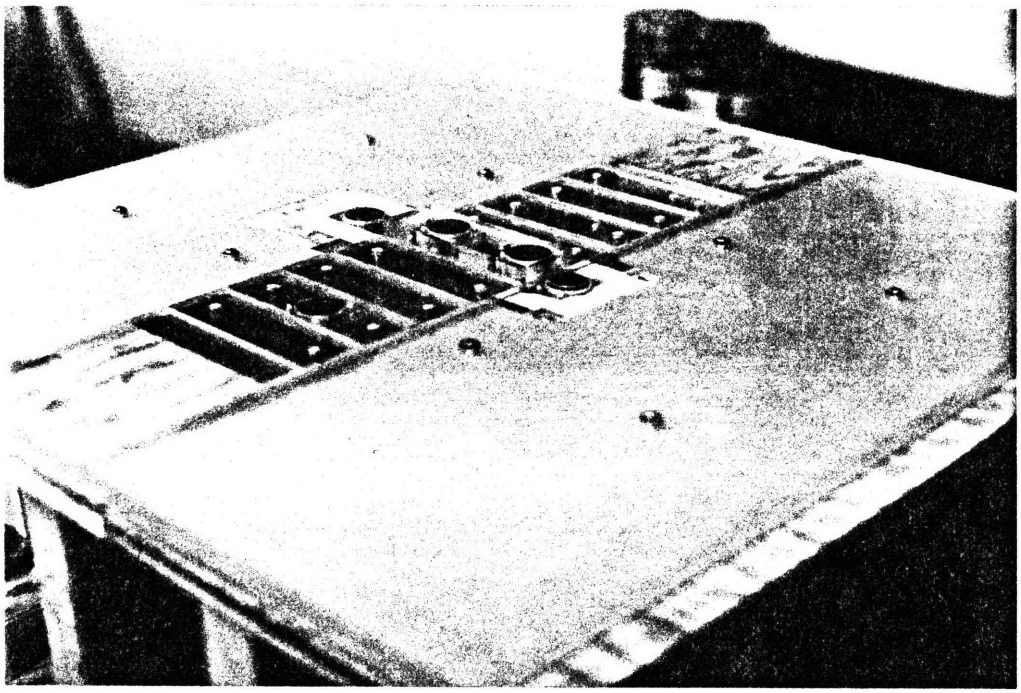

A.4 Trap Doors and Adjacent Stationary Base; Primary Test Apparatus

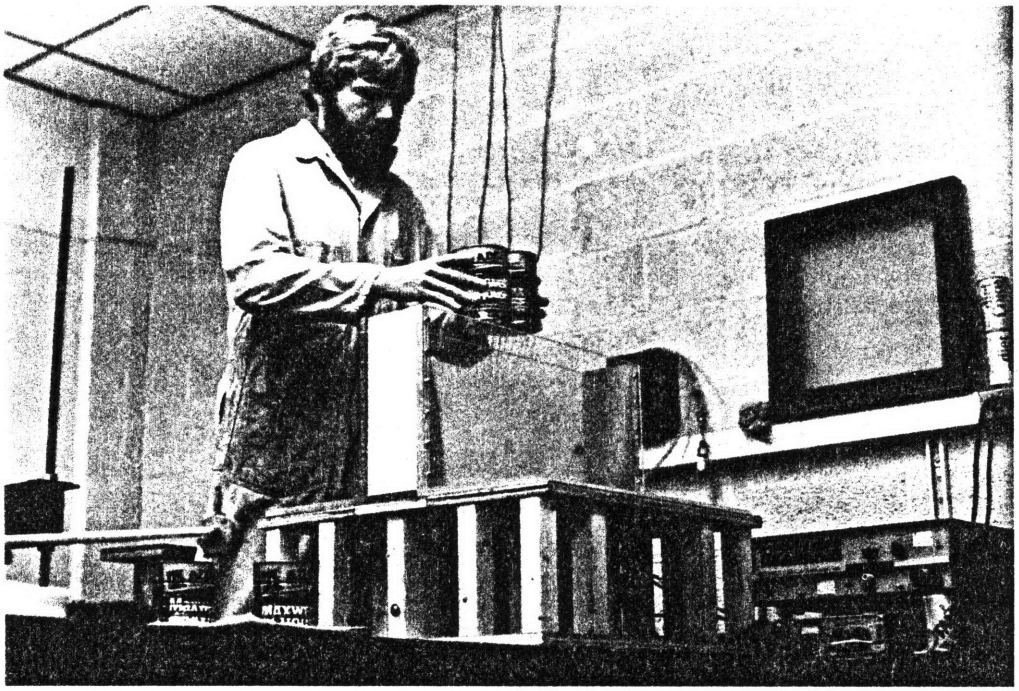

A.5 Primary Deposition Technique - Raining from Cans

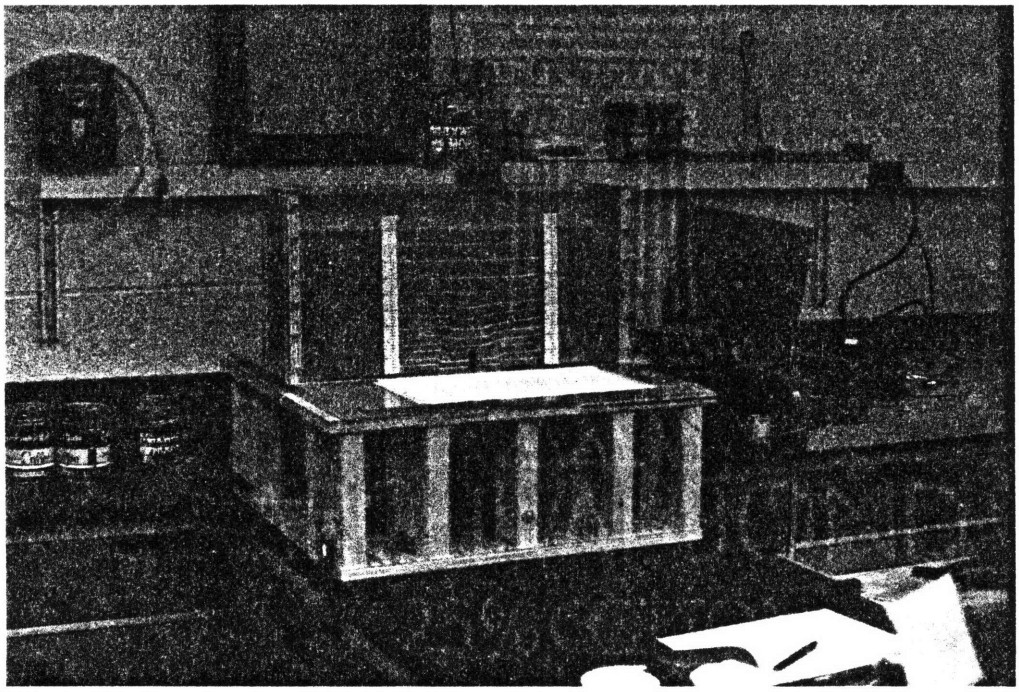

A.6 Test Configuration for Examining the Coefficient of Lateral Stress (K)

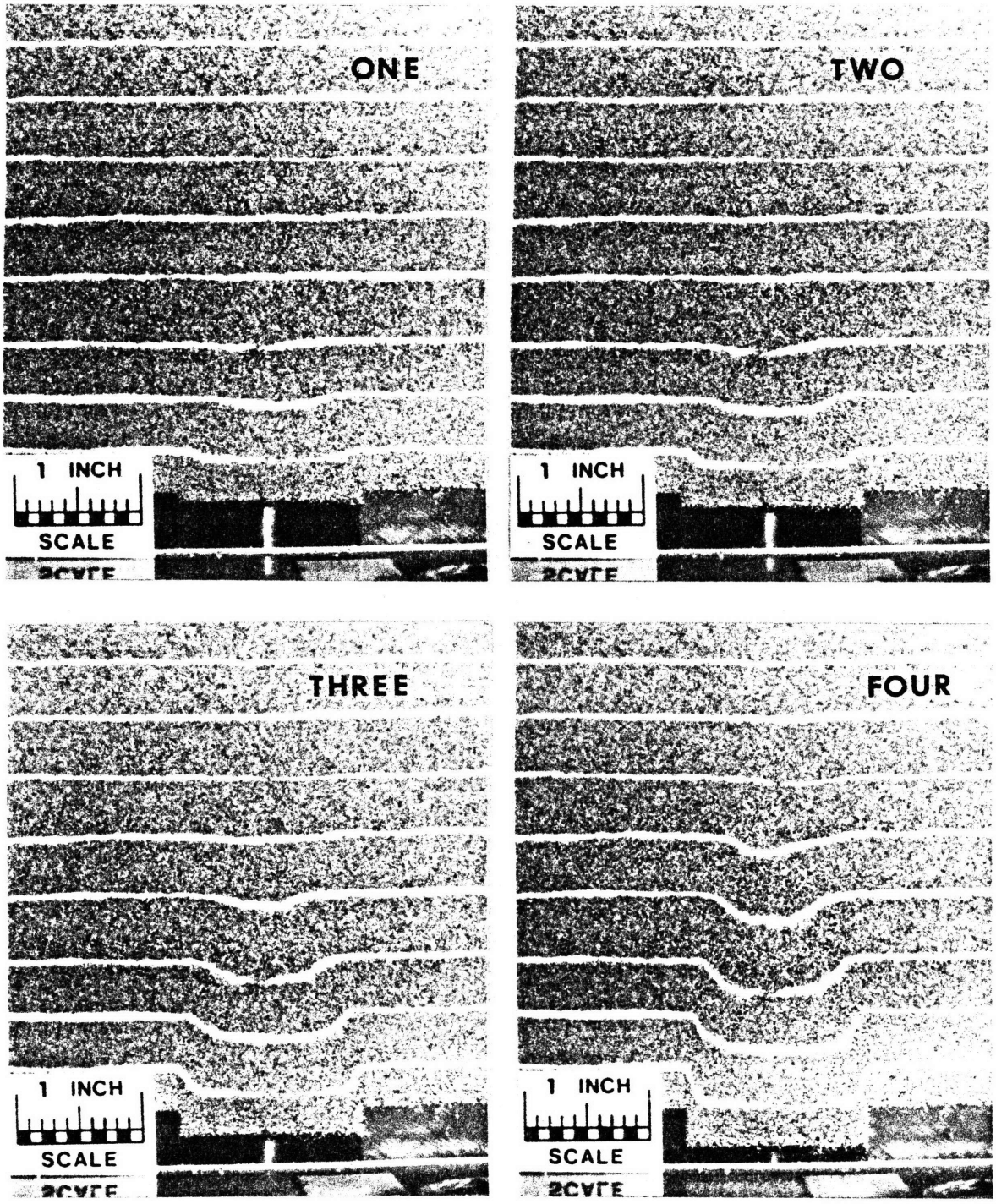

A.7 - A.10 Variations of Soil Displacement Pattern with Increasing Trap Door Displacement during an Active Arching Test

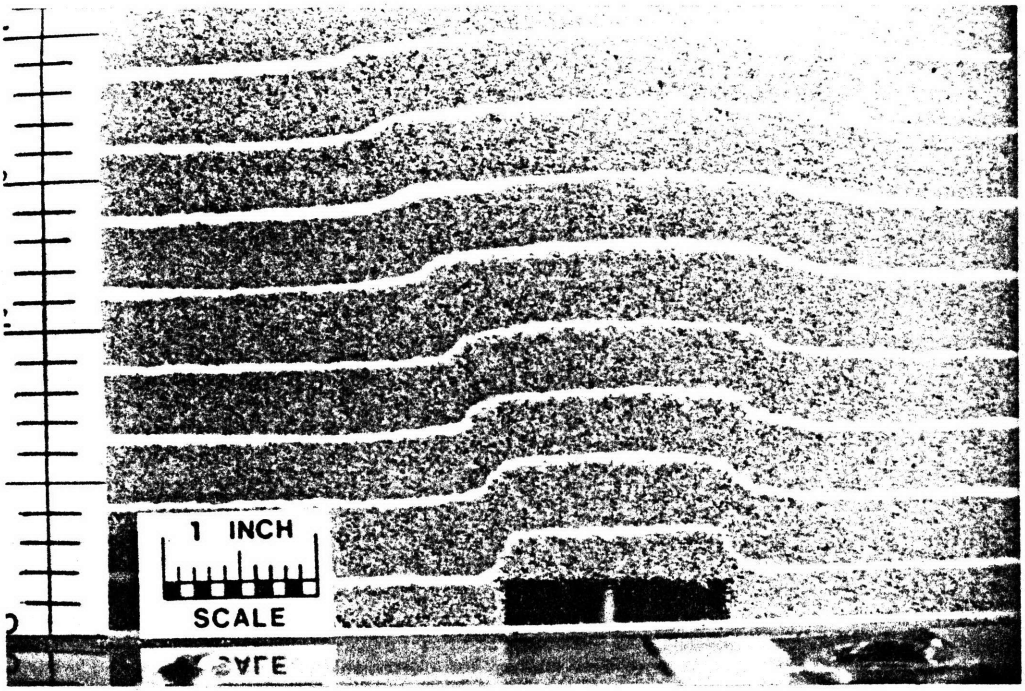

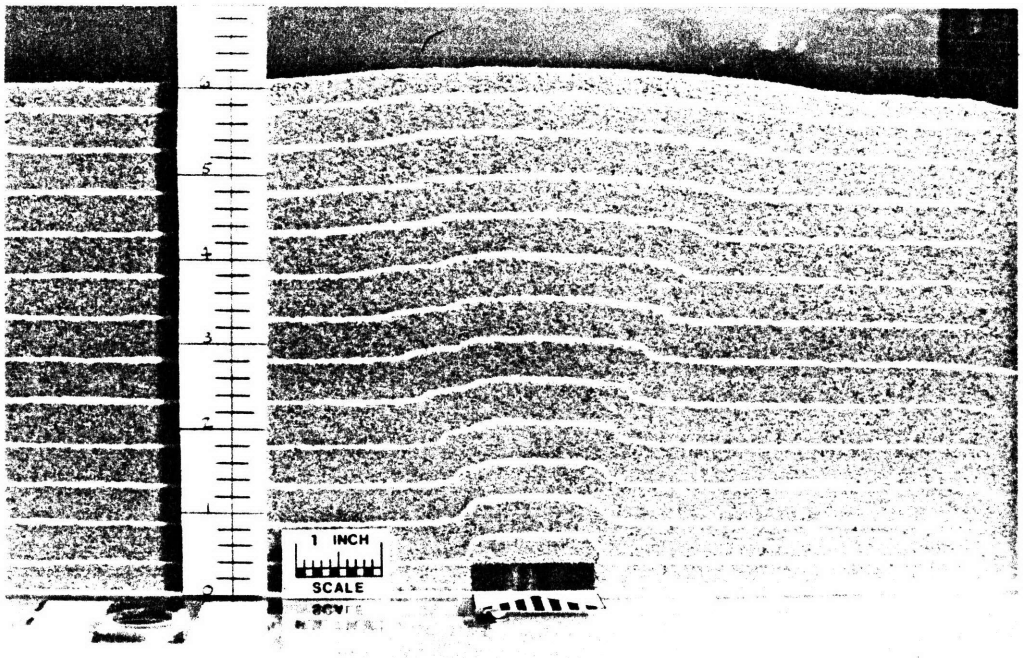

A.11 - A.12 Typical Patterns of Soil Deformation During Passive Arching Tests

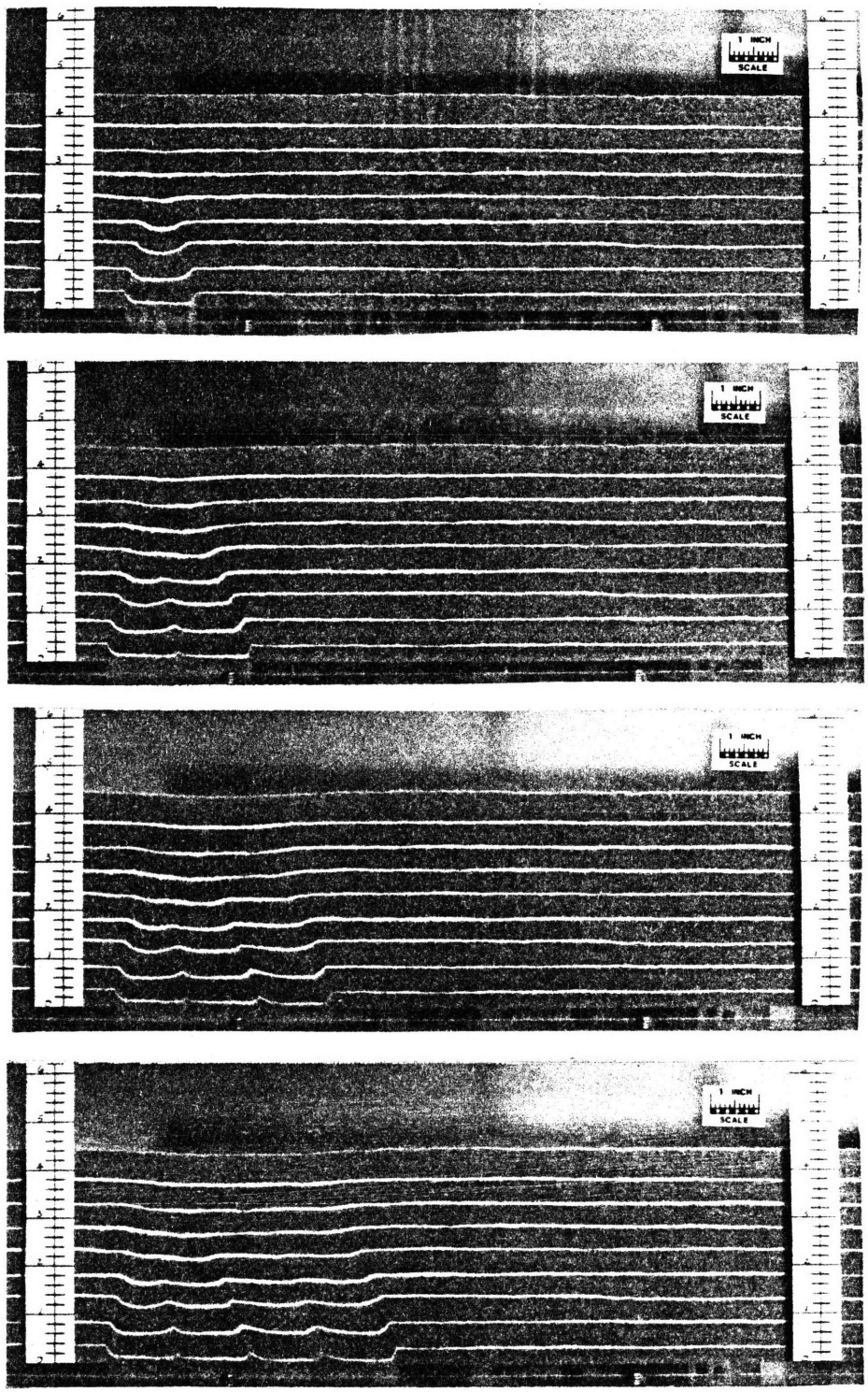

A.13 - A.16 Soil Deformations Above Trap Doors Lowered in Sequence (Active Arching)

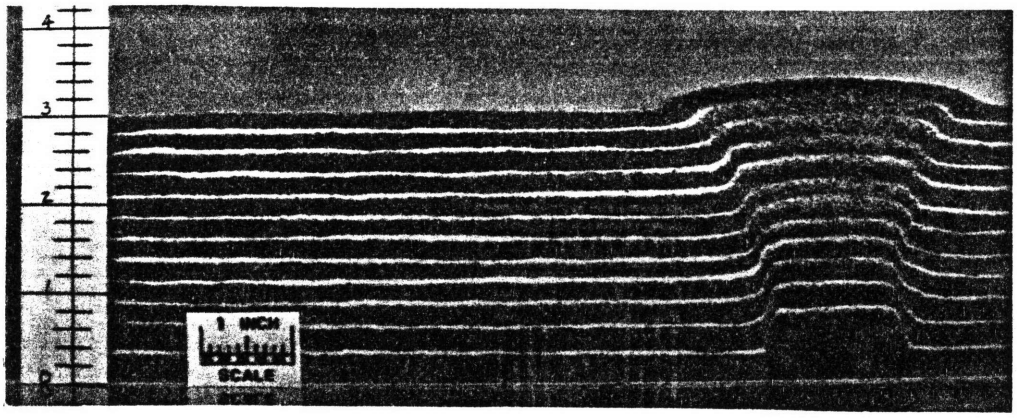

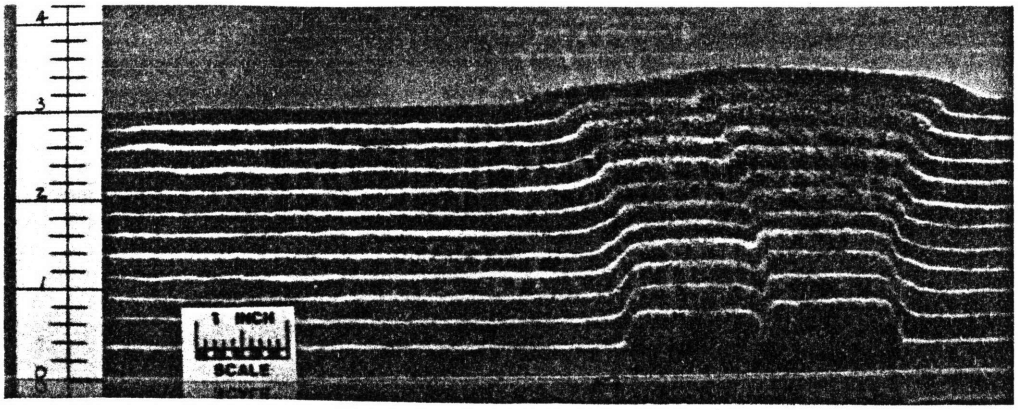

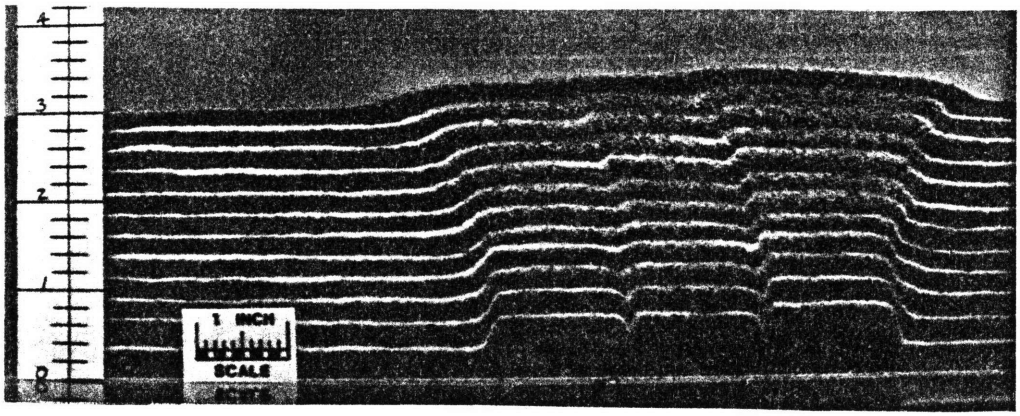

A.17 - A.19 Soil Deformations Above Trap Doors Raised in Sequence (Passive Arching)

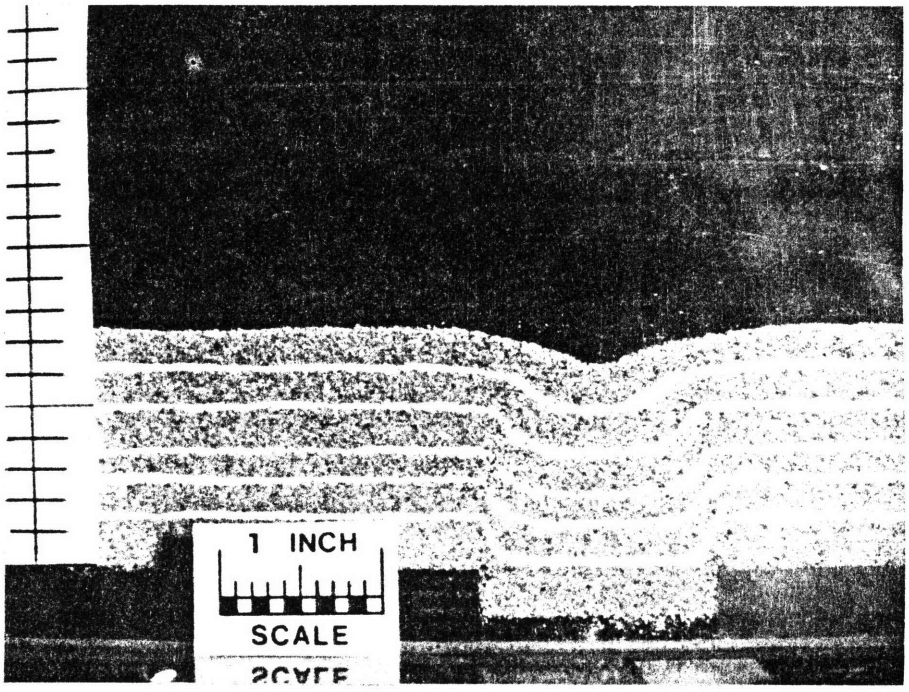

A.20 Observed Settlement Trough - Test Number 61

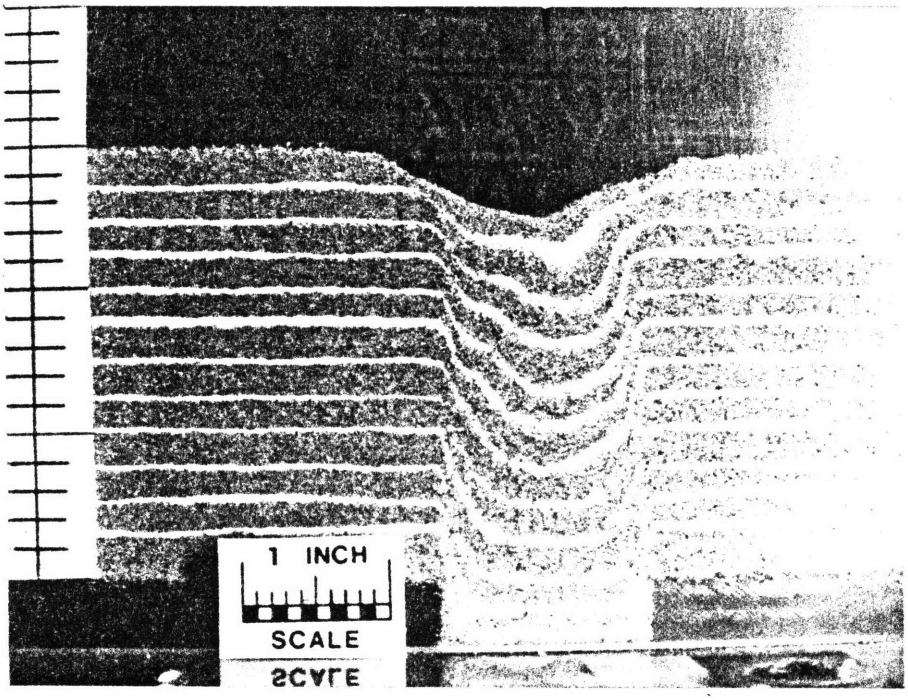

A.21 Observed Settlement Trough - Test Number 60

APPENDIX B

Summary of Tests Performed

This appendix summarizes the series of tests which were performed within the experimental portion of this research. The equipment and sands used, and the results obtained have been presented in Chapters 5 and 6. The actual raw and reduced data from these tests are not included in this document, but can be found compiled in a separate volume entitled "Laboratory Notes on Arching Tests, 1983".

Sixty-nine tests were performed with each numbered sequentially. To conserve space the sand types have been abbreviated as shown below:

F.L.B.S. - Fine Leighton Buzzard Sand
C.L.B.S. - Coarse Leighton Buzzard Sand
M.T.S. - Medium Tan Sand
F.W.S. - Fine White Sand

Tests numbered 1 through 16 were performed in the initial test apparatus.

Test No.	Sand Type	Depth of Sand (inches)	No. of Trans. Used	Description of Test
1	M.T.S.	$7\frac{1}{2}$	1	Tests 1 through 6 investigated the various deposition techniques (including the feasibility of vibration) as well as examining the performance of the transducer under loading. Densities and water contents were measured.
2	M.T.S.	$7\frac{1}{2}$	1	
3	M.T.S.	$7\frac{1}{2}$	1	
4	C.L.B.S.	$5\frac{1}{2}$	1	
5	C.L.B.S.	$5\frac{1}{2}$	1	
6	F.L.B.S.	6	1	
7	F.L.B.S.	6 3/4	1	Tests 7 through 10 were similar to those above with the addition of instrumented unload cycles and observations of temperature sensitivity of transducers. Instrumentation failed in test 9.
8	F.L.B.S.	6 3/4	1	
9	F.L.B.S.	6 3/4	1	
10	F.W.S.	8 3/4	1	
11	F.W.S.	$7\frac{1}{4}$	1	Tests 11 through 16 involved a lowering circular trap door. Results can be found summarized in Table 6.5.
12	F.W.S.	5	1	
13	F.W.S.	4	1	
14	F.L.B.S.	4	1	
15	F.L.B.S.	2	1	
16	M.T.S.	$3\frac{1}{2}$	1	

Tests numbered 17 through 32 were performed in the primary test apparatus with the planar soil deformation tank aligned parallel to the axis of the trap doors.

Test No.	Sand Type	Depth of Sand (inches)	No. of Trans. Used	Trap Door Displ.(δ) (inches)	Description of Test
17	M.T.S.	$4\frac{1}{4}$	1	0.46	Tests 17, 18, 19 and 21 involved lowering a single trap door with the transducer at its center. Results are summarized in Table 6.1.
18	M.T.S.	$4\frac{1}{4}$	1	0.86	
19	M.T.S.	$2\frac{1}{2}$	1	0.89	
20	M.T.S.	$4\frac{1}{4}$	1	Test stopped due to instrument failure.	
21	C.L.B.S.	$4\frac{1}{4}$	1	0.87	
22	M.T.S.	$4\frac{1}{4}$	1	0.15	Tests 22 through 27 involved lowering a set of three adjacent trap doors in succession while monitoring the stress at the center of the middle door. The objective was to check the primary test apparatus' trap door system while also obtaining data. Results are summarized in Table 6.1.
23	F.W.S.	$4\frac{1}{4}$	1	0.25	
24	F.L.B.S.	$4\frac{1}{4}$	1	0.25	
25	M.T.S.	$4\frac{1}{4}$	1	0.25	
26	M.T.S.	$2\frac{1}{4}$	1	0.25	
27	F.W.S.	$4\frac{1}{4}$	1	0.25	
28	M.T.S.	$2\frac{1}{4}$	1	0.31	In tests 28 through 31 a single trap door was raised while measuring stresses at its center. These tests examined passive arching with a summary of results found in Table 6.3.
29	M.T.S.	$2\frac{1}{4}$	1	0.16	
30	F.L.B.S.	$2\frac{1}{4}$	1	0.21	
31	F.L.B.S.	$2\frac{1}{4}$	1	0.30	
32	M.T.S.	$3\frac{1}{2}$	2	0.30	In Test 32 the nine trap doors were lowered in order while measuring stresses on the center door.

Tests numbered 33 through 51 were performed in the primary test apparatus with the three-dimensional soil deformation tank.

Test No.	Sand Type	Depth of Sand (inches)	No. of Trans. Used	H/B	δ/B
33	M.T.S.	4½	2	1	17%
34	M.T.S.	2¼	4	½	1%
35	M.T.S.	2¼	4	½	1%
36	M.T.S.	2¼	4	½	1%
37	M.T.S.	2¼	4	½	1%
38	M.T.S.	2¼	4	½	1%
39	M.T.S.	4½	4	1	1%
40	M.T.S.	4½	4	1	1%
41	M.T.S.	2¼	4	½	5%
42	M.T.S.	2¼	4	½	5%
43	M.T.S.	4½	4	1	1%
44	M.T.S.	2¼	4	½	5%
45	M.T.S.	4½	4	1	1%
46	M.T.S.	2¼	4	½	5%
47	F.W.S.	4½	4	1	1%
48	F.W.S.	2¼	4	½	1%
49	F.W.S.	2¼	4	½	1%
50	F.W.S.	4½	4	1	1%
51	M.T.S.	9	4	2	1%

Description of Test

Tests numbered 33 through 51 involved the sequenced lowering of the nine trap doors in order. The objective was to simulate an advancing tunnel while measuring stresses at specific points as the tunnel approaches and passes. Results can be found in Figures 6.18 through 6.23.

Test 51 - following sequenced 1% displacement, displacements of 5% and 1% were performed with stresses monitored.

Tests numbered 52 through 56 were performed in the primary test apparatus with the planar soil deformation tank aligned perpendicular to the axis of the trap doors.

Test No.	Sand Type	Depth of Sand (inches)	No. of Trans. Used	Description of Test
52	M.T.S.	4½	4	Tests 52 through 56 investigated the hysteretic behavior of the pressure transducers. Sand was deposited and then removed via vacuum with stresses measured. Typical results are presented in Figures 6.1 through 6.5.
53	M.T.S.	4½	4	
54	M.T.S.	2¼	4	
55	M.T.S.	2¼	4	
56	M.T.S.	Var.	4	Two load-unload cycles occurred.

Tests numbered 57 through 65 were performed in the primary test apparatus with the planar soil deformation tank aligned parallel to the axis of the trap door.

Test No.	Sand Type	Depth of Sand (inches)	No. of Trans. Used	H/B	Description of Test
57	M.T.S.	3	3	2	Plane strain active arching - Table 6.1.
58	M.T.S.	3	3	2	Door lowered followed by slow removal of sand via vacuum.
59	M.T.S.	6	0	4	In Tests 59 through 61 the sand was streaked with that of a contrasting color and photographs taken to illustrate soil movement during active arching. See appendix A.
60	M.T.S.	3	0	2	
61	M.T.S.	1½	0	1	
62	M.T.S.	1½	3	1	Tests 62 through 65 investigated plane strain passive arching with stresses measured on the translating doors. Summarized in Table 6.3.
63	M.T.S.	6	3	4	
64	M.T.S.	4½	3	3	
65	M.T.S.	3	3	2	

Tests numbered 66 and 67 were performed in the primary test apparatus with the planar soil deformation tank aligned perpendicular to the axis of the trap door.

Test No.	Sand Type	Depth of Sand (inches)	No. of Trans. Used	H/B	Description of Test
66	M.T.S.	4½	3	1	In Tests 66 and 67 horizontal and vertical stresses were measured so as to determine K. See Figure 6.25 and Table 6.1.
67	M.T.S.	9	3	2	
68	M.T.S.	7½	3	5	Tests 68 and 69 investigated plane strain active arching. Summarized in Table 6.1.
69	M.T.S.	6	3	4	